Journal of Energy in Southern Africa

Volume 26 Number 1 • February 2015

Sponsored by the Department of Science and Technology

Sponsored by the
Department of Science & Technology

This journal is accredited by the South African Department of Higher Education and Training for university subsidy purposes. It is abstracted and indexed in Environment Abstract, Index to South African Periodicals, and the Nexus Database System.

The journal has also been selected into the Science Citation Index Expanded by Thomson Reuters, and coverage begins from Volume 19 No 1. It is also on the Scientific Electronic Library Online (SciELO) SA platform and is managed by the Academy of Science of South Africa (ASSAf).

Administration and subscriptions
Ms Fazlin Harribi

Annual subscriptions (four issues)
Individuals (Africa): R160 (single copy R51)
Individuals (beyond Africa): US$109 (single copy US$39)
Corporate (Africa): R321 (single copy R103)
Corporate (beyond Africa): US$218 (single copy US$77)

Cost includes VAT and airmail postage.
Cheques should be made payable to the University of Cape Town and sent to the address given below.

Enquiries may be directed to:
The Editor, Journal of Energy in Southern Africa,
Energy Research Centre, University of Cape Town,
Private Bag, Rondebosch 7701, South Africa
Tel: +27 (021) 650 3894 Fax: +27 (021) 650 2830
E-mail: Richard.Drummond@uct.ac.za

Website: www.erc.uct.ac.za

It is the policy of the Journal to publish papers covering the technical, economic, policy, environmental and social aspects of energy research and development carried out in, or relevant to, Southern Africa. Only previously unpublished work will be accepted; conference papers delivered but not published elsewhere are also welcomed. Short comments, not exceeding 500 words, on articles appearing in the Journal are invited. Relevant items of general interest, news, statistics, technical notes, reviews and research results will also be included, as will announcements of recent publications, reviews, conferences, seminars and meetings.

Those wishing to submit contributions should refer to the guidelines given on the inside back cover.

© Energy Research Centre ISSN 1021 447X

JOURNAL OF ENERGY IN SOUTHERN AFRICA

Volume 26 Number 1 • February 2015

CONTENTS

SAURAN: A new resource for solar radiometric data in Southern Africa

Michael J Brooks[a]
Sven du Clou[a]
Wikus L van Niekerk[b]
Paul Gauché[b]
Corli Leonard[b]
Michael J Mouzouris [b]
Riaan Meyer[c]
Nic van der Westhuizen[c]
Ernest E van Dyk[d]
Frederik J Vorster[d]

a. Department of Mechanical Engineering, University of KwaZulu-Natal, Durban, South Africa
b. Centre for Renewable and Sustainable Energy Studies, Stellenbosch University, South Africa
c. GeoSUN Africa (Pty) Ltd, Stellenbosch, South Africa
d. Centre for Energy Research, Nelson Mandela Metropolitan University, Port Elizabeth, South Africa

Abstract
A new resource for sun strength data in Southern Africa has been established with the commissioning of a regional network of solar monitoring stations. The Southern African Universities Radiometric Network (SAURAN) is an initiative of Stellenbosch University and the University of KwaZulu-Natal (UKZN), and consists of an initial set of ten ground stations equipped with secondary standard thermopile radiometers. SAURAN's aim is to provide a long-term record of sun strength in a region that shows excellent potential for the deployment of solar energy technologies. Instruments measuring direct normal irradiance (DNI), diffuse horizontal irradiance (DHI) and global horizontal irradiance (GHI) feed time-averaged data over 1-minute, hourly and daily intervals to a central archive from where they are accessible to the public via a website interface. Meteorological data is also provided by most of the stations. This paper gives a brief background to the SAURAN project and describes the network's operation, coverage and future expansion. Examples of solar energy irradiance plots are also provided to illustrate the information available from the SAURAN database.

Keywords: solar resource assessment, Africa, direct normal irradiance, diffuse irradiance, global irradiance

1. Introduction

The solar resource is exceptionally good over most of Southern Africa. Several of South Africa's provinces receive annual direct normal radiation levels high enough to implement concentrating solar power (CSP) projects (Fluri, 2009) and the Northern Cape has among the best resources of any region globally. South Africa's neighbours are also well-placed to exploit high levels of solar radiation. The Namibian government has recognized the untapped potential of solar energy (Namibia Ministry of Mines and Energy, 1998) and now subsidizes off-grid systems such as solar cookers and water-pumps. Botswana has identified solar energy as a key resource for reducing dependence on imported power (Mzezewa, 2009).

South Africa's Integrated Resource Plan for Electricity mandates the installation of 17.8 GW of renewable energy-based generating capacity by 2030 (Department of Energy, 2010). Of this, 8.4 GW is dedicated to photovoltaics (PV) and 1.0 GW to CSP. At present, 200 MW of CSP and 1048 MW of PV capacity are under development (Giglmayr *et al.*, 2014), with an emphasis on local content during construction to stimulate the development of an indigenous solar energy industry.

The roll-out of CSP and PV systems across Southern Africa, together with off-grid initiatives such as solar water heater programmes, has raised

the need for reliable solar resource data with which to plan projects and assess their performance. In some cases, this can be met with satellite models, however, their uncertainties are high when compared to ground stations. Vignola *et al.* (2007) reported root mean square errors (RMSE) ranging from 12 to 38% for hourly GHI data obtained from the GOES 8 satellite when compared to stations in the US Pacific Northwest. Myers (2013) lists RMSE values from a number of studies that fall between 18.3 and 36.1%. Although satellite-derived measurements offer greater spatial coverage, ground-based sensors will remain an essential component of integrated resource assessment programmes for the foreseeable future.

Although the Republic of South Africa (SA) has a history of sporadic radiometric monitoring campaigns, there has been no coordinated deployment of high-quality ground measurement stations for some years. From the 1980s to the mid-90s the South African Weather Bureau, now the Weather Service (SAWS) maintained a network of thermopile sensors, however, this fell into disrepair and its rehabilitation is only recently getting underway. SAWS archived data is not freely available to the public. Ciolkosz (2009) presented results from a network of silicon-based sensors operated by the Agricultural Research Council, however, these do not output research-grade data nor is the archive easily accessible.

In the last fifteen years, several universities have started radiometric measurement and research programmes, including Mangosuthu University of Technology (Brooks, 2005; Zawilska and Brooks, 2011), Stellenbosch University and the University of KwaZulu-Natal (Lysko, 2006; Brooks and Roberts, 2009; Kunene *et al.,* 2013). Given the potential for expanding these efforts, and considering the lack of a long-term, coherent record of sun strength in Southern Africa, Zawilska *et al*. (2012) argued for the establishment of a formal radiometric network utilizing instrumentation at universities and elsewhere.

2. Solar monitoring networks

Although there are many solar monitoring stations operated throughout the world by government agencies, weather services, research institutes and universities, there are relatively few formal networks dedicated to the provision of data for public use. Some of these are national initiatives in which the operating agency owns the measurement stations and others are clearing houses for data obtained from instrumentation that is owned by others. Stoffel *et al.* (2010) provide a useful summary of data sources, including satellite-derived measurements.

Examples of ground-based solar monitoring initiatives are given in Table 1. Networks are important to research and to the success of solar energy programmes because they centralize the management of the data gathering effort, institute systematized maintenance programmes for sensors and apply quality controls that regulate the standard of data, enhancing its usefulness. They also broaden public access to data, encourage the standardization of measurement techniques and promote sound methods of data analysis.

The Baseline Surface Radiation Network (BSRN) is an initiative of the World Climate Research Programme and gathers data from over 50 stations located on seven continents. Rigorous quality checks are performed on the data (Zhang *et al.,* 2013) before it is made available to the public free of charge, via a website. The World Radiation Data Centre (WRDC) is based in Russia and publishes measurements from over 1 000 stations, mainly as daily totals of global irradiance (Stoffel *et al*., 2010). The Surface Radiation Network (SURFRAD) operates seven stations across the continental United States and is funded by the National Oceanic and Atmospheric Administration. The Atmospheric Radiation Measurement (ARM) programme is oprated by the US Department of Energy and has instruments located mainly in the USA, with three sites in the Western Pacific. The University of Oregon's Solar Radiation Monitoring Laboratory (SRML) operates a regional network of ground stations across five states of the Pacific Northwest. The data record extends back to 1977 for certain of the locations. The Bureau of Meteorology in Australia maintains a network of 10 active stations across the continent and makes historical data available to the public from several more.

Table 1: Examples of active solar radiometric networks and data archives

Data source	*Website access*
Baseline Surface Radiation Network (BSRN)	www.gewex.org/bsrn.html
World Radiation Data Centre (WRDC)	wrdc-mgo.nrel.gov
Surface Radiation Network (SURFRAD)	www.esrl.noaa.gov/gmd/grad/surfrad/
Atmospheric Radiation Measurement (ARM)	www.arm.gov
University of Oregon Solar Radiation Monitoring Laboratory (SRML)	solardat.uoregon.edu/index.html
Australian Bureau of Meteorology (BOM)	www.bom.gov.au/climate/data-services/solar/
Southern African Universities Radiometric Network (SAURAN)	www.sauran.net

In 2014 the Southern African Radiometric Network (SAURAN) was established to address the regional lack of publicly accessible, long-term, high-quality solar data of high-temporal resolution. The network is an initiative of the Centre for Renewable and Sustainable Energy Studies (CRSES) at Stellenbosch University and the Group for Solar Energy Thermodynamics at the University of KwaZulu-Natal in Durban. This paper describes the coverage and operation of the network, which offers analysts and researchers an online source of meteorological and sun-strength data from instrumentation that is carefully maintained in a centrally coordinated monitoring programme.

3. The SAURAN network

3.1 Spatial coverage

SAURAN is being implemented over several phases as monitoring stations are acquired and commissioned. In its initial phase, SAURAN consists of ten ground stations across South Africa, marked in black in Figure 1. Each station is given a three-letter identification code that forms part of the filename when data is downloaded. Six stations are located on university campuses in the cities of Stellenbosch (SUN), Port Elizabeth (NMU), Durban (KZH and KZW), Pretoria (UPR) and Bloemfontein (UFS). Four are on farms in rural areas near the towns of Vanrhynsdorp (VAN) in the Western Cape, Vryheid (VRY) in KwaZulu-Natal, Graaff-Reinet (GRT) in the Eastern Cape and near Alexander Bay in the Richtersveld region of the Northern Cape (RVD).

The location of the ten sites covers a range of climate and vegetation conditions, from desert through to coastal sub-tropical. Some of the stations, including SUN, KZH, KZW and NMU are existing facilities that have also contributed historical data to the archive that predate the SAURAN project. Table 2 gives the geographic coordinates of the ten SAURAN stations and a brief description of each location's surrounding topography.

In the project's second phase, stations are planned in the far northern province of Limpopo (UVT), near the town of Alice in the Eastern Cape (UFH) and at the Mangosuthu University of Technology (STA) south of Durban. Further stations are planned in the Namibian capital city of Windhoek (PNW), at Gaborone in Botswana (UBG) and on the Indian Ocean island of Reunion (URN). Subsequent phases will see the expansion of the network into Southern Africa so as to fill gaps in the network's coverage.

3.2 Instrumentation

The primary aim of the SAURAN initiative is to build a high-quality, long-term dataset of high temporal resolution for public use. To this end, the ten initial stations use research-grade secondary standard thermopile radiometers that are properly maintained and cleaned regularly. All sites measure direct normal, diffuse and global irradiance independently so that cross-checking of the radiometric

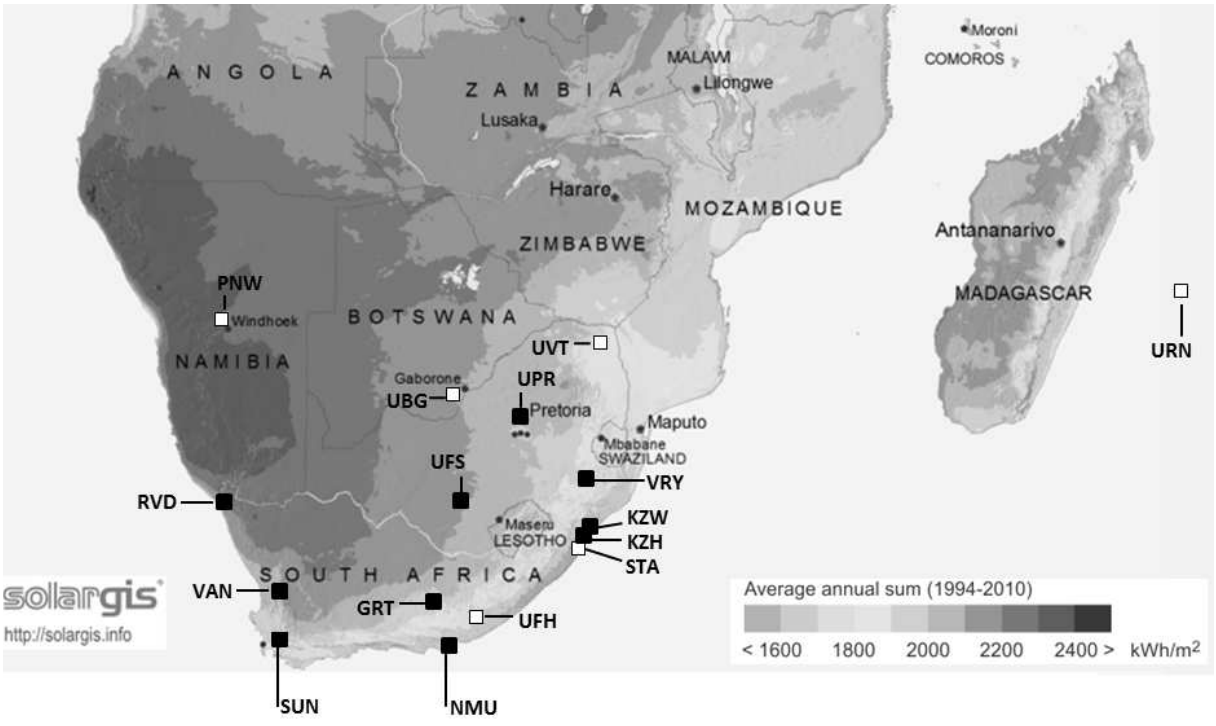

Figure 1: Location of the ten active SAURAN stations (in black) and six planned stations (in white) overlaid on a satellite-derived map of annual average global horizontal radiation for Southern Africa *(GeoSUN Africa (Pty) Ltd, 2014)*

Table 2: Metadata for the ten initial SAURAN stations

Code	Location	Lat.[deg]	Long.[deg]	Elevation [m]	Site and topography
GRT	Near Graaff-Reinet, Eastern Cape	-32.4854	24.5858	660	Inside enclosure on flat scrubland with clear horizons
KZH	Durban, KwaZulu-Natal	-29.8709	30.9769	150	On building rooftop with clear horizons except for partial obscuration on north western side
KZW	Westville, Durban, KwaZulu-Natal	-29.8169	30.9449	200	On building rooftop with clear horizons except for partial obscuration on southern side
NMU	Port Elizabeth, Eastern Cape	-34.0085	25.6652	35	On building rooftop with mainly clear horizons
RVD	Near Alexander Bay, Northern Cape	-28.5608	16.7615	141	Inside enclosure in desert region with clear horizons
SUN	Stellenbosch, Western Cape	-33.9281	18.8654	119	On building rooftop with horizons partially obscured by mountains
UFS	Bloemfontein, Free State	-29.1107	26.1850	1491	On building rooftop with mainly clear horizons
UPR	Pretoria, Gauteng	-25.7531	28.2286	1410	On building rooftop with mainly clear horizons
VAN	Near Vanrhynsdorp, Western Cape	-31.6175	18.7383	130	Inside enclosure on flat scrubland with clear horizons
VRY	Near Vryheid, KwaZulu-Natal	-27.8282	30.5000	1277	Inside enclosure on flat grassland with clear horizons

components at a given location is possible through the closure equation:

$$E = E_{bn} \cos Z + E_d \quad (1)$$

where E, E_{bn} and E_d are measured values of GHI, DNI and DHI respectively. The responsibility for maintaining sensors belongs to the partner universities that own the stations. Data is provided to website users as 1 minute, hourly and daily averages from sensor scans conducted at sub-6 second intervals, and the time base for all readings is South African Standard Time (SAST). Users who wish to conduct further analysis of SAURAN data, such as cross-checking component values using equation (1), must supply solar vector information, such as the zenith angle. This should be adjusted to accommodate for the difference between SAST and solar time in the download files.

A list of the instruments in use at each of the initial ten stations is given in Table 3. Some of the sites host additional radiometers for research purposes. Stellenbosch University (SUN) operates a CMP11 under a shading ring to provide additional diffuse measurements and UVS-AB-T sensor for recording ultraviolet radiation in the wavelength ranges of 280 to 315 nm and 315 to 400 nm. UKZN Howard College (KZH) has a CUV5 sensor for UV radiation

Table 3: Instruments in use and measured parameters at the ten initial SAURAN stations

Instrument Type	*Parameter, [unit]*	*GRT*	*KZH*	*KZW*	*NMU*	*RVD*	*SUN*	*UFS*	*UPR*	*VAN*	*VRY*
Kipp & Zonen CHP1/ SOLYStracker	DNI, [W/m^2]	✓	✓	✓	✓	✓	✓	✓	✓	✓	✓
Kipp & Zonen CMP11	GHI, [W/m^2]	✓	✓	✓	✓	✓	✓	✓	✓	✓	✓
Kipp & Zonen CMP11/ Shad. ball/SOLYS	DHI, [W/m^2]	✓	✓	✓	✓	✓	✓	✓	✓	✓	✓
Kipp & Zonen CUV5	Total UV, [W/m^2]		✓								
Kipp & Zonen UVS-AB-T	UV-A and UV-B, [W/m^2]						✓				
Delta-T ✓SPN1	DHI and GHI, [W/m^2]		✓								
Eppley PSP/Perforated shadow band	DHI and GHI, [W/m^2]		✓								
Kipp & Zonen CMP11/ Shading ring	DHI, [W/m^2]						✓				
Campbell Scientific CS215	Air temperature, [°C]	✓	✓		✓	✓	✓	✓	✓	✓	✓
Campbell Scientific CS215	Relative humidity, [%]	✓	✓		✓	✓	✓	✓	✓	✓	✓
Vaisala PTB110	Barometric pressure, [mbar]	✓	✓		✓	✓	✓	✓	✓	✓	✓
Texas TR525I or TE525	Rainfall, [mm]	✓	✓			✓		✓	✓	✓	✓
R.M.Young 05103 or 03001	Wind speed/direction, [m/s/°]	✓	✓	✓	✓	✓	✓	✓	✓	✓	✓

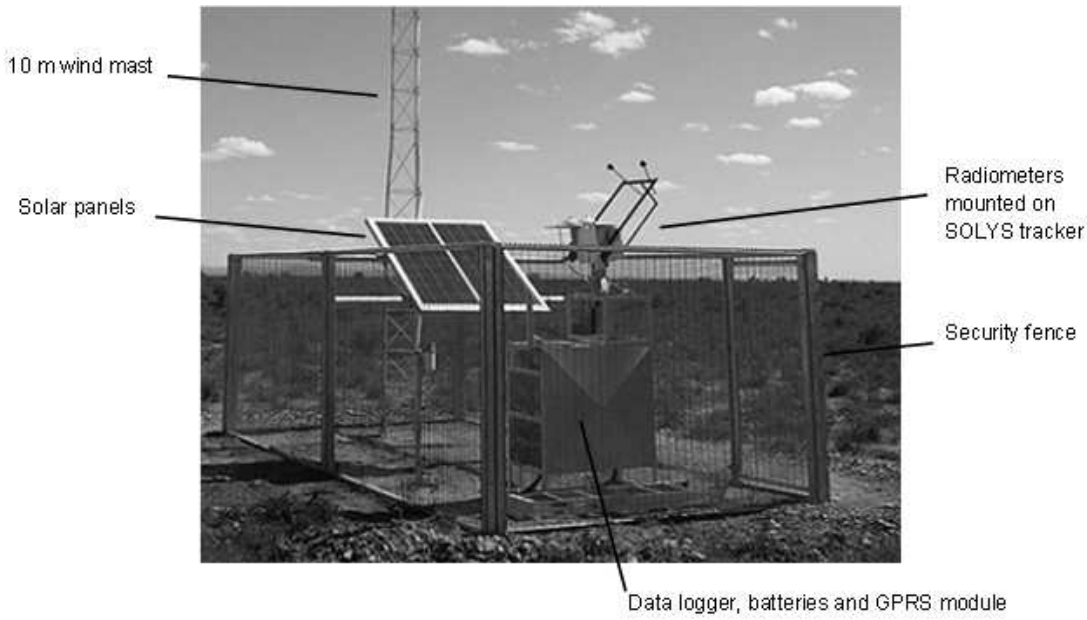

Figure 2: SAURAN station at Graaff-Reinet in the Eastern Cape province of South Africa

in the 280 to 400 nm range. The KZH station also hosts instruments for parallel research projects, including a Delta-T SPN1 pyranometer and an Eppley Precision Spectral Pyranometer fitted with a perforated shadow band (Brooks, 2010).

Figure 2 shows the SAURAN GRT installation located on a farm outside the town of Graaff-Reinet in the Eastern Cape Province of South Africa. As with most stations in the network, the Kipp & Zonen radiometers are mounted on a SOLYS tracker, including a CHP1 measuring DNI, a CMP11 under a shading ball measuring DHI and an exposed CMP11 for GHI. Radiometric and meteorological data, typically including air temperature, barometric pressure, wind speed, wind direction and humidity, are recorded by a CR1000 logger housed inside a waterproof enclosure and cage. All of the SAURAN stations are secured against interference and most are powered by photovoltaic systems to ensure continuity of operation and independence from the electrical grid. The GRT station is powered by two 125 W solar panels with excess energy stored in four 102 Ah batteries. The communications system includes a GPRS module that connects the station to its university-operator via the cellular telephone network.

Stations in the SAURAN network either use a similar remote communications setup or are connected directly to a local university network. Operators communicate with the stations using Loggernet software to monitor instrumentation output, battery voltages and tracker operation. This is done independently of the SAURAN database infrastructure, which is managed separately and harvests data from the stations multiple times daily to maintain the archive.

Meteorological measurements such as wind, temperature and pressure are provisioned for as supporting data to the radiometric data. While the additional measurements are recorded with good quality instruments, they are not all installed in typical meteorological measurement locations and the data is not intended for use other than to support the radiometric data. Stations located on rooftops, typically on university campuses, will record wind and temperature data only relevant to the immediate proximity of the station. The more remote stations such as GRT (near Graaff-Reinet) have meteorological stations that are more typical with 10 m mast height for wind speed and direction.

3.3 Database infrastructure and website

The information flows and architecture of the SAURAN network are represented schematically in Figure 3. The archive resides on the UKZN research server cluster to provide data security, automatic backups and an uninterruptable power supply. Radiometric data is retrieved from station loggers using Loggernet software according to a download schedule that limits the drain on storage batteries at remote locations. Most stations use modems operating on the Global System for Mobile Communications (GSM) standard. Measurements are first stored in a primary database as three tables per station; one each for minute-, hour-, and day-averaged readings. The primary database is isolated from the secondary SAURAN archive that serves the website whenever a user downloads measurements. This is to protect the primary data record. The SAURAN database is generated using custom code that automatically transfers new measurements from the primary archive at regular intervals. The website does not offer real-time data, but the time lags are typically less than 10 hours.

The SAURAN database is structured according to the entity-attribute-value (EAV) model, where the station is the entity, each instrument (Instr) is an attribute and the measurements constitute the values. This permits commonality of instrument names across the network and the structured ordering of columns in download files, regardless of their position in logger tables. In addition, the model facilitates data manipulation and allows administrators to add or remove instruments and quality control flags at specific stations.

The website user interface includes a map of Southern Africa with radio buttons for accessing each station in the network. Users can also access data through a list of stations that includes an updated record of the years and months containing measurements. Each station's page includes a photograph of the installation, the geographic coordinates, a list of the measurements available at the site, downloadable supporting documents and the data download tool. Supporting documents include a description of the quality control flags, acronyms and instrument calibration dates.

The data download tool packages measurements as a radiometric time-series in an ASCII text file for a specified date range at a particular station. The downloaded file is named according to the format YYYYMMDD_***_T.dat, where YYYY is the year, MM is the month and DD is the start date of the time series. To facilitate file handling, the three letter station code (***) is embedded in the filename with the averaging period (T) designated as M for minute, H for hour or D for day. Quality control flags are downloaded if the appropriate checkbox is selected. The website also provides administrative access for configuring new stations, editing instrument names and managing quality control data flags.

3.4 Data quality control

Initially, SAURAN offers a limited quality control feature in the form of downloadable flags for minute-interval measurements at selected stations. The flags are intended to warn users of potential problems in the archive and are similar to those employed by Jacovides *et al.* (2006). A flag, denoted as '1' in the data file, is triggered when any one of the following conditions is met:

$$E_d > 1.1E \quad (2)$$

$$E > 1.2E_o \quad (3)$$

$$E_d > 0.8E_o \quad (4)$$

$$E - E_d > E_o \quad (5)$$

$$E < 5 \quad (6)$$

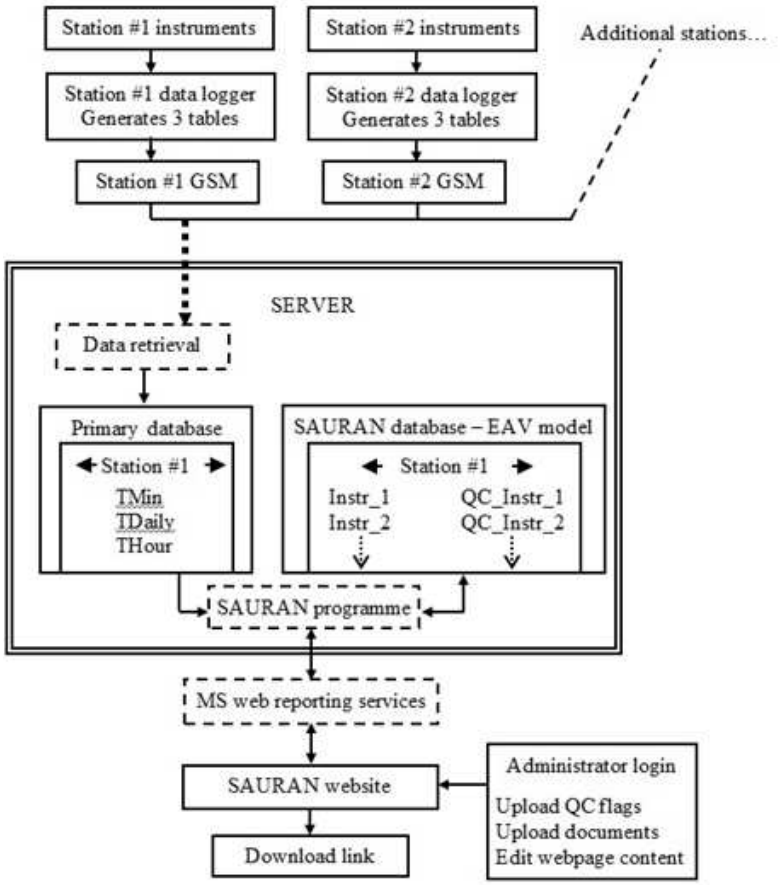

Figure 3: Flow chart of data handling in the SAURAN network

$$E_d < 5 \quad (7)$$

$$|E_{bn} - E_{bn\_calc}| > 50 \text{ where } E_{bn\_calc} = (E - E_d)/\cos Z \quad (8)$$

$$|E - E_d| < 5 \text{ and } E_{bn} < 1.5 \text{ and } E > 600 \quad (9)$$

In the above, E_o is the extra-terrestrial global horizontal irradiance. Equations (2) to (5) identify non-physical limits for DHI, GHI and DNI. Equations (6) and (7) eliminate night values and data close to sunrise or sunset where the cosine effect compromises pyranometer readings. Equation (8) uses the measurement redundancy of the station to identify egregious discrepancies between the calculated DNI and its measured equivalent. Equation (9) can be used to identify problems with the tracking system. In the event of a tracker failure, the misaligned pyrheliometer will read zero and the shading ball will no longer occlude the sun, such that $E_d \approx E$. Fulfilment of the third condition in equation (9) suggests a non-zero DNI-component, discounting normal occlusion of the radiometers by cloud and triggering the flag for possible tracker malfunction.

In addition to the above, a quality control flag is triggered when the time difference between successive measurements is not equal to 1 minute. This

identifies data gaps or anomalies related to the logger clock time. A manual flag is also provided to indicate any other known station malfunction that does not affect data in the normal way. It should be noted that the flag system is for alarm purposes only and SAURAN users are advised to run their own quality checks on all data from the site.

4. SAURAN data examples

Data can be downloaded for any period of time in minute-averaged, hour-averaged or day-averaged format. It should be noted that the selection of minute-averaged data can lead to significant volumes of data being downloaded, for example, a single day will result in 1 440 lines of information. The following examples illustrate some of the functionality and value of the SAURAN network in graphical form.

Figure 4 plots DNI measured at the Vanrhynsdorp (VAN) station on 1 May 2014. Hour-averaged DNI is superimposed on the finer resolution minute-averaged DNI data. The break in DNI during the day illustrates the differences between the average values and the range of values during that period. In order to appropriately represent that data, the hour-averaged values are shifted 30 minutes earlier, representing the mid-point of the elapsed hour.

Figure 5 additionally plots GHI, DHI, wind speed and air temperature for the same location and timeframe in order to illustrate further the value of measured minute-averaged data. Not shown are other typical measurements such as relative humidity and wind direction. The value of SAURAN as a network of stations is perhaps best demonstrated by the graphical representation of solar data at five stations on 8 May 2014 in Figure 6.

The five SAURAN stations (SUN, NMU, UFS, UPR, KZH) are more-or-less ordered from west to east and from south to north. It is clear that as the day progresses, one or more weather events causing significant degradation of DNI occur. The western and southern regions experience poor weather early. This poor weather is not experienced in Bloemfontein (central region) until early afternoon. Only Durban on the east coast shows no signs of these weather systems on that day.

Many other examples could be shown including quality control flag cases, longer time series, data validation and calibration.

5. Conclusion

The SAURAN network offers solar resource analysts simplified access to research-grade radiometric ground data in a region sparsely served by monitoring stations. Apart from its usefulness to commercial developers, agricultural planners, municipal

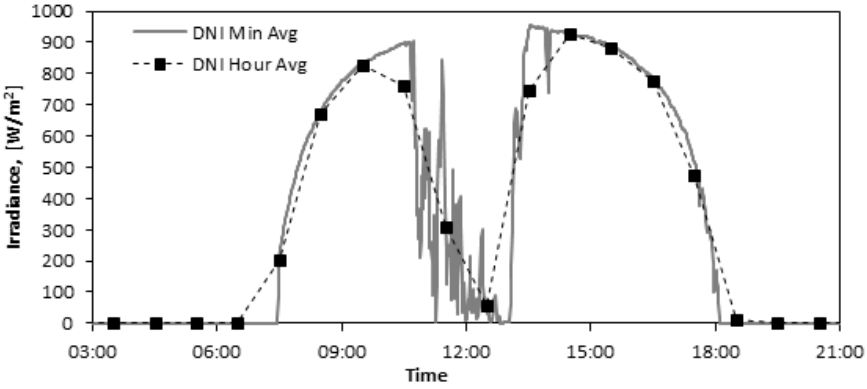

Figure 4: DNI (minute-averaged and hour-averaged) at the Vanrhynsdorp station on 1 May 2014

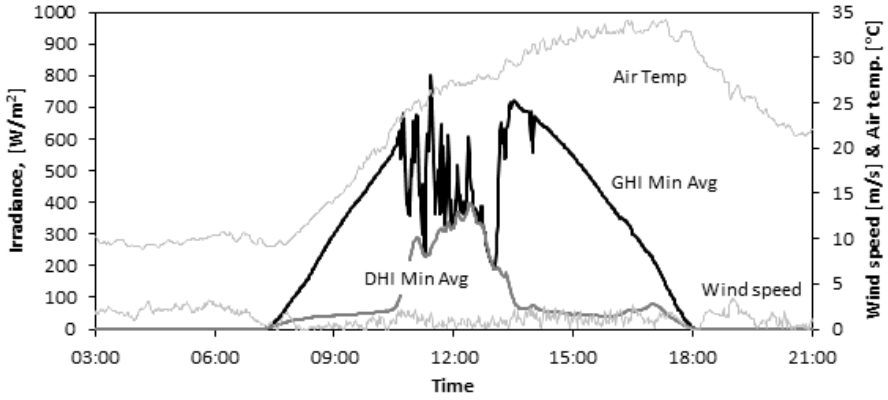

Figure 5: GHI, DHI, wind speed and air temperature (all minute-averaged) at the Vanrhynsdorp station on 1 May 2014

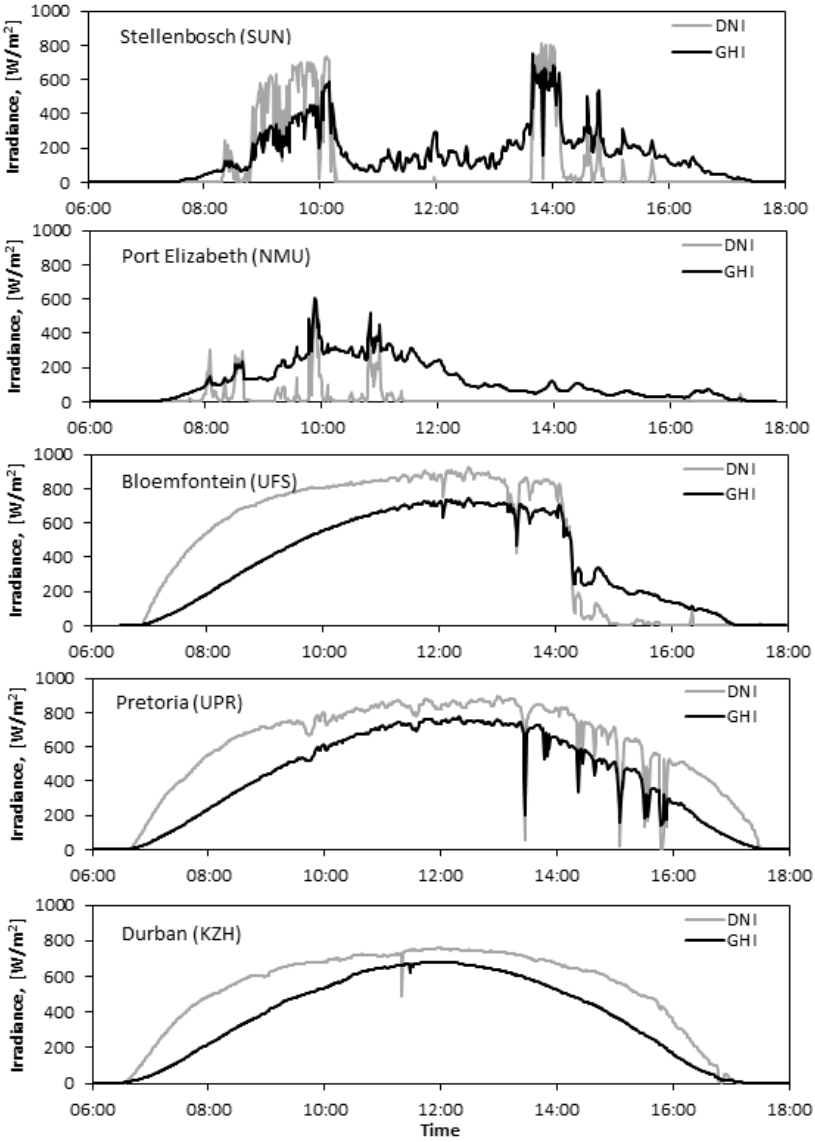

Figure 6: DNI and GHI measurements at 5 spatially distributed SAURAN stations on 8 May 2014

energy departments and researchers, the database can also be used to refine satellite models of the solar resource over Southern Africa.

SAURAN measurements can be utilized with other data streams in the region for climate studies and atmospheric research. For example, aerosol optical depth (AOD) data are available from the Council for Scientific and Industrial Research in Pretoria through the Aerosol Robotic Network (AERONET). These can be used with irradiance data from the UPR station to verify and develop radiometric transmittance models. SAURAN's spatial coverage will be enhanced through further expansion of the network. It is hoped that the database will be used extensively by researchers to promote sustainable energy initiatives in sub-Saharan Africa.

Acknowledgements

The authors appreciate the support of the Deutsche Gesellschaft für Internationale Zusammenarbeit (GIZ), the eThekwini Municipality, the United States Agency for International Development (USAID), Eskom and the National Research Foundation. We also thank Dr. Alan Matthews, Paulene Govender, Jason Freeman, Kai Broughton, Donald Fitzgerald and CS Africa for their support and assistance.

References

Brooks, M.J., (2005). The development and impact of an outdoor solar thermal test facility. *Journal of Energy in Southern Africa* 16:4, 67–71.

Brooks, M.J., (2010). A perforated shadow band for separation of diffuse and direct components from global irradiance. *Solar Energy* 84:12, 2179–2194.

Brooks, M.J., & Roberts, L.W., (2009). Establishment of a broadband radiometric ground station on the

South African east coast. In: Proceedings: SPIE Conference on Optical Modelling and Measurements for Solar Energy Systems III, 7410-1, San Diego.

Kunene, K.R., Brooks, M.J., Roberts, L.W. &, Zawilska, E., (2013). Introducing GRADRAD: The greater Durban radiometric network. *Renewable Energy*, 49, 259–262.

Ciolkosz, D., (2009). SASRAD: An hourly-timestep solar radiation database for South Africa. *Journal of Energy in Southern Africa* 20:1, 25–34.

Department of Energy, (2010). Integrated resource plan for electricity (IRP) 2010-2030: Update report. Government of South Africa.

Fluri, T.P., (2009). The potential of concentrating solar power in South Africa. *Energy Policy* 37, 5075–5080.

GeoSUN Africa (Pty) Ltd, Accessed on 21 March 2014. http://geosun.co.za/solar-maps/.

Giglmayr, S., Brent, A., Gauche, P., & Fechner, H., (2014). Utility-scale PV power and energy supply outlook for South Africa in 2015. In proceedings: 2nd South African Solar Energy Conference (SASEC), Port Elizabeth.

Jacovides, C.P., Tymvios, F.S., Assimakopoulos, V.D., & Kaltsounides, N.A., (2006). Comparative study of various correlations in estimating hourly diffuse fraction of global solar radiation. *Renewable Energy* 31, 2492–2504.

Lysko, M., (2006). Measurement and Models of Solar Irradiance. PhD Thesis, Norwegian University of Science and Technology.

Myers, D.R., (2013). Solar Radiation: Practical Modelling for Renewable Energy Applications, Taylor and Francis.

Mzezewa, C.T., (2009). National Energy Policy for Botswana: Final draft.

Namibia Ministry of Mines and Energy, (1998). Energy Policy White Paper.

Stoffel, T., Renné, D., Myers, D., Wilcox, S., Sengupta, M., George, R., & Turchi, C., (2010). Best practices handbook for the collection and use of solar resource data. National Renewable Energy Laboratory, NREL/TP-550–47465.

Vignola, F., Harlan, P., Perez, R., & Kmiecik, M., (2007). Analysis of satellite derived beam and global solar radiation data, *Solar Energy* 81, 768–772.

Zawilska, E., & Brooks, M.J., (2011). An assessment of the solar resource for Durban, South Africa. *Renewable Energy* 36:12, 3433–3438.

Zawilska, E., Brooks, M.J., & Meyer, A.J., (2012). A review of solar resource assessment initiatives in South Africa: The case for a national network, In Proceedings: The World Renewable Energy Forum, Denver, Colorado.

Zhang, T., Stackhouse Jr, P.W., Gupta, S.K., Cox, S.J., Mikovitz, J.C., & Hinkelman, L.M., (2013). The validation of the GEWEX SRB surface shortwave flux data products using BSRN measurements: A systematic quality control, production and application approach, *Journal of Quantitative Spectroscopy & Radiative Transfer* 122, 127–140.

Received 30 May 2014; revised 6 February 2015

The inter-relationships between regulation and competition enforcement in the South African liquid fuels industry

Reena Das Nair[a]
Pamela Mondliwa[a]
Simon Roberts[ab]

a. Centre for Competition, Regulation and Economic Development, University of Johannesburg, South Africa
b. Department of Economics and Econometrics, University of Johannesburg, South Africa

Abstract
The competition authorities have devoted considerable time and energy to investigating anticompetitive conduct in the broad area of liquid fuel, gas and related products, where regulation sets rules for firm conduct. Competition cases have included the Sasol-Engen merger, collusive arrangements in gas distribution and the pricing of bitumen for road construction projects, and alleged coordination through information exchange in diesel. Drawing on a review of these matters we assess the inter-relationships between regulation and competition enforcement. We argue that regulation can be designed to enable greater competitive rivalry, while anti-competitive conduct can also be better remedied through recognition of the role of regulation.

Keywords: regulation, competition, liquid fuels

1. Introduction

There has been much debate in South Africa as elsewhere about the relationships between competition authorities and regulators, and between competition and regulation.[1] There have also been court cases regarding the boundaries of the jurisdiction of regulators and the competition authorities, especially in telecommunications (Moodaliyar and Weeks, 2009). We focus on the inter-relationships between the two to better understand the nature of tensions and of complementarities between the two regimes.

At the outset we caution that it should not be assumed that there is a standard form of economic regulation nor of competition/antitrust. For example, some (Ginsberg, 2009) contrast antitrust and economic regulation in terms of objectives, observing that antitrust has consumer welfare as its objective while economic regulation typically has economic development and sector-specific goals. However, South Africa's competition law has a total welfare standard and has a range of objectives encompassing participation in the economy and addressing the legacy of concentration of control bequeathed by apartheid. International reviews also reveal a range of objectives, standards and frameworks (Fox, 2003; Singh, 2002).

We start by briefly characterising economic regulation and competition law and note some of the tensions that have been identified in the literature. In section 2, we then focus on the liquid fuels regime, describing its evolution and the proposed Sasol-Engen merger. Section 3 examines how previous regulation (and the role of the state) set up challenges for competition enforcement, drawing on a review of competition cases. In section 4 we then reflect back from the competition challenges to the ways in which regulation and competition can work better together, with clarity on roles and responsibilities.

The economic regulation which we have today in South Africa, as in many other countries, is in the main about regulating the natural monopoly parts of the economy that were state owned and have been privatised. Regulation is generally understood as *ex ante* because, in the absence of competitive discipline on market power, the regulators set rules

within which businesses make forward-looking investment and production decisions (Viscusi *et al.,* 2000). Regulators seek to ensure that a fair return is earned on investments made but not an exploitative one (Newbery, 1997). Three decades ago, it was widely believed that regulation would 'wither away' as competition developed. However, it has become evident that regulation is required to ensure the competitive space remains open and to govern aspects such as access to critical infrastructure. Indeed, regulation may seek to create what Ginsberg (2009) has termed 'synthetic competition' where the dynamic gains from rivalry, such as in terms of product and service development, are judged to merit several competitors where scale economies imply that only one firm would minimise costs.

Competition enforcement is most effective in dealing with firms' conduct in markets that would support competition absent the targeted behaviour. It is about evaluating conduct in *ex post* assessments of whether competition has been harmed (OECD, 1999; Buigues, 2006; de Streel, 2004). Contraventions are deterred through penalties on such conduct. Remedies in competition cases can, however, also involve changes to conduct (such as banning exclusive dealing or types of loyalty inducing rebates) and/or changes to structure.

Tensions between competition and regulation can arise in instances where regulation limits the scope of competition laws and instances where regulation makes it increasingly difficult to enforce the competition law. The former is not an issue in the South African context as the Competition Act was amended to give the competition authorities jurisdiction over all sectors including those that have sector regulators. The latter arises where regulation creates a structure which is not conducive to competition (ICN, 2004).

Economic regulation and competition law may be complementary even while their goals differ (de Streel, 2004). For example, regulation and competition law may work together to support entrants and smaller rivals in markets with an entrenched incumbent that have been recently opened to competition. Competition can be facilitated if the regulator has intervened to alleviate the potential competition problems (ICN, 2004).

This complementarity also stems from the tools that are at the disposal of the two authorities. In circumstances where the intervention required is extensive and/or frequent, or where the remedies that are available to competition authorities are insufficient to address such conduct, then it may be better to use *ex-ante* regulation (Buigues, 2006; Geradin & O'Donoghue, 2005). By comparison, competition law typically has stronger powers of investigation and sanction to uncover anticompetitive practices which may be undermining the objectives of regulation, including where a firm is using benefits from regulation in one market to engage in anti-competitive conduct in another (ICN, 2004; Buigues, 2006). Without overlapping jurisdiction of regulators and competition authorities, the risk is that there may be gaps where neither competition law nor regulation applies. This could occur as an unintended consequence of regulation creating a position of market power in a related market that the firm claims is not covered by the competition law.[2]

It is against this backdrop that we reflect on the South African energy value chains, and argue for regulation *for* competition, to complement competition law and to facilitate better market outcomes.

2. The legacy of liquid fuels policy and objectives under apartheid[3]

The history of regulation in the refining and marketing of petrochemical products entrenched a long-standing culture of coordinated behaviour between oil companies. Government intervened extensively in petrochemical markets to develop a synthetic fuels industry to reduce dependency on imported crude oil and vulnerability to sanctions in the apartheid period. Low grade coal supply in the inland region allowed the formation by the state of a synthetic fuels producer, South African Coal, Oil and Gas Corporation Limited, later Sasol Limited, in the 1950s.

In 1954, government brokered the Main Supply Agreement (MSA) between Sasol and other crude oil refining companies, obliging the other oil companies (OOCs) to purchase Sasol's production to meet their inland fuel demand. The OOCs were committed to purchase all of Sasol's production volumes pro-rata to their market shares. The regulation here effectively represented a bargain between the multinational refiners present in the country (including Shell, BP, Total and Chevron) and Sasol together with the South African state (Rustomjee *et al*, 2007). This favoured Sasol's growth and dominance in the inland region.

Sasol sold to the OOCs at import parity prices, where hypothetical transport costs were added to a free-on-board international price to arrive at a local South African price as though the refined product was imported. This pricing structure was initially known as the In Bond Landed Cost (IBLC) and later evolved into the 'basic fuel price' (BFP) and was the foundation for the wholesale list selling price for petroleum products (Corbett *et al.,* 2010). In certain instances, key policy issues were not legislated, rather, a system of 'gentlemen's agreements' was put in place by the oil companies to regulate the industry (Rustomjee *et al.,* 2007).

Support was given to compensate the crude oil refiners for having to mothball a substantial portion of their refining capacity. The arrangements meant

the crude oil refiners agreed to purchase all Sasol's output in exchange for a guaranteed margin[4] at the marketing level, which Sasol agreed not to enter. Competition between fuel producers was essentially removed in the interests of supporting the profitability of Sasol (Rustomjee, 2012).

Sasol was also supported by a dispensation[5] where synthetic fuel producers (which included Mossgas) received tariff protection when crude oil prices fell below a defined floor price and had to put additional revenue into an Equalisation Fund when crude oil prices rose above a ceiling price (Rustomjee *et al.,* 2007).

Extensive regulation of the liquid fuels industry continued despite the government's liberalisation policy as articulated in the Energy White Paper of 1998. When the Competition Act came into effect in 1999 it was intended to be part of an evolution to less regulation, and the oil companies applied for and were granted an exemption from the Competition Act for certain arrangements to ease the transition from a heavily protected environment to a more liberalised one. In 2002, Sasol applied for and was granted another exemption from the collusion provisions of the Competition Act for a number of market allocation agreements with the OOCs. The exemption was granted until 31 December 2003. At the end of 1998, Sasol gave the required 5 year notice to end the Main Supply Agreement in December 2003. In 1998 the Government also released Sasol from the obligation to repay any outstanding subsidies it had received during the 'Pim Goldby' era provided it continued to develop the petrochemicals sector (National Treasury, 2007). From the end of 2003 Sasol has been free to enter and expand into the marketing and retailing of fuel, and the OOCs have not been required to buy Sasol products.

According to the Competition Tribunal (2006), the MSA had amounted in effect to a cartel:

> In our view and, we note again, this view is essentially uncontroverted – the South African fuel market, from the refinery level through to the level of the retail service station, was cartelised for many years. The MSA was in effect the market sharing agreement entered into by the participants in the cartel with the price of refined product based on import parity or BFP which was then used to build up to the wholesale price and the retail pump price. (Para 122 p 46)

It appears as if the new government's change in the basis of calculating the wholesale price in the price build-up from the IBLC to the 'Basic Fuel Price' and intention to de-regulate the market stimulated Sasol's termination of the MSA as Sasol anticipated competitive pressure (Competition Tribunal, 2006, para 123). Sasol wanted to be able to enter and expand in the downstream retail markets (para 125). At the same time, it sought to entrench its dominant position inland and extend its retail presence nationally through the proposed merger of its fuel business with Engen in a merger to create a new entity to be termed uHambo.

The uHambo merger sought to secure a downstream retail and distribution footprint as well as to control refining capacity at one of the large crude oil refineries on the coast. The importance of these objectives can be appreciated by understanding the competitive threat to Sasol that was expressed in the bargaining games that occurred at the end of the MSA as the OOCs were no longer obliged to uplift all of Sasol's synfuels production (Corbett *et al.,* 2011; Competition Tribunal, 2006). At the time, the OOCs had excess capacity at the coast and were exporting products which they could have sold locally had they not been required to buy all of Sasol's production. After 2003, in purchasing inland volumes from Sasol, they therefore sought discounts off the inland BFP (set as the import parity price), as Sasol had a surplus of product, did not have its own distribution network, and also had very low production costs. Sasol on the other hand only wanted to offer product at the BFP to protect it as the benchmark price, and thus had to credibly threatened to reduce supply, either by reducing production (which it did at the Natref refinery) or by exporting product (Competition Tribunal, 2006).

The uHambo transaction would simultaneously provide Sasol with a route to market for its own product (through the Engen network, the largest in the country) without having to rely on the OOCs, and refinery capacity at the coast (the Engen refinery). The Tribunal prohibited the merger due largely to the effect of the former, judging that Sasol could credibly threaten to 'foreclose' (not supply) OOCs as customers for bulk supply of fuels, the impact of which was exacerbated by capacity constraints on the Durban-Johannesburg Pipeline which limited OOCs from bringing in the product from the coast, and as competitors in retail and commercial markets. The merger was contested by all the OOCs in Tribunal hearings involving detailed scrutiny of Sasol's operations and intentions. The Competition Commission at first supported the merger, and then altered its position (Competition Tribunal, 2006). The Competition Tribunal ultimately prohibited the merger and Sasol has had to expand in the downstream market through incrementally adding forecourts and obtaining commercial customers.

The other major threat to Sasol has been a possible change in the taxation and/or regulatory regime. This was most obviously in the form of the mooted windfall tax on excessive profits. National Treasury established a task team to evaluate the arguments which recommended such a tax should

be pursued. National Treasury rejected the recommendations of the Task Team on grounds which included the fact that Sasol had committed to 'significantly expand its synthetic fuel production capacity' in the interests of 'fuel security' and development of petrochemicals (National Treasury, 2007:4).[6] Having headed off the possible windfall tax, it appears that certain projects will not be pursued without very substantial participation and support from the state.

Sasol's continued hold over supply of fuels in the inland market in particular has been reinforced by their position as joint owner in the exploitation of Mozambican gas and in the pipeline delivering it to Secunda. The pricing of the gas has been subject to maximum regulation for the first ten years from 2004 to 2014, with the volume weighted price not to exceed an average price of selected European countries, while individual customers can be charged up to a maximum determined as the price of their alternative energy source (including the cost of physically switching to gas). This latter provision is effectively the monopoly price in any case as it is the maximum price that Sasol could offer in order to attract the individual buyer to switch to natural gas.

The legacy of the apartheid liquid fuels policies has resulted in the concentrated markets that are found throughout these value chains and has further placed Sasol in a particular position of influence in terms of fuel supply. The barriers to entry are substantial, as is witnessed by the slow rate of entry, particularly of historically disadvantaged South Africans (Mokoena and Lloyd, 2005). Over the last decade, the Competition Commission has uncovered cartels in related products, such as bitumen and piped gas; referred a case of coordinated conduct in diesel to the Competition Tribunal and has pursued a number of enforcement cases as explained below.

3. Regulation in the petroleum industry and competition enforcement

As of 2013, the prices of certain products, such as petrol at the retail/pump level, loose illuminating paraffin at the retail level and liquid petroleum gas at the refinery gate and retail level, are still regulated by the Department of Energy (DoE). These prices are posted on the department website and published monthly in the Government Gazette.

Diesel is referred to as a 'controlled' product. Government measures the return being made on the marketing of controlled products and sets the prices of regulated products (for example, of retail petrol) in order to yield a rate of return for the industry on marketing assets of between 10% and 20% (Rustomjee *et al.,* 2007*)*. Although not regulated by legislation, the wholesale list selling price (WLSP) of diesel is published on DoE's website. The industry has used this posted WLSP as the list price for wholesale diesel sales. Competition between the oil companies is therefore largely through discounts off this wholesale list price and through quality of service.

Certain information has been required from the oil companies for the calculations relating to the regulatory framework. However, the oil companies also exchanged such information between each other. The exchange of information between the oil companies began as early as the 1960s with a single company tasked to gather and disseminate information. The National Energy Council in 1989 requested that this data be submitted to government on a more disaggregated level for research purposes and to inform policy (Corbett *et al.,* 2010). There was, however, no requirement and no justification from a regulatory perspective to exchange this information, particularly company specific information, between the oil companies themselves.

In 1994, the South African Petroleum Industry Association (SAPIA) was created. SAPIA, an industry organisation to which all the oil companies still belong, was originally created for the oil industry to engage with the new African National Congress (ANC) government and other stakeholders. It also undertook the handling of information between oil companies, and between oil companies and government.

The history of regulation in the petroleum industry has created well understood, focal pricing points that could allow for coordinated behaviour to continue in markets which are no longer regulated and in which exemptions from competition law no longer apply (Corbett *et al.,* 2010). This transparency was further enhanced through the highly disaggregated information exchanged via the SAPIA platform. For unregulated products like commercial diesel, these published prices could act as focal points of which competition would occur only through discounting. If secret discounting is discouraged through the exchange of disaggregated information (such as detailed information on sales volumes) which increased the ability to monitor market shares, then competition is stifled, particularly in an oligopolistic industry such as the oil industry.

A player has no incentive to secretly discount to gain market share if it knows that this action is immediately visible to its competitors through the information exchange (Corbett *et al,* 2010). The Competition Commission referred a case against the main oil companies, alleging that such information exchange amounted to a contravention of the cartel provisions of the Act.[7]

Information exchange was also part of the conduct in the bitumen arrangements. The Commission referred to the Competition Tribunal a

cartel case against the oil companies on price fixing in the bitumen market, a petroleum product used to make tar to pave roads. This was in contravention of Section 4(1)(b)(i) of the Act. Sasol, the leniency applicant in this case admitted to continued coordination in the post-exemption period based on import parity pricing formulae established in the exemption period and suitable escalations.[8] Masana/BP, Shell and Engen all subsequently settled with the Commission and admitted that the arrangements contravened section 4(1)(b)(i) which addresses direct and indirect price fixing.

During the exemption period, the petrochemical companies jointly calculated the prices for bitumen with reference to an industry-wide retail price list, the Wholesale List Selling Price (WLSP). After the exemption lapsed in the latter part of 2000, there was no longer a standard method by which list prices for bitumen could be changed according to the changes in crude oil prices. The primary producers agreed to set the WLSP each month by setting a 'starting' price for February 2002 and escalating this by a factor determined through a formula, the Bitumen Price Index (BPI) which later became the Bitumen Price Adjustment Factor (BPAF). This was deemed an appropriate price escalation factor for long-term road construction contracts.

The development and implementation of the BPAF was done through another industry association, South African Bitumen Industry Association (SABITA). Information was exchanged through regular e-mail communications where BPAF percentages and/or Rand per ton escalation figures were circulated to the oil companies. The BPAF then would be added to the present month's WLSP to arrive at the following month's WLSP. It was therefore clearly forward-looking and gave an indication of what the market was likely to do in terms of magnitude of list price increases the next month and amounted to collusive conduct (Boshoff, 2013). In addition to such information exchange via emails, there were bilateral communications between oil companies. While the agreement did not fix the transaction prices of bitumen, it had the effect of dampening competition, undermining discounting below list prices and, as a result, underpinning higher prices.

The Competition Commission has also assessed coordinated conduct in the piped gas market. Pricing of piped gas is regulated by NERSA through provisions in the Gas Act 2001 (Act No. 48 of 2001) and Schedule One of the Agreement Concerning the Mozambican Gas Pipeline between the Government of the RSA and Sasol Limited. Possible contraventions of Section 4 of the Competition Act, particularly involving market allocation, were brought to the Commission's attention through a leniency application by Sasol Gas Ltd in 2009.[9]

Sasol is the main producer of natural gas sourced from Mozambique as well as methane rich gas produced in its Secunda plant. These gases are transported via pipeline to industry and household users. Sasol applied for leniency for participating in a series of agreements entered into with Spring Lights Gas in KwaZulu-Natal and Egoli Gas in Johannesburg, both competitors to Sasol Gas. These agreements contained non-compete clauses that amounted to market allocation by region (which therefore implied allocation of regional customers too), a contravention of Section 4(1)(b)(ii) of the Competition Act.

Spring Lights Gas further applied for an exemption from the Competition Act seeking to maintain the non-compete clauses in the agreement on grounds that it needed the exemption to survive and grow its business, particularly in light of the fact that its sole supplier is Sasol, with whom it also competes. The Commission found that the non-compete clauses were not necessary for Spring Lights to effectively compete with Sasol, given protection offered through the regulatory framework,[10] and rejected the exemption application.

In these circumstances, the Commission viewed the Competition Act as a secondary defence and that the regulatory framework was sufficient to ensure existing and new gas traders were protected from any potential abuses of dominance by Sasol.

There have thus been a number of cases of anti-competitive conduct which are closely related to past and current regulatory framework for liquid fuels. In addition, there have been competition cases in by-products of liquid fuels production and their derivatives in fertilizer and polymer chemicals (Makhaya and Roberts, 2013).

4. What are the appropriate roles of competition law and regulation?

Traditionally competition law is presented as being about addressing structural changes (mergers) and conduct in the absence of which there would be competition, while economic regulation controls market power in instances where competition is either not possible or is not desirable (de Streel, 2004; Lang, 2009). This fits neatly with the distinction drawn between the *ex-ante* nature of regulation and *ex-post* nature of competition law intervention in markets. However, it does not accord with the reality of how markets work and firms' strategies to create and protect rents from the exercise of market power.

Leaving aside mergers, cartel enforcement would appear to be the most straightforward area where, in the absence of cartel agreements, there would be competition. However, in tight oligopolies of 'insiders', who have well established norms for maintaining the status quo, collusive outcomes may exist without the need for explicit arrangements.

These arrangements may well have been developed under past regulatory arrangements or in an environment where coordination was tolerated or even encouraged, such as where the policy and regulatory framework had been 'captured' by the industry. This accords with the coordinated arrangements uncovered by the Competition Commission in several markets such as cement, bitumen and fertilizer. In each of these markets, after the ending of such formal arrangements for coordination as existed, firms established their own mechanisms. While the Commission has tackled such mechanisms, it may require entry to destabilise the collective understanding in place. Even in industries with apparently low barriers to entry, collusive outcomes can persist for some time (Khumalo *et al.,* 2014).

Entry barriers due to scale economies may be further reinforced by vertical integration on the part of incumbents implying that an entrant at one level needs to source inputs from firms associated with its rivals. As Geroski and Jacquemin (1984: 22) caution: 'when, however, small asymmetries can be solidified into dominant positions that persist, the inequities they create become institutionalized, creating long-term problems in the performance of the economic system which cry out for policy attention'.

In relatively small industrial economies, such as South Africa, there is also a greater prevalence of markets dominated by a single firm (Chabane *et al.,* 2006; Roberts, 2012). The large open markets of the USA and the EU are outliers when viewed against the conditions characterising most economies in the world.

Imperfect competition is thus commonplace, rather than an aberration resulting from readily identifiable anti-competitive arrangements. As such, it is important to understand the way in which competition works in practice and to guard against oversimplifying it, for example, by simplistically seeking to separate out natural monopoly elements for regulation, and assuming there will be 'free' competition elsewhere (Helm and Jenkinson, 1998: 2). Against the reality of competitive rivalry, choices about both competition law and regulation are about setting the 'rules of the game' or deciding on the 'economic constitution' of a country (Gerber, 2010). These are part of a set of rules and institutions which influence who has access to economic opportunities and on what terms, and whether the economy tends towards being inclusive or extractive (Acemoglu and Robinson, 2012).

We now consider these issues in terms of the objectives, analytical framework and tools of regulatory bodies and competition authorities, drawing on the cases discussed above.

The *objectives* of regulators may appear wider than those of competition authorities, in including the development of the economy, and more particular, in addressing the development of a selected sector. However, competition law can have a wide mandate as part of economic welfare. For example, the objectives of the South Korean Fair Trade Commission (KFTC) are to encourage free and fair competition, prevent the concentration of economic power and thereby promote 'balanced development' (Wise, 2000). This is given that the early stages of rapid industrialisation were viewed as 'unbalanced', requiring an active competition policy addressed at dominant firms in that country (Fox, 2002; Fox, 2003). The mandate of the KFTC therefore includes evaluating 'unreasonable' practices and 'unjustifiable' restrictions on competition (Fox, 2003; KFTC, 2011). The South African Competition Act has a range of objectives that reflect the importance of addressing the apartheid legacy of the concentration of control, although arguably these objectives only find expression in the provisions for merger evaluation which include a public interest test.

Relevant to the cases examined here, regulation of liquid fuels had originally been part of the apartheid state's objective to ensure local production, by Sasol in particular. Security of supply remains a natural government concern. However, this is not necessarily in conflict with competitive outcomes over time. Supply of refined product means ensuring logistics and transport capacity to get product to market, consistent with vigorous competition between suppliers to meet demand. Regulation and competition law seeking to ensure dynamic rivalry, increased access and competitive pricing could thus take quite a different stance to the past regulation which sought to guarantee margins of oil companies, as the 'insiders'. In addition, the unintended consequences of regulatory provisions that entrench market power in related products should be taken into account by regulatory bodies and competition authorities.

The *analytical framework* for regulators and competition authorities is substantially the same (Piergiovanni *et al*., 2009). It is essentially about evaluating firm conduct and outcomes in static and dynamic terms. This includes the effect of arrangements that undermine competition as well as the impact of arrangements on efficiency and investment. The main difference is that competition authorities make findings in specific instances, while regulators make determinations about the necessary arrangements to achieve efficient outcomes (or approximate effective competition) looking forwards. Even this is an over-generalisation. Competition authorities in some jurisdictions (including in South Africa) have market enquiry powers, that is, powers to investigate widely to address competition problems in a market and make far-reaching findings on necessary remedies. Conversely, regulators in some regimes, including in

South Africa, have to make findings of 'inadequate competition' in order to trigger regulatory powers.[11] Even where this is not explicit, the analysis of regulators of what is necessary going forwards will likely take into account what has happened in the past.

The more important distinction is the in-depth industry knowledge and the on-going monitoring that a specialist regulator embodies as compared with the generalist that is a competition authority. Seen in these terms, the relative scope of regulation and of competition enforcement is just a matter of choice for a given country. This also applies to particular responsibilities within a sector, such as where the regulator has powers to determine conditions of access and/or issue licences along with, for example maximum price caps, while the competition authority investigates anti-competitive conduct. In this world, the interplay of competition and regulation is not so-much about drawing lines as it is about understanding the complementarities in the work of the institutions. In several countries, such as the Netherlands and Australia, the common analytical base has led to important regulatory bodies being combined with the competition authority. The separate application of different laws, competition and regulatory, does not prevent the development of knowledge and expertise. In South Africa, the separate regulators and competition bodies have not established effective mechanisms to build on the complementarities while maintaining distinct roles. Instead, the impression is of the emphasis of their independence as an obstacle, rather than as a starting premise from which to build constructive engagement.

The third area is the *tools*, by which we mean the powers to change or set boundaries on behaviour. In competition law, remedies are available to competition authorities include those that are behavioural and structural, as well as sanctions in the form of administrative fines (de Streel, 2004). Administrative penalties perform a deterrence role, assuming that it is simply about deterring the conduct in the absence of which there will be adequate competition (and the efficient outcomes therefrom). Remedies seek to stop the anti-competitive conduct of the respondent and to restore competition (Marsden, 2008).

Structural remedies will, at least on the surface, require less monitoring than behavioural undertakings and tend to be preferred for competition authorities (OECD, 2004; de Streel 2004). At one extreme is divestiture, which seeks to create more competition through structural change. At the other is a behavioural remedy on pricing, such as to address a margin squeeze which results from the upstream and downstream prices of a vertically integrated firm. Pricing remedies are viewed as the tools more associated with regulators. However, there are many other types of conduct that are less easily categorised in terms of the structural/behavioural separation. For example, loyalty rebates are prices that seek to achieve *de facto* exclusivity and can be seen as substitutable with pricing offered for exclusive contracts.

In South African case law, administrative fines and remedies are primarily used as deterrent and corrective tools. There has however only been one instance where a structural remedy was adopted for an abuse of dominance under section 8 of the Act of 1998. This was in the complaint of abuse of dominance in the market for ammonia derivative products against Sasol Chemical Industries.[12] The remedy involved a combination of commitments regarding pricing (not to discriminate by location of customer) with divestiture of all but one downstream blending operation. The pricing remedy does not therefore stipulate maximum prices nor require ongoing monitoring on a month by month basis. In other cases such as *SAA* and *Patensie* the remedies have simply been the ending of the conduct being the form of rebates in *SAA* and the exclusivity in *Patensie* (Roberts, 2012).

The cases discussed above illustrate that the competition authorities have been pursuing alleged anti-competitive conduct, while the firms are subject to regulation in important areas of their business, which relate to their market power in associated products. The worlds of regulators and competition enforcers have not been talking to each other. One consequence is the long and drawn out competition investigations and prosecutions where, if proven, the remedies would be of a quasi-regulatory nature, even if implemented by the competition authorities. These cases could be strengthened by appropriate regulatory measures, if the competition concerns have merit. Rather than drawing what may be unhelpful distinctions between structural and behavioural measures, it is therefore more appropriate to recognise the skills and capabilities of regulators and competition authorities assessed against the nature of the problem. For example, whether the position of the dominant firm is linked to licencing arrangements, and/or there is regulation of some of the products, should be taken into account.

5. Regulating for competition?

The institutional make-up of regulators and competition authorities mean they have a natural tendency to certain types of arrangements which might blinker them to the benefits of competition and regulation when combined. Regulators by their nature engage with a small number of large firms on which they develop detailed information and with which they have extensive interactions. The relationships that develop will naturally lead to an appreciation of the firms' capabilities, the importance of the incumbents in ensuring security of supply, and a tenden-

cy to under-estimate the value of opening up to new rivals. However, there are likely to be substantial dynamic benefits from regulating for competition in terms of incentivising new ideas, service, quality and product offerings. While it will intrinsically be less stable in the short term, greater access and rivalry generates information for the regulator, and tests assumptions in the established system which can make it more robust in the longer-term.

On the side of the competition authorities, the tendency is to have very discrete interventions and to deter anticompetitive conduct (rather than to regulate it). However, in industries by their nature characterised by entrenched firms seeking to protect their positions, this simply means repeated extensive investigations and drawn-out legal processes. This could therefore mean as much detailed enquiry into a firm by the competition authority as is undertaken by the regulator. And, in terms of addressing the conduct, powers that can be portrayed as 'regulatory', whether in the hands of a regulator or the competition authorities, are necessary and appropriate to address the anti-competitive conduct in a way that is credible and ensures more competitive outcomes in practice. In addition, regulatory measures tailored to enable entrants and smaller rivals will ensure less need for such invasive remedies in the future. Regulatory measures can provide certainty in advance that can facilitate entry into markets, critical in markets where dominant firms have engaged in reputational strategies to discourage entry or have entrenched dominance (Lang, 2009: 30). The facilitation of entry and promotion of effective rivalry creates a landscape for competition to work more effectively.

Notes

1. See, for example, papers at the Annual Conference on Competition Law, Economics and Policy, available at www.compcom.co.za
2. This was contended by Telkom in the case brought by Value Added Network Service providers to the Competition Commission. After the Commission's referral on 24 February 2004 there were over five years of litigation over jurisdictional points brought by Telkom including over the proper application of regulation and competition, until the Supreme Court of Appeal decision on 27 November 2009.
3. This draws substantially on Rustomjee *et al*. (2007); Competition Tribunal (2006); Rustomjee (2012).
4. Until 1989, refining margins were guaranteed along with returns on marketing assets. From 1989 only the returns on marketing assets were regulated through setting retail prices to allow this return. Bulk supply prices (wholesale prices) for refined products were regulated at import parity.
5. Following an investigation by Pim Goldby consultants.
6. In particular, Sasol had undertaken to pursue the Mafutha project, of a large new coal to liquids plant in the Waterberg.
7. See Competition Commission media release, 'Commission refers a case of collusion against oil companies' 24 October 2012, www.compcom.co.za accessed 20 November 2012.
8. Competition Commission media release, 'The Commission refers its price fixing findings against major oil companies' 4 March 2010, www.compcom.co.za accessed 10 June 2012.
9. www.compcom.co.za/assets/Uploads/AttachedFiles/MyDocuments/March-09-Newsletter-31.pdf, accessed on 29 August 2012
10. For instance, through non-discrimination requirements, access on commercially reasonable terms to facilities as well as powers by the regulator to investigate complaints relating to issues of supply and excessive prices or tariffs, amongst others.
11. As under the Gas Act, section 21(1)(p), for NERSA to regulate maximum prices for piped gas.
12. The consent and settlement agreement was confirmed by the Tribunal on 20 July 2010. See www.comptrib.co.za

References

Acemoglu, D. and J. Robinson (2012), *Why Nations Fail.* New York: Crown Publishers.

Boshoff, W.H. (2013). 'Illegal Cartel Overcharges in Markets with A Legal Cartel History: The South African Bitumen Market', CCRED Working Paper 3/2013. www.uj.ac.za/ccred.

Buigues, P. (2006), 'Competition Policy versus Sector Specific Regulation in Network Industries – The EU experience'. Submitted to UNCTAD's Seventh Session of the Intergovernmental Group of Experts on Competition Law and Policy, Geneva, 30 October – 2 November 2006.

Chabane, N., Goldstein, A. and Roberts, S. (2006) 'The changing face and strategies of big business in South Africa: Ten years of political democracy', *Industrial & Corporate Change*, 15, 549–578.

Competition Tribunal (2006) Decision in Sasol – Engen Merger, case 101/LM/Dec04.

Corbett, C., das Nair, R. and Roberts, S. (2011) 'Bargaining power and market definition: a reflection on two mergers'. *Journal of Economic & Financial Sciences*, 4, 147-166.

Corbett, C., das Nair, R., Grimbeek, S. and Mncube, L. (2010) 'The importance of information exchange in dampening competition in industries historically characterised by regulation – issues from South Africa', presented at Cresse Conference, Crete, 2-4 July 2010.

De Streel, A. (2004), 'Remedies in the European Electronic Communications Sector', in Geradin, D. (ed) *Remedies in Network Industries: EC Competition Law vs Sector-specific regulation*, Antwerp: Intersentia

Dobreva, R. (2006). 'Value Chains, Market Power and

Competitiveness: Understanding the Performance of the Plastics Sector', in S. Roberts, (ed) *Sustainable manufacturing? The Case for South Africa & Ekurhuleni,* Cape Town: Juta.

Fox, E (2002) 'What is harm to competition? Exclusionary practices and anticompetitive effect.' *Antitrust Law Journal* 70: 372–411.

Fox, E. (2003) 'We protect competition, you protect competitors', *World Competition*, 26(2), 149–165.

Geradin, D. and O'Donoghue, R (2005) 'the Concurrent Application of Competition Law and Regulation: The Case of Margin Squeeze Abuses in the Telecommunications Sector'. GCLC Working Paper No. 04/05. Available at SSRN: http://ssrn.com/abstract=671804.

Gerber, D. (2010) *Global Competition: Law, Markets and Globalisation,* Oxford University Press.

Geroski, P. and A. Jacquemin (1984) 'Dominant firms and their alleged decline', *International Journal of Industrial Organisation*, 2(1), 1-27.

Ginsberg, D.H. (2009) 'Synthetic Competition', in Lévêque, F. and Shelanski, H. (eds) *Antitrust and Regulation in EU and US: Legal and economic perspectives.* Cheltenham: Edward Elgar Publishing Limited.

Helm, D. and T. Jenkinson (eds.) (1998) *Competition in Regulated Industries*. Oxford: OUP.

ICN (International Competition Network). (2004) Enforcement Experience in Regulated Sectors, Third Annual Conference, Seoul, 21-22 April, 2004.

Khumalo, J, J. Mashiane, and S. Roberts (2014) 'Harm and Overcharge in the South African Precast Concrete Products Cartel', *Journal of Competition Law and Economics*, 10(3), 621-646.

Korea Fair Trade Commission (KFTC) (2011) *Annual Report 2011 Special Edition 30 Years of KFTC, Looking Back, Moving Forwards*. KFTC, Seoul.

Lang, J.T. (2009) 'European Competition Policy and Regulation: Differences, Overlaps and Constraints'. in Lévêque, F. and Shelanski, H. (eds) *Antitrust and Regulation in EU and US: Legal and economic perspectives.* Cheltenham: Edward Elgar Publishing Limited.

Makhaya, G. and S. Roberts (2013). 'Expectations and outcomes – considering competition and corporate power in South Africa under democracy', *Review of African Political Economy* 138, 556-571.

Marsden, P. (2008). 'Article 82 and Structural Remedies after Microsoft' *presented at International Competition Forum. St. Gallen, 22-23 May 2008*

Mokoena, J.K.J. and P.J.D. Lloyd (2005) 'A business model to overcome barriers to entry in the South African downstream petroleum industry', *Journal of Energy in Southern Africa*, 16(2), 4-13.

Moodaliyar, K. and K. Weeks (2009) 'A framework for promoting competition in electronic communications: clarifying the role of the Competition Authority and the sector regulator' presented at the Third Annual Competition Conference, Johannesburg, 3-4 September 2009.

National Treasury (2007) 'Windfall Taxes in the Liquid Fuels Industry. Response to the task team report on windfall products in the liquid fuels industry.'

Newbery, D.M (1997) 'Determining the regulatory asset base for utility price regulation', *Utilities Policy*, 6(1), 1-8.

OECD (Organisation for economic Cooperation and Development). (2008). 'Remedies and Sanctions for Abuse of Market Dominance', Accessed June 2012, http://www.oecd.org/dataoecd/17/44/41814852.pdf.

Piergiovanni, M. (2009) 'Competition and Regulation in the energy Sector in Europe in the Post Sector Enquiry Era', *Competition Law International*, http://www.ibanet.org/Publications/publications_CLI_June_2009.aspx.

Roberts, S. (2010) 'Competition policy, competitive rivalry and a developmental state in South Africa', Chapter 11 in O. Edigheji ed. Constructing a Democratic Developmental State in South Africa: Potentials and Challenges, HSRC Press, Pretoria.

Roberts, S. (2012) 'Administrability and business certainty in abuse of dominance enforcement: an economist's review of the South African record', *World Competition*, 35(2), 269-296.

Rustomjee. Z., Crompton. R., Mehlomakulu. B. and Steyn. G. (Windfall Task Team) (2007) 'Possible reforms to the fiscal regime applicable to windfall profits in South Africa's liquid fuel energy sector, with particular reference to the synthetic fuel industry', report for National Treasury, 9 February 2007.

Rustomjee, Z. (2012) Witness Statement in Competition Commission v Sasol Chemical Industries. case number 48/CR/Aug10 (non-confidential).

Singh, A. (2002). 'Competition and competition policy in emerging markets: international and developmental dimensions.' UNCTAD G-24 Discussion Paper Series No.18. New York/Geneva: United Nations.

Viscusi, WK, J Vernon, and J. Harrington (2000) *Economics of Regulation and Antitrust*. Cambridge Mass: The MIT Press.

Wise, M. (2000) 'The Role of Competition Policy in Regulatory Reform – Review of Competition Law and Policy in Korea', *OECD Journal of Competition Law and Policy*. 3(2), 128-180.

Received 3 November 2013; revised 29 January 2015

Investigation of common-mode voltage and ground leakage current of grid-connected transformerless PV inverter topology

Atanda K Raji

Mohamed T E Kahn

Centre for Distributed Power Electronics Systems, Cape Peninsula University of Technology, South Africa

Abstract

The problems of increasing electricity demand by the unabated population and economy growth can be solved by employing sustainable distributed generation technologies. Convectional primary energy sources such as coal, liquid hydrocarbons' and natural gasses create environmental degradation and energy security problems. Even though the cost of solar energy is zero, the same cannot be said of a solar energy system. The system cost especially the initial capital investment has been hindering the rapid deployment of solar energy systems. One way of reducing the system cost of a solar energy system is to look into the constituent components and see where cost can be reduced without compromising the system efficiency and human safety. Eliminating the isolation transformer reduces the cost and increases the system overall efficiency. However, the galvanic connection between the PV array and the utility grid creates a safety problem for people and system equipment. We present a simplified model for the investigation of the common mode voltage and ground leakage current that can lead to electromagnetic interference. The leakage current level is used for the determination of the suitability of the investigated PV inverter topology for grid connection without isolation transformer.

Keywords: common-mode voltage, grid-connected transformerless PV inverter topology; ground leakage current

Introduction

The problems of increasing electricity demand by the unabated population growth can be solved by employing sustainable distributed generation technologies. Convectional primary energy sources such as coal, liquid hydrocarbons' and natural gasses create environmental degradation and energy security problems (Binal, 2000). Alternative energy sources such as wind, solar, wave, tidal, geothermal and ocean are renewable sources that are sustainable and environmentally friendly. Amongst these renewables, solar energy is in pole position to be adopted as distributed generation integrated into a low voltage system. The abundance and everywhere availability of solar energy provides easy site for system setup, reduced transmission losses and eliminate utility grid extension cost for very low load centres such as remote villages (Bull & Billman, 2000)

Even though the cost of solar energy is zero, the same cannot be said of a solar energy system. The system cost especially the initial capital investment has been hindering the rapid deployment of a solar energy system (Bouffard & Kirschen, 2008). Many governments around the world have provided incentives and subsidies to promote fast adoption of renewable energy systems. However, such policy is not sustainable in the longer terms and it is highly dynamic (Winkler, 2005).

One way of reducing the system cost of a solar energy system is to look into the constituent components and see where cost can be reduced without compromising the system and human safety (Arnam & Zhong, 1997). 25% of the solar system cost constitutes the inverter system cost out of which 15% is the cost of the transformer that is used to isolate the PV array from the AC grid system for

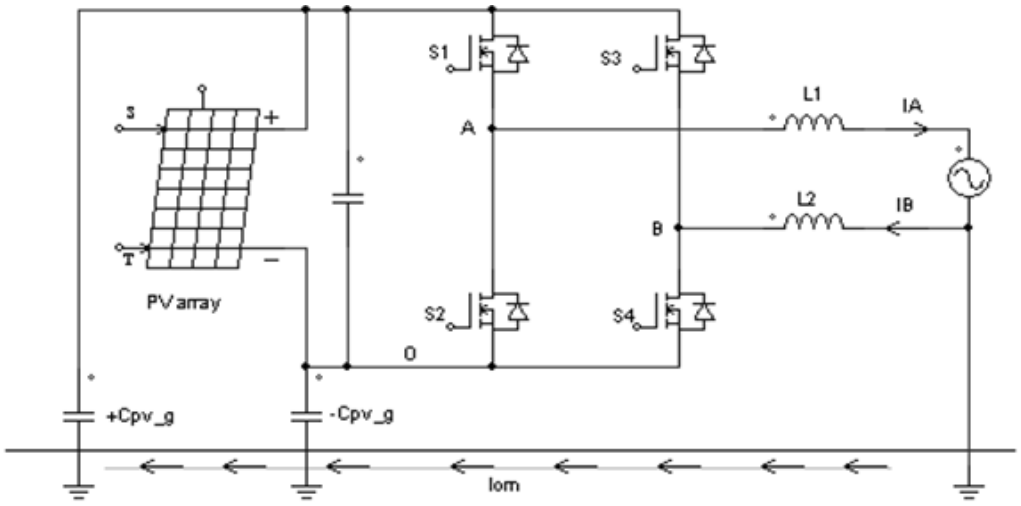

Figure 1: H bridge grid connected PV module

safety reasons. The percentage contribution of the inverter system cost may increase in longer terms as the cost of PV module continues to decrease. Eliminating the isolation transformer reduces the cost and increases the system overall efficiency. However, the galvanic connection between the PV array and the utility grid creates a safety problem for people and system equipment (IEEE Standard 1547, 2003).

The PV array parasitic capacitance between the PV array and the ground causes leakage current to flow (Barater et al., 2009) Many PV inverter topologies with different switching strategies have been proposed in the technical literature to mitigate the problem of common-mode voltage (CMV) and ground leakage current (Francke *et al*., 2010; Photong *et al.,* 2010).

The next section presents the analysis of a simplified model suitable for the investigation of common-mode voltage and ground leakage current for a convectional full bridge inverter topology with unipolar switching strategy. Section three models, simulates the presented model using PSIM software and presents the simulation results. Conclusion of the work is presented in the final section.

Simplified model for CMV and GLC

The full bridge inverter topology used in this work is presented in Fgure 1. Switches S1/S4 and S3/S2 switched with unipolar modulation strategy. An L output filter is used to ensure that the injected AC current complies with the harmonics requirements stated in the grid codes (Azri & Rahim, 2011).

In the full bridge circuit shown in Figure 1, voltages V_{AO} and V_{BO} are controlled by the four switches S1, S2, S3 and S4. The principle of superposition is used for the analysis. Each of the voltage sources is considered acting alone and the total effect of all is obtained from the algebraic sum of the individual current produced by each source acting alone.

PV parasitic capacitance value of 100nF is used for the investigation (Bassoon, 2018). The parasitic capacitance depends on such factors as weather, PV cell technology, distance between the PV cells and the frame etc. (Azri & Rahim, 2011; Arajo *et al.,* 2010; Lopez *et al,* 2007; Photong, 2010).

When the upper switch is on, the corresponding voltage is equal to V_{DC} while the lower switch corresponding voltage is zero (reference O). Therefore, we can replace the DC bus and switches with two PWM voltage sources as shown in Figure 2.

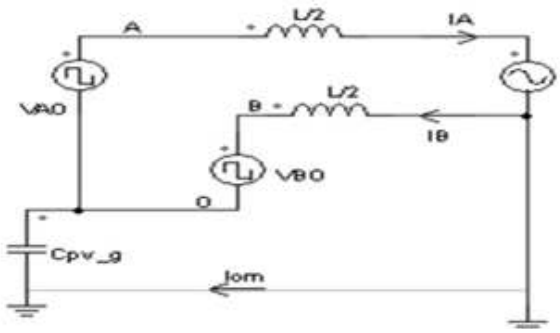

Figure 2: Equivalent common-mode currents

According to the superposition theorem, the total leakage current is the sum of the currents generated by the grid and the two PWM voltage sources. Figure 3 shows the leakage current generated by the grid. The leakage current generated by the two PWM voltage sources is shown in Figure 4.

As shown in Figure 3, the leakage current i_{cm1} generated by the grid can be given as:

$$i_{cm1} = \frac{-\frac{1}{2} j v_{grid}}{-\frac{1}{4}\omega_{grid} L + \frac{1}{\omega_{grid} C_{pv\_g}}} \quad (1)$$

As shown in Figure 4, the leakage i_{cm2} and i_{cm3} generated by the PWM voltage sources can be given as:

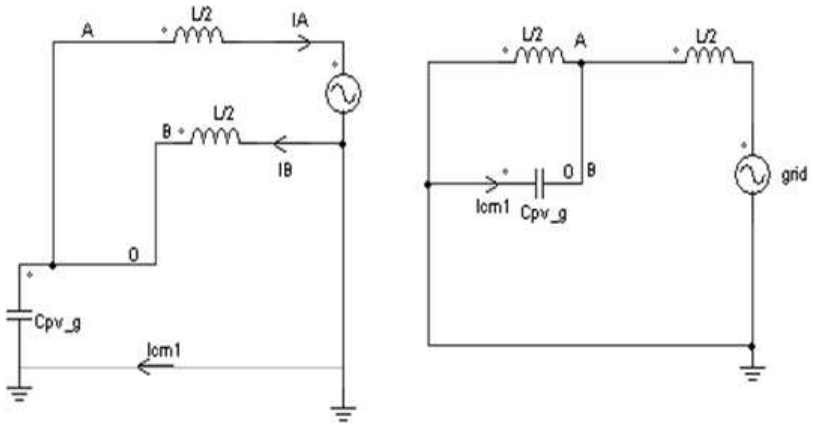

Figure 3: Generated grid leakage currents

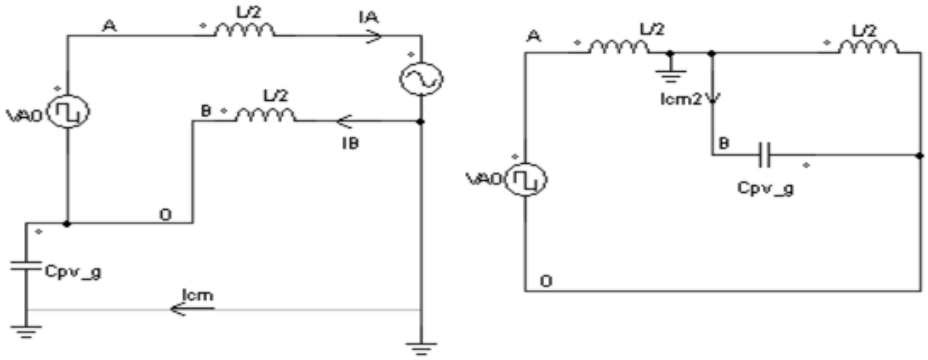

Figure 4: Generated PWM for each inverter leg

$$i_{cm2} = \frac{\frac{1}{2} j v_{AO}}{-\frac{1}{4}\omega L + \frac{1}{\omega C_{pv\_g}}} \quad (2)$$

$$i_{cm3} = \frac{\frac{1}{2} j v_{BO}}{-\frac{1}{4}\omega L + \frac{1}{\omega C_{pv\_g}}} \quad (3)$$

Compared to the switching frequency, the grid frequency is low, thus I_{cm1} can be ignored. In literature cases, the leakage current caused by the grid is not discussed, but it truly exists even when the common mode voltage is kept constant during all commutation states.

Combining equations 2 and 3, the total leakage current i_{cm} and common mode voltage v_{cm} are given in equations 4 and 5 respectively.

$$i_{cm} = \frac{j v_{cm}}{-\frac{1}{4}\omega_{cm} + \frac{1}{\omega_{cm} C_{pv\_g}}} \quad (4)$$

$$v_{cm} = \frac{1}{2}\left(v_{AO} + v_{BO}\right) \quad (5)$$

According to equation 5, the equivalent circuit model of common mode leakage current can be obtained as shown in Figure 5.

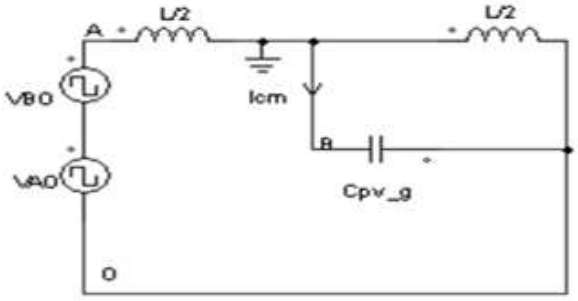

Figure 5: Combined inverter leg generated common-mode currents

As shown in Figure 5 it is concluded that if the common mode voltage is kept constant during all the commutation states, leakage current could be restricted to nearly zero (assuming that the leakage current contribute by the grid is negligible).

Simulations and results

The inverter ouput voltage is shown in Figure 6 changing from positive peak value to zero and then to negative peak values. The three voltage vector states enable the topology to be switched with half the switching frequency with the same component parameters as a full bridge with bipolar switching strategy. This provides the advantage of lower filter requirements and reduce the core lossess of the filter inductor.

The common mode voltage imposed on the PV array parasitic capacitance is shown in Figure 7.

The PV array terminal voltage across the PV array parasitic capacitance is shown in Figure 8 to contain harmonics of switching frequency.

The leakage current through the PV array parasitic capacitance is shown in Figure 9. It contains harmonics of the switching frequency. The peak value of the ground leakage current is 3,552 A and the average value is 1,164 A while the root mean square value is 1,345 A.

Figure 10 shows the FFT of the ground leakage

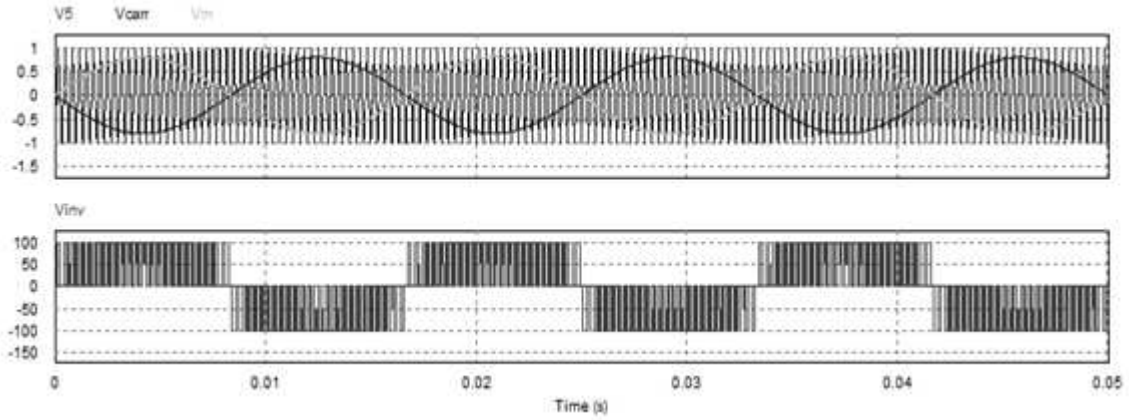

Figure 6: Unipolar inverter output voltage

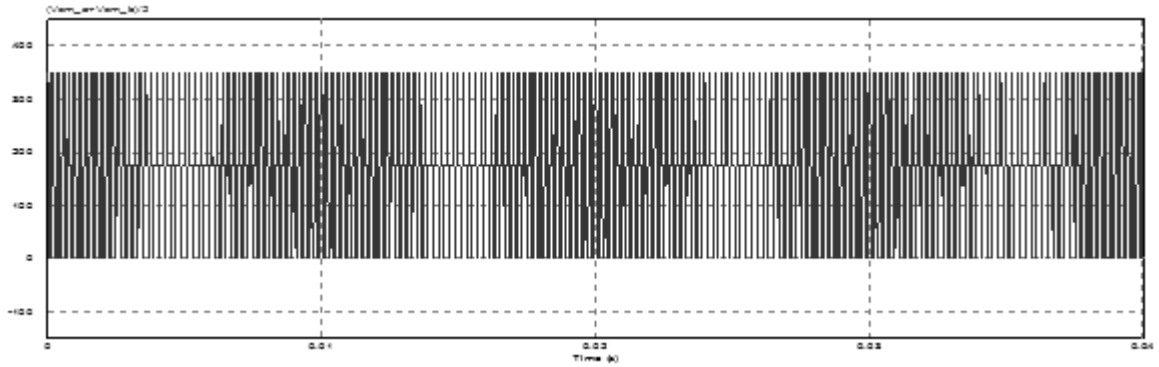

Figure 7: Common mode voltage

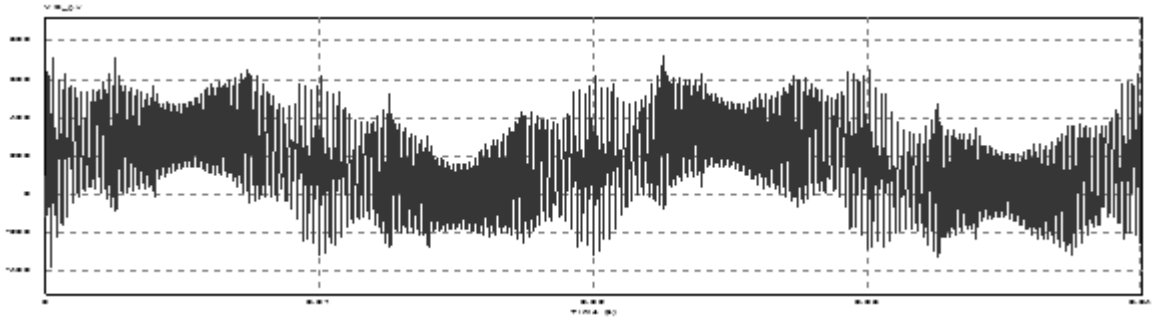

Figure 8: PV array terminal voltage

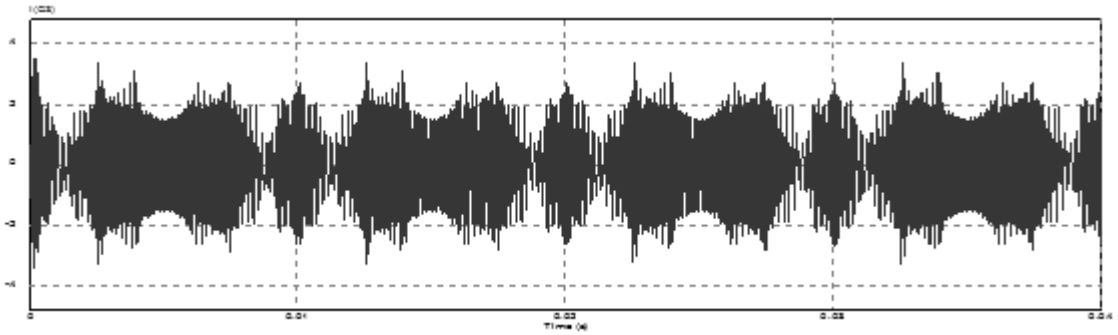

Figure 9: Ground leakage current

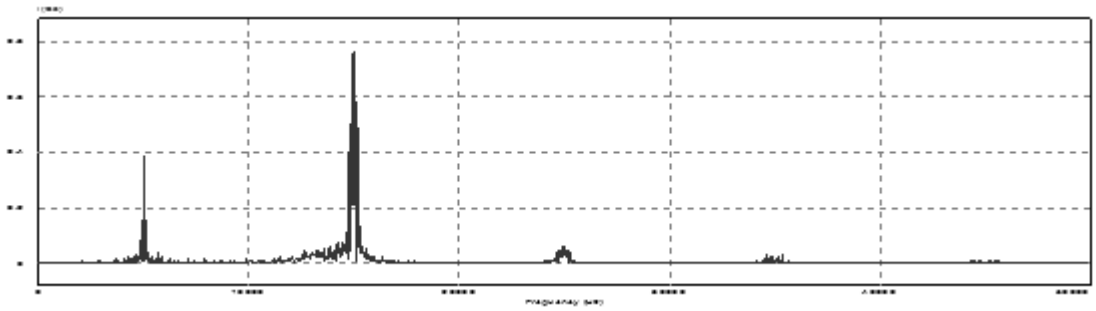

Figure 10: FFT of the ground leakage current of the simulated PV inverter topology

current of the simulated PV inverter topology.

Conclusion

A simplified model of a grid-connected transformerless PV inverter topology for the investigation of the common-mode voltage and ground leakage current is presented in this paper.

A convectional full bridge (FB) inverter topology with unipolar switching is used as an example to carry out the investigation.

Based on the simulation results, the FB with unipolar switching is not acceptable for PV transformerless configuration because it does not comply with the safety requirement of VDE 0126-1-1.However, similar investigation was carried out of same topology but with bipolar switching scheme and found to be compliant with respect to VDE 0126-1-1 safety requirements. This methodology can be extended to other transformerless topologies for grid-tied technical requirements compliance test. The benefit of reduced system cost and increased energy efficiency of grid connected transformerless PV topology will accelerate solar energy system deployment in developing countries such as South Africa.

References

Arajo S., V., Zacharias P., and Mallwitz R., (2010). Highly Efficient Single-Phase Transformerless Inverter for Grid-Connected Photovoltaic Systems, IEEE Transaction on Industrial Electronics, Vol. 57, no. 9, pp. 3118-3128.

Arman M. F and Zhong L., (1997). A new transformerless, photovoltaic array to utility grid interconnection, in Proceeding International Conference in Power Electronics and Drive Systems, May 26–29, 1997, vol. 1, pp. 139–143.

Azri M. and Rahim N. A., (2011). Design Analysis of Low-Pass Passive Filter in Single-Phase Grid-Connected Transformerless Inverter, IEEE First Conference on Clean Energy and Technology CET, pp. 348-353.

Barater D., Buticchi G, Crinto A. S., Franceschini and Lerenzani E (2009), A new proposal for ground leakage current reduction in Transformerless Grid-Connected Converters for Photovoltaic Plants. Industrial Electronics, IECON 09. 35th Annual Conference of IEEE pp.4531-4536.

Bassoon T. S., (2008). High-Penetration, Grid-Connected Photovoltaic Technology Codes and Standards, 33rd IEEE Photovoltaic Specialists Conference San Diego, California, pp. 1-4.

Bimal K. B. (2000) Energy, Environment, and Advances in Power Electronics, IEEE Transaction on Power Electronics, Vol. 15, No. 4, pp. 688-701.

Bouffard F. and Kirschen D. S., (2008). Centralized and Distributed electricity systems, Energy Policy, Vol. 36, pp. 4504-458.

Bull S R and Billman L. L, (2000).Renewable Energy: Ready to meet Its Promise?, The Center for Strategic and International Studies and International Studies and the Massachusetts Institute of Technology, The Washington Quarterly, 23:1, pp. 229-244.

Dicorato M. and Travato G. F., (2008),. Environmental-concerned energy planning using energy-efficiency and distributed-generation facilities, Renewable Energy, Vol. 33, pp. 1297-1313

Franke W.-Toke, Oestreich N. and Fuchs F. W., (2010), Comparison of Transformerless Converter Topologies for Photovoltaic Applications concerning Efficiency and Mechanical Volume, pp. 724-729

IEEE Standard 1547, (2003). IEEE Standard for Interconnecting Distributed Energy Resources with Electric Power System, 28 July, pp.1-16.

Kerekes T, R Teodorescu and U Borup, (2007). Transformerless Photovoltaic Inverters Connected to the Grid, Applied Power Electronics Conference, APEC 2007 - Twenty Second Annual IEEE, pp.1733-1737

Lopez O., Teodorescu R., Freijedo F. and DovalGandoy J., (2007). Leakage current evaluation of a single phase transformerless PV inverter connected to the grid, Applied Power Electronics Conference, APEC 2007 - Twenty Second Annual IEEE , pp. 907-912.

Photong C., Klumpner C and Wheeler P., (2010). Evaluation of Single-Stage Power Converter Topologies for Grid-Connected Photovoltaic, Industrial Technology (ICIT), IEEE International Conference on, pp.1161-1168.

Winkler, H. (2005), Renewable energy policy in South Africa: policy options for electricity, Energy Policy, Vol. 33, pp. 27-38.

Received 5 August 2012; revised 14 February 2015

New markets for renewable industries: Developing countries – Turkey, its potential and policies

Durmus Kaya
Department of Energy Systems Engineering, Faculty of Technology, Kocaeli University, Umuttepe, Kocaeli, Turkey

Fatma Canka Kilic
Department of Electric and Energy Technologies, Air Conditioning and Refrigeration Technology, Kocaeli Vocational School, Kocaeli University, Kullar, Basiskele, Kocaeli, Turkey

Abstract
For today's world, energy is a huge requirement for economic, industrial and social life. The necessity of energy is increasing quite rapidly to keep pace with the technological and economical advancements and this brings about many energy problems like, dependence on energy importation, environmental pollution, global warming, increasing cost of energy expenses and inefficiency in energy use etc. Countries are working very hard to solve these problems. To supply the energy needs and protect our planet's future safety, it is very important to generate clean energies. In this context, governments give huge amounts of incentives for renewable energy generations and support related investments in many countries. In this study, the importance of renewable energy usage, recent incentives, renewable energy policies in Turkey and some developed countries are investigated and compared. It is also aimed to examine the real situation of renewables in Turkey by giving the latest numbers and make a contribution of future developments for these clean energies in Turkey. In this regard, some barriers and recommendations are also submitted.

Keywords: renewable energy, renewable energy resources, renewable energy policies, renewable energy incentives, Turkey

1. Introduction

Turkey is the 17th largest economy of the World (International Energy Agency, 2010). Considering total primary energy consumption in the world, Turkey was ranked 22nd according to a report published by the Ministry of Energy and Natural Resources of Turkey in 2012. As for Turkey's place in the energy sectors on a global scale, the country was ranked 20th in the world's electricity production list (Republic of Turkey, Ministry of Energy and Natural Resources, 2012).Turkey's economy has been developing strongly for the last twelve years. This fast industrialization, increasing energy demand and the needs of urbanization require more energy production. The demand for electrical energy in Turkey is expected to be 580 billion kWh by the year 2020 (Bilgen *et al*.,2008). Also, Turkey's primary energy demand reached the value of 119.5 million tons of oil equivalent (Mtoe) in 2012, the share of natural gas was 32 percent, coal was 31 percent, oil was 26 percent, hydropower was 4 percent, and other renewable energy sources were 7 percent in this total. When examining Turkey's primary energy demand by sectors, the usage distribution were 27 percent in the industrial sectors, 26 percent in residential and service sectors, 14 percent in transportation sectors and 24 percent in the conversion sectors (Republic of Turkey, Ministry of Energy and Natural Resources, 2013). Along with Turkey's economic development, its crude oil and natural gas consumption has increased over recent years, but Turkey has very limited domestic reserves; therefore, the country imports almost all of its oil and natural gas supplies, which costs are high for its economy. Despite all these, Turkey plays an increasingly crucial role in the transit of oil because the country is strategically located at the crossroads between Former Soviet Union countries, the Middle East, and the Europe. Also, Turkey has a strategic

role for distribution of natural gas between the world's second largest natural gas market, Europe, and the large gas reserves of the Caspian Basin and the Middle East.

In Turkey new investments and studies have been initiated to meet growing energy demand and needs. For this purpose, different types of renewable energies are seen as effective solutions for Turkey's energy problems and its sustainable development. Turkey has many renewable energy sources for extensive energy production and use. The country's main renewable energy resources are hydroelectric, solar, wind, biomass, and geothermal energy (Kilic, 2011). While hydro power accounts for most of the total renewable energy supply in Turkey; biomass increasingly has a good share in the last few years. As for solar, geothermal and wind energy, they are expected to increase for the near future (International Energy Agency, 2010).

To reduce the amount of the cost of energy, it is necessary to generate renewable energy which is inexpensive, permanent, reliable, clean and sustainable and it is also the solution for the World's future of energy use. Therefore, Turkey has improving energy policies, strategies, and programs to take the right steps for the country's clean energy development. To realize the economic goals and energy targets, Turkey needs important investments in renewable energies, particularly in the electricity generation. This requirement is not only for its people's welfare, but also for the continuation of its rapid economic growth. To attract new investments for energy production from renewable energies are being supported by the government. At the end of 2010, the Turkish Government has enacted a new law that designs the new incentives for renewable energy productions (The Republic of Turkey, Turkish Official Journal, No: 6094, 2010), thereby; Turkey plans to increase energy production from alternative energy sources.

In this study, the evaluation of renewable energy and the importance of renewable energy use, the new incentives for renewable energy production, the renewable energy policies in Turkey and some developed countries are investigated and compared. In this regard, some barriers and recommendations are submitted for better understanding about the importance of the topic.

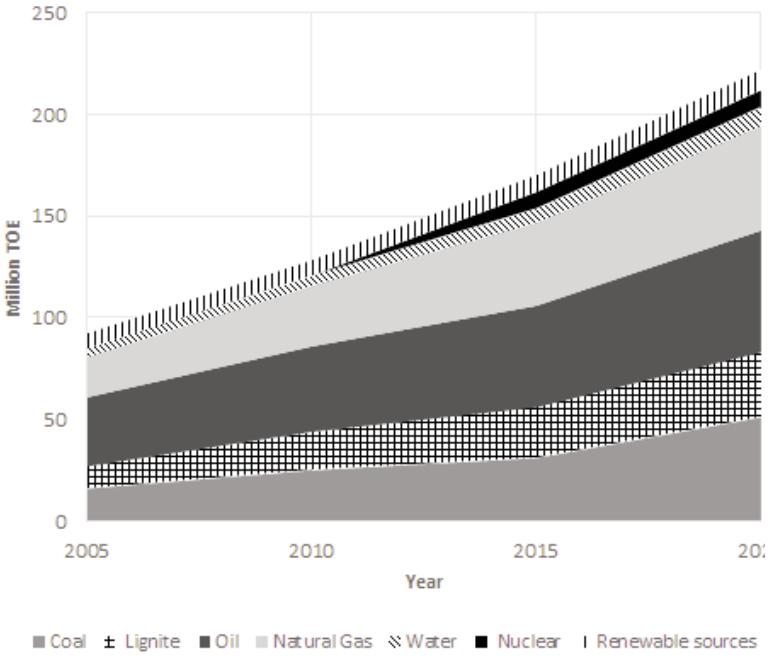

Figure 1: Turkey's Primary Energy Demand Projections by 2023
(Republic of Turkey, Ministry of Energy and Natural Resources, 2013)

2. Current and future energy status of Turkey

In Turkey, electricity is mostly produced in thermal power plants (TPPs) by using coal, lignite, natural gas and fuel oil. The production of electricity from renewables is small. As for nuclear power, it is new and very limited. On the other hand, Russia and Turkey signed a $20 billion agreement in May 2010 for the construction of a four-reactor Nuclear power plant near the coastal city of Mersin (in Akkuyu). Although there is opposition from environmental organizations to nuclear energy, Turkey wants to launch the nuclear power industry to diversify its energy mix and supply its soaring demand (www.rferl.org). The Turkish Government encourages domestic and foreign private sectors to carry out the country's power generation projects on a built operate transfer basis (Demirbas and Bakıs, 2004).

The distribution of electrical energy generation by primary energy sources in Turkey (in %, October 2013) is given in Table 1.

Table 1: Distribution of electrical energy generation by primary energy sources in Turkey (in %, October 2013)
(Republic of Turkey, Ministry of Energy and Natural Resources, 2013)

Geothermal	0.5%
Natural gas	41.3%
Hydraulic	29.2%
Wind	2.8%
Renewable and waste	0.4%
Coal	24.2%
Oil	1.6%

Primary energy demand in Turkey is expected to reach the value of 218 million tons of oil equivalent (Mtoe) with the increase of 90 percent by the year 2023. Also, the predictions for the share of coal will be 37 percent, the share of natural gas will be 23 percent, the share of oil will be 26 percent, the share of hydropower will be 4 percent, the share of

nuclear energy will be 4 percent, and the share of renewable and other energy sources will be 6 percent in primary energy demand by 2023. Turkey's primary energy demand projections by 2023 can be examined in Figure 1 (Republic of Turkey, Ministry of Energy and Natural Resources, 2013).

As it can be seen in Tables 2a and 2b, the total energy productions in Turkey is expected to be 58.20 Mtoe and 71.68 Mtoe by the years 2020 and 2030, respectively. On the other hand, total energy consumption is expected to be 279.18 Mtoe and 463.24 Mtoe by the years 2020 and 2030, respectively. Turkey has large coal reserves and hopes to multiply their use over the next decade to generate electricity.

Table 3 (Kilic, 2011) shows renewable energy potential in Turkey; including energy type, usage purpose, natural capacity, technical and economical values.

One of the main energy goals of Turkey is to increase the share of renewable energy sources in the country's energy supply. Due to its geographical location and geological structure, Turkey is rich in renewable energy resources. Effective use of these resources will contribute to not only security of energy supply but also help the formation of new employment areas. While Turkey's installed capacity was 12,305 MW in renewable energy sources in 2002; this value has reached the number of 24,947 MW at the end of October in 2013. The electricity generation from renewable sources was 34 billion kWh in 2002, with an increase of 92 percent this number reached to 65.3 billion kWh in 2012.

The installed capacity of new commissioning power plants based on renewable energy sources in the first ten months of 2013 has been around 2,757 MW. The power plants that sharing this value can be listed as follows:

- 428.3 MW of wind,
- 2,114 MW of hydro power,
- 148.6 MW of geothermal,
- 65.5 MW of landfill gas, biomass and waste heat sourced electricity generation power plants.

Considering the power plants that were commissioned and put into service in the years of 2012 and 2013, have the power of 9085 MW, 64 percent of this value is coming from renewable, 36 percent is coming from thermal sources. These numbers demonstrate that renewable energy studies and applications for Turkey are improving and bringing

Table 2a: Present and future (estimated) total energy production in Turkey (Mtoe)
(Koyun, 2007)

Energy sources	*1990*	*2000*	*2005*	*2010*	*2020*	*2030*
Coal and Lignite	12.41	13.29	20.69	26.15	32.36	35.13
Oil	3.61	2.73	1.66	1.13	0.49	0.17
N. gas	0.18	0.53	0.16	0.17	0.14	0.10
Com. renewables and wastes*	7.21	6.56	5.33	4.42	3.93	3.75
Nuclear	-	-	-	-	7.30	14.60
Hydropower	1.99	2.66	4.16	5.34	10.00	10.00
Geothermal	0.43	0.68	0.70	0.98	1.71	3.64
Solar/wind/other	0.03	0.27	0.22	1.05	2.27	4.28
Total energy production	25.86	26.71	34.12	39.22	58.20	71.68

* *Comprises solid biomass, biogas, industrial waste and municipal waste.*

Table 2b: Present and future (estimated) total energy consumption in Turkey (Mtoe)
(Koyum, 2007)

Energy sources	1990	2000	2005	2010	2020	2030
Coal and lignite	16.94	23.32	35.46	39.70	107.57	198.34
Oil	23.61	31.08	40.01	51.17	71.89	102.38
N. gas	2.86	12.63	42.21	49.58	74.51	126.25
Com. renewables and wastes*	7.21	6.56	5.33	4.42	3.93	3.75
Nuclear	-	-	-	-	7.30	14.60
Hydropower	1.99	2.66	4.16	5.34	10.00	10.00
Geothermal	0.43	0.68	1.89	0.97	1.71	3.64
Solar/wind/other	0.03	0.27	0.22	1.05	2.27	4.28
Total energy consumption	53.01	77.49	129.63	152.22	279.18	463.24

* *Comprises solid biomass, biogas, industrial waste and municipal waste.*

Table 3: Renewable energy potential in Turkey (annual)

Energy type	*Usage purpose*	*Natural capacity*	*Technical*	*Economical*
Solar energy	Electric (billion kWh)	977.000	6.105	305
	Thermal (Mtoe)	80.000	500	25
Hydropower	Electric (billion kWh)	430	215	124.5
Wind direct energy	Electric (billion kWh)	400	110	50
– land	Electric (billion kWh)	–	1801	–
Direct energy – off shore	(billion kWh)	150	18	–
Wave energy				
Geothermal energy	Electric (10^9 kWh)	–	–	1.4
	Thermal (Mtoe)	31.500	7.500	2.843
Biomass energy	Total (Mtoe)	120	50	32

to successful conclusions for the country's economy (Republic of Turkey, Ministry of Energy and Natural Resources, 2013).

Turkey gives great importance to the security of energy supply. To meet the increasing demand for energy, the country executes crucial projects and studies within the framework of policies for the security of energy supply. In this context, the studies for reducing the risks that result from the security of energy supply can be listed as follows:

1. To ensure diversification of sources by giving priority to domestic and renewable energy sources,
2. To enhance the investment and trade environment for businesses,
3. To diversify of energy sources, transport routes and energy technologies in order to ensure the sustainability of the energy sector,
4. To evaluate Turkey's underground and aboveground resources properly to gain and provide higher values to the country's national economy,
5. To increase the energy efficiency in the whole chain of energy supply and demand in the country,
6. To contribute to the security of electricity supply and provide interconnection to the neighbouring countries to assure the uninterrupted, qualified and adequate energy supply.
7. To integrate the nuclear energy to the whole system,
8. To reduce Turkey's dependence on foreign energy supply and decrease the energy costs in the country's economy and the current deficit (Republic of Turkey, Ministry of Energy and Natural Resources, 2013).

Turkey's renewable energy potential can be seen as a great opportunity from an economic, environmental and national security perspective (Kilic, 2011). Turkey's dependency on foreign energy resources for heating and electricity is planning to be lessened because of its high costs for the country. Developing and using domestic alternative energy resources will support security of energy.

Renewable energy sources in Turkey are the second largest source after coal in terms of energy production, and an important portion of the renewable energy production is met by biomass (Kilic, 2011). The annual biomass potential of Turkey is around 32 Mtoe. The current and projected biomass energy production in Turkey is presented in Table 4. Almost all of biomass energy is consumed in residences mostly for cooking and heating purposes. Wood is the main heating fuel for 6.5 million residences in Turkey. The Paper industry also uses wood wastes to provide 60% of needed energy for their production plants (Baris and Kucukali, 2012).

Table 4: Present and estimated biomass energy production of Turkey
(Baris and Kucukali, 2012)

Year	*Total biomass production (ktoe)*
2000	6982
2005	7260
2010	7414
2015	7320
2020	7520
2025	7810
2030	8205

The biomass sources of Turkey and corresponding potentials can be seen in Table 5.

Table 5: Biomass sources and their potentials
(WEC, 2007)[*]

Resource	*Raw material potential (million tons)*
Municipal solid wastes	25
Wood	3.52
Forestry/wood processing	3.56
Agricultural residues-straw+stalk	13.2
Agricultural residues-seed, shells, wood chips	4
Fertilizers	13.8

In Turkey, biomass has important potential to provide rural energy services based on forest and agricultural residues. Biomass has a significant place for Turkey because its share of total energy consumption is very high. Table 6 shows Turkey's annual biomass energy potential (Gokcol, 2009).

Table 6: Turkey's annual biomass energy potential
(Gokcol, 2009)

Type of biomass	*Energy potential (Mtoe)*	*Annual potential (Mt)*
Annual crops	14.9	55
Perennial crops	4.1	16
Animal wastes	1.5	7
Forest residues	5.4	18
Residues from agro industry	3.0	10
Residues from food industry	1.8	6
Other	1.3	5
Total	32.0	117

According to data received from the Energy Market Regulatory Authority (EMRA) in Turkey, operating capacity of power plants that generate electricity from biomass is around 138.7 MW in businesses. The capacity of power plants that are under construction for biomass energy generation is 13.4 MWe. Power plants capacity for biomass energy generation is 45.8 MWe, which in the form of projects. Turkey's energy generation plants from biomass can be grouped as follows:

- Energy production from waste gas,
- Power generation from organic waste through anaerobic fermentation,
- Energy production from biomass in the combustion plants,
- Energy production from organic wastes by using the method of gasification.

As for geothermal energy in Turkey, the country is one of the leading countries in terms of potential for geothermal energy applications. It has seen some important improvements in the geothermal sector in the last few years. The geothermal potential of Turkey is estimated as 31500 MW. This potential is around 77.9% and mainly takes place in Western Anatolia. With today's numbers, 13% of geothermal energy potential which is 4000 MW has been made available by General Directorate of Mineral Research and Exploration (MTA) under the management of Ministry of Energy and Natural Resources. In Turkey 55% of the total geothermal areas are suitable for heating applications (Kilic and and Kilic, 2013).

Since 2005, the rate of geothermal site exploration has been increased by the General Directorate of Mineral Research and Exploration (MTA). The number of discovered geothermal fields increased from 170 in 2005 to 187 in 2008 (Baris and Kucukali, 2012). As it can be seen in Table 7, geothermal usage in Turkey has reached the amount of 114.2 MWe at the end of 2012 (Kilic, 2013).

Table 7: Geothermal use in Turkey in 2012
(Kilic and Kilic, 2013)

Usage	*Capacity 2012 (MW)*
Electricity generation	114.2 MWe
Residence heating	805 MWt
Thermal tourism	402 MWt
Greenhouse heating	507 MWt

In addition to geothermal resources, there are 1 000 hot water and mineral water sources and wells available in Turkey. 170 of these wells have the temperature above 40 °C. 13 of these sources are considered the most valuable ones by the sector for the generation of electrical energy. The potentials of geothermal electricity generation and source temperatures of these regions are given in Table 8.

Table 8: Potentials of Turkey in electric energy generation form geothermal sources
(Kilic F and Kilic, 2013)

Geothermal region	*Temp. (°C)*	*Potential of electric energy generation (MW)*
Denizli Kızıldere	200-242	80
Aydın-Germencik	200-232	130
Manisa-Alaşehir-Kavaklıdere	213	15
Manisa-Salihli-Göbekli	182	15
Çanakkale-Tuzla	174	80
Aydın-Salavatlı	171	65
Kütahya-Simav	162	35
İzmir-Seferihisar	153	35
Manisa-Salihli-Caferbey	150	20
Aydın-Sultanhisar	145	20
Aydın-Yılmazköy	142	20
İzmir-Balçova	136	5
İzmir-Dikili	130	30
Total		**550**

The installed capacity of new commissioning power plants based on renewable energy sources in the first ten months of the year (2013) has been around 2 757 MW. The geothermal power plants sharing this total value can be defined as 148.6 MW of geothermal sourced electricity generation power plants (Republic of Turkey, Ministry of Energy and Natural Resources, 2013).

Currently, there are 13 geothermal power plants that are available based on geothermal energy

sources in Turkey. While geothermal installed capacity was only 17.5 MW in 2002, it has reached the value of 310 MW as at the current numbers.

On the other hand, in 2012 the applications of geothermal greenhouse heating have reached the value of 2 832 thousand square meters with an increase of 466 percent compared to 2002 and also the residential heating has reached a number of about 89 443 dwellings with an increase of 198 percent.

The private sector began to take part in geothermal studies in Turkey with the Law Number 5686: The Geothermal Resources and Natural Mineral Water Act came into force in 2007. Between the years 2008-2013, the geothermal 90 fields in total have been transferred to investors, 16 pieces of these fields are for electricity generation and 74 of them for heating and thermal tourism oriented. Thus, the total tender price of these geothermal fields is $547 million, brought to the country's economy (Republic of Turkey, Ministry of Energy and Natural Resources, 2013).

It can be seen in Table 9, the largest share of the country's total energy consumption comes from natural gas (31.8%), followed by oil (29.9%) and coal (27.3%). Renewable energy sources (with the exception of hydro) are currently small fractions of Turkey's energy supply (Erdem, 2010).

Turkey has progressed well in all areas of energy policy since 2005 and there are obvious signs of a better future balance in energy policy goals (IEA, 2010). The Energy sustainability country index leaders by economic groupings can be seen in Table 10 (World Energy Council Report, 2010).

3. Renewable incentives in Turkey

There are some incentives and regulations related to renewable energy sources in Turkey. In our previous studies (Kilic, 2011; Kilic, and Kaya, 2007; Kilic, 2011; Kaya, 2006; Kaya *et al.,* 2008) these regulations have been investigated in depth. Law No. 5346 on the Use of Renewable Energy Sources for the Purpose of Electrical Power Generation dated 10 May 2005 ('Renewable Energy Law') has been amended by Law No. 6094 (Hence forward 'Amendments'). The Amendments were published in the Official Gazette for Promulgation of Law: 8 January 2011. In this study, the incentives according to Law No: 6094 have been examined in detail in the following sub topic.

3.1. Incentives for renewable energy in Turkey

At the end of 2010, the Turkish Grand National Assembly (TBMM) passed a new renewable energy bill determining regulations and feed-in tariffs in the renewable energy sector (Kilic, 2011). The New Law raises the guaranteed prices for the sale of electrical energy by renewable energy sources ('RES') certificate holders. According to law, producers of renewable energy who started operation between May 18, 2005 and December 31, 2015, are being guarantied for power purchase (purchasing of electricity that being produced is guaranteed) for a period of ten years. Such guaranteed prices for the incentives (Feed-in Tariffs) are determined in 'Dollar cents'. According to this new law, the renewable energy production incentives can be seen in Table 11 (Turkish Official Journal, 2010).

The Council of Ministers is also authorized to determine new purchase prices, which should not exceed the current prices, for facilities established after December 31, 2015. Renewable energy producers that got their operation license before December 31, 2015 are entitled to receive an additional subsidy ranging from USD 0.004 to USD

Table 9: Comparison of energy consumption amounts between the rorld and Turkey (%)
(*Erdem, 2010)*

	Oil	*Natural gas*	*Coal*	*Nuclear*	*Renewables (including hydropower)*
World (2007)	34.0	20.9	26.5	5.9	12.7
Turkey (2008)	29.9	31.8	27.3	-	11.0

Table 10: Energy Sustainability: Country Index Leaders (by economic groupings)
***S**ource: Multiple (IEA, EIA, World Bank, IMF, WEF etc. 2007)*

GDP/capita (USD)	*> 33,500*	*14,300 – 33,500*	*6,000 – 14,300*	*< 6,000*
Positioning				
1	Switzerland	Spain	Colombia*	Indonesia*
2	Sweden	Portugal	Argentina	Egypt
3	France	Slovenia	Brazil	Cameroon
4	Norway*	Italy	Mexico*	Philippines
5	Germany	New Zealand	Turkey	Swaziland

* *Net energy exporters (others are net energy importers).*

Table 11: Renewable energy (Law No: 6094) subsidies
(Turkish Official Journal, 2010)

The plant type of the generation of energy from renewable resources	*The prices that will be applied (USD cent/kWh)*
A hydroelectric power plant	7.3
A wind power plant (A wind farm)	7.3
A geothermal energy plant	10.5
A biomass supplier (including landfill gas)	13.3
A solar energy plant	13.3

0.035 per kWh for a period of five years if they use locally-produced equipment and technology for their plants, which can be seen in Table 12. License procedures will be handled by the Energy Market Regulatory Authority (EPDK) in cooperation with the Energy Ministry, Interior Ministry and the State Waterworks Authority (DSI).

4. Renewable energy subsidies in EU

Governments' energy policies play important roles to augment investments in renewable energies (International Energy Agency, 2008). Increasing incentives, notably feed-in tariffs, direct subsidies, and tax credits can make the risk/revenue of renewable energy investments more attractive. The pro-

Table 12: Additional support amounts for companies with facilitates that use locally produced equipment and components
(Turkish Official Journal, 2010)

Plant type	*Locally produced equipment and components*	*Domestic contribution supplement (USD cent/kWh)*
A: Hydroelectric power plant	1. Turbine	1.3
	2. Generator and power electronics	1.0
B: A wind power plant (A wind farm)	1. Propeller	0.8
	2. Generator and power electronics	1.0
	3. Turbine Tower	0.6
	4. Rotor and all mechanical components in the nasel group (the exception of payments made for propeller group with generators and power electronics.)	1.3
C: Facilities of photovoltaic solar panels	1. Integration of PV panels and manufacture of the structural mechanics of the solar PV panels	0.8
	2. PV modules	1.3
	3. Cells that make up PV modules	3.5
	4. Inverter	0.6
	5. Beam materials that focusing solar energy on the solar PV module	0.5
D: Plants based on concentrated solar power	1. Radiation pick-up tube	2.4
	2. Reflective surface plate	0.6
	3. Solar Tracking System	0.6
	4. The mechanical parts of the thermal energy storage system	1.3
	5. Mechanical parts of the steam production system by collecting the solar beam on the tower	2.4
	6. Sterling engine	1.3
	7. The panel integration and structural mechanics of the solar panel	0.6
E: Facilities based on biomass energy	1. Fluidized-bed steam boiler	0.8
	2. Liquid or gas-fired steam boiler	0.4
	3. Gasification and gas cleaning group	0.6
	4. Steam or gas turbine	2.0
	5. Internal combustion engine, or Stirling engine	0.9
	6. Generator and power electronics	0.5
	7. Cogeneration system	0.4
F: Facilities based on geothermal energy	1. Steam or gas turbine	1.3
	2. Generator and power electronics	0.7
	3. Steam injector or a vacuum compressor	0.7

ceeds from carbon and energy taxes or from phasing out fossil fuel subsidies could be used to uphold such incentives. As far as project financing is concerned, public finance mechanisms, which can range from simple grants to complex conditional funding structures, can be deployed to support R&D, technology transfer, and skill building. These can complement private capital, particularly in developing countries, or broaden the market for renewable energies. Thus, governments have increasingly been taking action; in early 2010, for example, 85 countries have set national targets for renewable energy, more than half of which are in developing countries like Turkey (UNEP Green Economy Report, 2011).

According to the European Commission's Brussels, 17.10.2012, COM (2012) 595 final 2012/0288 (COD), said in the section of Explanatory Memorandum that 'Directive 2009/28/EC1 on the promotion of the use of energy from renewable sources (the 'Renewable Energy Directive') established mandatory targets to be achieved by 2020 for a 20% overall share of renewable energy in the EU and a 10% share for renewable energy in the transport sector. At the same time, an amendment to Directive 98/70/EC2 ('the Fuel Quality Directive') introduced a mandatory target to achieve by 2020 a 6% reduction in the greenhouse gas intensity of fuels used in road transport and non-road mobile machinery'.

While the 2005 share (measured in terms of gross final energy consumption) was 8.5% (9.2% in 2006), and the EU 2020 target is 20% (European Commission, 2012). In all European countries, production of electricity from renewable resources is supported. In many countries and a minimum price system is used widely, which require an electricity utility to purchase a portion of its electricity requirement, as green energy, at a minimum price defined. Legally defined, minimum prices change according to the country; some of them can be seen in Table 13 (Erdogdu, 2009).

Table 13: Minimum price of renewable electricity in some European countries (Eurocent/kWh) *(Erdogdu, 2009)*

Country	*Price (USD cents)*
Netherlands	11.9-12.27
France	10.41
Austria	9.66
Portugal	9.29-9.79
Greece	7.93
Spain	7.81-9.29
Germany	7.68-10.53
Turkey*	6.2-6.82

* *Turkey has changed the prices by new law at the end of 2010, which is given in Table 11 and Table 12.*

5. Analysis of the current situation in Turkey and EU

There are many support mechanisms for dissemination of renewable energy usage in Turkey, but the most important and distinctive one has been enacted at the end of December, 2010, which has been given in this study, section 3.1 as Law on Utilization of Renewable Energy Resources for the Purpose of Generating Electrical Energy (The Republic of Turkey, Turkish Official Journal, 2010). It has taken so much effort to be realized with some crucial modifications. For example, the most critical change in the tariff is the purchase price. Incentive mechanisms in Turkey are presented in section 3 and applications of EU are presented in section 4. The following conclusions can be inferred if these two sections and references (Boewe 2012; Ghosh and Gangania, 2012; Gipe, 2010; Renewable energy: Gross employment 2006; BMU – Brochure, Internet Update, 2007; Camadan and Erten, 2011; Kilic, 2011) are examined carefully.

- It can be seen that the unit purchase price of electricity which is generated from renewable energy sources (RES) are low when compared to other developed countries. For example, while purchase price of biogas is approximately 12.39 USD cent/kWh in Turkey, it can reach to 24.78 USD cent/kWh in Germany, 35.93 USD cent/kWh in Italy, and 30.97 USD cent/kWh in England. This effects affordability of the facility installation and can make it difficult to find investment financing.
- The highest tariff purchase in Turkey is 13.3 Dollar cent/kWh, applied to the biomass and solar. As of July 2014, feed-in tariffs for photovoltaic systems range from 15.95 USD cents per kWh for small roof-top system, down to 11.05 USD euro cents per kWh for large utility scaled solar parks. Feed-in tariffs are restricted to a maximum system capacity of 10 megawatts (MW). The feed-in tariff for solar PV is declining at a faster rate than for any other renewable technology in Germany (Feed-in tariffs in Germany, 2014).
- In Turkey, the implementation of a procurement schedule of biomass energy is higher than other resources' of energy production subsidies. The reason is that biomass production facilities have higher local installation potential than other facilities. Moreover, incentives for biogas mean the indirect incentives for agricultural sector.
- In Turkey, The Law No: 6094 for renewable energy production assures purchase guarantee for electrical energy generation, it does not comprise of heat or CHP (Combined Heat and Power) applications. However, some developed countries have additional subsidies for CHP applications that using RES (Renewable Energy Sources) as a source.

- While guaranteed purchase of electricity in Turkey is 10 years, this period is 20 years in countries like Germany, Greece, OECD countries and BRICS (Brazil, China, Russia and India) ((International Energy Agency, 2008).
- Using domestic products for the installation of the facility is encouraged by this law in Turkey. Renewable energy producers that got their operation license before 31 December 2015 are entitled to receive an additional subsidy ranging from USD 0.004 to 0.035 per kWh for a period of five years if they use locally-produced mechanical, electromechanical and other equipment and technology for their plants. This is called 'local contribution'.
- The law also limits the total production of licensed solar energy companies to 600 MW annually until 31 December 2013, and then authorizes the cabinet to determine the limits afterwards in Turkey.
- Although intense discussion has been made for the last decade to disseminate the usage of renewable energy resources in Turkey, not much progress can be seen especially in the figures of the employment in renewable energies. But, considering the employment in this sector in Germany, the numbers are quite high. For example in 2006 Germany has reached the number of the employment in total of 235 000 people in the renewable energy sector, which was 160 500 in 2004 (Renewable energy: Gross employment, 2006).
- The effect of the use of renewable energy resources is so important to reduce greenhouse gas emissions. Turkey's contribution to the reduction of greenhouse gases will be increased by the expansion of the use of renewable energy resources (Internet Update BMU- Brochure, 2007).
- While the Turkish Parliament has approved a new renewable energy law that sets short-term standards, the renewable energy sector's long term prospects should be left in the hands of the nation's cabinet.
- It can also be said that Turkey has great wind and solar energy potential, and still needs important improvements.

6. Conclusion

In this paper, the evaluation of renewable energy and the importance of renewable energy usage, the feed in tariffs for renewable energy generation, the renewable energy policies in Turkey and some developed countries are investigated and compared. In this regard, some barriers and recommendations are submitted for better understanding about the importance of the subject. With this study, the following items were identified or accomplished:

1. Turkey is an energy-importing country. In order to be less dependent on other countries in energy, Turkey needs to use its sustainable sources. From this point of view, renewable energy is a very attractive choice, since it is reliable, endless, domestic, sustainable and environmentally friendly. Furthermore, due to its geographical position, Turkey has many advantages having renewable energy resources; such as, hydraulic, solar, wind, geothermal and biomass. Although there has been an important progress recent years in RES exploitation, there are still some barriers; such as, economic, lack of legislative and regulatory framework and poor infrastructure.
2. According to the International Energy Agency (2009) Turkey Report, Turkey is tenth among the 28 IEA countries. To examine the renewable energy sources of Turkey by comparison, its renewable energy sources account for more than 40% of TPES (Total Primary Energy Supply) in Norway (which is basically hydropower), and around 1/3 in New Zealand and Sweden. Allowing for the electricity generation, in 2009, renewable sources provided 37.8 TWh of electricity, or 19.6% of the total power generation in Turkey, which is the 12th highest portion among the 28 IEA countries. Hydropower accounted for 95% (35.9 TWh) of this total and wind power for 4% (1.5 TWh). The remaining 1% came from biomass (0.3 TWh) and geothermal energy (0.5 TWh). Hydropower generation varies according to rainfall. The Turkish government is planning to realize the target of electricity production from renewable energy sources as around 30% in the share of energy generation by 2023. (Turkish Republic Ministry of NR and Energy, 2014).
3. As for heat, firewood is the largest source of heat from renewable sources in Turkey (Kilic, 2011). In 2008, 5.0 Mtoe of firewood was used for heating in rural areas. Other forms of biomass are negligible. The second-largest source of heat from renewable sources is geothermal, 0.9 Mtoe of which was used in 2008.
4. In Turkey, energy sectors are the main contributor to Turkey's greenhouse gas emissions, which increasing rapidly. The Turkish government is therefore focusing on clean energy development, such as from domestic renewable resources and introducing incentives and the feed in tariffs in energy production from RES, so it is aimed to increase the share of renewables in the electrical energy mix. By enacting this new law (Law No:6094), Turkey offers guaranteed prices for power generated from renewable resources and pays more if the producers use locally-made equipment (Kilic, 2011).
5. Current levels of investment in renewable energy are still lower than expected. The major bar-

riers and policy responses may be grouped as:

a) Some risks and incentives associated with renewable energy investments, including fiscal policy instruments. For example, the purchase prices specified in the 6094 Act (according to the renewable laws) will be valid until the end of 2015. The prices will be determined by the Council of Ministers for the investments that will be realized after 2015, and these new prices will not to exceed the price indicated in the law. This uncertainty poses risks for potential investments.
b) Relative costs of renewable energy projects and financing. For example, some of projects may not be feasible considering the region that the investment will be realized, the type and the quality of renewable energy sources and the amount of resources that will be used.
c) Electricity infrastructure and regulations,
d) Sustainability criteria.

6. To achieve the required returns, incentive mechanisms such as feed-in tariffs need to be guaranteed for 15-20 years instead of 10 years.
7. Feed in tariffs need to be judiciously designed and applied. Subsidies will most likely need to be adjusted over time in order to be efficient, and such changes are likely to be opposed by businesses or consumers who benefit from them. Such support also needs to take into account requirements of international agreements, in particular the rules and regulations of the World Trade Organization.
8. EU policy and legislation relevant to renewable energy resources should be more researched and summarized. These policies are believed to be the most developed in the world for this topic, and they serve as a solid base for development of recommendations for Turkish energy policy.
9. The importance of the role of the government in formulating and implementing favourable policies for renewable energy resources exploitation is stressed. It is also important for efficiency and effectiveness that communication and mechanisms for coordination/cooperation between ministries (i.e. energy, agricultural, and environmental) be improved. Successful policymaking and implementation can lead to an ultimately important outcome.
10. Since the private sector has the capacity to mobilize needed funds, development of incentives would motivate the private sector to become more involved in the advancement of renewable energy.

Disclaimer

Although some data has been taken from governmental documents, this paper is not necessarily representative of the views of the government.

References

Baris, K., and Kucukali, S. (2012). Availability of renewable energy sources in Turkey: Current situation, potential, government policies and the EU perspective. *Energy Policy*, 42 (2012) 377–391.

Bilgen, S., Keles, S., Kaygusuz, A. Sarı A., and Kaygusuz K. (2008). Global warming and renewable energy sources for sustainable development: A case study in Turkey. *Renewable and Sustainable Energy Reviews* 12 (2008) 372–396.

BMU – Brochure, Internet Update (2007). 'Renewable energy sources in figures-national and international development' Version: November 2007; provisional figures.

Camadan, E., and Erten, İ. E. (2011). An evaluation of the transitional Turkish electricity balancing and settlement market: Lessons for the future. *Renewable and Sustainable Energy Reviews* 15 (2011) 1325–1334.

Demirbas, A., and Bakıs, R. (2004). Energy from Renewable Sources in Turkey: Status and Future Direction. Energy Sources, Part A: Recovery, Utilization, and Environmental Effects, (2004) 26:5, 473-484, Taylor & Francis Inc. ISSN: 0090-8312 print/1521-0510 online, DOI: 10.1080/00908310490429759.

Erdem, Z. B. (2010). The contribution of renewable resources in meeting Turkey's energy-related challenges. *Renewable and Sustainable Energy Reviews* 14 (2010) 2710–2722.

Erdogdu E. (2009). On the wind energy in Turkey Renewable and Sustainable Energy Reviews 13 (2009) 1361–1371.

Gokcol, C., Dursun, B., Alboyaci, B., and Sunan, E. (2009) Importance of biomass energy as alternative to other sources in Turkey *Energy Policy*, 37, pp. 424-431.

http://ec.europa.eu/energy/renewables/targets_en.htm. European Commission Brussels (2012). 17.10.2012, COM (2012) 595 final 2012/0288 (COD). Proposal for a Directive of The European Parliament and of the Council amending Directive 98/70/EC relating to the quality of petrol and diesel fuels and amending Directive 2009/28/EC on the promotion of the use of energy from renewable sources, 2012. (Accessed 29 November 2014).

http://greenbuildest.blogspot.com/2010/11/renewable-energy-opportunities-in.html. Renewable energy opportunities in Turkey. (2010). (Accessed 29 November 2014).

http://www.iea.org/textbase/pm/?mode=re&id=4910&action=detail. Ghosh A. & Gangania H. (2012). Governing Clean Energy Subsidies: What, Why, and How Legal? ICTSD (International Centre for Trade and Sustainable Development) Global Platform on Climate Change, Trade and Sustainable Energy. August 2012. (Accessed 8 December 2014).

http://www.mayerbrown.com/publications/article.asp?id

=11934. Mayer- Brown, Boewe M. A. (2012). The German Renewable Energy Act of 2012. (Accessed 15 November 2014).

http://www.rferl.org/content/russia_turkey_to_build_nuclear_plant/2340411.html. (Accessed 30 November 2014).

http://www.wind-works.org/FeedLaws/TableofRenewableTariffsorFeed-InTariffsWorldwide.html. Gipe, P. (2010). French Tariffs Raise Price for Solar, Geothermal, and Biomass Solar Advocates Warn of Overheating French PV Market. January 30, 2010. (Accessed 21 November 2014).

IEA, (International Energy Agency). (2008). In support of the G8 Plan of action, Deploying Renewables: Principles for effective policies. IEA Publications, 9, Rue de la Fédération, 75739 Paris Cedex 15, Printed in France By Stedi Media, (61 2008 06 1P1) ISBN: 978-92-64-04220-9-2008.

IEA, (International Energy Agency). (2010). Energy policies of IEA countries, Turkey 2009 Review. (2010). IEA Publications, 9, Rue de la Fédération, 75739 Paris Cedex 15, printed in France by Soregraph, July 2010, (61 2009 06 1P1) ISBN : 978-92-64-06041-8.

Kaya, D. (2006). Renewable Energy policies in Turkey. Renewable and Sustainable Energy Reviews, 10: 152-163.

Kaya, D., Çanka Kılıç, F., Baban, A., and Dikeç, S. (2008). Administrative, institutional and legislative issues on agricultural waste exploitation in Turkey. Renewable and Sustainable Energy Reviews, 12 (2008) 417-436.

Kilic, F.C, and Kilic, M. K. (2013). Geothermal Energy and Turkey. ('Jeotermal Enerji ve Türkiye' in Turkish) TMMOB (Turkish Union of Chambers of Mechanical Engineers and Architects), Mühendis ve Makina Dergisi, ISSN: 1300-3402, Volume: 54, Issue: 639, Pages: 45-56; April 2013.

Kilic, F.C. (2011). Biyogaz, önemi, genel durumu ve Türkiye'deki yeri. General outlook of biogas, the importance of its usage and biogas in Turkey. June 2011. TMMOB (Turkish Union of Chambers of Mechanical Engineers and Architects) Mühendis ve Makina Dergisi, ISSN:1300-3402, Volume: 52, Issue: 617, Pages: 94-106.

Kilic, F.C. (2011). Recent renewable energy developments, studies, incentives in Turkey. Energy Education Science and Technology Part A: Energy Science and Research, 2011 Volume (Issue) 28 (1): pages 37-54.

Kilic, F.C. (2011). Türkiye'deki Yenilenebilir Enerjilerde Mevcut Durum ve Teşviklerindeki Son Gelişmeler. Current renewable energy situation and renewable subsidies in Turkey. March 2011. TMMOB (Turkish Union of Chambers of Mechanical Engineers and Architects) Mühendis ve Makina Dergisi, ISSN:1300-3402, Volume: 52, Issue: 614, Pages: 103-115.

Kilic, F.C., and Kaya, D. (2007). Energy production, consumption, policies, and recent developments in Turkey. Renewable and Sustainable Energy Reviews. (2007) 11: 1312-1320.

Koyun, A. (2007). Energy Efficiency and Renewable Energy, Turkey-National Study's Summary. Mediterranean and National Strategies for Sustainable Development, Energy and Climate Change, Yildiz Technical University, Plan Bleu, Regional Activity Centre, Sophia Antipolis, March 2007.

Renewable energy: Gross employment 2006, final report of the proposal (2007). 'Effect of increased use of renewable energies on the German labour market-Follow up' Version: September 2007.

Republic of Turkey, Ministry of Energy and Natural Resources (2011).The Presentation of the Ministry's Budget for The Year 2012 at The Plenary Session of The Turkish Grand National Assembly (TBMM), Republic of Turkey, Ministry of Energy and Natural Resources.

The Republic of Turkey, Turkish Official Journal (2010). Law No: 6094. 29th December 2010, Ankara.

UNEP Green Economy Report, (2011). Part II, Chapter 1, Renewable energy Invest in energy and resource efficiency, United Nations Environment Programme, 2011.

WEC, (2007). World Energy Council, Survey of Energy Resources, 2007.

World Energy Council Report. Pursuing sustainability: (2011). 2010 Assessment of country energy and climate policies, 2010.

Received 5 November 2013; revised 12 December 2014

Production of biodiesel from chicken wastes by various alcohol-catalyst combinations

Chia-Wei Lin

Shuo-Wen Tsai

Department of Food Science and Biotechnology, National Chung Hsing University, Taiwan

Abstract

An environmentally friendly biorefinery process for producing biodiesel from chicken wastes was performed for this study. Low acid value (0.13±0.01 mg KOH/g) chicken oil was obtained by preparing chicken wastes with moderate heating and filtration processes that minimized damage to the lipids and thus facilitated subsequent reactions. Methanol-lipids in a molar ratio of 6:1 and a methanol-ethanol-lipids mixture in a molar ratio of 3:3:1 were both reacted with 1% KOH catalyst for transesterification. Furthermore, ethanol-lipids in a molar ration of 6:1 were analogously transesterified with 1% sodium ethoxide. The amounts of biodiesel were 771.54 mg/mL±15.28, 722.98 mg/mL±37.38, and 714.86 mg/ mL±29.99 from methanol, ethanol, and a mixture of methanol/ethanol (3:3), respectively, after transesterification. The total amount of ethyl ester was comparable with the total amount of methyl ester. In addition, ethanol is a renewable resource and a biorefinery concept can be contributed for biodiesel production. Furthermore, transesterification of chicken oil with a mixture of methanol/ethanol (3:3) only needed a relatively short reaction time of an hour. Densities, viscosities, sulphur contents, acid values, and flash points of all esters were within the specifications of CNS 15072 and EN 14214. The transesterification system for chicken oil in ethanol and mixed methanol/ethanol (3:3) demonstrated in this study is a potential candidate for biodiesel production.

Keywords: biodiesel, chicken oil, transesterification, ethanol, methanol-ethanol mixture

1. Introduction

In recent years, the price of gasoline has remained consistently high. It is almost a common consensus that its price shows an ascending trend. Therefore, an alternative fuel supply as a substitute for petroleum would be a welcomed resource to help alleviate high cost expenditures. Biodiesel can be used as a fuel or mixed with petroleum-based diesel. The advantages of biodiesel are present in its nontoxic nature, biodegradability, and minimal chemical emissions characteristics. Biodiesel also benefits the environment by aiding carbon dioxide recycling over short periods (Jeong *et al*., 2009; Wang *et al*., 2007; Bianchi *et al*., 2010). As shown in Figure 1, biodiesel can be produced by the transesterification process of triacylglycerides (from animal fats or vegetable oils) and alcohol with the assistance of a proper catalyst (Hoque *et al*., 2011).

The raw materials employed in biodiesel production are ordinarily categorized into animal fats, vegetable oils, and waste oils (Kim *et al*., 2010; Marulanda *et al*., 2010; Issariyakul *et al*., 2007). Clean vegetable oils such as palm oil (Gutiérrez *et al*., 2009), rapeseed oil (Warabi *et al*., 2004), soybean oil (Kim *et al*., 2010), cottonseed oil (Joshi *et al*., 2012), and sunflower oil (Ahmad *et al*., 2010), are the most commonly used feedstocks for biodiesel production. However, the utilization of edible vegetable oil sources serves to not only increase the production cost but also directly competes with the human food supply. It is estimated that the cost of raw materials represents approximately 85% of the cost of biodiesel production. Therefore, the development of cheap, abundant, and high-quality feedstock from waste by-products is considered important for the biodiesel industry's progress (Bianchi *et al*., 2010).

Previous researchers have effectively utilized mutton (Mutreja *et al*., 2011), chicken fat (Alptekin and Canakci, 2010; Marulanda *al*., 2010; Boey *et*

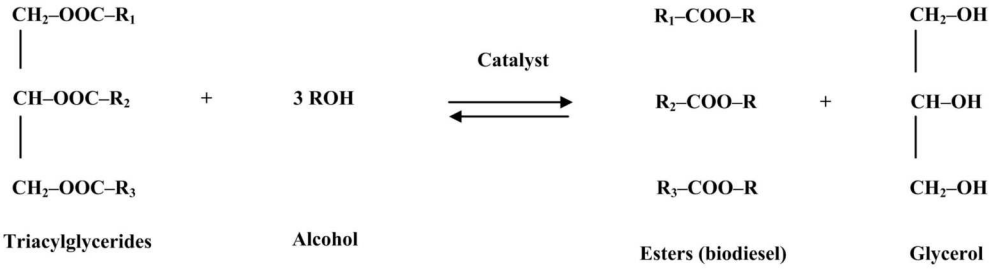

Figure 1: The transesterification process for biodiesel synthesis
Source: Hoque et al. (2011)

al., 2011; Gugule *et al*., 2011), lard (Jeong *et al*., 2009), beef tallow (Hoque *et al*., 2011), and waste cooking oil (Lam and Lee, 2011) as alternative sources for transesterification processes. In this research, the fat from chicken waste is suggested as a raw material for biodiesel.

Mege *et al*., (2006) indicated that chicken can have a 30% fat content of the total poultry meat. According to Arnaud *et al*., (2004), Marulanda *et al*., (2010) and Boey et al., (2011) chicken fat is composed of 26.5%–30.3% saturated fatty acids and 63.9%–73.5% unsaturated fatty acids; with major components being palmitic, stearic, linoleic, and oleic acids (Gugule *et al*., 2011). Large amounts of chicken by-products such as fat, skins, and tissues are discarded as wastes. The chicken fat can be simply and economically separated from wastes without chemical solvent treatment (Kondamudi *et al*., 2009).

Biodiesel production is frequently performed by alkali-catalysis transesterification. Typically methanol reacts with triglycerides to form fatty alkyl methyl esters (FAMEs) and glycerol. Currently, methanol is considered to be a cheap and convenient source for biodiesel production. However, there is rising interest in exploiting the use of ethanol as a replacement for methanol, since bio-ethanol is an environmentally friendly renewable resource that may relieve the dependency on petroleum-based synthetic methanol, which may become subject to shortages (Issariyakul *et al*., 2007). Methyl and ethyl esters are the most common esters used as biodiesel. However, the preparation processes show both advantages and disadvantages. Methanol shows poor oil solubility compared with ethanol, which limits reaction rates due to the slow mass transfer rate (Kulkarni *et al*., 2007). However, ethanol is presently more expensive than methanol, hence restricting its use for commercial biodiesel production (Joshi *et al*., 2012). Furthermore, transesterification of ethanol results in serious emulsion problems, which obstruct further processes (Issariyakul *et al*., 2007).

Previous reports in the literature have stated that using mixtures of methanol and ethanol for transesterification greatly improves the solvent properties and thus provides balanced biodiesel conversion (Issariyakul *et al*., 2007; Kulkarni *et al*., 2007). The objective of this research is to provide a less complicated method for producing biodiesel from chicken wastes. A gentle oil extraction is adopted to minimize deterioration, and thus, facilitate the subsequent processes. Methanol and ethanol as well as methanol/ethanol mixtures were used as the substrates with proper catalysts for transesterification. The compositions of major methyl and ethyl esters were analysed to study the reactions during the processes. In addition, the fuel characteristics of the fatty alkyl esters were analysed and compared to the standards.

2. Experimental section

2.1 Chicken fat extraction and separation

Figure 2 shows the biorefinery flowchart for synthesizing biodiesel from chicken wastes. Fresh chicken wastes obtained from the local market were the processing by-products, which mainly composed of chicken skin, fat, and a few other tissues. The chicken wastes were frozen, stored and then thawed at room temperature just before use. Thawed chicken wastes were filtered to separate the aqueous liquid and solid. The semi-solid chicken wastes were then placed in a container with a 100 °C water bath for one hour to melt the chicken fat**.** The melted mixtures were centrifuged at 3500×g for 20 minutes to separate the liquid chicken oil and solid remains. Freshly extracted chicken oil was directly used for the characterization experiments. Large-scale prepared chicken oil was temporary stored in a freezer until it was processed.

2.2 Characterization of chicken oil

Characterization of the chicken oil was achieved by measuring the saponification number, acid value (Chinese National Standards 13568, 1995), and fatty acid composition (Association of Official Analytical Chemists official method 996.06, 1996).

2.2.1 Acid value

The acid value (Av) was evaluated according to CNS 13568 (1995). The acid value was calculated by the following equation:

$$Av\ (mg\ KOH/g) = 5.611 \times a \times F)/S \quad (1)$$

The constant 5.611 represents 5.611 mg potas-

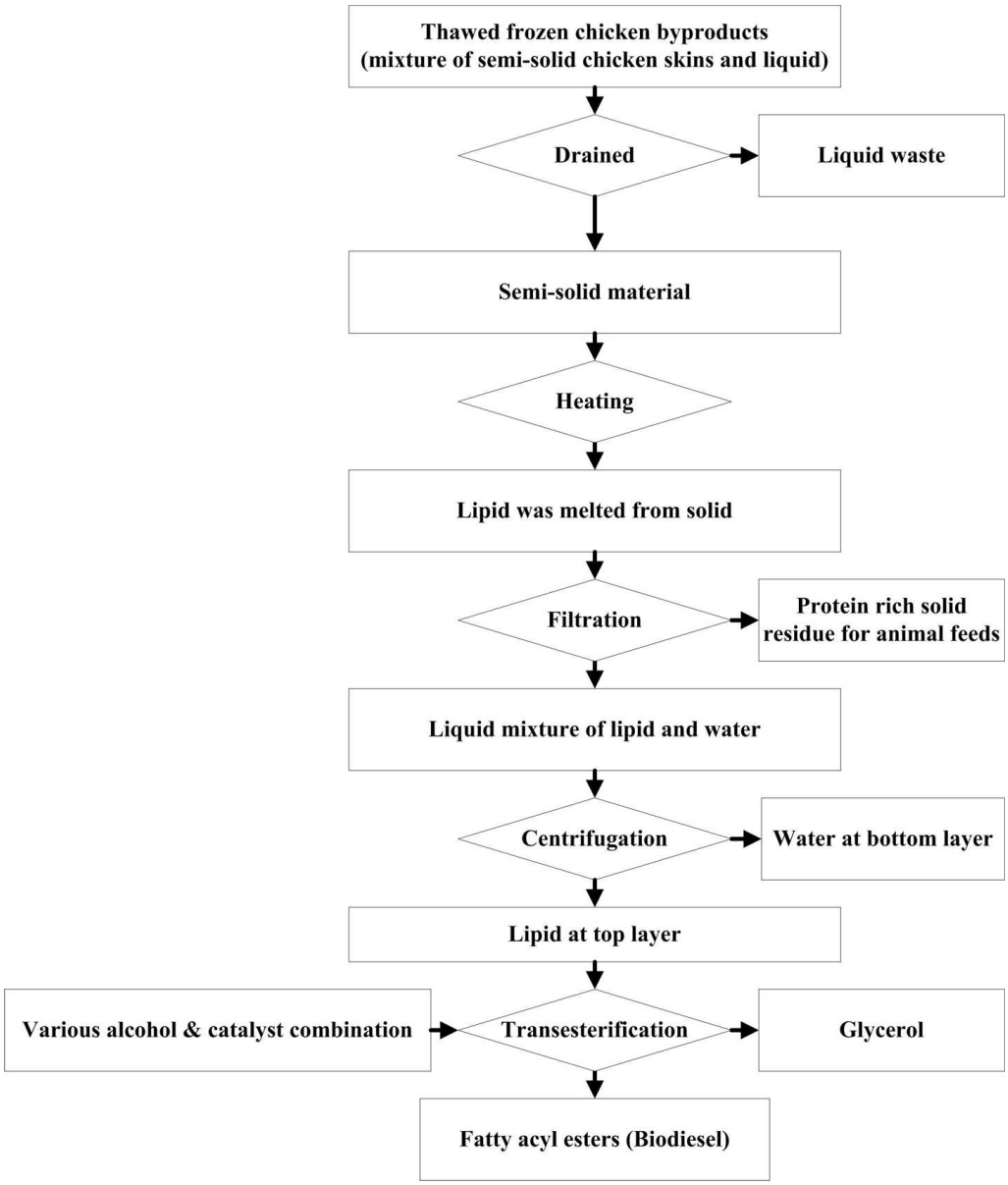

Figure 2: Flowchart for biodiesel production from chicken wastes

sium hydroxide in 1 mL solution (0.1 N); the variable 'a' is the consumption volume (mL) of N/10 KOH; 'F' is the potency of N/10 KOH; and 'S' is the weight (g) of the chicken oil sample.

2.2.2 Saponification number

The saponification number (Sn) was evaluated according to CNS 13568 (1995). The saponification number was calculated by the following equation:

$$Sn\ (mg\ KOH/g) = 28.05 \times (a - b) \times F/S \quad (2)$$

The constant 28.05 represents 28.05 mg potassium hydroxide in 1 mL solution (0.5 N); the variable 'a' is the titer (mL) of 0.5 N HCl for the blank and 'b' is the titer (mL) of 0.5 N HCl for the lipid sample; 'F' is the potency of 0.5 N HCl; and 'S' is the weight (g) of the chicken oil sample.

2.2.3 Fatty acid composition

Fatty acid composition of extracted chicken oil was analysed according to the official method of AOAC 996.06 (1996) by gas chromatography equipped with a capillary column (SP2560) (100 m × 0.25 mm × 0.20 μm) and a flame ionization detector. Helium was used as the carrier gas with a flow rate of 0.75 mL/min. Injection was accomplished with a split ratio of 200:1. The temperature of the injector and detector were 225 °C and 285 °C, respectively. The column temperature was preheated at 100 °C for 4 minutes then gradually raised to 240 °C at a slope of 3 °C/min then maintained for 15 minutes. The percentage of saturated lipid was calculated by the following equation:

$$\text{Saturated lipid (\%)} = (\Sigma \text{ saturated } W_i / W_{\text{test portion}}) \times 100\% \quad (3)$$

The variable 'Σ saturated W_i' represents the total weight of saturated lipid and '$W_{test\ portion}$' represents the weight of the test sample.

The percentage of monounsaturated lipid was calculated by the following equation:

$$\text{Monounsaturated lipid (\%)} = (\Sigma \text{ monounsaturated } W_i / W_{test\ portion}) \times 100\% \quad (4)$$

The variable 'Σ monounsaturated W_i' represents the total weight of monounsaturated lipid (*cis* form) and '$W_{test\ portion}$' represents the weight of the test sample.

The percentage of polyunsaturated lipid was calculated by the following equation:

$$\text{Polyunsaturated lipid (\%)} = (\Sigma \text{ polyunsaturated } W_i / W_{test\ portion}) \times 100\% \quad (5)$$

The variable 'Σ polyunsaturated W_i' represents the total weight of polyunsaturated lipid and '$W_{test\ portion}$' represents the weight of the test sample.

2.3 Transesterification of chicken oil

2.3.1 Fatty acid methyl esters

The preparation of fatty acid methyl esters was modified from the methods of García *et al*., (2011) and Kulkarni *et al*., (2007). The temporarily frozen chicken oil was pre-thawed at room temperature and homogenized at 50 °C. Fatty acid methyl esters were synthesized from the substrates of methanol and oil in a molar ratio of 6:1 with 1% (w/w) potassium hydroxide as catalyst. 40 g of chicken oil was loaded into the 60 °C thermostatic reactor with gentle stirring. Afterward 7.69 g methanol with 0.4 g dissolved potassium hydroxide was added to the reactor and allowed to reflux for 2 hours.

Reacted products were separated by separation funnel. The lower layer mainly consisted of glycerol and the upper layer consisted of fatty acid methyl esters (biodiesel) and unreacted remains. The upper layer of biodiesel was carefully washed with hot water (70 °C) to remove the residues of catalyst, glycerol, and alcohol. The washed biodiesel was further dried by a rotary vacuum evaporator to remove the fine residual water and methanol. The evaporation was continued until the weight of biodiesel remained constant. Residual water can be further removed by adding anhydrous sodium sulphate.

2.3.2. Fatty acid ethyl esters

The preparation of fatty acid ethyl esters was similar to the processes for fatty acid methyl esters that slightly modified the method of García *et al.*, (2011). The temporarily frozen chicken oil was pre-thawed and homogenized as the previous section described. Fatty acid ethyl esters were synthesized from the substrates of ethanol and oil in a molar ratio of 6:1 with 1% (w/w) sodium ethoxide as catalyst. 40 g of chicken oil was loaded into the 78 °C thermostatic reactor with gentle stirring. Afterward 11.06 g ethanol with 0.4 g dissolved sodium ethoxide was added to the reactor and allowed to reflux for 3 hours.

Reacted products were separated by separation funnel. The lower layer mainly consisted of glycerol and the upper layer consisted of fatty acid ethyl esters (biodiesel) and unreacted remains. The upper layer of biodiesel was washed with hot water (70 °C) to remove the residues of catalyst, glycerol, and alcohol. The organic layer was further washed with acidified water (pH 2, sulfuric acid, room temperature). The washed biodiesel was further dried as described in the previous section.

2.3.3 Mixture of fatty acid methyl/ethyl esters

The preparation of fatty acid methyl/ethyl esters was slightly modified from the methods of Issariyakul *et al*., (2007) and Kulkarni *et al*., (2007). The temporarily stored chicken oil was pre-thawed and homogenized as the previous section described. Fatty acid methyl/ethyl esters were synthesized from the substrates of methanol, ethanol, and oil in molar ratios of 5:1:1, 4:2:1, 3:3:1 and 2:4:1, respectively. An additional 1% (w/w) potassium hydroxide was utilized as a catalyst. Chicken oil was loaded into the 50 °C thermostatic reactor with gentle stirring. Afterwards, methanol and ethanol with dissolved potassium hydroxide were added to the reactor and allowed to reflux for 1 hour.

Reacted products were separated by separation funnel. The lower layer mainly consisted of glycerol and the upper layer consisted of fatty acid methyl/ethyl esters (biodiesel) and unreacted remains. The upper layer of biodiesel was washed with hot 0.1% (w/w) tannic acid solution (70 °C) to remove the unfavourable residues. The washed biodiesel was further dried as described in the previous section.

2.4 Characterization of biodiesel

Fatty acid methyl esters, ethyl esters, and mixtures of methyl/ethyl esters were analysed according to the modified AOAC method 996.06 (1996). The fatty acid profiles were established by a gas chromatograph (GC 9800) equipped with a DB-WAX (125-7032, Agilent) column (30 m×0.54 mm×1.00 μm).

The temperatures of the injector and detector were both set at 250 °C. 1 μL of sample was injected and the carrier gas used was helium. The column temperature program was held at 140 °C and subsequently ramped to 180 °C at 15 °C/min, then ramped to 200 °C at 5 °C/min and held for 20 min. Fatty alkyl esters such as methyl palmitate, methyl

stearate, methyl oleate, methyl linoleate, ethyl stearate, ethyl palmitate, ethyl oleate, and ethyl linoleate were chosen as references. The contents (mg/mL) of fatty alkyl esters in the prepared biodiesel were calculated by the standard curves.

The qualities of the prepared biodiesel were evaluated by a certificated organization according to the following methods: density at 15 °C (CNS 14474, 2000), viscosity at 40 °C (CNS 3390, 1972), flash point (CNS 3574, 1973), sulphur content (CNS 14505, 2001), water content (CNS 4446, 1978), and acid value (CNS 14906, 2005).

2.5 Statistical analysis

Experimental data was analysed by the SYSTAT Statistical Software (Version 11.0) using the *t*-test mode.

3. Results and discussion

3.1 Characterization of chicken oil

The experimental results and previous reports of acid values, saponification numbers, and molecular weights of extracted chicken oil are summarized in Table 1 (Marulanda *et al*., 2010; Boey *et al*., 2011; Gugule *et al*., 2011; Baião and Lara, 2005). The measured acid value of our chicken oil was 0.13±0.01 mg KOH/g, which is significantly lower than the values of 0.8976 and 4.1 mg KOH/g in previous reports (Gugule *et al*., 2011; Boey *et al*., 2011). A lower acid value is a desirable indicator for lipid extraction processes since it implies minimal damage to the lipids and thus will facilitate the further transesterification reactions (Alptekin and Canakci, 2010). It is important to estimate the molecular weight of the fatty acids for setting the

Table 1: Properties of chicken oil

Properties	*Chicken fat*	*Baião and Lara (2005)*	*Gugule et al., (2011)*	*Marulanda et al., (2010)*	*Boey et al., (2011)*
Acid value (mg KOH/g)	0.13±0.01		0.8976		4.1
Saponification no.(mg KOH/g)	148.62±6.18	190–196	55.8756		
Molecular weight (g/mol)	1131.86±47.38			867	
Data is presented in means standard deviations that were calculated from triple determinations.					

Table 2: Fatty acid composition of chicken oil

Fatty acid	*Present work (%)*	*Marulanda et al. (2010) (%)*	*Arnaud et al. (2004) (%)*	*Boey et al. (2011) (%)*	*Lee and Foglia (2000) (%)*	*Arnaud et al. (2006) (%)*
Saturated	31.75					
Caprylic acid (C8:0)	0.02					
Lauric acid (C12:0)	0.03					
Myristic acid (C14:0)	0.96			0.6	0.7	0.5
Pentadecanoic acid (C15:0)	0.10					
Palmitic acid (C16:0)	24.57	21.0	24.0	24.7	25.2	24.0
Margaric acid (C17:0)	0.15					
Stearic acid (C18:0)	5.80	5.5	5.8	4.5	5.9	5.8
Arachidic acid (C20:0)	0.07					
Behenic acid (C22:0)	0.05					
Unsaturated	68.25					
Myristoleic acid (C14:1)	0.18			0.2	0.3	
Palmitoleic acid (C16:1)	4.83	7.7	5.8	6.3	7.8	5.8
Oleic acid (C18:1)	39.81	48.5	38.2	44.1	40.5	38.2
Linoleic acid (C18:2)	20.52	17.3	23.8	18.4	18.4	23.8
Linolenic acid (C18:3)	2.10	traces	1.9	0.2	0.7	1.9
Octadecatetraenoic acid (C18:4)	0.05					
Gadoleic acid (C20:1)	0.10			1.0	0.5	
Eicosadienoic acid (C20:2)	0.15					
Eicosatrienoic acid (C20:3)	0.33					
Eicosapentaenoic acid (C20:5)	0.08					
Docosapentaenoic acid (C22:5)	0.04					
Docosahexaenoic acid (C22:6)	0.06					

appropriate molar ratio during biodiesel production. The average molecular weight of the total of three fatty acids on a triacylglyceride molecule from our partially purified chicken oil was 1131.86±47.38 g/mol, which was calculated by the experimental saponification number of 148.62±6.18 mg KOH/g.

In Table 2 we summarize the fatty acid compositions of the chicken lipids used in this research and previous research. The compositions of saturated fatty acids and unsaturated fatty acids present in the chicken oil were 31.75% and 68.25%, respectively. Monounsaturated oleic acid was the major component of the chicken lipids (39.81%). Our results showed that oleic acid (C18:1), palmitic acid (C16:0), linoleic acid (C18:2), and stearic acid (C18:0) altogether share 91% of the total fatty acids, which were comparable with values in the previous literature (Marulanda *et al*., 2010; Boey *et al*., 2011; Arnaud *et al*., 2004; Lee and Foglia, 2000; Lee and Foglia, 2000; Arnaud *et al*., 2006).

3.2 Molar ratios of alcohol to oil

The 6:1 molar ratio of alcohol to oil was chosen to prepare fatty acyl esters in accordance with the previous literature (Issariyakul *et al*., 2007; Kulkarni *et al*., 2007; García *et al*., 2011) and our practical experience. The major fatty acyl esters produced by the transesterification of alcohol and oil mixtures were analysed by gas chromatography. Figure 3 (A) and (B) present typical chromatograms of the classic fatty acyl esters produced by alcohols and chicken oil in a molar ratio of 6:1. The three obvious peaks in the chromatogram indicate the three major fatty acyl esters (16:0; 18:1; 18:2) which correspond to the fatty acid profiles of the original chicken oil. Assorted peaks in the chromatogram of Figure 3 (C) confirm the diversified fatty acyl esters produced by mixed alcohol to oil in a molar ratio of 3:3:1 (methanol: ethanol: oil).

Quite a few reports in the literature describe biodiesel produced from methanol with various lipid sources (Hoque *et al.*, 2011; Boey *et al.*, 2011). Methanol is commonly selected for the reasons of cost and efficiency. However, bioethanol is prospectively expected to be a preferable substrate for biodiesel when the price of petroleum-based methanol is boosted. The ratios of methanol to ethanol in the alcohol mixture were varied for studying the formation of methyl esters or ethyl esters.

As shown in Table 3, the transesterification of various alcohol combinations with chicken oil resulted in different methyl and ethyl ester profiles. The ratio of methyl/ethyl esters products does not perfectly correspond with the ratio of the methyl/ethyl alcohol substrate. Chicken oil that transesterified with alcohols having a molar ratio of 3:3 (methanol: ethanol) produced approximately double the methyl esters compared to ethyl esters. The profile of fatty acyl esters is consistent with a previous report that used canola oil as the lipid source (Kulkarni *et al.*, 2007). The extensive production of methyl esters rather than ethyl esters

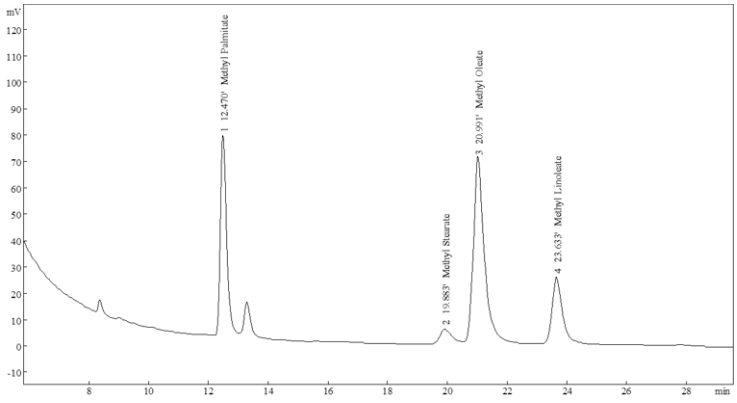

(A) Biodiesel produced by methanol and chicken oil in a molar ratio of 6:1

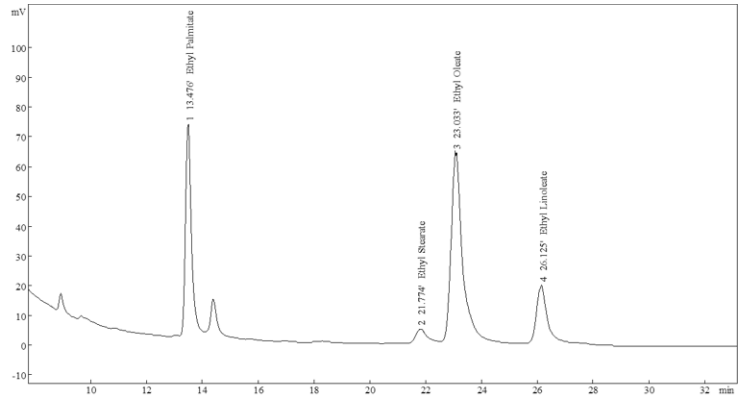

(B) Biodiesel produced by ethanol and chicken oil in a molar ratio of 6:1

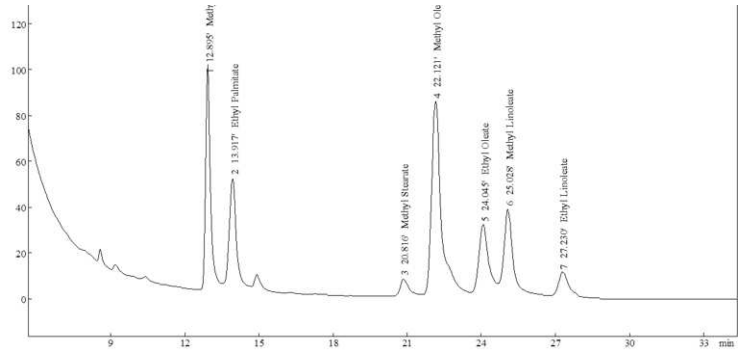

(C) Biodiesel produced by methanol, ethanol and chicken oil in a molar ratio of 3:3:1

Peaks in the chromatograms indicate (a) methyl palmitate, (b) methyl stearate, (c) methyl oleate, (d) methyl linoleate (e) ethyl palmitate, (f) ethyl stearate, (g) ethyl oleate, (h) ethyl linoleate

Figure 3: Gas chromatograms of fatty acyl esters

Table 3: The relative composition (%) of fatty acyl esters transesterified from chicken oil

	Substrate ratio of methanol to ethanol to oil			
Fatty acyl esters	*5:1:1*	*4:2:1*	*3:3:1*	*2:4:1*
C16:0 (Methyl)	16.86	16.63	14.96	9.83
C16:0 (Ethyl)	7.97	9.72	12.53	14.56
C18:0 (Methyl)	6.19	5.57	3.97	3.18
C18:0 (Ethyl)	N.D.	N.D.	N.D.	N.D.
C18:1 (Methyl)	36.21	32.89	30.49	21.48
C18:1 (Ethyl)	10.46	11.87	13.78	26.29
C18:2 (Methyl)	16.11	16.48	15.63	11.18
C18:2 (Ethyl)	6.19	6.84	8.64	13.48

N.D. = not detected.

The relative composition (%) of fatty acyl esters is calculated as the concentration of the individual fatty acyl ester divided by the sum of the 8major fatty acyl esters

may be attributed to the higher nucleophilicity of methoxide ions (Sridharan and Mathai, 1974). The intrinsic lower reaction rate of ethanol and the availability of alcohol molecules may explain the differences between the expected composition of the fatty acyl esters and their formulated substrates (Issariyakul *et al.,* 2007; Kulkarni *et al.*, 2007). However, increasing the ethanol in the substrate formula did increase the ethyl esters in the products. On the balanced consideration of the versatile substrate availability and reaction efficiency, we chose the 3:3:1 (methanol: ethanol: chicken oil) ratio for further discussion.

3.3 Fatty acyl esters preparation

The major fatty acyl esters produced by simple alcohol with chicken oil and mixed alcohol with chicken oil are presented in Table 4. The major components in the produced biodiesel roughly corresponded to the fatty acid composition in the original chicken oil. The dominant fatty acyl ester in the biodiesel was oleyl ester (316.50–375.94 mg/mL, 44.27–48.74%), which is consistent with previous research (oleyl ester 40.9–45.83%), (Wyatt *et al*., 2005; Gugule *et al*., 2011). The sum of the unsaturated fatty acyl esters (489.99–510.50 mg/ mL, 66.17–68.55%) is significantly higher than that of the saturated fatty acyl esters (224.88–261.04 mg/ mL, 31.45–33.83%).

The literature indicates that saturated esters show higher calorific values and cetane numbers than unsaturated esters (Canoira *et al*., 2008; Lebedevas and Vaicekauskas, 2006). However, animal fat derived saturated biodiesel has been repeatedly challenged on its application in cold environments (Lebedevas and Vaicekauskas, 2006; Foglia *et al*., 1997). On the other hand, the intrinsic unsaturated double bonds are more susceptible to chemical deterioration, such as autoxidation and polymerization. A previous research revealed that soy oil based biodiesel with a high level of unsaturated fatty esters may lead to the formation of engine deposits and the deterioration of engine lubricating oil (Mittelbach, 1996).

The saturation degree of biodiesel derived from chicken oil is between that derived from tallow (52.6% unsaturated fatty acyl esters and 38.2% saturated fatty acyl esters) and soy oil (82.8% unsaturated fatty acyl esters), thus chicken oil derived biodiesel becomes an interesting alternative (Wyatt *et al*., 2005).

The results in Table 4 demonstrate that the conventional methyl transesterification, the alternative ethyl transesterification, and the compromising mixed methyl/ethyl transesterification all obtained similar sums of acyl esters. It is worth mentioning that the sum of the methyl esters (771.54 mg/mL±15.28) prepared from the simple methanol formula (6:1) shows no significant difference with the sum of ethyl esters (722.98 mg/mL±37.38) from the simple ethanol formula (6:1) on a statistical basis ($P > 0.05$). Several previous papers have reported that transesterification of ethanol with lipids is not as good as using methanol (Issariyakul *et al*., 2007; Lam and Lee, 2011). However, as the data shows, similar amounts of ethyl esters (in three hours) and methyl esters (in two hours) can be achieved via our modified processes. We consider these results to be an encouragement for the utilization of bioethanol in the future.

Comparable results for mixed methyl/ethyl esters (714.86 mg/mL±29.99) can be achieved in a relatively short period (one hour). In previous work, before a one hour transesterification process, Issariyakul *et al*., (2007) used an esterification process which took five hours to decrease the acid value of waste fryer grease and Lam and Lee (2011) spent a total of eight hours manufacturing a complex catalyst. However, we are able to offer a simplified process to produce a mixture of fatty acid methyl/ethyl esters that only takes one hour.

Consequently, ethanol and a mixture of methanol/ethanol (3:3) transesterification are methods that have enormous potential for biodiesel pro-

Table 4: Fatty acyl esters (mg/mL) transesterified by simple alcohol or mixed alcohol with chicken oil

Fatty acyl esters		*Substrate formula for producing biodiesel*		
	methanol to oil (6:1)	*ethanol to oil (6:1)*	*Methanol to ethanol to oil (3:3:1)*	
Palmityl	Methyl ester	202.88 mg/mL±5.82		106.97 mg/ mL±10.64
(C16:0)	Ethyl ester		168.16 mg/ mL±10.58	89.55 mg/ mL±4.12
Sum of palmityl esters		202.88 mg/ mL±5.82 [a]	168.16 mg/ mL±10.58 [b]	196.52 mg/ mL±12.62 [a]
Stearyl	Methyl ester	58.16 mg/ mL±0.81		28.36 mg/ mL±1.46
(C18:0)	Ethyl ester		64.50 mg/ mL±8.03	N.D.
Sum of stearyl esters		58.16 mg/ mL±0.81 [a]	64.50 mg/ mL±8.03 [a]	28.36 mg/ mL±1.46 [b]
Oleyl	Methyl ester	375.94 mg/ mL±0.91		217.96 mg/ mL±8.77
(C18:1)	Ethyl ester		322.43 mg/ mL±23.34	98.54mg/ mL±6.94
Sum of oleyl esters		375.94 mg/ mL±0.91 [a]	322.43 mg/ mL±23.34 [b]	316.50 mg/ mL±13.88 [b]
Linoleyl	Methyl ester	134.56 mg/ mL±8.13		111.71mg/ mL±1.43
(C18:2)	Ethyl ester		167.89 mg/ mL±4.49	61.79 mg/ mL±3.98
Sum of linoleyl esters		134.56 mg/ mL±8.13 [a]	167.89 mg/ mL±4.49 [b]	173.49 mg/ mL±5.37 [b]
Sum of the methyl esters		771.54 mg/ mL ±15.28		464.99 mg/ mL ±20.53
Sum of the ethyl esters			722.98 mg/ mL ±37.38	249.87 mg/ mL±14.84
Sum of the esters		771.54 mg/ mL ±15.28[a]	722.98 mg/ mL ±37.38[ab]	714.86 mg/ mL ±29.99[b]

Means±SDs were calculated from triple determinations.

[a–b] The different letters in the same column indicate significant differences (P < 0.05) by t-tests.

duction due to the considerable amount of acyl esters delivered and the reaction time.

3.4 Biodiesel characterization

The methyl esters, ethyl esters, and mixed methyl/ethyl esters that were produced from chicken oil and various alcohol combinations were subjected to a regular biodiesel evaluation. Fuel characteristics, Chinese National Standards (CNS) 15072 and EN 14214, are summarized in Table 5. The fuel characteristics of all the esters except water content were within the ranges of CNS 15072 and EN 14214.

The densities of the fatty acyl esters prepared from chicken oil and various alcohols were close to those reported in the previous literature, with values of 879.6 kg/m^3 (methyl esters); 874.7 kg/m^3 (ethyl esters), and 879.6 kg/m^3 (methyl/ethyl esters) (Boey et al., 2011; Lam and Lee, 2011).

The viscosities of methyl esters, ethyl esters, and mixed methyl/ethyl esters were 4.469, 4.594, and 4.822 mm^2/s respectively, which are all within the range of CNS 15072 and EN 14214.

Sulphur contents of all the esters were much lower than the limit of maximum sulphur content of CNS 15072 and EN 14214. The low sulphur contents represent the positive impact on exhaust emissions and less engine corrosion (Joshi *et al*., 2012).

The water contents of all the esters exceeded the specifications of CNS 15072 and EN 14214 and we presume the reason to be that the final vacuum evaporation processes were not optimized. This problem may be addressed through further investigation.

The oxidation stability of biodiesel is related to its free fatty acid content, which is measured by the acid value (Kulkarni *et al*., 2007). Therefore, experimental results reveal ester's low acid value which help long term operation of the engine and make it an ideal candidate for biodiesel production. Flash point, a characteristic that must be considered when estimating the flammability risks of all esters, was used to ensure that esters will remain in a stable state during transportation. The resulting flash

Table 5: Fuel characteristics of methyl esters, ethyl esters, and mixed methyl/ethyl esters produced from chicken oil and various alcohol combinations

Characteristics	*Methyl esters from methanol and oil (6:1)*	*Ethyl esters from ethanol and oil (6:1)*	*Mixed methyl/ethyl esters from methanol, ethanol and oil (3:3:1)*	*CNS 15072/ EN 14214*
Density at 15 °C (kg/m^3)	879.6	874.7	879.6	860-900
Viscosity at 40 °C (mm^2/s)	4.469	4.594	4.822	3.5-5.0
Sulphur content (ppm)	1.3	1.5	1.210.0 max	
Water content (ppm)	1390	1707	1852	500 max
Acid value (mg KOH/g)	0.144	0.183	0.301	0.5 max
Flash point (°C)	170	186	174	101 min

All measurements were achieved by a certificated organization with corresponding CNS methods

points of methyl esters, ethyl esters, and a mixture of methyl/ethyl esters (3:3) were 170, 186, and 174 °C, respectively. Furthermore, the experimental results for flash points were higher than for the flash point reported in previous research (150 °C, chicken fat methyl esters) (Wyatt *et al*., 2005).

In summary, fuel characteristics of methyl esters, ethyl esters, and a mixture of methyl/ethyl esters (3:3) principally met the specifications of CNS 15072 and EN 14214. Moreover, the fuel characteristics were principally consistent with previous literature on methyl esters from chicken fat (Boey *et al*., 2011).

4. Conclusions

The present work has successfully developed a potential process for producing biodiesel from chicken oil. Chicken oil with a lower acid value was obtained by a moderate extracting method that would later benefit the transesterification reaction.

The slightly modified methods for fatty acid ethyl ester and methyl/ethyl ester preparation can obtain similar amounts of ethyl esters and methyl esters and comparable amounts of a mixture of fatty acid methyl/ethyl esters in one hour, which is a relatively short reaction time. Thus, our results suggest that using ethanol or a methanol/ethanol mixture (3:3) to transesterificate chicken oil can be good alternative methods for biodiesel production. Fuel characteristics of methyl esters, ethyl esters, and a mixture of methyl/ethyl esters (3:3) such as density, viscosity, sulphur content, acid value, and flash point were all within the specifications of CNS 15072 and EN 14214.

Currently, our group is working on integrating the two biodiesel production processes along with our previous work on collagen extraction (Lin *et al*., 2013) into a chicken waste biorefinery chain to replace its traditional use as feed and further enhance its added value.

Acknowledgement

This work was supported by National Chung Hsing University.

References

Ahmad, M., Ahmed, S., Hassan, F.U., Arshad, M., Khan, M.A., Zafar, M., & Sultana, S., (2010). Base catalysed transesterification of sunflower oil biodiesel. *Afr. J. Biotechnol*. 9, 8630-8635.

Alptekin, E., & Canakci, M., (2010). Optimization of pre-treatment reaction for methyl ester production from chicken fat. *Fuel*. 89, 4035-4039.

AOAC official method 996.06, (1996). Fat (Total, Saturated, and Unsaturated) in Foods. Hydrolytic Extraction Gas Chromatographic Method.

Arnaud, E., Relkin, P., Pina, M., & Collignan, A., (2004). Characterisation of chicken fat dry fractionation at the pilot scale. *Eur. J. Lipid Sci. Technol*. 106, 591–598.

Arnaud, E., Trystram, G., Relkin, P., & Collignan, A., (2006). Thermal characterization of chicken fat dry fractionation process. *J. Food Eng.* 72, 390-397.

Baião, N.C., & Lara, L.J.C., (2005). Oil and fat in broiler nutrition. *Braz. J. Poultry Sci.* 7, 129-141.

Bianchi, C.L., Bof□to, D.C., Pirola, C., & Ragaini, V., (2010). Low temperature de-acidi□cation process of animal fat as a pre-step to biodiesel production. *Catal. Lett*. 134, 179-183.

Boey, P.L., Maniam, G.P., Hamid, S.A., & Ali, D.M.H., (2011). Crab and cockle shells as catalysts for the preparation of methyl esters from low free fatty acid chicken fat. *J. Am. Oil Chem. Soc*. 88, 283-288.

Canoira, L., Rodríguez-Gamero, M., Querol, E., Alcántara, R., Lapuerta, M., & Oliva, F., (2008). Biodiesel from low-grade animal fat: Production process assessment and biodiesel properties characterization. *Ind. Eng. Chem. Res.* 47, 7997-8004.

CNS 3390, (1972). Method of test for kinematic viscosity of transparent and opaque liquids (and calculation of dynamic viscosity).

CNS 3574, (1973). Method of test for flash point by Pensky-Martens closed cup tester.

CNS 4446, (1978). Method of test for determination of water in petroleum products, lubricating oils, and additives by coulometric Karl Fisher titration.

CNS 13568, (1995). Methods of test for acid value, saponification value, ester value, iodine value, hydroxyl value and unsaponificable matter of chemical products.

CNS 14474, (2000). Method of test for density and relative density of liquids by digital density meter.

CNS 14505, (2001). Method of test for total sulphur in light hydrocarbons, motor fuels and oils by ultraviolet fluorescence.

CNS 14906, (2005). Method of test for acid number of petroleum products by potentiometric titration.

Foglia, T.A., Nelson, L.A., Dunn, R.O., & Marmer, W.N., (1997). Low-temperature properties of alkyl esters of tallow and grease. *J. Am. Oil Chem. Soc.* 74, 951-955.

García, M., Gonzalo, A., Sánchez, J.L., Arauzo, J., & Simoes, C., (2011). Methanolysis and ethanolysis of animal fats: A comparative study of the influence of alcohols. *Chem. Ind. Chem. Eng. Q*. 17, 91-97.

Gugule, S., Fatimah, F., & Rampoh, Y., (2011). The utilization of chicken fat as alternative raw material for biodiesel synthesis. *Animal Production*. 13, 115-121.

Gutiérrez, L.F., Sánchez, Ó.J., & Cardona, C.A., (2009). Process integration possibilities for biodiesel production from palm oil using ethanol obtained from lignocellulosic residues of oil palm industry. *Bioresour. Technol*. 100, 1227-1237.

Hoque, M.E., Singh, A., & Chuan, Y.L., (2011). Biodiesel from low cost feedstocks: The effects of process parameters on the biodiesel yield. *Biomass Bioenergy*. 35, 1582-1587.

Issariyakul, T., Kulkarni, M.G., Dalai, A.K., & Bakhshi, N.N., (2007). Production of biodiesel from waste fryer grease using mixed methanol/ethanol system. *Fuel Process. Technol*. 88, 429-436.

Jeong, G.T., Yang, H.S., & Park, D.H., (2009). Optimization of transesteri□cation of animal fat ester using response surface methodology. *Bioresour. Technol*. 100, 25-30.

Joshi, H., Moser, B.R., & Walker, T., (2012). Mixed alkyl esters from cottonseed oil: Improved biodiesel properties and blends with diesel fuel. *J. Am. Oil Chem. Soc*. 89, 145-153.

Kim, M., Yan, S., Salley, S.O., & Ng, K.Y.S., (2010). Competitive transesteri□cation of soybean oil with mixed methanol/ethanol over heterogeneous catalysts. *Bioresour. Technol*. 101, 4409-4414.

Kondamudi, N., Strull, J., Misra, M., & Mohapatra, S.K., (2009). A green process for producing biodiesel from feather meal. *J. Agric. Food Chem.* 57, 6163-6166.

Kulkarni, M.G., Dalai, A.K., & Bakhshi, N.N., (2007). Transesteri□cation of canola oil in mixed methanol/ethanol system and use of esters as lubricity additive. *Bioresour. Technol*. 98, 2027-2033.

Lam, M.K., & Lee, K.T., (2011). Mixed methanol–ethanol technology to produce greener biodiesel from waste cooking oil: A breakthrough for $SO_4^{2-}/SnO_2–SiO_2$ catalyst. *Fuel Process. Technol*. 92, 1639-1645.

Lebedevas, S., & Vaicekauskas, A., (2006). Use of waste fats of animal and vegetable origin for the production of biodiesel fuel: Quality, motor properties, and emissions of harmful components. *Energy Fuels*. 20, 2274-2280.

Lee, K.T., & Foglia, T.A., (2000). Synthesis, purification, and characterization of structured lipids produced from chicken fat. *J. Am. Oil Chem. Soc*. 77, 1027-1034.

Lee, K.T., & Foglia, T.A., (2000). Fractionation of chicken fat triacylglycerols: Synthesis of structured lipids with immobilized lipases. *J. Food Sci.* 65, 826-831.

Lin, C.W., Loughran, M., Tsai, T.Y., & Tsai, S.W., (2013). Evaluation of convenient extraction of chicken skin collagen using organic acid and pepsin combination. *J. Chin. Soc. Anim. Sic*. 42, 27-38.

Marulanda, V.F., Anitescu, G., & Tavlarides, L.L., (2010). Biodiesel fuels through a continuous flow process of chicken fat supercritical transesterification. *Energy Fuels*. 24, 253-260.

Marulanda, V.F., Anitescu, G., & Tavlarides, L.L., (2010). Investigations on supercritical transesteri□cation of chicken fat for biodiesel production from low-cost lipid feedstocks. *J. Supercrit. Fluid*. 54, 53-60.

Mege, R.A., Manalu, W., Kusumorini, N., & Nasution, S.H., (2006). Pengaruh superovulasi terhadap produksi anak babi. *J. Anim. Prod*. 8, 14-18.

Mittelbach, M., (1996). Diesel fuel derived from vegetable oils, VI: Specifications and quality control of biodiesel. *Bioresour. Technol.* 56, 7-11.

Mutreja, V., Singh, S., & Ali, A., (2011). Biodiesel from mutton fat using KOH impregnated MgO as heterogeneous catalysts. *Renewable Energy*. 36, 2253-2258.

Sridharan, R., & Mathai, I.M., (1974). Transesterification reactions. *J. Sci. Ind. Res.* 22, 178-187.

Wang, Y., Ou, S., Liu, P., & Zhang, Z., (2007). Preparation of biodiesel from waste cooking oil via two-step catalysed process. *Energy Convers. Manage*. 48, 184-188.

Warabi, Y., Kusdiana, D., & Saka, S., (2004). Reactivity of triglycerides and fatty acids of rapeseed oil in supercritical alcohols. *Bioresour. Technol*. 91, 283-287.

Wyatt, V.T., Hess, M.A., Dunn, R.O., Foglia, T.A., Haas, M.J., & Marmer, W.N., (2005). Fuel properties and nitrogen oxide emission levels of biodiesel produced from animal fats. *J. Am. Oil Chem. Soc*. 82, 585-591.

Received 19 December 2013; revised 7 December, 2014

Aggregate and regional demand for electricity in Malaysia

Saeed Solaymani[a]

Sayed Mohammad Bager Najafi[a]

Fatimah Kari[b]

Nurulhuda Binti Mohd Satar[b]

a. Department of Economics, Faculty of Social Science, Razi University, Kermanshah, Iran
b. Department of Economics, Faculty of Economics and Administration, University of Malaya, Kuala Lumpur, Malaysia

Abstract
The main objective of this paper is the analysis of electricity consumption in Malaysia as a whole and its three regions, namely, Peninsular Malaysia, Sabah and Sarawak. This analysis has been carried out using distinguished data in sectoral level for 44 quarters (2000Q1-2010Q4). For this purpose, two log-log static and dynamic panel demand functions are estimated. The dynamic model, which is based on a partial adjustment approach, is used to compare with the static model. The aggregate and the three regional models are estimated based on their economic sectors in both the dynamic and static methods. This study seeks to reveal some features of electricity consumption in Malaysia and its regions. It is found that the short and long- run price elasticities of electricity demand in all regions of Malaysia are inelastic. Consumers' responsiveness to changes in electricity prices in the short-run is low, while they have a high response to the long-run changes in the entire Malaysian economy and its regions. This means that, while the short and long-run price elasticities of electricity demand are lower than one, the magnitudes of the long-run elasticities are greater than the short-run elasticities. Moreover, all elasticities in the dynamic models are smaller than the static models. The estimated short and long-run cross-price elasticities of Liquefied Petroleum Gas (LPG) are negative which suggests that LPG and electricity are complementary goods.

Keywords: electricity, Malaysia, elasticity

1. Introduction

Malaysia consists of thirteen states and three federal territories divided between Peninsular Malaysia (P.M.), which is part of mainland Southeast Asia, East Malaysia consisting of Sabah, and Sarawak, which are located on the northern edge of the island of Borneo. Most of the industries, commercial centres and, especially, the capital and main political centre are located in Peninsular Malaysia. The three differ in many respects such as differences in population, Gross Domestic product (GDP) and its growth, unemployment, level of industrialization and consumption of energy. For example, the Peninsular's GDP share of total GDP of Malaysia averaged 84.3% since 1997, and these shares for Sabah and Sarawak regions are 6.3% and 9.4%, respectively.

The energy demand is a function of the level of industrialization in the region. For instance, since 1997, in both Peninsular Malaysia and Sarawak, the industrial sector has had a high consumption of electricity, followed by the commercial sector. In constant, in Sabah, the reverse is the case, with the commercial sector being the highest electricity consumer, followed by the domestic sector and, in third position, the industrial sector.

Moreover, the average percentage shares of electricity consumption during this period in Peninsular Malaysia, Sabah and Sarawak have been 91.6%, 3.5% and 4.8%, respectively. Empirical evidence has shown that the electricity consumption has a significant impact on the economic growth of Malaysia (Chandran et al., 2010; Lean and Smyth, 2010a, 2010b; Tang, 2008; Tang and Tan, 2013; Yoo, 2006). The demand for elec-

tricity has facilitated Malaysia's overall economic growth while economic development of Malaysia's regions depended upon the availability of electricity supply to stimulate economic growth. Therefore, it is of utmost importance for this study to estimate the demand for electricity in Malaysia as a whole and in its three regions. The major contribution of this study is in applying the dynamic panel data models in Malaysia and its regions. As noted by Bond (2002), estimating the dynamic version of a static model is necessary because ignoring the estimation of the basic dynamic model leads to poor estimation results and significant information might be lost. If a dynamic model is estimated, while the coefficient on the lagged dependent variable is not of interest, dynamics are allowed for in the underlying processes, which are necessary for the recovery of consistent estimates of other parameters.

The reasons that increase the interest to study the demand for electricity in Malaysia are as follows: first, the electricity demand in Malaysia among the five ASEAN founding economies is the second highest, and third highest among all members (Figure 1). The electricity consumption per capita grows rapidly in this country as well as in other ASEAN countries, except for Indonesia and the Philippines. In 2010, the electricity consumption per capita in Malaysia has increased rapidly from 2577kWh per capita in 2000 to 3867kWh per capita. Second, in Malaysia, the electricity intensity, kWh/GDP (Kilowatt hours / 2005 USD), is the second highest among all ASEAN members. In 2010, the electricity intensity for Thailand was 0.67 while it was 0.62 for Malaysia. Third, to the best of the authors' knowledge, only a number of studies have examined demand for electricity in Malaysia such as Bekhet and Othman (2011) and Bazmi *et al*. (2012). Bazmi *et al*. (2012), by applying a Neuro-Fuzzy Network, estimated the demand for electricity in the state of Johor in Malaysia, while Bekhet and Othman (2011) estimated electricity consumption in rural and urban areas using a time series approach over the 1980-2009 period. In addition, the study by Aman *et al*. (2011) employed top-down and bottom-up approaches and thereby forecast demand for electricity in large steel mills industry, whereas Akhwanzada and Tahar (2012) applied a simulation based on system dynamics, and thereby forecast demand for electricity in the whole of the Malaysia economy.

By using a dynamic panel data, this study will differ from other studies on this subject, and by such means will form a significant contribution to the existing literature.

This study differs from previous studies on the subject in two ways. First, it uses both static and dynamic panel data approaches to compare the outcomes of both methods. Brañas-Garza *et al.* (2011) revealed that using a dynamic panel data in terms of experiments allows unravelling new relationships between experimental variables and highlighting new paths in behaviours. Second, despite using recent quarterly data on consumption of electricity, the focus of the paper is to estimate the demand for electricity at the aggregate level of the Malaysian economy and especially in its three regions.

The next section provides a review of literature, section 3 describes the methodology and the data employed. In section 4 the estimation results and their analyses are presented and finally, in section 5, conclusions are provided.

2. Review of literature

Demand for electricity has a strong background in international literature. In the aggregated level of demand for electricity, Amusa *et al* (2009), by using an autoregressive distributed lag (ARDL) method, estimated the aggregate demand for electricity in South Africa during the 1960-2007 period. The findings show that the main determinant of electricity demand in the long-run is only income, while in

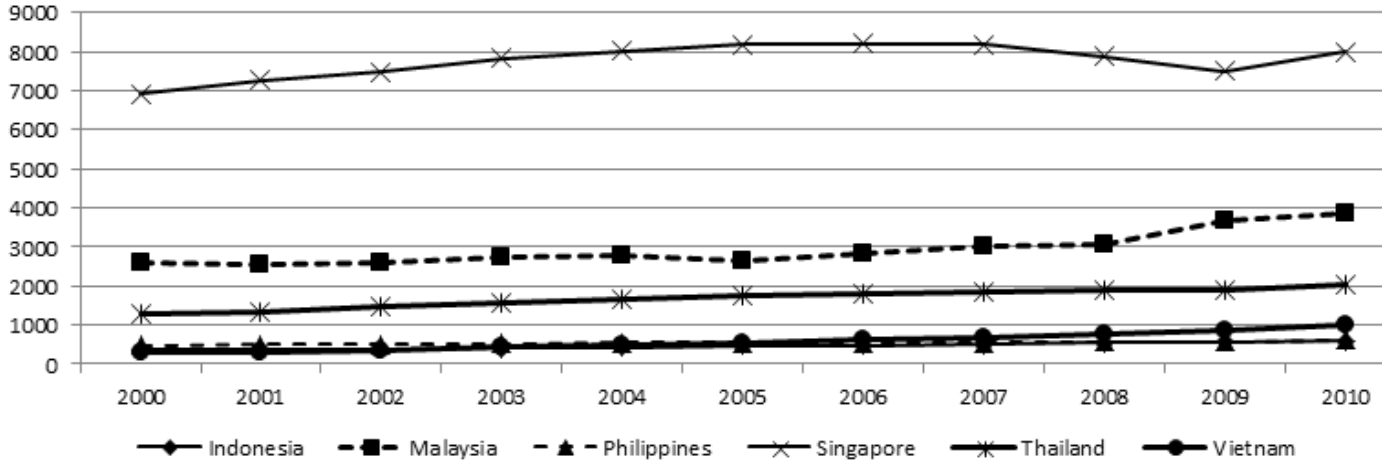

Figure 1: Electricity consumption (KWh) per capita in five ASEAN founding countries
Source: Authors' elaboration with data from EIA, the world band database

the short-run both income and electricity prices are significant. Similarly, Adom *et al.,* (2012), using the ARDL bounds cointegration approach, examined the determinants of electricity demand function in the short and long-run in Ghana during 1975-2005. The results indicate that in the short-run, real per capita GDP, industry efficiency, and degree of urbanization are the main drivers of aggregate domestic electricity demand and long-run price and income elasticities are lower than the short-run estimates. Gam and Rejeb (2012) analysed the aggregated demand for electricity in Tunisia using annual data from 1976 to 2006 in a VAR method. The empirical findings suggest that in the long-run the price of electricity has a negative effect on electricity consumption, while the GDP and the past value of electricity consumption have positive effects. Amarawickrama and Hunt (2008) also examined the electricity demand for Sri Lanka by applying six econometric techniques (Static Engle and Granger method, Dynamic Engle and Granger method, Fully modified ordinary least squares method, Pesaran, Shin and Smith method, Johansen method, and Harvey approach). They found that the range of long-run income elasticity is from 1.0 to 2.0 and price elasticity is from 0 to -0.06. Therefore, the main determinants of electricity demand are GDP and prices of electricity with different methods, also long-run income and price elasticities are greater than those of the short-run.

Dilaver and Hunt (2011a) by applying the structural time series model to annual data over the period from 1960 to 2008 and Halicioglu (2007), using the bounds testing procedure to cointegration during 1968-2005, found that the long-run income and price elasticities of the residential electricity demand in Turkey are greater than the short-run elasticities. Ziramba (2008) applied the bounds testing approach to cointegration analysis to estimate residential electricity demand in South Africa during the 1978-2005 period. The results indicated that income is the main determinant of electricity demand in the short and long-run, while electricity price is insignificant.

In the industrial and manufacturing sectors, there are a number of studies on electricity demand in developing countries. For example, Dilaver and Hunt (2011b) estimated the demand function for the industrial sector using the structural time series technique over the 1960-2008 period. Their results show that both industrial output and price elasticities have a significant impact on electricity consumption and are inelastic in the long-run. Bölük and Koc (2010) estimated four demand functions for four production factors, namely capital, labour, intermediate input and electricity, using a translog cost function over the 1980-2001 period. The results indicate that the price of electricity is inelastic and electricity-labour and electricity-capital inputs are complementary.

Therefore, it can be concluded that the price of electricity and income are the main determinants of electricity demand functions with different methodologies and their long-run elasticities are greater than the short-run. As the literature shows, applying dynamic panel data to estimate the electricity demand in developing countries is a new method which is used in this study, while it has been used in many studies in developed economies such as Alberini and Filippini (2011), Filippini (2011), Alberini *et al.,* (2011) and Leesombatpiboon and Joutz (2010).

3. The models and the data

3.1. The model

The production function of the composite energy commodity, *E*, is a function of electricity consumption, *Ec*, and capital stock of appliances, *K*, as follows (Filippini, 1999; 2011):

$$E = E\,(Ec,K) \tag{1}$$

We also assumed that the consumer has a utility function with the usual properties of differentiability and curvature. The consumer utility is a function of the composite energy commodity, *E,* and aggregate consumption of good *X* that directly yields a utility. The utility function is influenced by other variables, *D,* such as household characteristics, weather and geographic characteristics which is illustrated by equation (2).

$$U = U\,(E\,(Ec, K), X; D) \tag{2}$$

The consumer is then assumed to maximize its utility subject to the equation (1) and the budget constraint,

$$I = P_E.E + P_X.X \xrightarrow{P_X = 1} I - P_E.E - 1.X = 0 \tag{3}$$

Where *I* is income, is the price of the composite energy commodity, and is the price of composite numeraire good *X*. (For more details of consumer production theory to electricity demand analysis see Filippini (1999) and Francisco (1988).)

Finally, the demand functions for electricity and capital stock can be obtained as:

$$Ec^* = Ec^*(P_{Ec}, P_K, I; D) \tag{4}$$

$$K^* = K^*(P_{Ec}, P_K, I; D) \tag{5}$$

According to Filippini (2011), equations (4) and (5) show the long-run equilibrium of the consumers. This model is static in that it assumes instant adjustment in the equipment stock to variations in electricity demand, so that the short and long-run elasticities are similar.

Based on equation (4), along with available data and using a log-log functional form, the following static empirical model of electricity demand can be specified as:

$$LnEc_{it} = \beta_0 + b1LnEpit + \beta_2 LnGDPper_c + \beta_3 LnGDPp_{it} + \varepsilon_{it} \quad (6)$$

Where, the consumption of electricity, *Ec*, is a function of real price of electricity, *Ep*, per capita gross domestic product, *GDPper (GDP by sector / number of electricity consumers)*, and the real price of Liquefied Petroleum Gas, LPGp, as a complimentary good. Filippini and Pachauri (2004) and Athukorala and Wilson (2010) used LPG prices in their models to test the hypothesis of whether this fuel is complimentary to or substitutes for electricity. All variables are measured in logarithm.

The subscript *i* denotes economic sectors, namely residential, commercial, industrial, and mining in both models for aggregate and Peninsular Malaysia electricity demand. Since mining is not a major consumer of electricity in Sabah and Sarawak, it is not included in the models for Sabah and Sarawak. The subscript *t* denotes the duration of data (2000Q1-2010Q4).

The sign for *LnEp* is expected to be negative following the demand theory. On the other hand, an increase in income is expected to increase the demand for electricity on the assumption that it is a normal good. Therefore, the sign of GDP is positive. The sign of *LPGp* nonetheless depends on how consumers perceived the use of LPG, whether it is complementary or substitute to electricity. For the case of Malaysia, the initial expectation for the sign on LPGp is negative since LPG and electricity are often consumed together, one of them for lighting and use in electrical instrument and another for heating. Since all variables are logarithmic values, the coefficients of them can be directly interpreted as demand elasticities.

It is equally vital to consider that the actual consumption of electricity may differ from the long-run equilibrium consumption, because the equipment stock may not be able to adjust easily to the long-run equilibrium. To cope with this situation, researchers normally make use of a partial adjustment as suggested by Houthakker *et al*. (1974), Berndt and Samaniego (1984), Filippini (2011), and Alberini and Filippini (2011). This model assumes that the actual change between time periods *t* and *t-1* in the quantity of electricity consumption- which is demanded- is equal to a fraction, λ, of the long-run change. Formally,

$$LnEc_t - LnEc_{t-1} = \lambda(LnEc_t^* - LnEc_{t-1}) \ , \ 0 < \lambda \leq 1 \quad (7)$$

Where $(LnEc_t - LnEc_{t-1})$ is the actual change, and $(LnEc_t^* - LnEc_{t-1})$ is the desired change.

The dynamic versions of the electricity demand model can be specified by combining equations (6) and (7). The equation (6) can be rewritten as:

$$LnEc_{it} = \lambda\beta_0 + \lambda\beta_1 LnEp_{it} + \lambda\beta_2 LnGDPper_{it} + \lambda\beta_3 LnLPGp_{it} + (1-\lambda)LnEc_{it-1} + \lambda\varepsilon_{it} \quad (8)$$

Summarizing the coefficients, the dynamic model can be declared as:

$$LnEc_{it} = \alpha_0 + \alpha_1 LnEc_{it-1} + \alpha_2 LnEp_{it} + \alpha_3 LnGDPper_{it} + \alpha_4 LnLPGp_{it} + \varepsilon_{it} \quad (9)$$

Where, Ec_{t-1} is electricity consumption in the previous period (t-1). It is expected that the sign of this variable will be positive, because the consumption of the previous period has a positive impact on current consumption due to economic growth.

To estimate the dynamic equation derived from a partial adjustment approach, this study used a dynamic panel data method in order to take account of the correlation of the lag of electricity consumption with the error term in the right side of the equation 6.

As noted by Berndt and Samaniego (1984) and Alberini and Filippini (2011), short-run price and income elasticities based on equation (8) are constant and equal to:

$$\in_p^{SR} \equiv \frac{\partial LnEc_{it}}{\partial LnEp_{it}} = \lambda\beta_1 \quad (10)$$

$$\in_{GDPper}^{SR} \equiv \frac{\partial LnEc_{it}}{\partial LnGDPper_{it}} = \lambda\beta_2 \quad (11)$$

And accordingly, the cross-price elasticity can be written as below:

$$\in_{LPGp}^{SR} \equiv \frac{\partial LnEc_{it}}{\partial LnLPGp_{it}} = \lambda\beta_3 \quad (12)$$

When the processing of the capital stock adjustment has been completed, the corresponding long-run elasticities are:

$$\in_p^{LR} = \beta_1 \ , \ \in_{GDPper}^{LR} = \beta_2 \ \text{and} \ \in_{LPGp}^{LR} = \beta_3$$

3.2. The data

The data for all variables in this study are quarterly data from the first quarter of the year 2000 to the fourth quarter of the year 2010 and comes from all three regions of Malaysia. The data on electricity consumption and real prices of electricity by states and sectors are collected from both the National Energy Balances and the Energy Commission of Malaysia. Household expenditure, GDP, and population data by states and activities are gathered from

the Department of Statistics, and the website of the Economic Planning Unit.

Real LPG prices by states are collected from the Economic Planning Unit website and the databank of the Bernama Library & Infolink Service (BLIS) website. The electricity consumption data is measured in terms of Kilowatt hours (kWh), the value of the GDP in terms of Million Malaysian Ringgit (RM) and, finally, the scales of real prices of electricity and LPG are in terms of Ringgit per kWh and Ringgit per litre, respectively.

4. Econometric methodology and estimation results

4.1. Econometric approach

We estimate equations (6) and (9) for a static and dynamic model, respectively. Since in the dynamic models one of the explanatory variables is the lagged dependent variable and leads to correlation with the error term, we follow Arellano and Bond (1991) and Arellano and Bover's (1995) approach based on the Generalized Method of Moments (GMM) approach which produces less biases.

The current study is based on T= 44 and N= 3 or 4 (as '*i*' defined in section 4.1), and the dynamic panel models are estimated using the system GMM estimator. The panel root test was deployed based on Levin-Lin-Chu test. Table 1 reports the Levin-Lin-Chu t-test statistics along with the p-values.

4.2. Panel unit root test

The Levin-Lin-Chu t-test statistics along with the p-values are presented in Table 1. The p-values of this table show that the joint unit root null hypothesis for all variables at the 5 percent level of significance are rejected. This means that all variables are integrated in order of one and are stationary.

4.3. The estimation and the results

4.3.1. Results of the static model

The results of the static models from the demand function (6) are presented in Table 2. We add a dummy variable to take into account any structural break after the 2008 financial crisis. The results of Hausman specification tests show that in the aggregate model and the Sabah model the null hypothesis has been rejected. This means that there is no correlation between the individual effects and the explanatory variables in these models but, in the two other regions, namely, Peninsular Malaysia and Sarawak, the random effect estimators are consistent, and the null hypothesis has not been rejected. Because of a small difference between these two models and their random effect' estimations, only the fixed effect' estimations of these models are reported in Table 2.

The results of the aggregate model show that the coefficients of all variables are significant and have the expected signs. Since all regions experience instability in their electricity consumption during the

Table 1: Levin-Lin-Chu's panel unit root test results for all models
Source: Research results

Variable	*Unadjusted t*	*Adjusted t**	*Panel means (constant term)*	*Time trend*	*Lags*	*P-value for adjusted t**
Levin-Lin-Chu Unit-Root Test for Aggregate Model						
LnEc	-10.4966	-8.1143	Included	Included	1	0.0000
LnEp	-10.1291	-5.8194	Included	Included	1	0.0000
LnGDPper	-19.9001	-17.7000	Included	Included	1	0.0000
LnLPGp	-5.6870	-2.4534	Included	Included	1	0.0071
Levin-Lin-Chu Unit-Root Test for P.M. Model						
LnEc	-10.0851	-7.6498	Included	Included	1	0.0000
LnEp	-12.3286	-8.4516	Not Included	Not Included	1	0.0000
LnGDPper	-5.7869	-2.7672	Included	Included	1	0.0028
LnLPGp	-5.8088	-2.6458	Included	Included	1	0.0041
Levin-Lin-Chu Unit-Root Test for Sabah Model						
LnEc	-12.6455	-10.3607	Included	Included	1	0.0000
LnEp	-4.6418	-2.3762	Included	Included	1	0.0000
LnGDPper	-17.2340	-15.3286	Included	Included	1	0.0000
LnLPGp	-4.7858	-1.6705	Included	Included	2	0.0474
Levin-Lin-Chu Unit-Root Test for Sarawak Model						
LnEc	-12.5298	-10.0066	Included	Included	1	0.0000
LnEp	-5.4610	-2.7130	Included	Included	1	0.0033
LnGDPper	-17.2340	-15.3286	Included	Included	1	0.0000
LnLPGp	-5.0306	-2.2914	Included	Included	1	0.0110

Table 2: Static models, the estimation results of LSDV approach (dependent variable LEc)
Source: Research results

Variables	*Aggregate model*		*P.M. model*		*Sabah model*		*Sarawak model*	
	Coef.	*t-Stat.*	*Coef.*	*t-Stat.*	*Coef.*	*t-Stat.*	*Coef.*	*t-Stat.*
LnEp	-0.61*	-3.54	-0.23	-1.38	-0.41*	-3.74	-0.61*	-6.95
LnLPGp	-0.75*	-2.53	-0.43	-1.38	-0.50*	-2.60	-0.13	-0.85
LnGDPper	0.99*	7.92	1.08*	8.17	1.86*	20.13	1.35*	17.82
Yr2008	-0.19*	-3.5	-0.12*	-2.16	-0.13*	-2.96	-0.12*	-4.25
Constant	8.46*	4.55	10.36*	5.08	0.94	0.94	6.89*	6.98
Sample size	176		176		132		132	
R^2 within	0.37		0.31		0.86		0.88	
R^2 between	0.16		0.15		0.50		0.69	
R^2 overall	0.22		0.23		0.63		0.77	
Prob. of F-test for all u_i's	0.00		0.00		0.00		0.00	
Hausman's specification test	62.66†		0.56		67.22†		0.19	

** Significant at 5 percent level*
*** Significant at 10 percent level*
† Rejection of Null Hypothesis (Random Effect (RE) estimator is consistent) at 5 percent level of significant

time, the low R-sq. for the aggregate and P.M. models might be due to the fact that the electricity consumption in Malaysia depends more significantly on other variables such as government electricity and energy subsidies, population, consumption of other fuels and their prices, weather temperature and so on. However, there are many studies in the literature which have low levels of R-square. For example, Filippini (2011), Alberini and Filippini (2011), Alberini *et al*., (2011), Swadley and Yucel (2011), Gans *et al,*. (2013) found low values of R-sq in their static models. Therefore, in the whole of the economy, both the own-price elasticity and the per capita income are inelastic in the short-run.

According to the results of the regional estimates, the coefficients of electricity price in all three regions, except for P.M., are significant. The price elasticities of demand for electricity, in all regional models as well as the aggregated model, are inelastic. In all regional models, the income elasticities are greater than one and reveal that the electricity is a luxury good. However, the income elasticity of the aggregated model is less than one and shows that the electricity, in general, is a necessary good in Malaysia. In other words, the electricity consumption in the Malaysian regions reflects a strong reflect to the economic growth in those regions. The magnitude of the coefficients of own price of electricity, LPG price and per capita GDP for the P.M. model are smaller than all other models. This means that if each one of these variables changes one percent, the magnitude of the change in electricity demand in Peninsular Malaysia is less than the other regions and models. The negative values of the LPG price elasticities suggest that Liquefied Petroleum Gas (LPG) is a good complement commodity for electricity in Sabah and in the whole of the country. In comparison with the previous studies, this finding is similar to the Filippini and Pachauri (2004) study, but is inconsistent with Athukorala and Wilson (2010). This coefficient in Peninsular Malaysia and Sarawak models has a negative sign but an insignificant value. Furthermore, the coefficients of the dummy variable in all models are negative and significant and show that the financial crisis year has influenced the consumption of electricity in Malaysia and its regions.

4.3.2. Results of the dynamic model

Table 3 represents the estimated results of the dynamic equation (9) for the aggregate and regional models. The coefficients of the variables show that all variables have the expected signs. While the elasticities of electricity prices and LPG prices in all dynamic models are smaller than the static models, they are inelastic like the static models and have negative effects on demand for electricity. The elasticities of per capita income also are inelastic in all dynamic models, whereas they are elastic in all static models, except the aggregate model. In all dynamic models, the coefficients of the dummy variables are also smaller than the static models. These findings show that in the dynamic models the sensitivity of consumers to the shocks, which may acquire in the economy, are less than the static models.

The long-run own price and cross price elasticities are obtained and their results are reported in Table 4. The elasticity estimates suggest that consumers are more responsive to price and income

Table 3: Dynamic panel-data estimation results, difference one step GMM (dependent variable LEc)
Source: Research results

Variables	*Aggregate Model*		*P.M. Model*		*Sabah Model*		*Sarawak Model*	
	Coef.	*z-Stat.*	*Coef.*	*z-Stat.*	*Coef.*	*z-Stat.*	*Coef.*	*z-Stat.*
LagLEc	0.79*	26.51	0.81*	27.84	0.62*	26.9	0.54*	15.92
LnEp	-0.02*	-2.82	-0.02*	-2.95	-0.06	-1.40	-0.05	-0.85
LnLPGp	-0.39*	-3.16	-0.41*	-3.28	-0.03	-0.48	-0.24*	-2.9
LnGDPper	0.61*	10.95	0.62*	10.72	0.93*	20.27	0.96*	20.42
Yr2008	-0.09*	-4.03	-0.09*	-3.84	-0.03*	-2.32	-0.08*	-5.32
Sample size	168		168		126		126	
Arellano-Bond test AR(1)	-4.30		-4.28		-2.46		-3.14	
Arellano-Bond test AR(2)	-2.22		-2.30		-5.85		-2.82	
Sargan test of overid.	191.07		187.25		137.19		177.81	
Prob. of Wald chi2(5)	0.00		0.00		0.000		0.00	

, Signficant at 5% and 10% level*

Table 4: Short-run and long-run elasticities in the dynamic model
Source: Research results

		Aggregate	*P.M.*	*Sabah*	*Sarawak*
Short run	Own price elasticity	-0.02	-0.02	-0.06	-0.05
	Cross price elasticity of LPG	-0.39	-0.41	-0.03	-0.24
	Income elasticity	0.61	0.62	0.93	0.96
Long run	Own price elasticity	-0.10	-0.11	-0.16	-0.11
	Cross price elasticity of LPG	-1.86	-2.16	-0.08	-0.52
	Income elasticity	2.90	3.26	2.45	2.09

changes in the long run, exactly as predicted by economic theory.

The estimated short-run own price elasticity in both the regional and the aggregate model are almost similar to elasticity estimates reported by Berndt and Samaniego (1984). The long-run elasticities for own and cross prices are varied where the long-run elasticities of real prices of electricity and LPG and income are greater than their corresponding values in the short-run implying that consumption, in the long run, is more responsive to changes in economic variables.

The long-run elasticities for own and cross prices are varied. However, the long-run elasticities of real prices of electricity, LPG and income are greater than their corresponding values in the short-run. These results are consistent with economic theory in which consumption, in the long run, is more responsive to changes in economic variables than in the short run. In the context of this study, electricity demand behaviour in the Malaysia' economy is consistent with standard economic predictions. In both short and long-run, the price elasticity of electricity for P.M. is smaller than other regions. It means that the responsiveness of those people that live in the Peninsular region and a change in electricity prices is less than the other regions.

5. Conclusion

This study estimates the aggregate and regional demand functions for electricity in Malaysia using quarterly data from 200Q1 to 2010Q4. For this purpose, an aggregate demand model for the whole of Malaysia and three regional models for each one of the regions of this country, namely Peninsular Malaysia, Sabah and Sarawak, were estimated using both static and dynamic panel data methods.

The empirical results have highlighted some characteristics of Malaysia in the aggregate level and its regions. The results from the static model show that the prices of electricity and LPG in all models are inelastic, while the income is elastic and its coefficients differs from 1 to 1.86. In contrast, in the dynamic models all coefficients of the real prices of electricity and LPG as well as per capita income are inelastic and smaller than their corresponding coefficients in the static models. In addition, the long-run elasticities for electricity prices, LPG prices and income are greater than the short-run ones. Therefore, in the short-run, consumer reactions to increasing the prices and income are relatively small, while this reaction has increased in the long-run. Furthermore, the negative values of the short and the long-run cross-price elasticities of LPG show that LPG and electricity are complementary

goods.

The negative impacts and low-elasticities of the LPG prices indicate that the cross-price elasticities have important implications for policy makers. It suggests that increasing the price of electricity leads to an increase in the price of LPG. However, this impact is different in both the short and long-run from region to region. Given this, the complementary commodities, at least in the long-run, cannot be effective tools for achieving electricity conservation through raising the prices of these goods. In contrast, policy prices on substitution commodities such as natural gas, also peak and off-peak electricity price policy can be effective tools for electricity conservation. Nevertheless, the government regulatory structure of the electricity sector may impede any move to use prices as a mechanism to utilize the resources in an efficient manner. This has a significant implication in terms of the equity and distribution aspect of subsiding energy sectors in Malaysia. As such, this should be the future direction of research in terms of how the regulation on electricity price and tariff affects the economic well-being of the consumers across all sectors. In order to use electricity in an effective manner, we suggest rationalization of electricity tariffs in Malaysia and other countries. We suggest using general equilibrium models to find the impacts of this policy on a certain section of an economy, because these models have a potential structure to trace the impacts of government policies on the economy and the welfare of poor as well done by Solaymani and Kari (2013), Solaymani *et al.* (2014a) and Solaymani *et al*. (2014b) for Malaysia.

References

Adom, P.K., Bekoe, W., and Akoena, S.K.K., (2012). Modelling aggregate domestic electricity demand in Ghana: An autoregressive distributed lag bounds cointegration approach. *Energy Policy,* 42, 530-537.

Akhwanzada, S.A., and Tahar, R.M., (2012). Strategic Forecasting of Electricity Demand Using System Dynamics Approach. *International Journal of Environmental Science and Development*, 3(4), 328-333.

Alberini, A., and Filippini, M., (2011). Response of residential electricity demand to price: The effect of measurement error. *Energy Economics*, 33 (5), 889-895.

Alberini, A., Gans, W., and Velez-Lopez, D., (2011). Residential consumption of gas and electricity in the U.S.: The role of prices and income. *Energy Economics*, 33(5), 870-881.

Aman, S., Ping, H.W., and Mubin, M., (2011). Modelling and forecasting electricity consumption of Malaysian large steel mills. *Scientific Research and Essays*, 6 (8), 1817-1830.

Amarawickrama, H., and Hunt, L.C., (2008). Electricity Demand for Sri Lanka: A time series analysis. *Energy*, 33, 724-739.

Amusa, H., Amusa, K., and Mabugu, R., (2009). Aggregate demand for electricity in South Africa: An analysis using the bounds testing approach to cointegration. *Energy Policy*, 37(10), 4167-4175.

Arellano, M., and Bond, S.R., (1991). Some tests of specification for panel data: Monte Carlo evidence and an application to employment equations. *Review of Economic Studies*, 58, 277-297.

Arellano, M., and Bover, O., (1995). Another look at the instrumental variable estimation of error-components models. *Journal of Econometrics*, 68, 29-51.

Athukorala, P.P.A.W., and Wilson, C., (2010). Estimating short and long-term residential demand for electricity: New evidence from Sri Lanka. *Energy Economics*, 32, S34-S40.

Bazmi A.A., Davoody, M., and Zahedi, G., (2012). Electricity Demand Estimation Using an Adaptive Neuro-Fuzzy Network: A Case Study from the State of Johor, Malaysia. *International Journal of Chemical and Environmental Engineering*, 3 (4), 284-295.

Bekhet, H.A., and Othman, N.S., (2011). Assessing the Elasticities of Electricity Consumption for Rural and Urban Areas in Malaysia: A Non-linear Approach. *International Journal of Economics and Finance*, 3 (1), 208-217.

Berndt, E.R., and Samaniego, R., (1984). Residential electricity demand in Mexico: a model distinguishing access from consumption. *Land Economics*, 60 (3), 268-277.

Bölük, G., and Koç, A.A., (2010). Electricity demand of manufacturing sector in Turkey: A translog cost approach. *Energy Economics*, 32, 609-615.

Bond, S., (2002). Dynamic panel data models: a guide to microdata methods and practice, CeMMAP Working papers CWP09/02, Centre for Microdata Methods and Practice, Institute for Fiscal Studies.

Brañas-Garza, P., Bucheli, M., and Garcia-Muñoz, T., (2011). Dynamic panel data: A useful technique in experiments. Universidad de Granada, Working papers, 10-22.

Chandran, V.G.R., Sharma, S., and Madhavan, K., (2010). Electricity consumption-growth nexus: the case of Malaysia. *Energy Policy*, 38(1), 606-612.

Dilaver, Z., and Hunt, L.C., (2011a). Modelling and forecasting Turkish residential electricity demand. *Energy Policy*, 39 (6), 3117-3127.

Dilaver, Z., and Hunt, L.C., 2011b. Industrial electricity demand for Turkey: A structural time series analysis. *Energy Economics*, 33 (3), 426-436.

Erdogdu, E., (2007). Electricity demand analysis using cointegration and ARIMA modelling: A case study of Turkey. *Energy Policy*, 35, 1129-1146.

Filippini, M., (1999). Swiss residential demand for electricity. *Applied Economics Letters*, 6 (8), 533-538.

Filippini, M., (2011). Short- and long-run time-of-use price elasticities in Swiss residential electricity demand. *Energy Policy*, 39 (10), 5811–5817.

Filippini, M., and Pachauri, S., (2004). Elasticities of electricity demand in urban Indian households. *Energy Policy*, 32, 429-436.

Francisco, C.R., (1988). Demand for electricity in the Philippines: implications for alternative electricity pricing policies. The Philippine Institute for Development Studies, 1988.

Gam, I., and Rejeb, J.B., (2012). Electricity demand in Tunisia. *Energy Policy,* 45, 714-720.

Gans, W., Alberini, A., and Longo, A., (2013). Smart meter devices and the effect of feedback on residential electricity consumption: Evidence from a natural experiment in *Northern Ireland. Energy Economics* 36, 729-743.

Halicioglu, F., (2007). Residential electricity demand dynamics in Turkey. *Energy Economics*, 29, 199-210.

Houthakker, H.S., Verleger, P.K..J., and Sheehan, D.P., (1974). Dynamic Demand Analyses for Gasoline and Residential Electricity. *American Journal of Agricultural Economics*, 56(2), 412-418.

Lean, H. H., and Smyth, R., (2010a). On the dynamics of aggregate output, electricity consumption and exports in Malaysia: Evidence from multivariate Granger causality tests. *Applied Energy*, 87, 1963-1971.

Lean, H.H., and Smyth, R., (2010b). Multivariate Granger causality between electricity generation, exports, prices and GDP in Malaysia. *Energy*, 35 (9), 3640-3648.

Leesombatpiboon, P., and Joutz, F.L., (2010). Sectoral demand for petroleum in Thailand. *Energy Economics* 32, S15–S25.

Solaymani S, Kardooni, R., Kari, F., and Yusoff, S., (2014a). Economic and environmental impacts of energy subsidy reform and oil price shock on the Malaysian transport sector. Travel Behaviour and Society. DOI 10.1016/j.tbs.2014.09.001

Solaymani S, Kari F, and Hazli R., (2014b). Evaluating the role of subsidy reform in addressing poverty level in Malaysia: A CGE poverty framework. *Journal of Development Studies,* 50 (4), 556-569.

Solaymani S, and Kari F., (2013). Environmental and economic effects of high petroleum prices on transport sector. *Energy*, 60, 435-441. http://dx.doi.org/10.1016/j.energy.2013.08.037

Swadley, A., and Yucel, M., (2011). Did residential electricity rates fall after retail competition? A dynamic panel analysis. Energy Policy, 39, 7702–7711.

Tang, C.F., (2008). A re-examination of the relationship between electricity consumption and economic growth in Malaysia. *Energy Policy*, 36 (8), 3077-3085.

Tang, C.F., and Tan, E.C., (2013). Exploring the nexus of electricity consumption, economic growth, energy prices and technology innovation in Malaysia. *Applied Energy*, 104, 297-305.

Yoo, S.H., (2006). The causal relationship between electricity consumption and economic growth in the ASEAN countries. *Energy Policy*, 34 (18), 3573-3582.

Ziramba, E., (2008). The demand for residential electricity in South Africa. *Energy Policy,* 36, 3460-3466.

Received 7 November 2013, revised 21 December 2014

Optimization analysis of solar-powered average temperature Stirling heat engine

Khaled M Bataineh
Department of Mechanical Engineering, Jordan University of Science and Technology, Irbid, Jordan

Abstract
This paper investigates the performance of the solar powered dish-Stirling engine using the non-linearized heat loss model of the solar dish collector and the irreversible cycle model of the Stirling engine. Finite time thermodynamic analysis is used to investigate the influence of the finite-rate heat transfer, operating temperatures, heat leak coefficient, and ratio of volume during regeneration processes, regenerator losses, thermal bridges losses on the maximum power output and the corresponding overall efficiency. The maximum overall system efficiency is 32% corresponding to absorber temperature and concentrating ratio of 850 K and 1300, respectively. The present analysis provides the basis for the design of a solar-powered mean temperature differential Stirling engine powered by solar dish system.

Keywords: Stirling engines, finite time thermodynamic, thermal losses, performance, regenerator effectiveness, numerical simulations.

Nomenclature

A	area, m^2
C	collector concentration ratio
C_v	specific heat capacity, J mol^{-1} k^{-1}
K_o	heat leak coefficient, W K^{-1}
h	heat transfer coefficient, WK^{-1} or WK^{-4}
I	direct solar flux intensity, Wm^{-2}
n	the mole number of the working fluid, mol
M	regenerative time constant, K s^{-1}
P	power, W
Q	heat transfer, J
q_u	heat gain, W
R	gas constant, J mol^{-1} k^{-1}
t	time, s
W	work, W
λ	ratio of volume during regenerative
τ	cyclic period, s
η	thermal efficiency
ε	emissivity factor
σ	Stefan's constant, W m^{-2} K^{-4}
x	effectiveness of the regenerator

Subscripts

b	absorber
HC	high temperature side convection
HR	high temperature side radiation
L	heat sink
LC	low temperature side convection
m	the system
R	regenerator
t	Stirling engine
o	process ambient or optics
1-4	the processes

1. Introduction

Solar energy is one of the most attractive renewable energy sources. Stirling heat engines convert heat energy into mechanical energy. Stirling engines work with an external heat supply. This makes them more reliable with lower maintenance requirements and their operation is relatively silent. Moreover, they can operate using low quality fuels and they can also use heat sources that do not depend on any combustion. The working gas can be maintained within the engine and need not be changed between the cycles. The fact that Stirling engines are driven by an external heat supply makes them appropriate for solar thermal applications. Furthermore, as they can combine different heat sources in one application, they are also appropriate for hybrid operations.

In a dish-Stirling system, a dish collector may be used to focus solar energy to supply power. The dish-Stirling system is comprised a parabolic dish collector and a Stirling heat engine. The resulting

conversion unit is relatively small compared to other CSP systems. Among the three well- known and established concepts of CSP (Parabolic trough power plants, solar tower power plants, and dish-Stirling systems) the dish-Stirling system has achieved the highest efficiency (Mancini and Heller, 2003; Sahin, 2001).

The first solar application of the Stirling engine is attributed to the Swedish-American inventor and mechanical engineer John Ericsson, who built the dish -Stirling device in 1872 Ericsson invented a solar-powered hot air engine using a reflector to heat the displacer cylinder hot-end. The modern dish-Stirling technology was developed in the late 1970s and in the early 1980s. Eight different dish-Stirling systems, ranging in size from 2 to 50 kW, have been built during the last 20 years (Mancini and Heller, 2003). The dish - Stirling energy system has the highest efficiency for converting solar energy into electricity. A parabolic dish concentrates only the direct radiation that enters the system parallel to its optical axis. So, the solar dish has to be oriented always towards the Sun. As it is a point-concentrating system, it requires two-axes tracking. A point-concentrating system offers the possibility of having very high concentration ratios compared to line- concentration system. With these point-concentrating systems the high concentration ratios result in high receiver temperatures. Receiver temperatures above 800°C have been achieved. Such high operating temperatures allow for a high thermal-mechanical energy conversion efficiency and, consequently, high solar-to-electric efficiencies. Nevertheless, under typical conditions, they have an average solar-to-electric efficiency between 16 and 25% (Mohr et al., 1999).

Finite time finite temperature difference thermodynamics deals with the fact that there must be a finite temperature difference between the working fluid/substance and the source/sink heat reservoirs (with which it is in contact) in order to transfer a finite amount of heat in a finite time interval. It is a modern powerful tool used for performance analysis of practical engineering cycles. Finite time thermodynamic originated with two independently published papers in 1957 (Chambadal, 1957; Novikov, 1957) and regained its popularity with another independent publication in 1975 by Curzon et al., (1975). Curzon et al. established a theoretical model of a real Carnot heat engine at maximum power output with a different efficiency expression from the well-known Carnot efficiency. Following that, several successful performance analyses and designs of dish – Stirling engine have been carried out during the past thirty years using finite time thermodynamic (Ladas and Ibraham, 1994; Popescu et al., 1996; Chen et al., 1998 Wu, 1998) to name a few. The results obtained by using finite time thermodynamic have even more realistic instructive significance for the optimal design of real solar-driven systems than those derived from traditional equilibrium thermodynamics. Analysing power, specific power and power density optimization of endoreversible and irreversible Stirling engine, and analysing the effect of heat transfer law and quantum characteristics of the working fluid on the Stirling engine performance have received significant attention be many researchers. Ibrahim et al. introduced the finite time analysis to the dynamic performance optimization of Stirling engines (Ladas and Ibrahim, 1994). They analyzed the Stirling engine cycle based on mass and energy balances with associated heat-transfer-rate equations. They concluded that there exists an optimum power output for a given engine design, based on engine speed and heat-transfer contact time. Radcenco and Popescu investigated the power optimization and the optimal distribution of heat transfer area of endoreversible and irreversible cycle with various laws (Popescu et al, 1996). Chen et al. investigated the performance of a solar-driven Stirling engine based on the linearized heat loss model of the solar collector and the irreversible cycle model of the Stirling engine (Chen et al, 1998). They pointed out that their method is valid for other heat loss models of solar collectors and the results obtained are also valid for a solar-driven Ericsson engine system using an ideal gas as its engine work substance .Wu et al. (1998) investigated the effects of heat transfer, regeneration time, and imperfect regeneration on the performance of the irreversible Stirling engine cycle. The results of their work provide a new theoretical basis for evaluating performance and improving Stirling engines. Kaushik and Kumar (2000) investigated the performance of an endoreversible Stirling heat engine using finite time thermodynamics. They found that an endoreversible Stirling heat engine with an ideal regenerator ($\varepsilon R=1.00$) has an efficiency that is equal to the efficiency of an endoreversible Carnot heat engine. Yan and Chen (1997) studied the optimal performance of an endoreversible cycle operating between a finite heat source and sink. Sahin (2001) investigated the optimum operating conditions of endoreversible heat engines with radiation and convection heat transfer between the heat source and working fluid as well as convection heat transfer between the heat sink and the working fluid based on simultaneous processes. Senft (1998) studied the theoretical limitations on the performance of a Stirling engine subject to limited heat transfer, external thermal and mechanical losses. The performance analysis and optimization of low temperature differential Stirling heat engines powered by low concentrating solar collectors have been conducted (Chen et al., 1998; Costea et al., 1999; Kongtragool and Wongwises (2003); Kongtragool and Wongvises, (2005); Shahrir et al., 2005; Jose, 2007).

Berchowitz et al. established several analyses and simulation methods of the engine (Costea et al., 1999). Kongtragool and Wongvises (2003) found a feasible solution which may lead to a preliminary conceptual design of a workable solar-powered low temperature differential Stirling engine. Results indicated that Stirling engines working with relatively low temperature air are potentially attractive engines of the future. Shahrir et al. (2005) presented a design of a low temperature differential double-acting Stirling engine for solar application. They concluded that there are optimal values of engine speed and swept volume and determined the critical engine parameters. Arenas (2007) described the design, manufacture and testing of a new portable solar kitchen with a large, parabolic solar reflector that folds up into a small volume. He found that the solar kitchen reaches an average power measurement of 175 W, with an energy efficiency of 26.6%. Li et al. (2011) developed a mathematical model of overall thermal efficiency of solar powered, high temperature differential dish-Stirling engine. When using the optimal parameters, their thermal efficiency reached 34%.

Previous studies have focused on high or low temperature Stirling engines, operating under mean temperature parameters, which have not received significant attention. Striling engines operating under mean temperatures do not require high grade expensive material selection nor do they require high-cost solar collectors because of their high concentration ratio. These advantages make Stirling engines very attractive and promising in terms of reliability and cost. The objective of this study is to investigate the optimal performance of solar-powered mean temperature differential dish-Stirling heat engines using finite-time thermodynamics. Thermal losses, imperfect regeneration, and both radiation and convective heat transfer modes are considered. The influence of major parameters such as operating temperatures, effectiveness of regenerator, heat leak coefficient, ratio of volume during regeneration processes, heat capacitance rate of heat source/sink external fluids, regenerator losses, thermal bridges losses on the maximum power output and the corresponding overall efficiency are investigated. Furthermore, this paper aims at providing the technical guidelines for the design of a solar-powered mean temperature differential Stirling engine powered by a solar dish system.

2. Solar – dish Stirling engine

The dish- Stirling engine system shown in Figure 1 uses a parabolic mirror to reflect and concentrate incoming direct insolation to receiver (focal point). Concentration of solar radiation is needed to achieve the temperatures required to effectively convert heat to work. The concentration ratio is one of the central parameters of the collector. To achieve adequate concentration of insolation the dish needs to track sun in two axes. The concentrated solar radiation is absorbed by the receiver (absorber) and transferred to the engine.

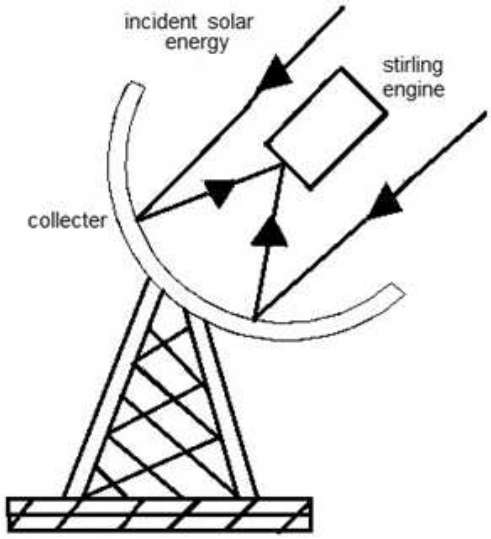

Figure 1: Schematic diagram of the dish system

2.1 Stirling Engine cycle

The Stirling cycle is a thermodynamic cycle in which thermal energy is transformed into mechanical energy. The working gas is compressed at lower temperatures and is expanded at higher temperatures. The net result of these processes is converting heat into mechanical work. Besides the isothermal compression and expansion at different temperature levels, the Stirling cycle includes isochoric heating and cooling in order to change from one temperature level to the other. The P-V and T-S diagrams for the ideal cycle (all processes are reversible, i.e. there is no dissipation) are shown in Figure 2. The four ideal cycle processes shown in Figure 2 are:

- Process 1-2: Isothermal compression of the working gas under heat release at low temperature.
- Process 2-3: Isochoric heating of the working gas.
- Process 3-4: Isothermal expansion of the working gas under heat absorption at high temperature.
- Process 4-1: Isochoric cooling of the working gas.

The Stirling engines need efficient heat exchangers in order to transport thermal energy over the engine boundaries. A key component of Stirling engines is the regenerator, which stores and releases thermal energy periodically. An ideal regenerator will store the heat that is released by the working gas in the process 4-1 (isochoric cooling) and gives the same amount of heat back to the working gas in

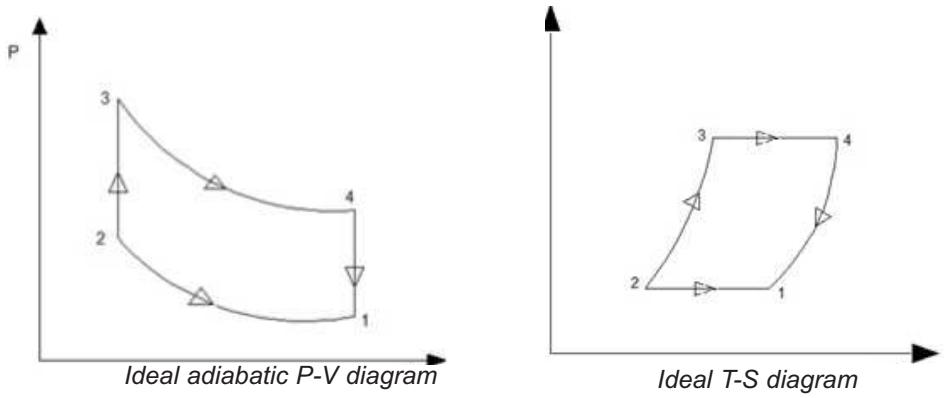

Figure 2: The P-V and T-S diagram for ideal Stirling cycle

the process 2-3 (isochoric heating). An idea regenerator considerably raises the efficiency of the engine by maintaining heat within the system that otherwise would be exchanged with the environment. It thereby increases the heat flow from the high temperature reservoir to the low temperature reservoir without any additional mechanical work.

The real Stirling engine cycle deviates from an ideal Stirling cycle. The efficiency of the conversion of thermal energy to mechanical work in the real cycle is lower than that in the ideal process even with the same upper and lower temperature limits and the same gas volumes and masses. Figure 3 compares the p-V diagrams of a real cycle and the p-V diagrams of an ideal cycle. It can be seen that the area enclosed by the curve of the real process, which indicates the released work, is smaller than that enclosed by the ideal cycle curve. This difference might be attributed to the following:

- Dissipation losses due to mechanical friction losses, pressure losses in the working gas, or gas leakage.
- Permanent temperature changes.
- Actual regenerator efficiency cannot be 100%.
- Heat loss through the engine material.
- Adiabatic losses (pressure losses due to the expansion and compression processes).
- Clearance (dead) volume, which impedes that the whole working gas is subject to the heating and cooling processes and which reduces the compression ratio.

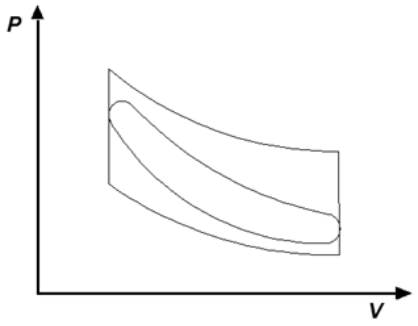

Figure 3: Ideal Stirling process compared to the real Stirling process in p-V diagram

2.2 Efficiency parameters of a dish – engine system

The overall efficiency of a dish – Stirling system, i.e. the solar-to-mechanical efficiency, depends on the following parameters:

- Solar irradiance: The mechanical power output and the respective system efficiency of the dish - engine system depends on solar radiation conditions. A higher power output is expected with higher average irradiance values. However, higher irradiance results in a high receiver temperature and may cause high thermal losses.
- Radiation concentration: A higher concentration ratio results in a higher temperature in the absorber increasing the thermal-to mechanic efficiency of the system. However, higher concentration ratios require expensive manufacturing processes (of the absorber or possibly the whole system).
- Intercept factor: A reduced intercept factor will reduce the energy flow to the receiver, but it may increase the mean radiant flux density when only the central parts of the Sun image hit the receiver aperture.
- Thermal receiver efficiency: The radiative and convective heat losses affect the receiver efficiency.
- Engine efficiency.

3. Finite time Thermodynamics analysis of the system

The objective of this paper is to develop a mathematical model for the dish solar collector, the Stirling engine, as well as the combination of the dish–Stirling engine system. Figure 4 is a schematic diagram of a Stirling heat engine cycle with finite-time heat transfer and regenerative heat losses as well as conductive thermal bridging losses from the absorber to the heat sink. We assumed finite heat exchanger areas, finite heat transfer coefficients and a finite rotation frequency, which induces speed-dependent fluid flows and time-dependent processes. The working substance in the Stirling cycle is assumed to be an ideal gas. Figure 5 is the Stirling heat engine T-S diagram. This cycle approximates

the compression stroke of a real Stirling heat engine as an isothermal heat rejection process (1-2) to the low temperature sink. The heat addition to the working fluid from the regenerator is modelled as the constant volume process (2-3). Since this external heat transfer process occurs in finite time across finite temperature differences, it is an irreversible isothermal process. The expansion stroke producing work is modelled as an isothermal heat addition process (3-4) from a high temperature heat source. Finally the heat rejection to the regenerator is modelled as the constant volume process (4-1). Similar to process 2-3, it is also considered an irreversible isothermal process. If the regenerator is ideal, the heat absorbed during process 4-1 should be equal to the heat rejected during process 2-3, however, the ideal regenerator requires an infinite area or infinite regeneration time to transfer a finite heat amount, and this is impractical. Therefore, it is desirable to consider a real regenerator with heat losses ΔQ_R. In addition, we also consider conductive thermal bridging losses Qo from the absorber to the heat sink.

3.1 Dish analysis

The useful thermal power provided by the solar collector denoted as q_h, considering conduction, convection, and radiation losses are given by (Kongtragool and Wongvises, 2005):

$$q_u = I\,A_c\eta_0 - A_b\left(h(T_H - T_0) + \varepsilon\sigma({T_H}^4 - {T_0}^4)\right) \quad (1)$$

where I is the direct solar flux intensity, A_c is the collector projected area, η_0 is the collector optical efficiency, A_b is the absorber area, h is the overall convective heat transfer coefficient, T_H is the absorber temperature, T_o is the ambient temperature, ε is the emissivity factor of the collector, and σ is the Stefan's constant.

Thermal efficiency η_s of the dish collector is:

$$\eta_s = \frac{q_h}{I\,A_{app}} = \eta_0 - \frac{1}{I\,C}[h(T_H - T_0) + \varepsilon\sigma({T_H}^4 - {T_0}^4)] \quad (2)$$

Where, C is the collector concentrating ratio.

3.2 Regenerative heat loss to the regenerator

It is important to consider the finite heat transfer through the regenerator. The regenerative processes are affected by internal thermal resistances to and from the thermal regenerator. Thus, regenerative losses are inevitable. Let DQ_R be the regenerative heat loss per cycle during the two regeneration processes, which is proportional to the temperature difference of the working fluid therefore the regenerative heat transfer is given by Kaushik and Kumar, (2001); Howell *et al.*, (1977):

$$\Delta Q_R = n\,C_v x(T_1 - T_2) \quad (3)$$

where C_v is the specific heat capacity of the working substance at constant volume in J/(kg K), and x is the fractional deviation from ideal regeneration (i.e. $x = 1$ for no- regeneration and x = 0 for ideal regeneration), and n is the number of mole. Then:

$$Q_R = n\,C_v\,(1 - x)(T_1 - T_2) \quad (4)$$

Due to the influence of irreversibility of the finite rate of heat transfer, the regenerative processes need a finite non-negligible time compared with

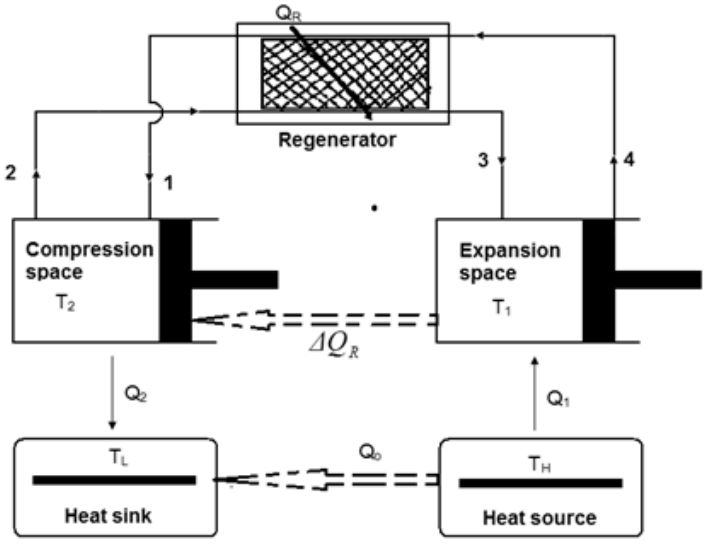

Figure 4: Schematic diagram of the Stirling heat engine cycle with losses

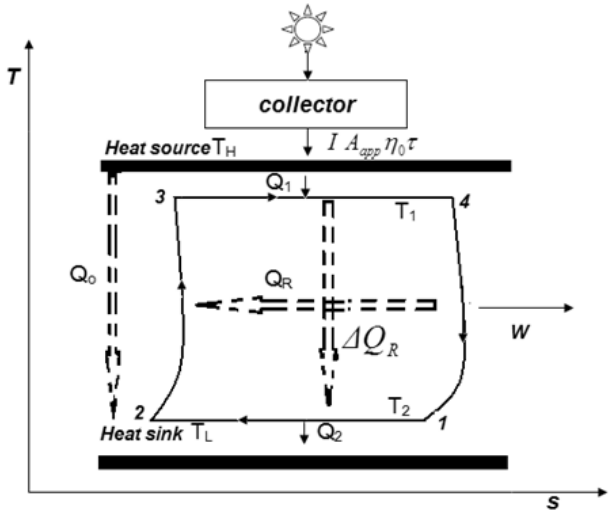

Figure 5: T-S diagram of solar dish-Stirling heat engine cycle with losses

the time of the two isothermal processes. In order to calculate the time of the regenerative processes, it is assumed that the temperature of the working substance in the regenerative processes is a function of time as given by Durmayaz *et al*, (2004) and is proportional to the temperature difference of the working fluid.

$$\frac{dT}{dt} = \pm M_i \tag{5}$$

Where M is the proportionality constant and is independent of the temperature difference but depends on the property of regenerative material, called regenerative time constant and the ± sign belong to the heating and cooling processes, respectively. The time of two regenerative processes is:

$$t_4 = \frac{T_1 - T_2}{M_2} \tag{6}$$

$$t_3 = \frac{T_1 - T_2}{M_1} \tag{7}$$

Where, t_3 and t_4 are the time taken during two regenerative processes 2–3 and 4–1, respectively.

3.3 Heat transfer across the Stirling cycle

We need to consider radiation and convection modes of heat transfer between the absorber and the working fluid. Convection heat transfer is assumed to be the main mode of heat transfer between the heat sink and the working fluid. There are always thermal resistances between the working substance and the external heat reservoirs in the Stirling engine. In order to obtain a certain power output, the temperature of the working substance must therefore be different from that of the heat reservoirs. The amounts of heat Q_1 and Q_2 absorbed from the heat source at temperature T_1 and released to the heat sink at temperature T_2 by the working fluid during the two isothermal processes are:

$$Q_1 = Q_H + \Delta Q_R = \left(h_{HC}(T_H - T_1) + h_{HR}(T_H{}^4 - T_1{}^4)\right)t_1 = nRT_1 ln\, v_1/v_2 + nC_v x(T_1 - T_2) \tag{8}$$

$$Q_2 = Q_L + \Delta Q_R = h_{LC}(T_2 - T_L)t_2 = nRT_2 \ln v_1/v_2 + nC_v x(T_1 - T_2) \tag{9}$$

Where h_{HC} is the high temperature side convection heat transfer coefficient, h_{HR} is the high temperature side radiation heat transfer coefficient, h_{LC} is the low temperature side convection heat transfer coefficient, n is the mole number of the working gas, R is the universal gas constant, t_1, t_2 are the times spent on the two isothermal processes at temperatures T_1 and T_2, respectively (process 3-4 and 1-2)., x is the fractional deviation from ideal regeneration (i.e. $x = 1$ for no-regeneration and $x = 0$ for ideal regeneration), and v_1 and v_2 are specific volumes of the working fluid along the constant-volume heating and cooling processes, in m^3/kg, and v_2/v_1 is the volume compression ratio during the regenerative processes λ, i.e.

$$\lambda = \frac{v_1}{v_2} \tag{10}$$

The conductive thermal bridging losses from the absorber at temperature T_H to the heat sink at temperature T_C is assumed to be proportional to the cycle time and is given by (Durmayaz *et al.*, 2004):

$$Q_o = k_o(T_H - T_L)\tau \tag{11}$$

where k_o is the heat leak coefficient between the absorber and the heat sink and τ is the cyclic period. Taking in account the major irreversibility mentioned, the net amount of heat released from the absorber Q_H at T_H and absorbed by the heat sink Q_L at T_L are given by:

$$Q_H = Q_1 + Q_0 \tag{12}$$

$$Q_L = Q_2 + Q_0 \tag{13}$$

Thus the total cycle time is given by:

$$\tau = t_1 + t_2 + t_3 + t_4 = \frac{nRT_1 \ln\lambda + nCvx(T_1 - T_2)}{h_{HC}(T_H - T_L) + h_{HR}(T_H{}^4 - T_L{}^4)} + \frac{nRT_2 \ln\lambda + nCvx(T_1 - T_2)}{h_{LC}(T_2 - T_L)} + \left(\frac{1}{M_1} + \frac{1}{M_2}\right)(T_1 - T_2) \tag{14}$$

For the thermodynamic cycle 1-2-3-4-1, the magnitude of the network for this finite time cycle is:

$$W = Q_H - Q_C \tag{15}$$

The power output and thermal efficiency are given by:

$$P = \frac{W}{\tau} = \frac{Q_H - Q_C}{\tau} \tag{16}$$

$$\eta_t = \frac{Q_H - Q_C}{Q_H} \qquad (17)$$

Now from equations (3)–(17) the power output and thermal efficiency of Stirling engine are given by:

$$P = \frac{T_1 - T_2}{\dfrac{T_1 + A_1(T_1 - T_2)}{h_{HC}(T_H - T_1) + h_{HR}({T_H}^4 - T_1^4)} + \dfrac{T_2 + A_1(T_1 - T_2)}{h_{LC}(T_2 - T_L)} + F_1(T_1 - T_2)} \qquad (18)$$

$$\eta_t = \frac{T_1 - T_2}{T_1 + A_1(T_1 - T_2) + (k_0(T_H - T_L)\left(\dfrac{T_1 + A_1(T_1 - T_2)}{h_{HC}(T_H - T_1) + h_{HR}({T_H}^4 - T_1^4)} + \dfrac{T_2 + A_1(T_1 - T_2)}{h_{LC}(T_2 - T_1)} + F_1(T_1 - T_2\right)} \qquad (19)$$

$$A_1 = \frac{Cvx}{R\ln\lambda}, \qquad F_1 = \frac{1}{nR\ln\lambda}\left(\frac{1}{M_1} + \frac{1}{M_2}\right)$$

Where,

For the sake of convenience, a new parameter y = T_2/T_1 is introduced into eqs. (18) and (19), then we have:

$$P = \frac{T_1 - yT_1}{\dfrac{T_1 + A_1(T_1 - yT_1)}{h_{HC}(T_H - T_1) + h_{HR}({T_H}^4 - T_1^4)} + \dfrac{T_1 + A_1(T_1 - yT_1)}{h_{LC}(yT_1 - T_L)} + F_1(T_1 - yT_1)} \qquad (21)$$

$$\eta_t = \frac{T_1 - yT_1}{T_1 + A_1(T_1 - yT_1) + (k_0(T_H - T_L)\left(\dfrac{T_1 + A_1(T_1 - T_2)}{h_{HC}(T_H - T_1) + h_{HR}({T_H}^4 - T_1^4)} + \dfrac{yT_1 + A_1(T_1 - yT_1)}{h_{LC}(yT_1 - T_L)} + F_1(T_1 - yT_1)\right)} \qquad (20)$$

To maximize the power output, take the derivative of eq. (18) with respect to the temperature T_1 and x and equate it to zero, namely

$$\frac{\partial P}{\partial T_1} = 0 \text{ and } \frac{\partial P}{\partial y} = 0,$$

the optimal working fluid temperature T_{1opt} and x_{opt} for this condition can be obtained from eq. (20) and (21), respectively:

$$D_1 T_{opt}^8 + D_2 T_{opt}^5 + D_3 T_{opt}^4 + D_4 T_{opt}^3 + D_5 T_{opt}^2 + D_6 T_{opt} + D_7 = 0 \qquad (22)$$

$$E_1 y_{opt}^3 + E_2 y_{opt} + E_3 = 0 \qquad (23)$$

where $D_1 = h_{HR}^2 B_{1x}$, $D_2 = h_{HR} y(2B_1 h_{HC} - 3B_2 h_{LC} y)$,

$D_3 = 2h_{HR} y(3B_2 h_{LC} T_L - B_1 B_3)$, $D_4 = -3B_2 h_{HR} h_{LC} T_L^2$,

$D_5 = h_{HC} y(B_1 h_{HC} - B_2 h_{LC} y)$, $D_6 = 2h_{HC} y(B_2 h_{LC} T_L - B_3 B_1)$,

$D_7 = B_1 x B_3^2 - B_2 h_{HC} h_{LC} T_L^2$, $B_1 = y + A_1(1 - y)$,

$B_2 = 1 + A_1(1 - y)$, $B_3 = h_{HC} T_H + h_{HR} T_H^4$,

$E1 = B\left(T_L^2 - Y1 T_c h_{Lc}\right)$, $E2 = B\left(Y_1 h_{Lc} T_1^2 - Y1 h_{Lc} T_1 T_c\right)$,

$E3 = -B_1 h_{Lc} T_1 (T_L + Y1T1) + T_1^2 h_{Lc}$,

$B = h_{HC}(T_H - T_1) + h_{HR}(T_H^4 - T_L^4)$

Solving eq. 22 for the optimal fluid working temperature, the maximum power output and the corresponding optimal thermal efficiency of the Stirling engine are:

$$P_{\max} = \frac{1-x}{\frac{1+A_1(1-x)}{h_{HC}(T_H - T_{1opt}) + h_{HR}(T_H^4 - T_{1opt}^4)} + \frac{x + A_1(1-x)}{h_{LC}(xT_{1opt} - T_L)} + F_1(1-x)} \quad (24)$$

$$\eta_{topt} = \frac{1-x}{1 + A_1(1-x) + (k_0(T_H - T_L))\left[\frac{1 + A_1(1-x)}{h_{HC}(T_H - T_{1opt}) + h_{HR}(T_H^4 - T_{opt}^4)} + \frac{x + A_1(1-x)}{h_{LC}(xT_{1opt} - TL)} + F_1(1-x)\right]} \quad (25)$$

The maximum power thermal efficiency of the system is the product of the thermal efficiency of the collector and the optimal thermal efficiency of the Stirling engine (Kongtragool and Wongvises, 2005) namely:

$$\eta_m = \eta_s \eta_{topt} \quad (26)$$

$$\eta_m = \left[\eta_0 - \frac{1}{IC}\left[h(T_H - T_0) + \varepsilon\delta(T_H^4 - T_0^4)\right]\right] * \left[\frac{1-x}{1 + A_1(1-x) + (k_0(T_H - T_L))\left[\frac{1 + A_1(1-x)}{h_{HC}(T_H - T_{1opt}) + h_{HR}(T_H^4 - T_{opt}^4)} + \frac{x + A_1(1-x)}{h_{LC}(xT_{1opt} - TL)} + F_1(1-x)\right]}\right] \quad (27)$$

4. Numerical results and discussion

In order to evaluate the effect of the absorber temperature (TH), the concentrating ratio(C), the effectiveness of the regenerator x, temperature ratio y, and the heat leak coefficient (ko) on the solar-powered dish-Stirling heat engine system, all the other parameters will be kept constant at

$h_{HC} = 200$ W/K, $h_{HR} = 4 * 10^{-8}\ W/K^4$,

$n = 1\,mol, \lambda = 2, R = 4.3\,J/mol, c_v = 15\,\text{J}/(\text{mol K})$,

$\varepsilon = 0.9, T_L = 320K, T_o = 300\ K, h = 20\,Wm^2/K, \sigma$

$= 5.76 * 10^{-8} W/mK, ((1/M_1) + (1/M_2)) =$

$2 * 10^{-5} s/K, I = 1000\,W/m.$

The above values are reasonable values corresponding to the typical operating condition of Stiring engines found in literature.

The effect of the absorber temperature T_H and the concentrating ratio C on thermal efficiency of the collector is shown in Figure 6. It can be seen that the thermal efficiency of the collector decreases rapidly with increasing temperature of the absorber T_H. The rate of this decrease is inversely proportional to the concentration ratio C. The reduction in the thermal efficiency is due to increase in convective and radiative heat losses at higher absorber temperature. Finally, at low temperature, the maximum thermal efficiency is nearly equal to the optical efficiency of the concentrator.

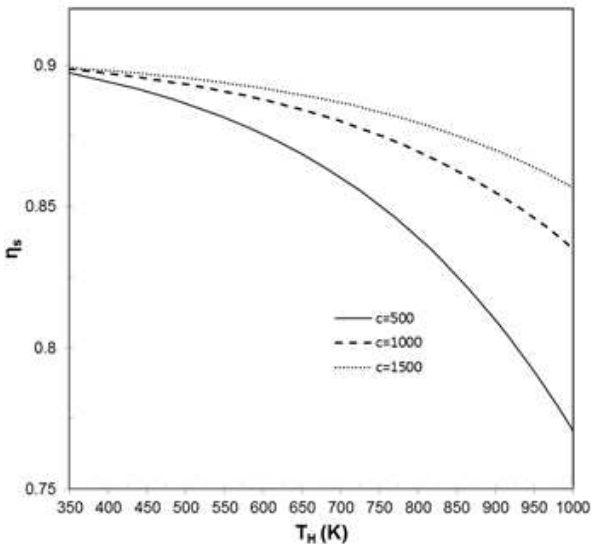

Figure 6: Effect of absorber temperature and the concentrating ratio on the thermal efficiency of the collector (e = 0.9)

The effect of absorber temperature and regenerator effectiveness on the optimal thermal Stirling efficiency is investigated and shown in Figure 7. It can be seen from Figure 7 that the thermal efficiency of the Stirling engine increases rapidly at the beginning until the absorber temperature reaches 750 K. The results of the model show that further increase in the absorber temperature will not improve the optimal efficiency of the engine significantly. The reason for this behaviour is due to the conductive thermal bridging losses, which increases with increasing absorber temperature. At high absorber temperature, the radiation losses start to dominate the heat transfer process. It is also found that the optimal thermal efficiency of the Stirling engine increases significantly along with regenerator efficiency.

Figure 8 shows the effect of the absorber temperature (T_H) on the thermal efficiency of dish-Stirling engine system (ηm) for several values of concentrating ratio. It can be seen that for a given concentrating ratio, the maximum power thermal efficiency increases with the increase of the absorber temperature until it reaches the optimal value, and then decreases with increasing absorber temperature. The reason for this decrease is due to increasing thermal losses at the absorber due to high temperature differences. Furthermore, the thermal system efficiency increases with the increase of the concentrating ratio. The rate of reduction of the system's efficiency at higher absorber temperatures is slowed down by high values of concentration ratios C. The highest thermal system efficiency is 32% corresponding to an optimum absorber temperature of 850 K, while the Carnot efficiency reaches about 50%.

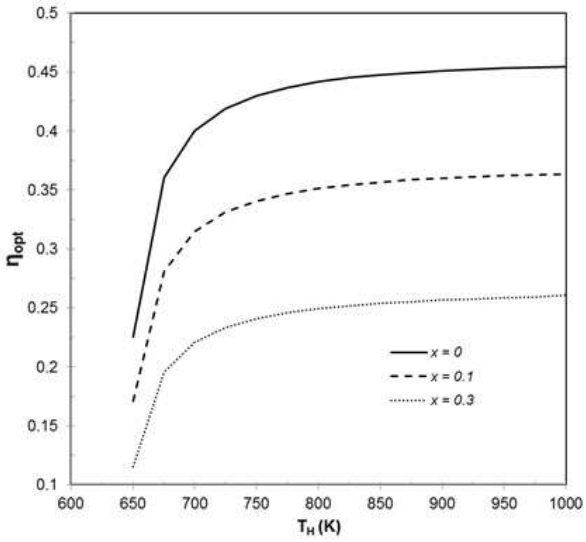

Figure 7: Variation of the optimal thermal efficiency of the Stirling engine for different absorber temperature and the effectiveness of the regenerator (y = 0.5, ko =2.5

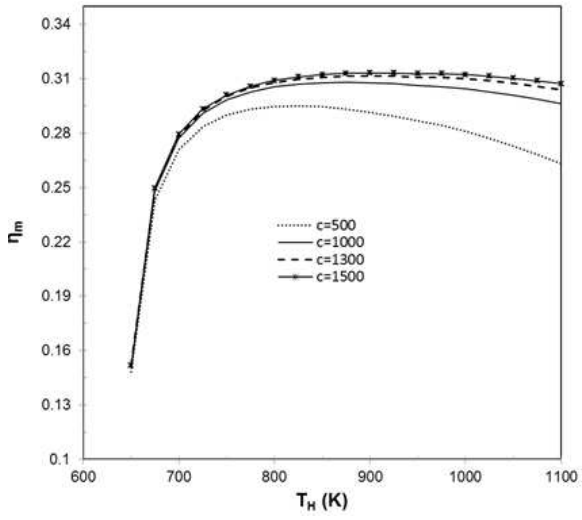

Figure 8: Effect of the absorber temperature on the maximum power thermal efficiency of the dish–Stirling engine system for several values of concentrating ratio

The effect of regenerator effectiveness on the maximum power thermal efficiency of the system is

shown in Figure 9. It is seen that the maximum power efficiency increases with the increase of the effectiveness of the regenerator. It is also observed that when there is no heat loss through the regenerator (x = 0), the Stirling heat engine attains an efficiency almost equal to the Curzon–Ahlborn efficiency CA = 39.49 of an endoreversible Carnot heat engine at T_H = 850K. Nevertheless, an endoreversible Stirling heat engine with an ideal regenerator is as efficient as an endoreversible Carnot heat engine but it is not practical since an ideal regeneration requires infinite time or infinite regenerative area. Furthermore, we see that if the regenerator effectiveness drops from 100% to 90%, the thermal efficiency will drop to around 30% for T_H = 850 K. Finally, the regenerator effectiveness has smaller effect on system efficiency for low values of T_H compared to high values of T_H.

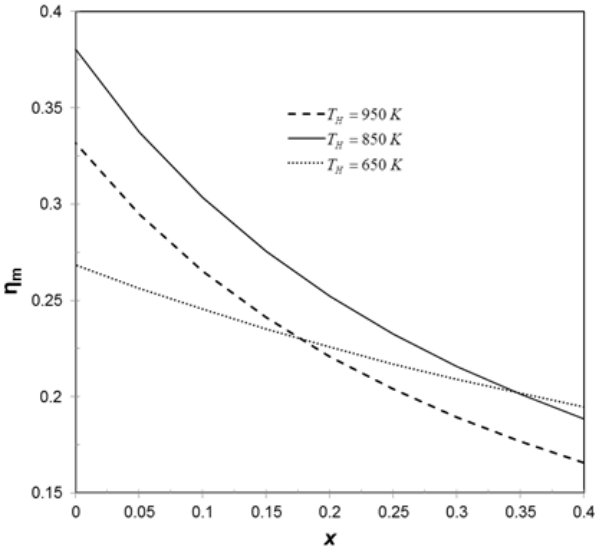

Figure 9: Effect of regenerator effectiveness on of the maximum power efficiency of the dish system for different absorber temperature (C = 1300, k_o=2)

The effect of the heat leak coefficient k_o on the system thermal efficiency is shown in Figure 10. It is seen from Figure 10 that the heat leak coefficient reduces the maximum power efficiency of the system. It is also observed that rate of decrease is higher at lower absorber temperature.

Figure 11 shows the variations of concentration ratio with maximum power efficiency of the dish-Stirling engine. According to this diagram, we can see that the system efficiency rises only slightly for concentration ratios over 1200. Taking the effect of a higher concentration ratio, the consequent higher receiver temperature and the higher thermal-to-mechanic efficiency isolated, we could suppose that the system efficiency should show a stronger dependence on the concentration ratio. However, higher thermal losses at higher temperatures reduce this dependence considerably. Taking this into consideration and taking into account the expected higher costs for the construction of dishes with a higher concentration ratio it may be not economical to aspire to concentration ratios higher than 1200.

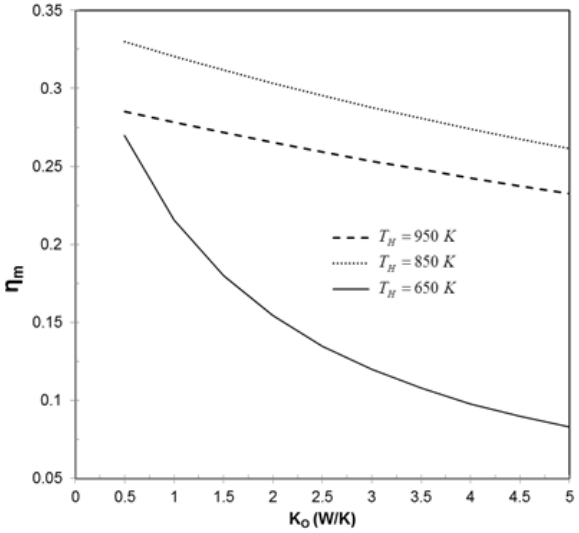

Figure 10: Variation of the maximum power thermal efficiency of the dish system for different heat leak coefficient and the absorber temperature (x = 0.1, C = 1300)

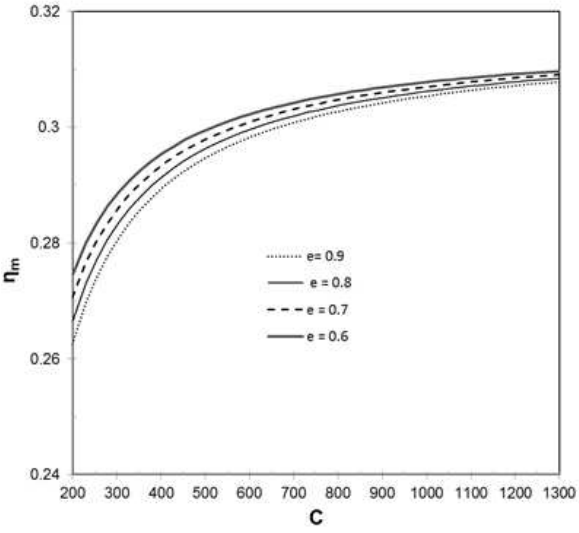

Figure 11: Variation of concentration ratio with maximum power efficiency (x = 0.1, ko = 2.5, T_H= 850 K)

Figure 12 shows the variation of maximum power output of the system with respect to absorber temperature for different combination of temperature ratio and regenerator effectiveness. It can be seen from Figure 12 that the maximum power increases with increasing absorber temperature. The rate of power increase at $T_1/T_2 = 0.5$ is higher than that corresponding to $T_1/T_2 = 0.7$. The rate of power increase with absorber temperature increases with increasing regenerator effectiveness.

Figure 13 shows the variations of system efficiency with the temperature ratios y. This increases

very rapidly with an increasing temperature ratio until it reaches a maximum value at $T_1/T_2 = 0.42$. It is shown that the system efficiency increases very rapidly when the temperature ratio increases until an optimal value is reached. Past the optimal temperature ratio, the efficiency rapidly descends. The value of the optimal temperature ratio decreases with the increase in absorber temperature.

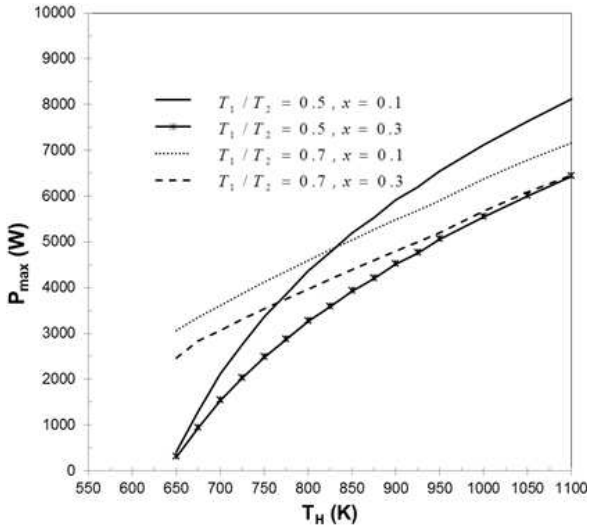

Figure 12: Effect of T_H on maximum power output for different regenerator effectiveness and temperature ratio (x = 0, k_o = 2.5)

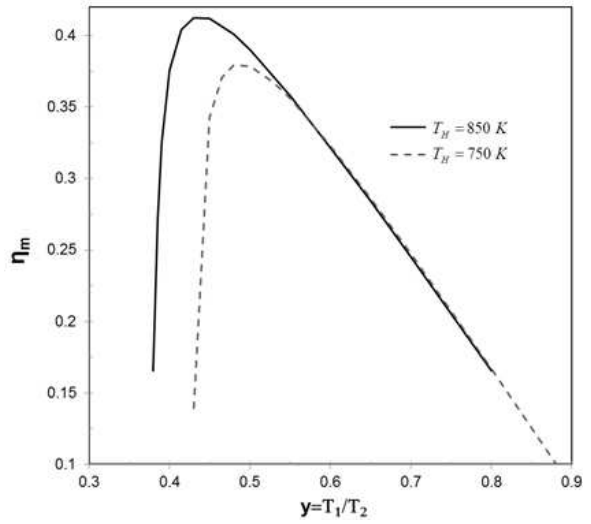

Figure 13: Effect of temperature ratio on maximum thermal system efficiency (x = 0, k_o = 2.5)

Figure 14 shows the effect of the volume ratio v_1/v_2 on maximum power output. The power output increases very rapidly when the volume increases and starts to level off sharply when the volume ratio reaches 2 for ideal regeneration. However, when regeneration effectiveness equals 0.2, the power output increases rapidly at the beginning and the increase will start slowing down with the volume ratio. It can be observed that for ideal regeneration, the power output after a certain ratio is no longer a function of volume ratio. This is not the case for non- ideal regeneration. It can be seen that the effect of volume ratio is more notable for the non-ideal regeneration than that for an ideal regeneration. Finally, in order to have high power output, the constant cooling volume should be as high as possible compared to the constant heating volume.

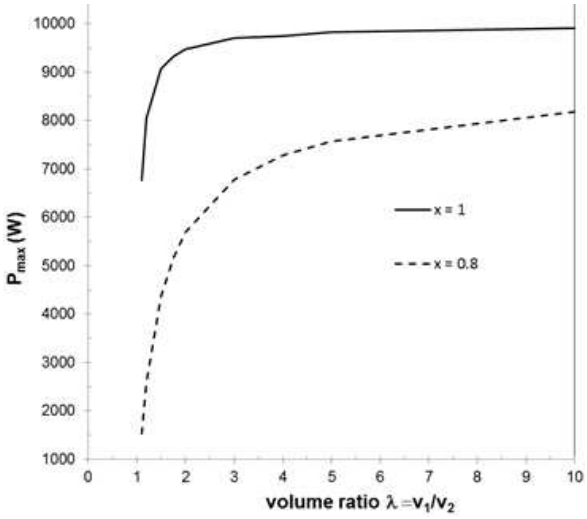

Figure 14: Effect of the volume ratio on maximum power output for different regenerator effectiveness (k_o = 2.5, T_H = 850 K)

5. Conclusion

Finite-time thermodynamics is used to optimize the power output and the thermal efficiency of the dish - Stirling engine when regenerative losses and thermal bridges losses are taken into account. The results show that the optimal thermal efficiency of the Stirling engine increases significantly with regenerator efficiency. It is also found that maximum power output increases with increasing absorber temperature. The highest thermal system efficiency is 32% when the corresponding optimum absorber temperature is equal to 850 K. For the non –ideal regenerator, maximum work output corresponds to high volume ratio values. The present analysis provides theoretical guidelines for the basis for the design, performance evaluation and system optimization of solar-powered mean temperature differential dish-Stirling engines powered by a solar dish system.

References

Arenas, Jose´ M. (2007). Design, development and testing of a portable parabolic solar kitchen. *Renewable Energy* 32, 257–266.

Chambadal, P., (1957). Les Centrales Nucléaires, Armand Colin, Paris, 41-58.

Chen Lingen, Yan Zijun, Chen Lixuan, and Andresen Biarne (1998). Efficiency Bound of a Solar-Driven Stirling Heat Engine System, *Int. J. Energy Res*., 22, 9, pp. 805-812.

Costea, M., Petrescu, S., and Harman, C. (1999). The Effect of Irreversibilities on Solar Stirling engine Cycle Performance, Energy Convers Manage, 40, 15-16, pp. 1723-1731.

Curzon, F. L., and Ahlborn, B. (1975). Efficiency of Carnot Heat Engine at Maximum Power Output, *Am. J. Phys, 43* (1975), 2, pp. 22-24.

Durmayaz, A., *et al.,* (2004). Optimization of Thermal Systems Based on Finite-Time Thermodynamics and Thermoeconomics, Prog Energy Combust Sci., 30, 2, pp. 175-271.

Howell, J. R., and Bannerot, R. B. (1977). Optimum Solar Collector Operation for Maximizing Cycle Work Output, *Solar Energy, 19*, 2, pp. 149-153.

Kaushik S.C. and Kumar S. (2000). Finite time thermodynamic analysis of endoreversible Stirling heat engine with regenerative losses. *Energy* 25: 989e1003.

Kaushik S.C. and Kumar S. (2001). Finite time thermodynamic evaluation of irreversible Ericsson and Stirling heat engines. Energy Convers Manage; 42:295e312.

Kodal Ali, and Sahin Bahri (2003). Finite size thermoeconomic optimization for irreversible heat engines. *Int J Thermal Sci*; 42:777e82.

Kongtragool Bancha and Wongwises Somechai (2003). A review of solar-powered Stirling engines and low temperature differential Stirling engines [J]. *Renew Sustain Energy* Rev; 7: 131e54.

Kongtragool Bancha, and Wongwises Somehai (2005). Optimum absorber temperature of a once-reflecting full conical concentrator of a low-temperature differential Stirling engines. *Renew Energy*; 30:1671-87.

Ladas H.G. and Ibrahim O.M. (1994). Finite-time view of the Stirling engine. *Energy*; 19(8):837–43.

Li Yaqi, He Yaling, Wang Weiwei (2011). Optimization of solar-powered Stirling heat engine with finite-time Thermodynamics. Renewable Energy 36 421-427.

Mancini, T., and Heller, P., (2003). Dish-Stirling Systems: An Overview of Development and Status [J], *J. Solar Energy Eng., 125*, 2, pp. 135-151.

Mohr, M., Svoboda, P., and Unger, H. (1999). Praxis solarthermischer Kraftwerke. Berlin, Heidelberg: Springer.

Novikov, H., 1957, Atomnaya Energiya, 3, 409-412.

Popescu G, Radcenco V, Costea M, and Feidt M. (1996). Optimization of an endo-exo-irreversible Stirling motor. *Rev. Gen. Therm*. (35):656–661.

Salah El-Din M.M. (1999). Thermodynamic optimization of irreversible solar heat engines. *Renew Energy;* 17:183–90.

Sahin, A. Z., (2001). Finite-Time Thermodynamic Analysis of a Solar Driven Heat Engine, *Exergy Int., 1*, 2, pp. 122-126.

Senft JR. (1998). Theoretical limits on the performance of Stirling engine. *Int J Energy Res*; 22:991–1000.

Shahrir Abdullah, Belal F. Yousif, and Kamaruzzaman Sopian (2005). Design consideration of low temperature differential double-acting Stirling engine for solar application. *Renewable Energy* 30, 1923–1941.

Thombarea D.G. and Verma S.K. (2008). Technological development in the Stirling cycle engines. Renewable and Sustainable Energy Reviews; 12:1–38.

Wang J.T. and Chen J. (2002). Influence of several irreversible losses on the performance of a ferroelectric Stirling refrigeration-cycle. *Appl Energy*; 72: 495–511.

Wu, F., *et al*., (1998). Performance and Optimization Criteria of Forward and Reverse Quantum Stirling Cycles, *Energy Conversion and Management*, 39, 8, pp. 733-739.

Wu F, Chen LG, Sun FR, *et al*. (2008). Performance optimization of Stirling engine and cooler based on finite-time thermodynamic. Beijing: Chemical Industry Press p. 59.

Yan Z, and Chen L. (1997). Optimal performance of an endoreversible cycle operating between a heat source and sink of finite capacities. *J Phys* A; 30: 8119–27.

Received 19 February 2014; revised 13 February 2015

Decomposition analysis of energy-related CO_2 emissions in South Africa

Ming Zhang

Shuang Dai

Yan Song

China University of Mining and Technology, Xuzhou, P.R. China

Abstract

South Africa has become one of the most developing countries in the world, and its economic growth has occurred along with rising energy-related CO_2 emission levels. A deeper understanding of the driving forces governing energy-related CO_2 emissions is very important in formulating future policies. The LMDI (Log Mean Divisia Index) method is used to analyse the contribution of the factors which influence energy-related CO_2 emissions in South Africa over the period 1993-2011. The main conclusions drawn from the present study may be summarized as follows: the energy intensity effect plays the dominant role in decreasing of CO_2 emission, followed by fossil energy structure effect and renewable energy structure effect; the economic activity is a critical factor in the growth of energy-related CO_2 emission in South Africa.

Keywords: CO_2 emission; LMDI method; South Africa

1. Introduction

Currently, global warming is considered among the most important environmental problems. Accelerating use of fossil fuels cause a significant increase in the anthropogenic greenhouse gases (GHG), which lead to global warming? Among six kinds of GHG, the largest contribution to the greenhouse effect is carbon dioxide (CO_2), and its share of the greenhouse effect is about 56% (IPCC, 2014). Thus, the acceleration of CO_2 emission with regard to ever-increasing energy consumption has raised the concern of energy analysts and policy makers.

South Africa has become one of the most developing countries in the world, and its economic growth has occurred along with rising energy-related CO_2 emission levels. It took the bold step at the end of 2009 to commit itself to the Secretariat of the United Nations Framework Convention on Climate Change (UNFCCC) in taking all the necessary actions to decrease the country's greenhouse gas emissions by 34% to below the 'business-as-usual' scenario by 2020 (Winkler *et al.*, 2010). A deeper understanding of the driving forces governing energy-related CO_2 emission is very important in formulating future policies. To accomplish this purpose, a robust approach is to decompose the evolution of energy-related CO_2 emission into possible affecting factors.

Nowadays, the Index Decomposition Analysis (IDA) technique has been used successfully to quantify the impact of different factors on the change of energy consumption and CO_2 emission. In the literature, two well-known IDA decomposition techniques, namely the Laspeyres index decomposition analysis and the Divisia index decomposition analysis, have been widely applied (Wang *et al.* 2011). So far many researchers have utilized the IDA method to identify the driving factors influencing the variation of energy consumption or related CO_2 emission. Based on the Laspeyres index decomposition analysis, an analysis had been made of energy consumption, efficiency and savings in China in the period 1980–94 by Sun (1998). The Laspeyres index decomposition analysis is also utilized by Reddy and Ray (2010) to study energy consumption and energy intensity in Indian manufacturing industries. Wang *et al*. (2005) applied the logarithmic mean Divisia index approach to study the influencing factor of the energy-related CO_2 emission. The LMDI technique was

also utilized by Tan *et al*. (2011) to examine the driving forces for reducing China's CO_2 emission intensity between 1998 and 2008.

The IDA method has been generalized to a different method, but there is no consensus among all IDA methods as to which is the `best' decomposition method. Ang (2004) compared various methods and their advantages and disadvantages and concluded that the LMDI method was the preferred method, due to its theoretical foundation, adaptability, ease of use and result interpretation, along with some other desirable properties in the context of decomposition analysis.

Currently, several studies have focused on energy consumption in South Africa. For example, Inglesi-Lotz and Blignaut (2011) conducted a sectoral decomposition analysis of the electricity consumption for the period 1993–2006 to determine the main drivers responsible for its increase. Inglesi-Lotz and Pouris (2012) examined the factors affecting the trends in energy efficiency in South Africa from 1993 to 2006 and particularly the impact of structural changes and utilization efficiency of the country's energy intensity. So far no study has been devoted to decomposing the energy-related CO_2 emission in South Africa. To deeper understand the driving forces governing energy-related CO_2 emission, this paper serves as a preliminary attempt to apply the LMDI method to analyse the contribution of the factors which influence energy-related CO_2 emission in South Africa over the period 1993-2011.

The remainder of this paper is organized as follows. The next section presents the methodologies of the study and related data. The decomposition results of CO_2 emission is presented in section 3. Finally, we conclude this study.

2. Methodology and data

In the first place, the method of estimation of CO_2 emission is presented in this section. Then we give the definition of effect factor and LMDI model formulation. In this paper, economic activity is measured by GDP (Gross Domestic Product), which is collected from SJGDP (2013).

The symbol definitions are as follows.

C^t: total CO_2 emission in year t (in Million tons (Mt));

C_i^t : total CO_2 emission based on fuel type i in year t;

E_i^t : total energy consumption of the fossil fuel type i in year t;

E_f^t : total fossil energy consumption in year t;

E^t : total energy consumption in year t;

$EF_i^t = C_i^t / E_i^t$: carbon emissions factor of the ith fuel in year t;

O_i: the fraction of carbon oxidized based on fuel type i;

M: the molecular weight ratio of carbon dioxide to carbon (44/12);

GDP^t : the value added in year t;

$EI^t = E^t / GDP^t$: the energy intensity in year t;

$ES_i^t = E_i^t / E_f^t$: the share of ith energy form to total energy consumption in year t;

$FS^t = E_f^t / E^t$: the share of fossil energy share to total energy consumption in year t.

2.1 Estimation of CO_2 emission

Following the method given by the IPCC (2014), total CO_2 emission from fuel combustion is estimated based on energy consumption, carbon emission factors by fuel as follows.

$$C^t = \sum_i C_i^t = \sum_i E_i^t \times EF_i^t \times O_i \times M \qquad (1)$$

The carbon emission factors for different fuel type are calculated based on the data given by IPCC, as listed in Table 1. These carbon emission factors have changed over time because of a change in grade of fuel. Because the study period 1993-2011 analysed in this paper is relatively short term, this paper assumes that the carbon emission factors of all energy forms are constant. Only three fuel types are considered in this paper, namely Oil, Coal, and Natural gas. The unit for energy is million ton oil equivalents (Mtoe). All energy data is collected from Statistical Review of World Energy (2012).

Table 1: Carbon emission factors and fractions of carbon oxidized
Source: IPPC (2014)

Fuel type	*Oil*	*Coal*	*Natural gas*
Carbon emission factor (Unit: Mt Carbon/Mtoe)	0.832	1.068	0.633
Fraction of carbon oxidized (Unit: %)	0.98	0.9	0.99

2.2 LMDI model formulation

The energy-related CO_2 emission in year () can be expressed as Eq. (2)

$$C^t = \sum_i C_i^t = \sum_i \frac{C_i^t}{E_i^t} \times \frac{E_i^t}{E_f^t} \times \frac{E_f^t}{E^t} \times \frac{E^t}{GDP^t} \times GDP^t = \sum_i EF_i^t \times ES_i^t \times FS^t \times EI^t \times GDP^t \qquad (2)$$

According to the LMDI method given by Ang

(2004), the change of CO_2 emission between a base year 0 and a target year t, denoted by ΔC^t_{tot}, can be decomposed into the following determinant factors:

(i) The economic activity effect (denoted by ΔC^t_{gdp}), which is defined as the total produced value added (GDP) from South Africa (measured in ZAR), reflecting changes in the development of economy (namely the theoretical CO_2 emission caused by economic activities).

(ii) The energy intensity effect (denoted by ΔC^t_{ei}), which is defined as the ratio of energy consumption to produced value added, reflecting changes in some variables like energy prices, energy conservation and energy-saving investments.

(iii) The fossil energy structure effect (denoted by ΔC^t_{es}), which is defined as the ratio of fossil energy forms to total fossil energy consumption, reflecting changes in the relative shares of different fossil energy type;

(iv) The renewable energy structure effect (denoted by ΔC^t_{fs}), which is defined as the ratio of total fossil energy consumption to total energy use, reflecting changes in the relative shares of renewable energy use;

(v) The emission-factor effect (denoted by ΔC^t_{ef}), which is defined by the ratio of CO_2 emission and energy consumption, reflecting changes in the fuel substitution, fuel quality and the installation of abatement technologies.

Thus, based on the LMDI method developed by Ang (2004), the difference ΔC^t_{tot} is decomposed into its components in additive form, as illustrated in Eq. (3):

$$\Delta C^t_{tot} = \Delta C^t_{gdp} + \Delta C^t_{ei} + \Delta C^t_{es} + \Delta C^t_{fs} + \Delta C^t_{ef} \quad (3)$$

Each effect in the right hand side of Eq. (5) can be computed as follows:

$$\Delta C^t_{gdp} = \sum_i L(C^t_i, C^0_i) \ln(\frac{GDP^t}{GDP^0}) \quad (3a)$$

$$\Delta C^t_{ei} = \sum_i L(C^t_i, C^0_i) \ln(\frac{EI^t}{EI^0}) \quad (3b)$$

$$\Delta C^t_{es} = \sum_i L(C^t_i, C^0_i) \ln(\frac{ES^t_i}{ES^0_i}) \quad (3c)$$

$$\Delta C^t_{fs} = \sum_i L(C^t_i, C^0_i) \ln(\frac{FS^t}{FS^0}) \quad (3d)$$

Because this paper assumes that the carbon emission factors (*EF*) of all energy forms are constant during the study period. The value of following formula (3e) is 0.

$$\Delta C^t_{ef} = \sum_i L(C^t_i, C^0_i) \ln(\frac{EF^t_j}{EF^0_j}) \quad (3e)$$

Here, $L(C^t_{ij}, C^0_{ij}) = \dfrac{C^t_{ij} - C^0_{ij}}{\ln C^t_{ij} - \ln C^0_{ij}}$.

In the index number, we form

$$(\frac{\Delta C^t_{gdp}}{\Delta C^t_{tot}} + \frac{\Delta C^t_{ei}}{\Delta C^t_{tot}} + \frac{\Delta C^t_{es}}{\Delta C^t_{tot}} + \frac{\Delta C^t_{fs}}{\Delta C^t_{tot}} + \frac{\Delta C^t_{ef}}{\Delta C^t_{tot}}) \times 100\% = 100\% \quad (4)$$

3. Results and discussion

Findings obtained from the decomposition analysis are shown in Table 2 and Figure 1. The components of the decomposition analysis, i.e. ΔC^t_{gdp} (economic activity effect), ΔC^t_{es} (fossil energy structure effect), ΔC^t_{ei} (energy intensity effect), ΔC^t_{fs} (renewable energy structure effect) and ΔC^t_{ef} (emission-factor effect) are calculated as given in Eqs. (3a-e), respectively. Our results show that energy intensity effect, fossil energy structure effect and renewable energy structure effect are the factors in decreasing energy-related CO_2 emission in South Africa. However, the economic activity effect plays a positive impact on the growth of energy-related CO_2 emission.

During the study period, the energy intensity effect played the dominant role in decreasing of CO_2 emission, followed by energy structure effect and fossil energy structure effect. The accumulated (period-wise) effect is a decrease of 66.28Mt, which accounts for 49.16% of the total change in absolute value. The change of South Africa's energy intensity for the study period is presented in Figure 2, illustrating a general decrease in energy intensities. The trend of energy intensity has three stages. The first stage is 1993-2002; in this stage the trend of energy intensity shows an inverted U-shape, and the energy intensity reached the highest in 1997. The next stage is 2002-2005, that trend also shows a small inverted U-shape. The third stage is 2005-2011, the energy intensity decreased continuously in this stage. The decreasing trend of energy intensity can be due to the use of new process, new technologies and new equipment, especially the extensive application of energy-saving technologies and the advancement of management level (Inglesi-Lotz and Pouris; 2012). The above reason can explain

Table 2: Complete decomposition of energy-related CO_2 emission change (1993-2011) (Unit: Mt)

	ΔC^t_{es}	ΔC^t_{fs}	ΔC^t_{ei}	ΔC^t_{gdp}	ΔC^t_{tot}
1993-1994	-2.09	-2.24	8.88	9.01	13.56
1994-1995	-0.42	-0.39	6.77	9.21	15.17
1995-1996	-0.26	-0.51	3.40	13.37	16.01
1996-1997	-0.74	-1.01	2.48	8.50	9.24
1997-1998	-0.80	-0.46	-1.76	1.67	-1.34
1998-1999	0.69	1.14	-12.83	7.90	-3.10
1999-2000	-0.77	-0.67	-12.74	13.62	-0.56
2000-2001	0.82	1.21	-12.33	8.79	-1.51
2001-2002	-0.66	-0.93	-1.26	12.12	9.26
2002-2003	1.75	1.34	9.97	10.16	23.23
2003-2004	-1.49	-0.62	3.80	16.47	18.16
2004-2005	0.15	1.44	-26.43	19.33	-5.51
2005-2006	0.16	0.58	-14.42	20.47	6.80
2006-2007	-0.41	-0.80	0.39	21.00	20.19
2007-2008	3.11	2.10	1.51	14.55	21.28
2008-2009	-2.22	-2.11	-12.62	-6.28	-23.24
2009-2010	-0.58	0.33	-1.18	12.25	10.81
2010-2011	0.10	0.21	-7.89	13.98	6.40
1993-2011	-3.66	-1.37	-66.28	206.13	134.82

why the energy intensity effect decreased CO_2 emission over 1993-2011.

As shown in Table 2, the fossil energy structure effect was another factor decreasing CO_2 emission over the study period. The accumulated effect is a decrease of about 3.66Mt CO_2 emissions, which only accounted for 2.72% of the total CO_2 emission change in absolute value. The tendency of fossil energy consumption structure over time is shown in Figure 3. There is a substitution between the increasing share of natural gas (from 1.13% in 1993 to 3.12% in 2011) and a decreasing share of coal (from 76.90% in 1993 to 75.58% in 2011) (authors' calculation based on Statistical Review of World Energy, 2012). The use of natural gas increased from 0.92Mtoe in 1993 to 3.84Mtoe in 2011, following an annual growth rate of 8.21%. However, the share of natural gas to total fossil energy consumption accounted for less than 3.2% over the period 1993-2011. During the study period, more than 75.0% fossil energy was coal in South Africa, which can explain why the energy structure effect on CO_2 emissions was relative small.

Table 2 also indicates that the renewable energy structure effect played a very minor role in decreasing CO_2 emissions in 11 out of 19 years. The accumulated effect is a decrease of about 1.37Mt CO_2 emission, which only accounted for 1.02% of the

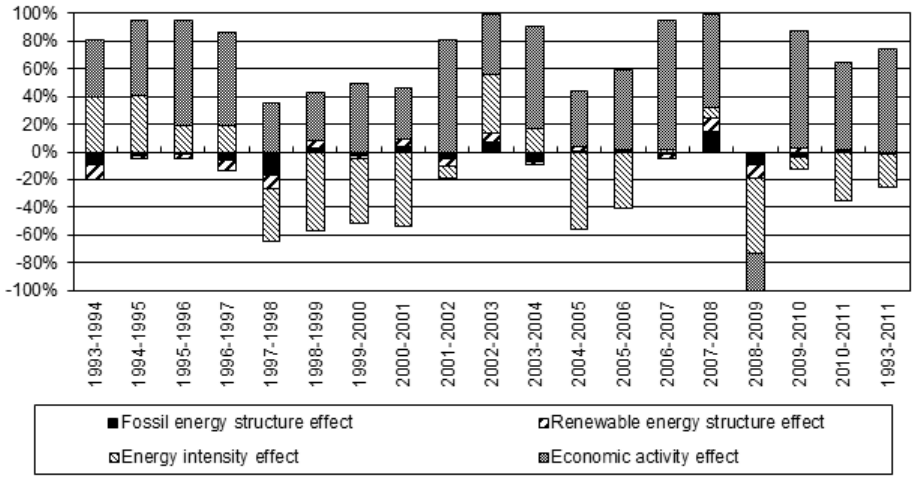

Figure 1: Complete decomposition of energy-related CO_2 emission change in percentage

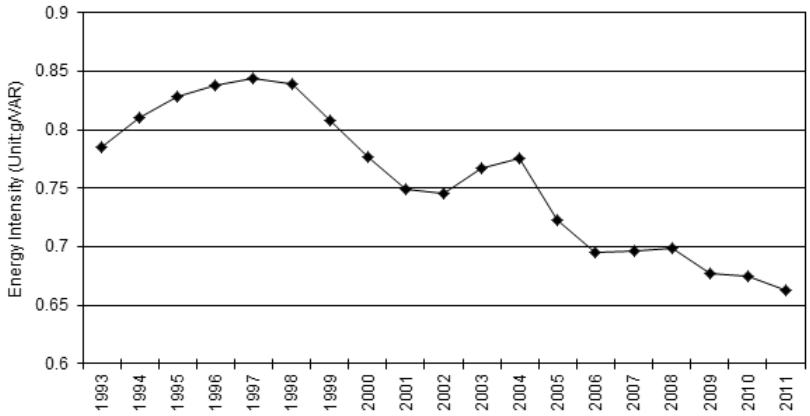

Figure 2: The change of South Africa's energy intensity over 1993-2011

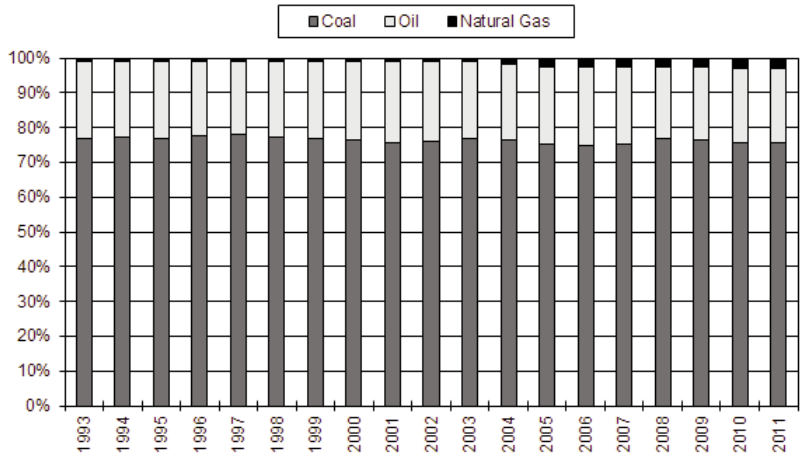

Figure 3: The tendency of fossil energy consumption structure over 1993-2011

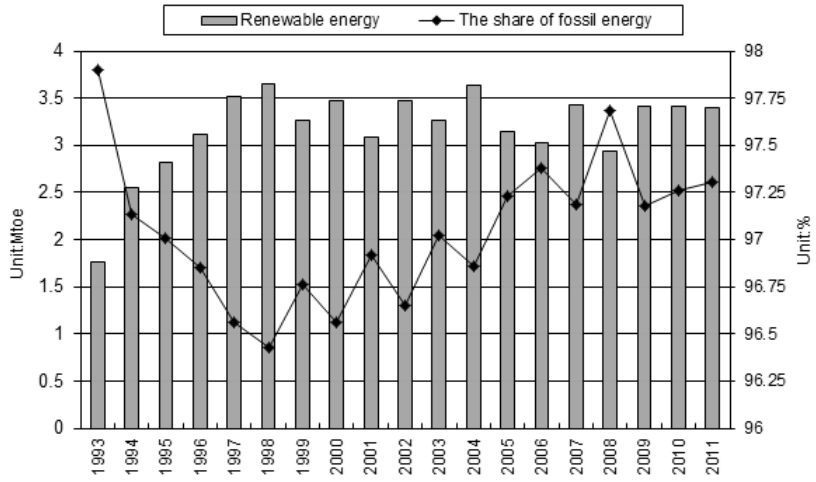

Figure 4: The tendency of the share of fossil energy consumption and renewable energy

total CO_2 emission change in absolute value. The tendency of the share of fossil energy consumption and renewable energy consumption over the period 1993-2011 is presented in Figure 4. During the study period, renewable energy consumption (including hydro power, nuclear power and other renewable energy) increased from 1.76Mtoe in 1993 to 3.39Mtoe in 2011, representing an annual average growth rate of 3.72%. That growth rate is faster than that of fossil energy (2.27%). Figure 4 also shows that the share of the fossil energy to total energy consumption declined from 97.89% in 1993 to 97.30% in 2011 (authors' calculation based on Statistical Review of World Energy, 2012). Though renewable energy increased quickly over 1993-2011, the decrease of the share of fossil energy was very small, which is the reason for the minor impact of renewable energy.

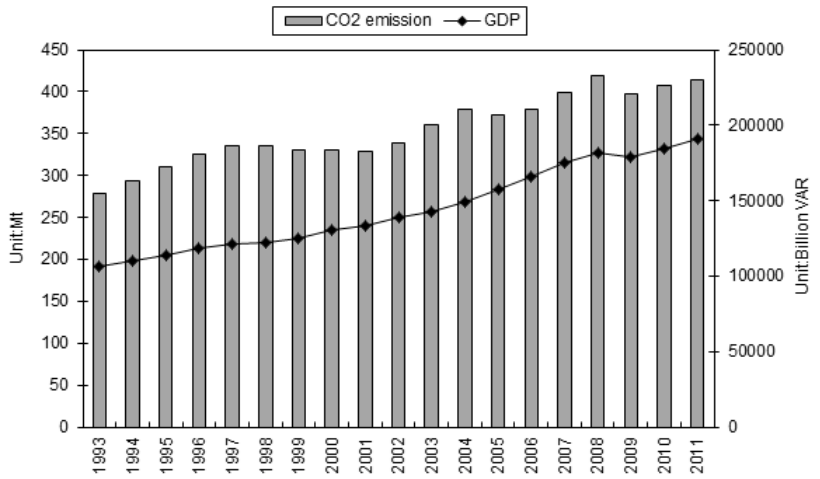

Figure 5: GDP and energy-related CO_2 emission in South Africa over 1993-2011

Our results show that economic activity is the critical factor in the growth of energy-related CO_2 emissions in South Africa. During 1993-2011, the economic activity effect made a continual increase of CO_2 emission except 2008-2009, as shown in Table 2. The accumulated (period-wise) effect is an increase of 206.13Mt, so accounts for about 152.89% of the total change in absolute value. The economic activity of South Africa (GDP) and energy-related CO_2 emissions are presented in Figure 5, which show an upward trend both in CO_2 emissions and GDP over this period. South Africa has experienced stable economic growth, with its GDP increasing at an average annual rate of about 3.27% over 1993-2011. Along with the economic development, energy –related CO_2 emission rose from 278.13Mt in 1993 to 414.32Mt in 2011, representing an annual average growth rate of 2.23%.

4. Conclusions

Global warming is considered among the most important environmental problems. How to relieve CO_2 emissions has become an urgent task of each country. South Africa has become one of the most developing countries in the world. Studying the driving forces governing energy-related CO_2 emissions may help to draw energy saving and a carbon reduction policy. Thus, the LMDI method is used to analyse the contribution of the factors which influence energy-related CO_2 emissions in South Africa over the period 1993-2011. The main conclusions drawn from the present study may be summarized as follows:

1. The energy intensity effect plays the dominant role in decreasing of CO_2 emissions, followed by the fossil energy structure effect and renewable energy structure effect; the economic activity is the critical factor in the growth of energy-related CO_2 emission in South Africa.
2. The change of South Africa's energy intensity illustrated a general decrease tendency during the study period, which also presented three different stages.
3. The tendency of the fossil energy consumption structure presented a substitution between the increasing share of natural gas and a decreasing share of coal during the study period. During the study period, renewable energy consumption increased faster than that of fossil energy.
4. During the 1993-2011, South Africa has experienced significant economic growth. Along with the economic development, energy–related CO_2 emission rose from 278.13Mt in 1993 to 414.32Mt in 2011.

Acknowledgments

The authors gratefully acknowledge the financial support from the Fundamental Research Funds for the Central Universities (2013W04).

References

Ang, B.W., (2004). Decomposition analysis for policy-making in energy: which is the preferred method? *Energy Policy* 32, 1131-1139.

BP (British Petroleum), (2012). BP Statistical Review of World Energy June 2012. Available from: www.bp.com.

Inglesi-Lotz, R., and Blignaut, J.N., (2011). South Africa's electricity consumption: A sectoral decomposition analysis. *Applied Energy* 88: 4779–4784.

Inglesi-Lotz, R., and Pouris, A., (2012). Energy efficiency in South Africa: A decomposition exercise. *Energy* 42:113-120.

IPCC, (2014). Greenhouse gas inventory: IPCC Guidelines for National Greenhouse Gas Inventories. United Kingdom Meteorological Office, Bracknell, England.

Reddy, B. S., and Ray, B.K., (2010). Decomposition of energy consumption and energy intensity in Indian manufacturing industries. *Energy for Sustainable Development* 14, 35–47.

SJGDP, (2013). http://www.sjgdp.cn/show.php?id=168.
Sun, J.W., (1998). Accounting for energy use in China, 1980-94. *Energy* 23, 835-849.
Wang, C., Chen, J.N., and Zou, J., (2005). Decomposition of energy-related CO_2 emission in China: 1957-2000. Energy 30, 73-83.
Tan, Z.F., Li, L., Wang, J.J., and Wang, J.H., (2011). Examining the driving forces for improving China's CO_2 emission intensity using the decomposing method. *Applied Energy* 88, 4496-4504.
Wang, W.W., Zhang, M., and Zhou, M., (2011). Using LMDI method to analyse transport sector CO_2 emissions in China. *Energy* 36(10): 5909-5915.
Winkler, H., Jooste, M., and Marquard, A., (2010). Structuring approaches to pricing carbon in energy and trade-intensive sectors: options for South Africa. Conference 2010 putting a price on carbon: economic instruments to mitigate climate change in South Africa and other developing countries. Energy Research Centre, University of Cape Town. p. 65.

Received 16 June 2013; revised 24 December 2014

Assessing possible energy potential in a food and beverage industry: Application of IDA-ANN-DEA approach

Oludolapo A Olanrewaju[a]

Josiah L Munda[a]

Adisa A Jimoh[b]

a Centre for Energy and Electric Power, Tshwane University of Technology
b. Department of Electrical Engineering, Tshwane University of Technology

Abstract
In the food and beverage industry, where growing, processing, packaging, distribution, storage, preparation, serving and disposing of food is the order of the day; energy consumption becomes an important input. Various energy models have been developed since the early 1970s, the period when energy caught the attention of policymakers due to the sudden price increase. Among the models are the index decomposition analysis (IDA), artificial neural network (ANN) and data envelopment analysis (DEA). The purpose of this study is to combine the strengths of these models, i.e., IDA, ANN and DEA, to allow biases in one model to offset biases in the other, so as to examine the effectiveness of energy management policies in a particular food and beverage industry. The integrated model applied to the food and beverage revealed that approximately 11% of energy consumed could be saved.

Keywords: IDA; ANN; DEA; integrated model; food and beverage industry

1. Introduction

A thorough analysis on how energy is consumed in an industry is important as it investigates the possibility of potential energy saving in the industry. Factors responsible for the consumption of energy are the activity, structure and efficiency changes. Understanding these factors will give insight into whether energy is used efficiently and the possibility of its saving.

Energy-saving is an important task today and in the future. The implementation of energy-saving policies can promote the structural adjustment of industries and products, and affect the enhancement of energy efficiency in production and processing (He *et al.*, 2011). The analyses of consumption patterns and the assessment of feasible energy conservation possibilities show that the potential for energy conservation in the industrial sector and in all sectors is substantial (Yang and Mingguang, 2011).

From energy studies, different tools have been successfully used to analyse the consumption of energy. These include index decomposition analysis (IDA), structural decomposition analysis (SDA), regression analysis, artificial neural networks (ANNs) and data envelopment analysis (DEA). The aim of this study is to combine the strengths of various energy research tools to analyse energy consumption and to assist in formulating sustainable policies for industries in the energy arena. The strengths of IDA, ANN and DEA are integrated for this study. The integration of these models has been successfully applied to Canadian industries (Olanrewaju, Jimoh & Kholopane, 2012), and South African industries (Olanrewaju, *et al.,* 2013). However, its application to a specific industry as opposed to a set of industries is yet to be carried out. This study focuses on a particular food and beverage industry, as a case study.

The rest of this paper is organized as follows: the next section introduces the literature review on studies regarding energy analysis. A description of the general integrated method based on IDA, ANN and DEA is presented. Details of the proposed method are discussed in section three. These include use of: the LMDI (Logarithmic Mean Divisia Index) for decomposition of the various factors responsible for energy consumption, the ANN model for prediction; regression analysis for authen-

tication; and, the DEA sub-model for energy optimization. The integrated model is applied to a particular food industry and beverage industry. Results and discussion are presented, as well as the conclusion on the case study, in the last section.

2. Literature review

IDA and SDA are similar, but differ in the fact that IDA is developed from index theory of economics, while SDA is based on an input-output table from statistics (Fengling, 2004). These decomposition methods make it possible to evaluate the relative contributions of various factors to changes in energy consumption, energy intensity and CO_2 emissions (Mairet and Decellas, 2009). Many studies have successfully carried out their investigation using decomposition analysis. Among the studies are APERC(APERC, 2001), where second decomposition analysis was conducted taking into account the composition of the service sector. It was discovered that activity and intensity effects were responsible for the changes in energy consumption compared with other effects. Golove and Schipper ((1997) found that the activity effect was the major factor affecting energy demand and drove energy consumption upward in their study to analyse changes in energy consumption in the United States from 1960 to 1963 using a decomposition method based on the Laspeyres index.

Gonzalez and Suarez (2003) studied the changes in electricity intensity in the Spanish industry by decomposition to explain the factors that contribute to the changes. Combined with electricity price analysis, the results of their study indicate poor contribution of structural change to substantial reductions in aggregate electricity intensity. Factors affecting the trends in energy efficiency in South Africa from 1993 to 2006 were examined by Inglesi-Lotz and Pouris (2012). It was determined that structural changes of the economy have played an important and negative role in the increasing economy-wide energy efficiency whereas the energy usage intensity was a contributing factor to the decreasing trend of energy efficiency.

Planning and conducting necessary measures to attain specified objectives is made possible by reliable prediction techniques. These techniques include regression analysis and neural networks, though the soft computing techniques (the neural networks) have proved to be superior to the conventional method (i.e., regression analysis). These techniques have been applied to energy studies successfully. Sozen and Arcaklioglu (2007) used artificial neural network to predict the net energy consumption of Turkey in order to determine the future level of the energy consumption and make correct investments. In their study, three neural network models were developed (Sozen and Arcaklioglu, 2007). South Korea's heavy dependence on imported energy sources led Geem and Roper (2009) to efficiently estimate the country's energy demand using ANN. The result of the ANN model proved superior to the regression and exponential models compared with Geem and Roper (2009).

ANN model has been successfully used to predict energy use in wheat production (Safa and Samarasighe, 2011). Several direct and indirect factors were considered in the study to create the ANN model, and it predicted energy use with an error margin of (+/-) 12% in the Canterbury farms. Ekonomou (2010) successfully used ANN to predict Greek long-term energy consumption for the years ahead, exploiting its computational speed, ability to handle complex non-linear functions, robustness and great efficiency even in cases where full information for the studied problem is absent.

DEA, an application of linear programming, has the ability to give a single index of performance, usually called the efficiency score, synthesizing diverse characteristics of decision making units (DMUs) (Azadeh *et al*., 2008). Among the energy related studies approached by DEA are the studies of Hu and Kao (2007) and Liu *et al*.., (2010). Hu and Kao (2007) set the energy-savings target using DEA for APEC economies without lowering their maximum potential gross domestic product in any year. It was found that China was in the lead with energy-saving goals. The operational performance of thermal power plants in Taiwan using data envelopment analysis was assessed by Liu *et al.,* (2010). The power plants investigated achieved acceptable overall operational efficiency from 2004-2006, with the combined cycle power plants being the most efficient.

From the literature review, it can be concluded that the decomposition tools focus on analysing and understanding historical data. Prediction techniques on the other hand serve as an aid for recommending and specifying opportunities to reduce irrational energy use (Kljajic *et al.,* 2012). DEA from various studies determines the efficiency and optimization capabilities.

IDA, ANN and DEA models are all powerful analytical tools as presented in this section, but have their weaknesses and limitations. Based on our survey, these models could be helpful to researchers in energy issues like identifying the relative contributions of different factors to changes in energy demand, prediction and forecasting of energy consumption for short- and long-term planning. Benchmarking performance to determine the potential of energy that could be saved has also been explored among the various industries. This research underlines the gaps of the individual energy models as far as energy analysis is concerned, and highlights the reasons why integration of the right models is necessary.

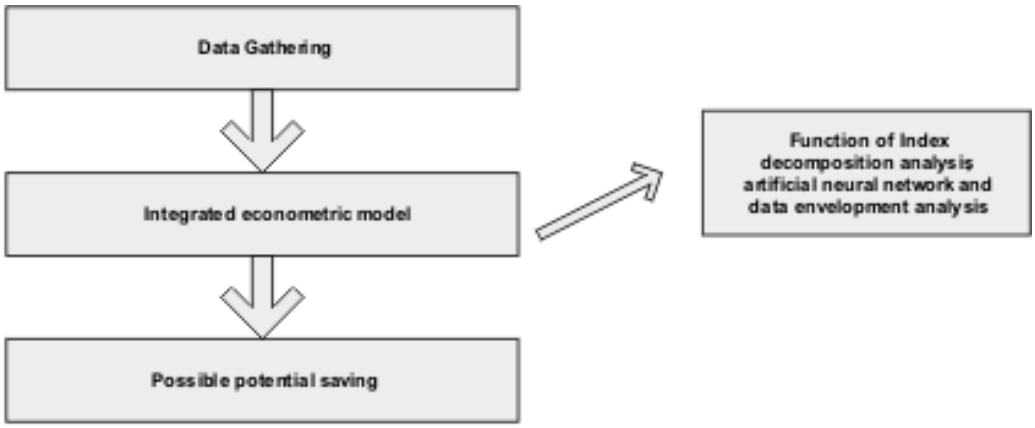

Figure 1: Structure of the integrated econometric model

3. Proposed method

Use of combined approaches is beneficial as these techniques seem to be able to take advantage of the best characteristics of all the techniques which comprise the combination. Combining different approaches allows biases in one technique to offset biases in other techniques (Bhattacharyya, 2011). The integrated econometric model developed for this investigation is an analytical tool to estimate how much energy saving could have been saved expressed by some variables that were given to the model. The model is a function of index decomposition analysis, artificial neural network and data envelopment analysis as depicted in Figure 1.

This study employs an integrated approach based on IDA, ANN and DEA for total energy efficiency assessment and optimization of energy consumption in the food industry. The model's conceptual framework is shown in Figure 2. Steps to be followed in the generic proposed model can be summarized as follows:

1. An IDA based on LMDI is performed to assess the respective contributions of activity, structural and intensity effects on the food industry.
2. Energy consumption baseline is predicted using ANN. Activity, structure and intensity effects are selected as the ANN inputs, while the observed energy consumption is the output indicator.

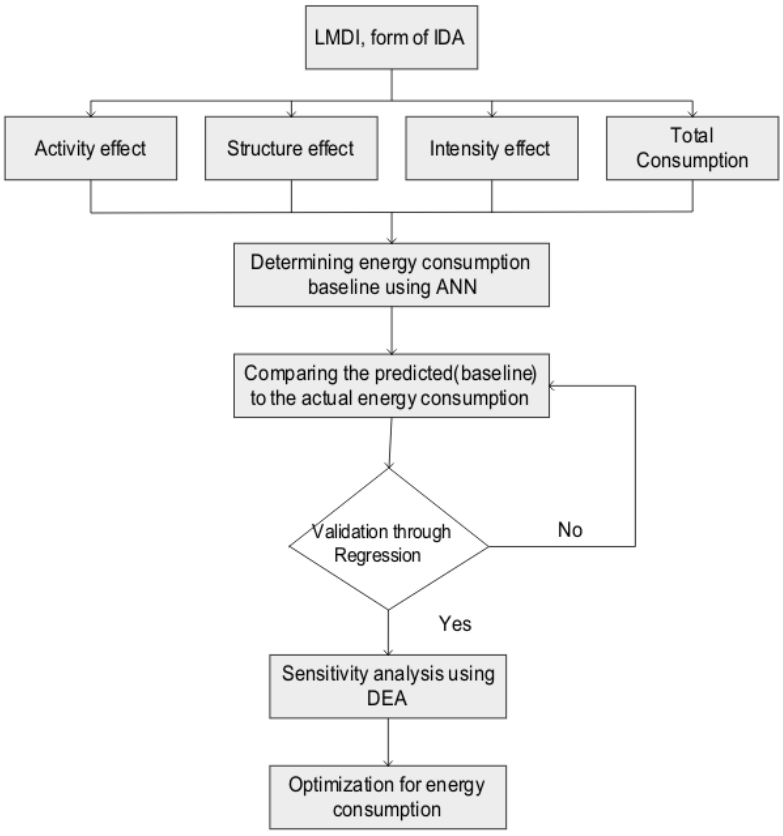

Figure 2: Schematic view of the general proposed model

3. The predicted baseline result is verified and validated using regression analysis.
4. With the aid of a super-efficient DEA sub-model, energy consumption is calculated using a sensitivity-analysis approach.
5. Suggestions for optimization of energy consumption are proposed to be applied in the food industry.

3.1 LMDI

There are various IDA methods, but the most preferred IDA is the LMDI, similar to other IDA methods, and can adopt either a multiplicative or an additive mathematical form in a time-series or base-year method. The differences between the time-series and the base-year method can be found (Granel, 2003) and (Ma and Stern, 2006). For our study, the time-series for both multiplicative and additive mathematical forms are adopted. The reason behind the use of additive form is to be able to understand easily the factors responsible for the consumption of energy, while multiplicative form is to assist in the integration model because of its non-negativity, especially when it concerns DEA application. The multiplicative and additive decomposition form decompose from the relative growth of an indicator I into determinant effects (Hoekstra and Bergh, 2003).

$$\frac{I^t}{I^{t-1}} = \text{effect x effect x effect x Residual} \quad (1)$$

The residual term for LMDI decomposition is always unity. Where energy consumption is the indicator for this study, equation (1) can be rewritten as:

$$\frac{E^t}{E^{t-1}} = D_{tot} = D_{act}.D_{str}.D_{\text{int}} \text{ (Multiplicative)} \quad (2)$$

$$\frac{E^t}{E^{t-1}} = \Delta V_{act.} + \Delta V_{str.} + \Delta V_{\text{int.}} \text{ (Additive)} \quad (3)$$

The LMDI (multiplicative) takes the following form

$$E = \sum_i E_i = \sum_i Q \frac{Q_i}{Q}\frac{E_i}{Q_i} = \sum_i Q S_i I_i \quad (4)$$

$$D_{act} = \exp[\sum_i w_i \ln[\frac{Q^T}{Q^0}]] \quad (5)$$

$$D_{str} = \exp[\sum_i w_i \ln[\frac{S^T}{S_i^0}]] \quad (6)$$

$$D_{\text{int}} = \exp[\sum_i w_i \ln[\frac{I^T}{I_i^0}]] \quad ; \quad (7)$$

Where

$$w_i = \frac{(E_i^T - E_i^0)/(\ln E_i^T - \ln E_i^0)}{(E^T - E^0)/(\ln E^T - \ln E^0)} \quad (8)$$

The LMDI (additive) takes the following form

$$\Delta V_{act} = \sum_i w_i \ln[\frac{Q^T}{Q^0}] \quad (9)$$

$$\Delta V_{str} = \sum_i w_i \ln[\frac{S^T}{S_i^0}] \quad (10)$$

$$\Delta V_{\text{int}} = \sum_i w_i \ln[\frac{I^T}{I_i^0}] \quad (11)$$

Where

$$w_i = \frac{(E_i^T - E_i^0)}{(E^T - E^0)} \quad (12)$$

The variables used for the decomposition analysis

E_i – Total energy consumption in sector *i*

E – Total energy consumption $(E = \sum_i E_i)$

Q_i – Value of production in sector *i* $(Q = \sum_i Q_i)$

Q – Total value of production $i\,(S_i = \frac{Q_i}{Q})$

S_i – Production share of sector

I_i – Intensity of energy consumption in sector $(I_i = \frac{E_i}{Q_i})$

Where D_{tot} and ΔV_{tot} represent the total energy consumption, D_{act} and ΔV_{act}, the activity involved, D_{str} and ΔV_{str}, the structural change and D_{int} and ΔV_{int}, the change in intensity. The derivation of the above equations can be found in (Ang, 2008).

3.2 ANN

ANNs are well-known massive, parallel computing models which exhibit excellent behaviour in solving problems associated with engineering, economics, etc. The most commonly applied network is the multilayer perceptron with the error backpropagation learning algorithm (Mata, 2011). For the neural network methodology, we refer interested readers to the paper (Rumelhart et al., 1986) for details of the methodology.

3.2.1 Problem formulation

The objective function chosen for this problem is the mean square error (MSE) between the outputs from the neural network and the target value which

is the energy consumption. The inputs are applied to the network; and similarly the network output is compared to the target. The error is calculated as the difference between the target output and the neural network output. The goal is to minimize the average of the sum of these errors.

$$mse = \frac{1}{Q}\sum_{k=1}^{Q} e(k)^2 = \frac{1}{Q}\sum_{k=1}^{Q} (t(k) - a(k))^2 \quad (13)$$

The least mean square error (LMS) algorithm adjusts the weights and biases of the linear network so as to reduce the mean square error. The architecture of this network comprises of three layers namely the input, hidden and output layers, with each layer having one or more neurons, in addition to the bias neurons connected to the hidden and output layers. The computational procedure of the network is described below (Hsu and Chen, 2003):

$$Y_j = f(\sum_i w_{ij} x_{ij}) \quad , \quad (14)$$

where *Yj* is the output of node *j*, the transfer function, w_{ij} the connection weight between node *j* and node *i* in the lower layer, and X_i the input signal from node in the lower layer. The backpropagation is based on the steepest descent technique with a momentum weight (bias function) which calculates the weight change for a given neuron. It is expressed as follows (Hsu and Chen, 2003, Huang *et al.*, 2002): let

$$\Delta w_{ij}^p(n)$$

denote the synaptic weight connecting the output of neuron *i* to the input of neuron *j* in the *pth* layer at iteration The adjustment $\Delta w_{ij}^p(n)$ to $w_{ij}^p(n)$ is presented as:

$$\Delta w_{ij}^p(n) = -\eta(n)\frac{\partial E(n)}{\partial w_{ij}^p} \quad , \quad (15)$$

where η (n) is the learning-rate parameter. By applying the chain rule of differentiation, the weight of the network with the backpropagation learning rule is updated, using the following formulae:

$$\Delta w_{ij}^p(n) = \eta(n)\partial_j^p(n) X_i^{p-1}(n) m(n) \Delta w_{ij}^p(n-1) \quad ,(16)$$

$$\Delta w_{ij}^p(n+1) = w_{ij}^p(n) + \Delta w_{ij}^p(n) \quad , \quad (17)$$

where $\partial_j^p(n)$ is the nth error signal at the *jth* neuron in the pth layer, $X_i^{p-1}(n)$ is the output signal of neuron *i* at the layer below and *m* is the momentum factor.

3.3 Linear regression analysis

Performance of neural networks can be measured to some extent by the sum squared error, but it is useful to investigate the response in more detail. One of the options is to perform a regression analysis between the network response and the corresponding targets (Gonzalez, 2008).

According to Gonzalez (2008), the validation analysis leads to 3 parameters. The first two m and b correspond to the slope with the y-intercept of the best linear regression, relating targets to neural network outputs. To ensure a perfect fit (outputs exactly equal to targets), the slope would be 1, and the y-intercept would be 0. The third parameter is the correlation coefficient (R-value) between the outputs and targets. There is a perfect correlation between the targets and outputs if the R-value is equal to 1.

3.4 DEA

This study makes use of the input-oriented Charnes-Cooper-Rhodes (CCR) model of a DEA. The input model reduces the inputs while satisfying the lowest given output (Liu *et al.*, 2010). The efficiency scores obtained from the input-oriented model for inefficient months/years (DMU) deal with the potential of conservation in the observed energy consumption.

The model to the CCR is given below (Liu *et al.*, 2010; Emmanuel, 2001):

$$\min \theta_k - \varepsilon \left(\sum_{i=1}^{m} s_{ik}^- + \sum_{r=1}^{s} s_{rk}^+ \right)$$

subject to:

$$\theta_k x_{ik} - \sum_{j=1}^{n} \lambda_j x_{ij} - s_{ik}^- = 0; i = 1,..,m$$

$$y_{rk} - \sum_{j=1}^{n} \lambda_j y_{rj} + s_{rk}^+ = 0; r = 1,..,s$$

$$\lambda_j, s_{ik}^-, s_{rk}^+ \geq 0 \; \forall \; i, j, r \quad (18)$$

where θ_k is the measure of efficiency of DMU 'k, the DMU in the set of $j = 1,2,..n$ DMUs rated relative to the others; ε an infinitesimal positive number used to make both the input and output coefficients positive; s^-_{ik} slack variables for input constraints, which are all constrained to be non-negative; s^+_{ik} slack variables for output constraints, which are all constrained to be non-negative; and λj the dual weight assigned to DMUs.

3.4.1 'Sensitivity analysis and optimization' using the DEA sub-model

The input-oriented, measure-specific super-

efficiency DEA model proposed by Zhu (2003) was adopted for the sensitivity analysis. Constant return to scale (CRS) was assumed. In the model 19, the k_{th} input is given priority to change to its value.

$$\min \theta_k$$

$$s.t \sum_{\substack{j=1 \\ j\neq 0}}^{..} \lambda_j x_{ij} \leq \theta_k x_{i0}, i = k,$$

$$\sum_{\substack{j=1 \\ j\neq 0}}^{n} \lambda_j x_{ij} \leq x_{i0}, i \neq k$$

$$\sum_{\substack{j=1 \\ j\neq 0}}^{n} \lambda_j y_{rj} \geq y_{r0}, r = 1,2,..,s$$

$$\theta_k, \lambda_j, (j \neq 0) \geq 0 \qquad (19)$$

The sensitivity analysis result for an efficient DMU will assist in determining the increase in energy consumption, yielding an inefficient DMU. It can be assumed that the decrease in energy consumption could make an efficient DMU of an inefficient DMU.

3.4.2 Optimization of energy consumed

The optimal value of a DEA sub-model shown in model 18 (θ^*) for an inefficient DMUo, is the minimum reduction in energy consumption that causes DMUo to be a best-practice DMU and an efficient DMU on the frontier for the observed energy consumption (input). When x_{i0} is the energy consumption of DMUo, $\theta^* x_{i0}$ is the amount of potential reduction in energy consumption that can be compared to the best observed DMU. The potential of a saving in energy consumption decreases as the optimal value of the energy consumption in model 18 increases. The reduction ($\theta^* x_{i0}$) in the input is the optimal reduction in energy consumption that makes DMUo an efficient DMU.

3.5 Case study

In this paper, we analyse a specific food and beverage industry for the possible energy potential that could be saved between January 2010 and April 2012 of one of the South African industrial sectors. Data used; Figures 3 and 4 are the energy consumption and output production data used for products A and B in the particular industry. The productions (Products A and B) are all given in tonnes and the energy consumption in gigajoules.

3.6 Results and discussion

3.6 1 LMDI Decomposition analysis

Both additive and multiplicative decomposition were employed for this case study because of the negativity result in energy consumption from additive decomposition. To be able to employ data envelopment analysis, the data inputted into the DEA model must be non-negative. Additive decomposition was employed to be able to understand the factors responsible for the consumption of energy in a simplified fashion. Multiplicative decomposition was employed because of the non-negativity result.

Factors responsible for the consumption of energy are the activity, structure and intensity changes. Understanding these factors give insight as to whether energy is used efficiently and the possibility of its saving. Figures 5 and 6 depict the effect of these factors.

The intensity effect measures improvements in energy efficiency, changes in technology, fuel mix changes, efficient energy management practice as well as any other factor which is not related to volume of output or composition. If this effect is positive, then it implies a worsening energy efficiency scenario. A negative intensity effect points to improvements in energy use. From Figure 5, the intensity effect gained unswerving positivity in

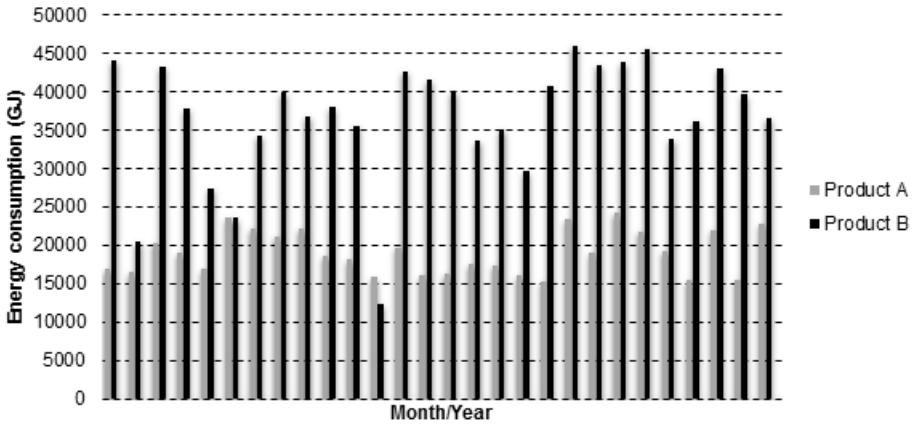

Figure 3: Energy consumption data

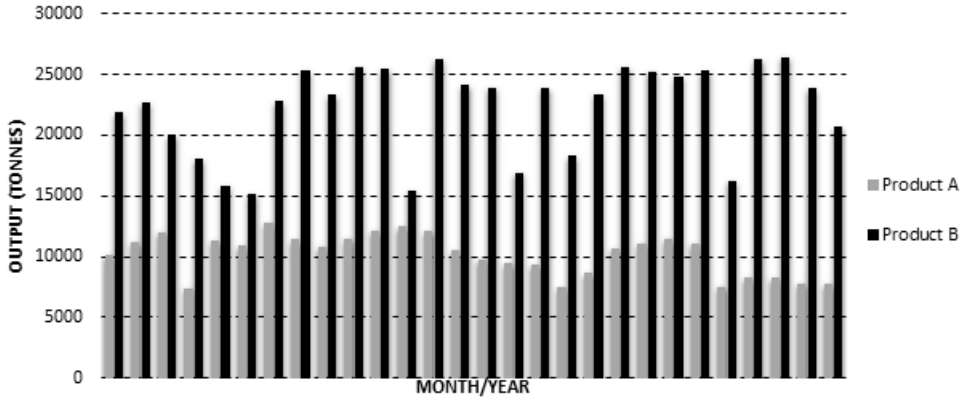

Figure 4: Output data

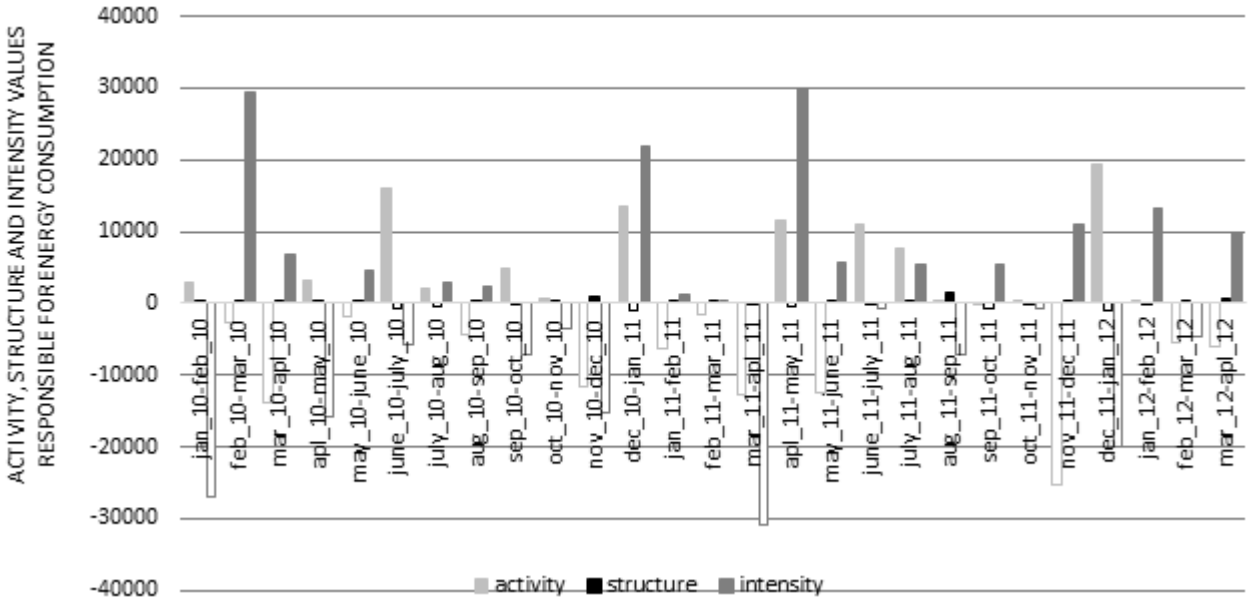

Figure 5: Factors responsible for the consumption of energy in a food and beverage industry

February 2010 – April 2010, July 2010 – September 2010, December 2010 – March 2011, and from April 2011 – June 2011. The structural effect measures the changes in composition. In general, if the structural effect is positive, there is a movement towards more energy intensity. From Figure 5, the structural effect gained unswerving positivity in March 2010 – June 2010, October 2010 – December 2010, January 2011 – March 2011, July 2011 – September 2011 and February 2012 – April 2012. The activity effect is positive when more output can be produced with the same energy use. This effect implies an improvement in energy efficiency when positive. From Figure 5, the activity effect gained unswerving positivity in June 2010 – August 2010, September 2010 – November 2010, June 2011 – September 2011 and December 2011 – February 2012. Figure 6 summarizes the total effects of these factors.

From Figure 6, the consumption of energy increased by 673% from the period January 2010-February 2010 and to the March 2012-April 2012 period. For activity effect, changes in the level of activity between 2010 and 2012 are considered, keeping the intensity and share of food industry in value addition unchanged in the initial year values. This implies that if activity would have changed alone, the energy demand for the food industry activities considered would have reduced by 11116.6 GJ.

For the structure effect, the structural change within the period is considered while keeping the other two factors unchanged. This suggests that the share of the food industry's activities in the industrial output has reduced and if this only had changed, the energy demand would have reduced 83.58GJ.

Finally for the intensity effect, we look at the changes in energy intensity within the period under investigation and keep the other two factors at their initial values. This suggests that the intensity in the food industry has increased and their intensity would have increased the energy demand by

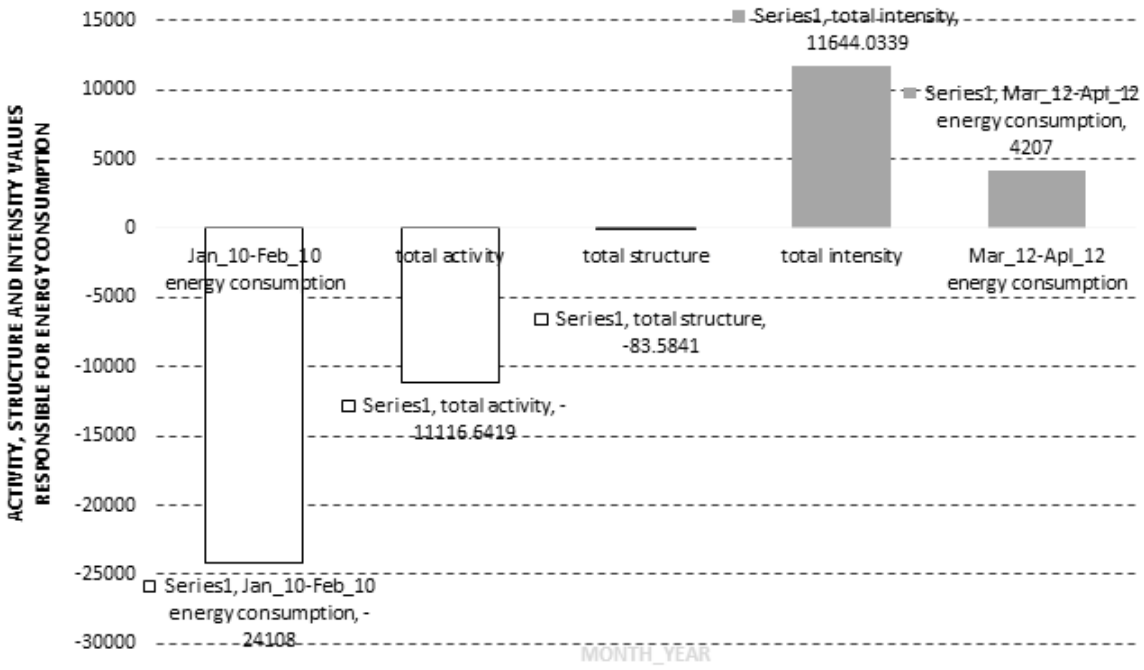

Figure 6: Summary of the factors responsible for the consumption of energy in a food and beverage industry

11644GJ between 2010 and 2012 if other things did not change. It can be concluded that from the period under investigation, energy has not been consumed efficiently from Figure 6.

3.6.2 ANN results

To attain the specified objectives of the study, the baseline was predicted using a reliable prediction technique, ANN. For the prediction technique; activity, structure and intensity were the inputs while the actual energy consumption was the output. It was discovered that a strong correlation exists between the baseline (predicted energy consumption) and the actual energy consumption. Figure 7 presents the results. For the prediction, '5' hidden neurons was used, with activation functions of tansig and purelin. Trainlm was used under Matlab 2010a software.

3.6.3 Regression analysis

To confirm and validate the ANN's result, linear regression analysis is a likely confirmation method to the neural network model between the predicted and corresponding energy consumption values. The analyses lead to a line $y=a+bx$ where y is the output (predicted energy consumption) and x is the input (observed energy consumption), b is the coefficient of the input (the gradient) and a is the slope with a correlation coefficient of R^2. A perfect prediction would give, $b=1$ and $R^2 = 1$.

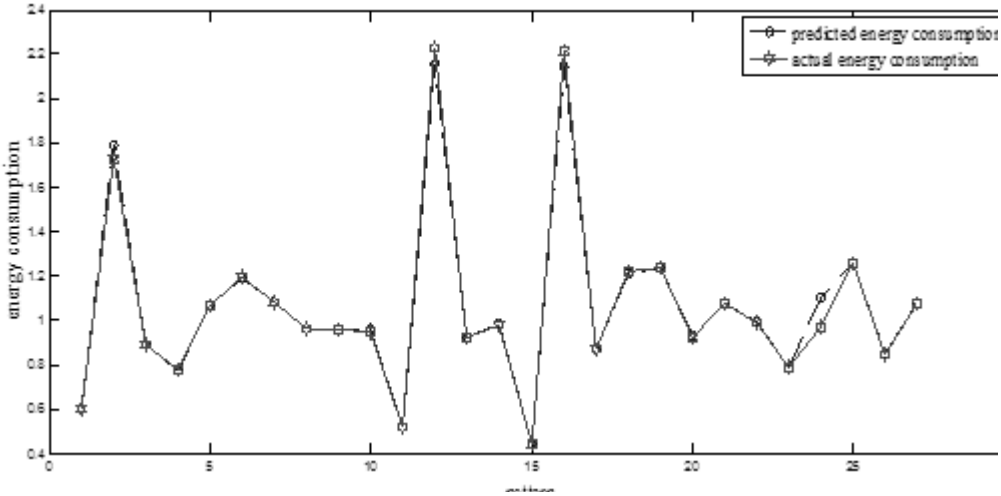

Figure 7: Prediction result for energy baseline

Table 1: Linear regression analyses parameters for the ANN validation of energy consumption

b=0.985
R^2 = 0.996

A graphical output provided by this confirmation analysis is depicted in Figure 8. The predicted energy consumption was plotted against the actual energy consumption. From Table 1 and Figure 8, the neural network can be seen to predict correctly. It should be noted that b and R^2 are very close to 1 respectively from Table 1.

3.6.4 DEA results

To be able to determine the possible energy saving for the period of study, DEA analysis was carried out. DEAFrontier software package on Excel has been employed to carry out the DEA analyses. The observed energy consumption was selected as the input whereas the predicted energy consumption was selected as the output data for the analyses. The efficiency scores of the food and beverage industry in different months/years (DMUs) are shown in Table 3. These efficiency scores are relative to the best performing months/years.

With internal benchmarking based on the month/year of consumption of energy, December 2011 – January 2012 was discovered to have performed better and can serve as the only benchmark to the other periods considered. Table 2 presents the efficiency score based on the comparison of the months/years following the CRS assumption. For this case study, the DMU was considered to have low energy consumption in comparison to the others. The inefficient DMUs should consider the efficient DMU as a peer to enable them to be efficient. To be able to register the energy consumption that will enable the inefficient years optimal in the DEA analyses, they must try to emulate the efficient month/year. The efficiency score of each DMU is a coefficient that indicates the amount of potential savings possible in energy consumption. The potential of energy consumption improvement can best be derived from the results of optimization analyses.

Table 2: Efficiency scores based on benchmarking of the food and beverage industry

DMU No.	*DMU Name*	*Efficiency*
1	jan10-feb10	0.8812
2	feb10-mar10	0.9146
3	mar10-apl10	0.8812
4	apl10-may10	0.87554
5	may10-jun10	0.8812
6	jun10-jul10	0.87738
7	jul10-aug10	0.8812
8	aug10-sep10	0.88129
9	sep10-oct10	0.8812
10	oct10-nov10	0.89121
11	nov10-dec10	0.8812
12	dec10-jan11	0.85321
13	jan11-feb11	0.8812
14	feb11-mar11	0.8848
15	mar11-apl11	0.8812
16	apl11-may11	0.85538
17	may11-jun11	0.8812
18	jun11-jul11	0.87256
19	jul11-aug11	0.8812
20	aug11-sep11	0.89362
21	sep11-oct11	0.8812
22	oct11-nov11	0.88645
23	nov11-dec11	0.8812
24	dec11-jan12	1
25	jan12-feb12	0.8812
26	feb12-mar12	0.88473
27	mar12-apl12	0.8812

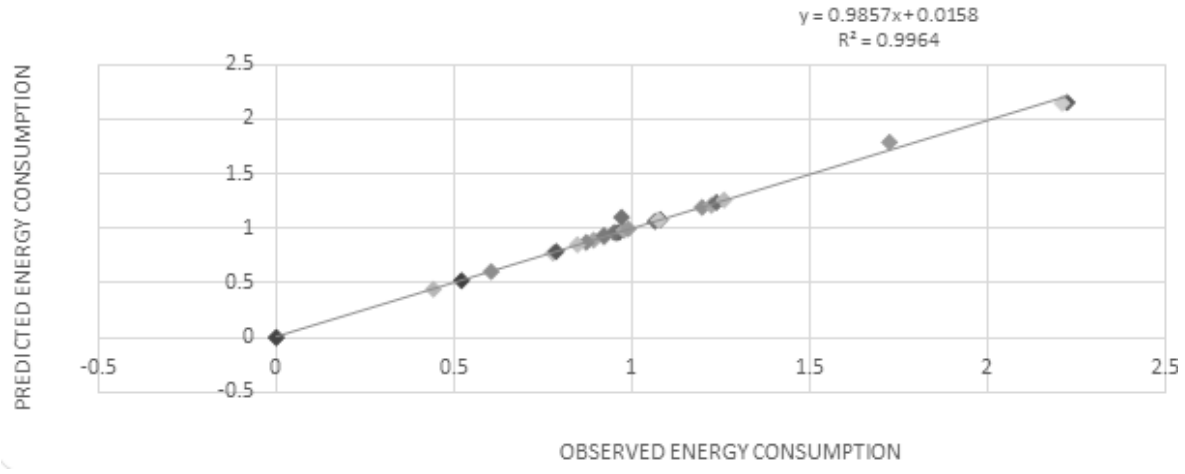

Figure 8: Graphical output provided by the validation analyses for food industry 'X'

3.6.5 Optimization of energy consumed

Optimization with the aid of model 19 has been applied. For example, industrial sectors in January 2010-Feruary 2010 will encounter a potential savings of (100-88.12 = 11.88) % in energy consumption compared to the best practice in December 2011-January 2012. Industrial sectors in January 2010-February 2010 can reduce their energy consumption by 11.88% and be an efficient industrial sector. Figure 9 relates the consumption to the percentage amount of energy that would have been saved if the periods emulated December 2011 – January 2012 practice. In summary, the amount of energy that could have been possibly saved is 11% of the total energy consumed for the whole period under study, which is equivalent to 171,533.78GJ.

4. Conclusion and discussion

Energy is a priority in the food industry. The food and beverage industry researched has plans in place to optimize the utilization of equipment to alleviate unnecessary running to reduce its energy consumption. To ensure the further reduction of its energy consumption, it becomes critical to conduct energy efficiency investigation to realize its dreams. Accordingly, to assess its energy efficiency potential, this investigation employed IDA-ANN-DEA approach. It was argued that seasonal effects could be the reason for the efficient period, i.e. December 2011-January 2012, though couldn't be confirmed. The seasonal effect argument is false as productivity is not the measure of output but the ratio of output to input. Considering the result obtained; other similar period, i.e. December 2010–January 2011 which is similar with the operations performed as the efficient period was inefficient, this simply nullifies the argument of seasonal effects. The result of the analyses identified factors responsible for the industry's energy consumption, baseline for energy consumed and possible potential saving. This study

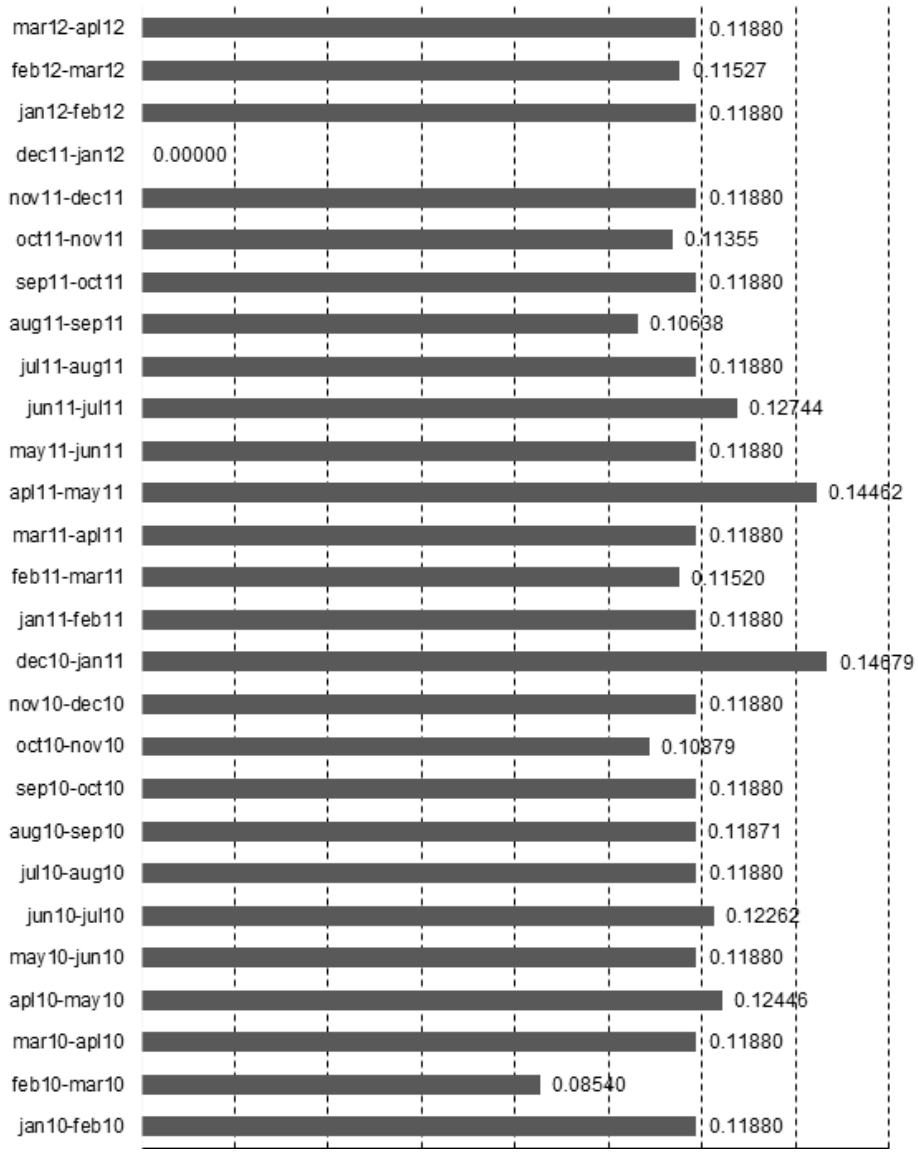

Figure 9: Possible potential energy saving for food and beverage industry

discovered possible potential saving of 171,533.78GJ during the period of investigation. Following the study carried out, existing energy efficiency strategies, energy conservation schemes and policies for the industry should be evaluated. The case study shows that energy intensity is an informative and practical indicator. Energy-conservation policy can be improved by considering the information from the analysis of the energy intensity. There is need for assistance in developing energy management capability and policy package to promote energy efficiency as required. It is required that the food and beverage industry needs a more aggressive energy-conservation policy to reduce its energy consumption.

5. Limitation and future research

Following the integrated model employed for this study, it should be noted that index decomposition analysis was performed on the Matlab 10.0 platform, artificial neural network o the Matlab 10.0 platform, and data envelopment analysis on the Excel platform (DEAFrontier). It is recommended that a programme that can integrate the three models on the same platform should be considered and this is ongoing for future research, as this will increase the simplicity of the system proposed.

References

Ang, B. W. (2008). Index Decomposition Analysis Using LMDI: A Simple Guide.

APERC (2001). Energy Efficiency .ndicators – A study of Energy Efficiency Indicators in APEC Economics, APERC, Tokyo.

Azadeh, A., Ghaderi, S. F. & Maghsoudi, A. (2008). Location optimization of solar plants by an integrated hierarchical DEA PCA approach. *Energy Policy*, 36, 3993-4004.

Bhattacharyya, S. C. (Ed.). (201)1. Energy Economics. Concepts, Issues, Markets and Governance: Springer-Verlog London Limited.

Ekonomou, L. (2010). Greek long-term energy consumption production using artificial neural networks. *Energy*, 35, 512-517.

Emmanuel, T. (ed.) (2001). Introduction to the Theory and Application of Data Envelopment Analysis: A Foundation Text with Integrated Software, Norwell, Massachusetts: Kluwer Academic Publishers.

Fengling, L. (2004). Decomposition Analysis Applied to Energy: Some methodological issues. A thesis submitted for the degree of Doctor of Philosophy. National University of Singapore.

Geem, Z. W. & Roper, W. E. (2009). Energy demand estimation of South Korea using artificial neural network. *Energy Policy,* 37, 4049-4054.

Golove, W. H. & Schipper, I. J. (1997). Restraining carbon emissions and measuring energy use and efficiency in the USA. *Energy Policy*, 25, 803-812.

Gonzalez, P. F. & Suarez, R. P. (2003). Decomposing the variation of aggregate electricity intensity in Spanish industry. *Energy,* 28, 171-184.

Gonzalez, R. L. (2008). Neural Networks for Variational Problems in Engineering., Technical University of Catalonia.

Granel, F. (2003). A Comparison Analysis of Index Decomposition Methods. Masters Degree, National University of Singapore.

He, Y. X., Zhang, S. L., Zhao, Y. S., Wang, Y. J. & Li, F. R. (2011). Energy-saving decomposition and power consumption forecast: The case of Liaoning province in China. *Energy Conversion and Management*, 52, 340-348.

HoekstrA, R. & Bergh, J. J. C. J. M. V. D. (2003). Comparing structural and index decomposition analysis. *Energy Economics,* 25, 39-64.

Hsu, C.-C. & Chen, C.-Y. (2003). Regional load forecasting in Taiwan-applications of artificial neural networks. *Energy conversion and Management*, 44, 1941-1949.

Hu, J.-L. & Kao, C.-H. (2007). Efficient energy-savings targets for APEC economies. *Energy Policy,* 35, 373-382.

Huang, H., Hwang, R. & Hsieh, J. (2002). A new artificial intelligent peak power load forecaster based on non-fixed neural networks. *Electric Power Energy Syst,* 24, 245-50.

Inglesi-Lotz, R. & Pouris, A. (2012). Energy efficiency in South Africa: A decomposition exercise. *Energy,* 42, 113-120.

KljajiC, M., Gvozdenac, D. & Vukmirovic, S. (2012). Use of Neural Networks for modeling and predicting boiler's operating performance. Energy, in press.

Liu, C. H., Lin, S. J. & Lewis, C. (2010). Evaluation of thermal power plant operational performance in Taiwan by data envelopment analysis. *Energy Policy,* 38, 1049-1058.

Ma, C. & Stern, D. I. (2006). China's Changing Energy Intensity Trend: A Decomposition Analysis. Rensselaer Working Papers in Economics.

Mairet, N. & Decellas, F. (2009). Determinants of energy demand in the French service sector : A decomposition analysis. *Energy Policy*, 37, 2754-2744.

Mata, J. (2011). Interpretation of concrete dam behaviour with artificial neural network and multiple linear regression models. *Engineering Structures*, 33, 903-910.

Olanrewaju, O.A., Jimoh,A.A., & Kholopane P.A. (2013). Assessing the energy potential in the South African industry. A combined IDA-ANN-DEA (Index Decomposition Analysis-Artificial Neural Network-Data Envelopment Analysis) *Energy*, 63, 225 – 232.

Olanrewaju, O.A., Jimoh,A.A., & Kholopane P.A. (2012). Integrated IDA-ANN-DEA for assessment and optimization of energy consumption in industrial sector. *Energy,* 46, 629 – 635.

Rumelhart, E., Hinton, G. E. & Williams, R. J. (eds.) (1986). Learning Internal Representations by Error Propagation in Parallel Distributed Processing 1, Cambridge, MA: MIT Press.

Safa, M. & Samarasighe, S. (2011). Determination and modelling of energy consumption in wheat production using neural networks: 'A case study in

Canterbury province, New Zealand'. *Energy*, 36, 5140-5147.

Sozen, A. & Arcaklioglu, E. (2007). Prediction of net energy consumption based on economic indicators (GNP and GDP) in Turkey. *Energy Policy,* 35, 4981-4992.

Yang, G. & Mingguang, L. (2011). Analysis on the degree of the industrial structure's impact on the energy consumption – Based on empirical study of Guangdong Province. *Energy Procedia,* 5, 1488-1496.

Zhu, J. (ed.) (2003). Quantitative models for Performance Evaluation and Benchmarking, Netherlands: Kluwer Academic Publishers.

Received 3 January 2013; revised 17 February 2015

Are solar tracking technologies feasible for domestic applications in rural tropical Africa?

Kant E Kanyarusoke[a]

Jasson Gryzagoridis[b]

Graeme Oliver[a]

a. Department of Mechanical Engineering, Cape Peninsula University of Technology, Cape Town, South Africa
b. Department of Mechanical Engineering, University of Cape Town, South Africa

Abstract
That solar tracking improves energy yields from solar harvest systems is not debatable. Nor is the under powering of tropical Africa amidst plenty of energy resources – including solar. This paper presents a review of recent literature on tracking as applied to domestic solar harnessing devices. The purpose is to find basic requirements in design of a suitable solar tracker for the region's rural homes. It is concluded that Single axis passive trackers possibly will stand better chances of acceptability in the region.

Keywords: tropical Africa, solar tracking, solar energy, domestic application

1. Introduction

It is an established fact that tracking improves energy yields from solar harvest devices. But there are doubts about the efficacy of this improvement for small systems and in high diffuse radiation areas. Mousazadeh *et al.* (2009), for example, advise against use of tracking for small systems because of disproportionate energy consumption by the tracking mechanisms. Elmer (2006) reported a lack of significant total energy gain from solar tracking in Great Britain because of excessive diffuse radiation. In Hanover, Germany, Beringer *et al.* (2011) reported that the tilt angle of fixed panels was nearly irrelevant as far as total annual yields were concerned. Does this mean tracking does not yield more energy? – Not necessarily. Kanyarusoke *et al.* (2012a) showed that at latitude (L), a fixed slope (β) surface receives radiation at a best angle on the day when the sun declination (δ) satisfies the condition in equation (1). Hence all fixed surfaces do so at their appropriate times. Whether the total annual yield for one inclination is higher than that at another depends on additional factors like climatic conditions.

$$\beta - \left| L - \delta \right| = \text{Minimum} \qquad (1)$$

Tracking enables multiple repetition of this condition – and hence can in general be expected to increase yield as reported by many researchers and inventers in different circumstances. Theoretical analysis on photovoltaic yields from a 180 Watt peak panel at 80 African weather stations (Kanyarusoke *et al.*, 2012b) seemed to suggest there can be substantial gains using various modes of tracking except in rainy equatorial and sandy, windy Sahel regions. There, effects of diffuse radiation were as important as in Elmer's case above. Focusing on systems for home use, this paper reviews available literature on tracking devices.

The paper is organized as follows: Section 2 gives a short brief about tropical Africa. Focus is on energy and technical issues affecting tracker marketing. Section 3 reviews the trackers. Section 4 summarises issues about the technologies in the target market segment.

2. Tropical Africa: Energy issues and solar tracking needs

Tropical Africa is that part of the continent lying between latitudes $\pm 23.5^{o}$. This means the sun is directly overhead twice annually. It also means the

sun's rays do come from the northern and southern directions at different times of the year. Hence, the use of fixed slope panels facing either direction poses problems of missing beam radiation at certain times of the year.

This region is described by the International Energy Agency (IEA) as underpowered because of inadequate grid power supply (IEA 2011). Hence, self-generation is a necessity in many situations. At village level, the easiest, safest and most convenient form of self-electric generation is to use photovoltaic (PV) systems. But PV systems' thermodynamic efficiencies are in the 10 to 16% range. Ideally therefore, they should be installed to track the sun so as to maximise incident energy if costs of doing so are justified by additional yield.

The only area where tracking is being used out of necessity is in concentrated solar power (CSP) systems. Nigeria has many documented research outputs on this. Between Oyetunji's (1989) work on composite conical concentrators, Oyetunji *et al.* (1989) and Abdulrahim's (2008) PhD work on bi focal solar tracking and (Abdulrahim *et al*., 2010), there were not less than seven significant contributions at honours and M Sc degree research levels in the area.

The extensive energy poverty in tropical Africa amidst an abundant solar resource supply and a growing middle class means that a large potential for innovative solar energy harvesting devices exists. The progressive efforts by African governments to increase the solar resource component in their energy mixes (Karekezi, 2002; Bugaje, 2006; UN, 2007; Brew-Hammond and Kemausuor, 2009) and to rural-electrify (UNEC, 2006; Fluri, 2009; Brent and Rogers, 2010; Pegels, 2010; UN, 2014) create opportunities for a mass market of suitably designed solar tracking devices not just to cater for PV and CSP but also for Solar Thermal (ST) applications.

In summary therefore: first, there is a big potential for solar engineering development for tropical African homes. Secondly, some of these applications need to track the sun. But even where systems are being developed, tracking is limited only to where it is absolutely essential.

3. Solar tracking technologies

Solar tracking is the act of making a solar collection surface change its orientation with the movement of the sun in the sky. There are two significant relative motions in the earth-sun system. The first is the diurnal movement due to the earth's rotation about its axis, causing day and night. This is responsible for the hourly variation of incident solar radiation on a surface. The second is the much slower movement due to the earth's elliptical voyage round the sun. Two factors in this motion combine to affect incident radiation. First, the actual sun-earth distance affects the extra-terrestrial radiation in accordance with an inverse square law. Secondly, the angle between the earth's equatorial plane and its orbit causes an apparent seasonal north-south range of travel of the sun in the upper celestial hemisphere. Figure 1 shows the relative motions.

Full control of solar harvest surface orientation is therefore a 2-degree of freedom problem. In practice, control is achieved by manipulating rotations about 2 of any 3 orthogonal axes. Commonly used axes are: West-East; North-South in the horizontal plane and the vertical Nadir-Zenith. Mousazadeh *et al.* (2009), Kelly and Gibson (2010), Barsoum and Vasant (2010), Seme *et al*. (2011), Tina and Gagliano, (2011) – among others – report the following pairs to constrain the rotation as to keep the surface facing the sun all day long.

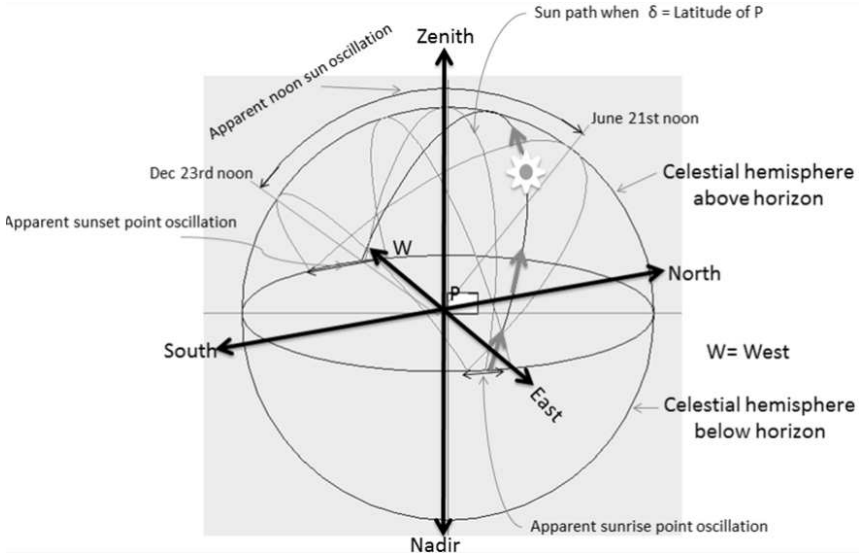

Figure 1: Apparent sun motion on the 'inside' surface of an inverted celestial hemisphere for a place 'P' within the tropics

- W-E and S-N
- S-N and Nadir – Zenith
- Nadir – Zenith and W-E

Rotation about these axes affects the surface slope β and its azimuth ψ. Tracking manipulates these angles to vary with the sun angles: the elevation α and the solar azimuth ψ_{ss}. These are dependent on the time and day of year. Hence, from a tracking point of view, they are independent variables. Figure 2 shows the four angles.

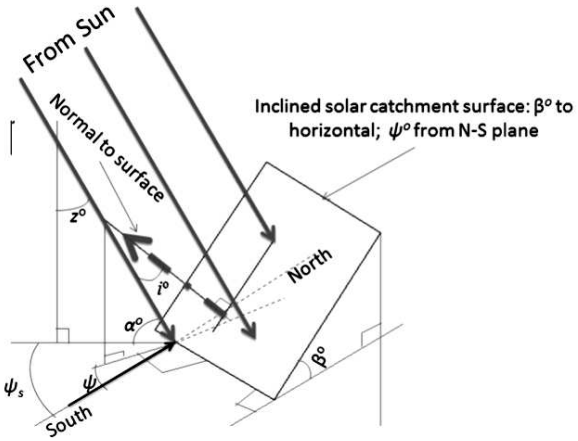

Figure 2: Important angles for a solar tracking surface: '*i*' is the incidence angle to be minimised

Broadly, the angles β and ψ track α and ψ_s using mechanisms classified according to two criteria (Helwa, *et al.*, 2000; Markvart, 2000; Chong and Wong, 2009):

- Passive or Active tracking
- One axis or Two axes tracking

3.1 Passive tracking

When the radiation catchment plane or aperture is adjusted without use of electrical power, the tracking is said to be passive.

Passive single axis trackers

Passive tracking on one axis is commonest in solar thermal systems employing tubular absorbers. These include (Winston, 2001; Kalogirou, 2007): compound parabolic collectors (CPCs), linear Fresnel reflectors (LFRs), parabolic trough collectors (PTCs) and cylindrical trough collectors (CTCs). The radiation catchment plane is directed to the sun usually in incremental steps about either a horizontal S-N or one parallel to the earth's rotational axis.

One example of a passive tracker is that by Zomeworks. It uses a refrigerant under suitable pressure in two cylinders running along the edges of the radiation catchment surface as shown in Figure 3. The cylinders are shaded and connected by a pipe/tube. When the incident radiation is not normal to the catchment plane, one of the cylinders is heated more than the other. Some of the refrigerant in the affected cylinder evaporates to create a new saturation pressure. The pressure rise forces some liquid into the cooler shaded cylinder, causing an extra torque to act on the structure's rotational axis. The shading is designed such that this torque turns the un-shaded cylinder towards shade. Damping helps stabilise the system quickly.

The main problems with the Zomeworks tracker are: lack of an evening/night return mechanism; slow wakeup response in the mornings due to limitation on the surface inclination angle β. Poulek (1994) and Full (2010) have faulted the use of refrigerants on account of environmental and safety concerns. Use of safer refrigerants like R134a can help address this issue.

Poulek developed a tracker using a shape memory alloy (SMA) to actuate the rotation. Two identical cylindrical actuators were symmetrically encased in a rotating cylinder with a lens at its opening as shown in Figure 4. Each actuator's one end joined a plane mirror attached to the rotating case while the other end was fixed to the frame (stator) sup-

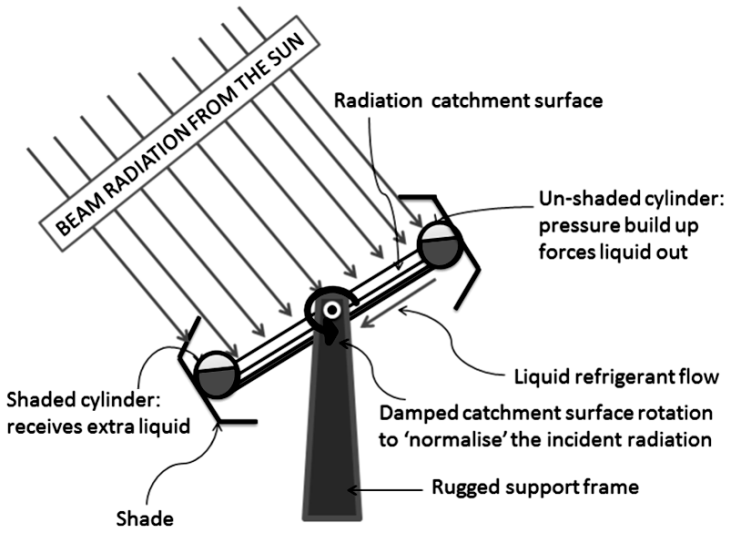

Figure 3: Zomeworks solar tracker – principle of operation

porting the radiation catchment plane. When the plane is properly oriented to the sun, the lens focuses the radiation onto the mirror which reflects it back preventing the SMAs from receiving it. On misalignment however, one of the SMAs receives the radiation, gets heated above its transformation temperature and then changes shape, rotating the mirror – and hence the plane – until radiation is again incident on the mirror.

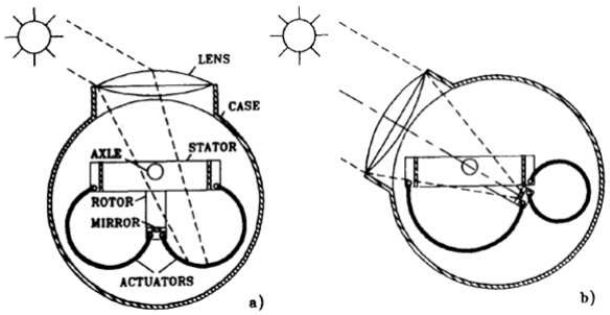

Figure 4: Poulek's single axis passive solar tracker
With permission from Elsevier: Solar Energy Materials and Solar cells: 33 (1994): 288 & 289

The tracker uses Cu-Zn-Al alloy. Because of the material's high damping characteristics, oscillations do not arise. It returns itself to morning conditions at night. Its downside is the 140° swing limit – meaning some energy harvest in the mornings and evenings is lost.

Clifford and Eastwood (2004) designed a tracker using the more common and robust aluminium/steel bimetallic strips. The strips are shaded and attached to the edges of the radiation catchment plane like the cylinders in the Zomeworks tracker. The more expansive aluminium is on the outside. Connected to the strips midpoints are masses which help amplify moments caused by the differential expansion on heating. The resulting net moment turns the radiation catchment plane to shade the hot strip. A mass-damper-thermally induced spring system was able to achieve a tracking range of 120° under lab conditions in the UK.

Although the design had equatorial regions in mind, it wasn't field tested in the target area. Full (2011) made a similar design in Kenya, using the strips and turning on a shaft from locally available bamboo plants. The tracker was reported to help increase photo-electricity generation by 38%. Still in rural Kenya, Mwithiga and Kigo (2006) developed a manually operated coffee beans dryer (see Figure 5). But the tracking labour cost could not be justified for a low value crop like coffee.

In his PhD thesis, Abdulrahim (2010) reviewed work that had been done in Nigeria especially on solar concentrators. Works by Oyetunji, *et* al. (1989) and by Suleiman, *et* al. (1989) at Ahmed Belo University (ABU) were cited. Oyetunji's group was reported to have worked on conical concentrators while the latter group worked on cylindrical collectors. All tracking was manual. In the 1990s, works by Musa, *et* al. (1992), Ajiya (1995), and Mshelbwala (1996) were reported. Musa's work group designed, constructed and tested a Fresnel concentrator which they manually tracked every 20 minutes. In spite of the improved performance, the labour requirement was too much to let the project proceed. Ajiya designed and tested a manually steerable parabolic cooker. It performed satisfactorily – achieving 30% energy efficiency. Mshelbwala modified the cooker by supporting the cooking pot to directly receive the reflected radiation. He reports to have raised the efficiency to 46.6%.

This century has seen improvements on earlier designs and further developments at many research centres across Nigeria – eventually culminating in the mechanically tracked bifocal collector of Abdulrahim's doctoral thesis in 2008. Ahmed (2001) improved parabolic trough collection at ABU. Pelemo, *et al*. (2002a, b, 2003) worked on circular parabolic concentrators – improving concentrating ability, and demonstrating applications in water distillation. Abdulrahim's mechanical tracker – the first recorded mechanical tracker in Nigeria –

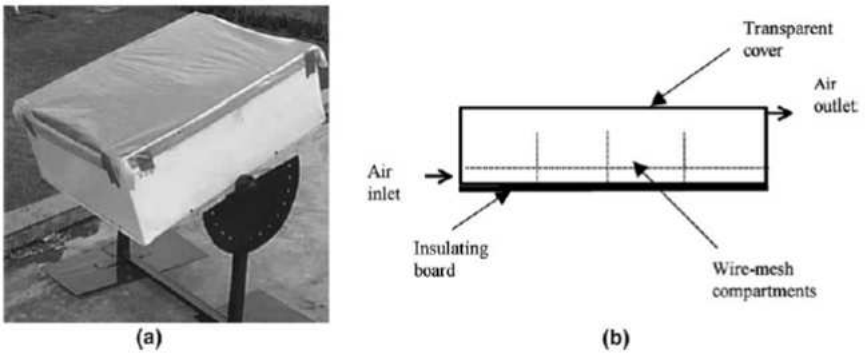

Figure 5: Mwithiga and Kigo's coffee bean manual sun tracking dryer
With permission from Elsevier: Journal of Food Engineering 74 (2006):248

was powered by a dropping weight that operates a clock mechanism driving the collector through a chain drive.

Outside Africa, only a few additional passive devices have been developed because focus has been on active systems. Hitchcock (1976) patented a buoyancy powered unit for the US navy. An array of Fresnel reflectors was kept pointed to the sun using water. Buoyancy produced movement whenever individual reflector elements were out of alignment. The issues with this tracker are that in morning hours, it takes about one hour to 'wake' up; it needs very precise manufacturing and assembly and uses a lot of water. It is big and not suitable for domestic applications.

Yi and Hwang (2009) patented a water driven tracker for Kun Shun University, China. A frame carries a pivoted radiation catchment surface. On either side of the pivot are spring supported water tanks with inlet and outlet valves. With the frame oriented in a W-E direction, one tank is filled with water at night while the other is emptied. This makes the surface face eastward. In the morning, the full tank is emptied in predetermined steps such that the frame incrementally tilts westward at an approximate uniform rate of 15° per hour. By solar noon, the tank is empty – and the frame takes on a horizontal position. When this happens, incremental filling of the western tank begins. Consequently, the catchment surface continues its westward rotation tracking the sun in the afternoon. The night operation of emptying the western tank and filling the other completes the cycle for the day.

The invention's merit is in its relative simplicity and automated filling and refilling of tanks as driven by a pre-programmed clock mechanism. It apparently has no 'wake up' issues. It is not clear if the water from one tank is preserved for use in the other and what mechanism is used to transfer the water in a night operation.

Passive two axes trackers

Many single axis trackers can be turned into full tracking types by providing independent means to turn about a second axis perpendicular to the first one. In fact, manual mobile types use this approach to orient the panel. The second axis for these cases is almost always vertical. An obvious problem is the additional cost and complexity for the expected energy gains. The single axis W-E tracking will have improved yields by 20 – 30% (Bekker, 2007; Rabinowitz, 2011; Kanyarusoke et al. 2012a, b; Sobamowo et al., 2012). The additional 5 to 10 percentage points may not easily be justified. This is particularly true in the tropics where the sun's noon zenith angle cannot exceed 47° and therefore the additional gain is at the lower end. The closer to the equator, the smaller will be the necessity to double track.

However, three recent patents have surfaced. Of these, only one is suitable for smaller domestic systems. It is similar to an 'improved' Zomeworks'. Djeu (2004) patented a passive full tracker for a solar concentrator that could be visualised as shown in Figure 6. A reflecting/refracting system focuses radiation onto a fixed collector. The energy receiving sub system is mirrored about a central plane for balancing purposes. One Gimbal rotates about an N-S axis and carries the optical system – with its balancing subsystem. The other rotates about an E-W axis. The fixed energy collection surface contains the point of intersection of the two axes. Refrigerant is held in shaded canisters at either end of the axes. The canisters for each axis are connected by piping as in the Zomeworks system.

The technical issues with this system are mainly to ensure proper balance of the gimbal and the usual 'wake up' and maximum inclination angle problems.

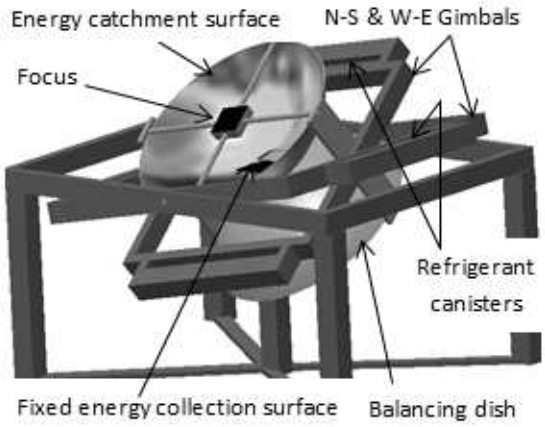

Figure 6: A 3-D visualisation of a typical Djeu's 2004 passive full tracker

3.2 Active tracking

Active trackers use electricity to drive the mechanism. They use any of 3 methods to sense the sun relative position: Light dependent resistors (LDRs), Photo transistors and Photocells. The devices are arranged in pairs to detect differential illumination which is transduced to an amplifiable voltage. The amplified signal is then used in a control circuit to drive a motor rotating the mechanism about an axis of interest. In general, each control axis will have its own sensing-control-motor–drive set up. Thus, single axis tracking has one set while two axes trackers have two sets.

Active single axis trackers

There are few active single axis trackers. Zerlaut and Heiskell (1977) patented a tracker with a clock override for Desert Sunshine Exposure Tests Inc. The override prevents fooling of the tracker by bright objects in the sky when the sun is occluded. Rizk and Chaiko (2008) designed a unit capable of

supporting an 8 kg 75 W panel using simple scrap parts. On a 9 Wp rated panel, they generated 6.3 W against 3.51 W when the panel was horizontal. While this is a substantial gain, it would have been more appropriate to compare yields with those from an inclined panel – since Australia is situated well south of the equator – and the optimal fixed slope panel is not expected to be zero. The tracker consumed 48 mW under no load conditions – or less than 1% of total power generated.

Active two axes trackers

Most amply reported active trackers are of the two axes type. Bakos (2006) reports use of 2 sets of LDRs as sensors to drive a 1370 rpm, 0.37 kW motor on the W-E axis and a 930 rpm, 0.75 kW one on the vertical. It is an electromechanical drive employing 4 relays and 2 electronic circuits connected to a computer with suitable software. A 46.46% energy gain when compared to a fixed 40° slope panel is reported. Louchene *et* al. (2007) report the use of fuzzy logic in generation of command signals to the drive motors.

Barsoum and Vasant (2010) report the design of a simplified full axes tracking system shown in Figure 7. It uses LDRs and varies the panel's azimuth and slope.

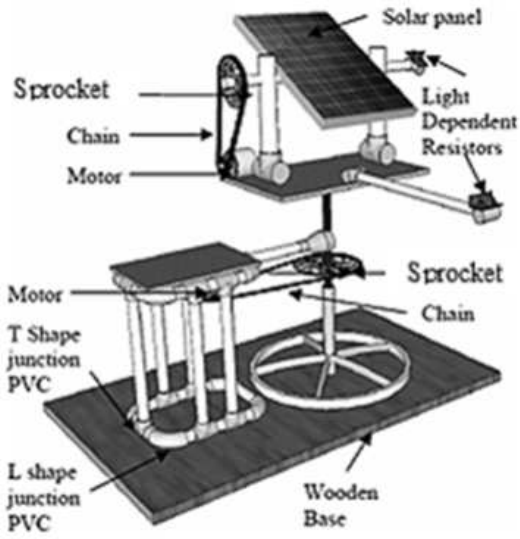

Figure 7: Barsoum and Vasant's solar tracking prototype

(With permission from: Global Journal on Technology and Optimisation Vol. 1, 2010 pp38-45)

Meyer (2010) patented a unit using lead screws driven by stepper motors to adjust the collection surface at two places. The surface was supported on spherical bearings at a third point. Martinez (2010) reports a bigger variant of linear positioning control. Hydraulic actuators in two orthogonal directions do the positioning. It is not suitable for rural African homes. Sobolewski *et al.* (2011) patented a roof mounted PV tracker at Rutgers, The State University of New Jersey, US. The tracker is mounted at the apex of an East-West roof to maximise tracking angles in these directions. Figure 8 gives the arrangement and the reported limit angles.

While this is an improvement on other roof mounted systems, it still leaves a big fraction of hours under non optimal tracking conditions.

4. The technologies and relevance in Tropical Africa's context

Research on tracking technology developments in tropical Africa is rather scarce. It is mainly Nigeria and Kenya showing some limited activity on the international scene. Fairly recent work in other developing countries has been reported, particularly in China, work by Wu Chun –Sheng *et al.* (2008) on automatic sun tracking and that by Chia-Yen Lee et al. (2009) on general tracking mechanisms. In the Middle East, Arafat et al. (2010) work was looked at. Quite earlier in the history of solar thermal electricity technology, Mill's global review is of interest. (Mill, 2004). So is Tomson's simplified two position tracker (Tomson, 2007). Recent work by Slama and Combarnous (2011) on orange peels drying in Tunisia can help improve performance of crop dryers using solar thermal systems.

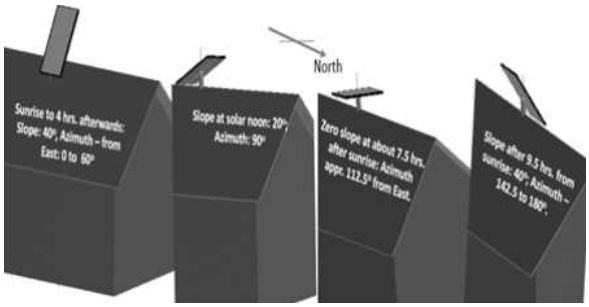

Figure 8: Sobolewski *et al.*'s roof apex mounted full tracker and the tracking angles progression across the day

The following works between 2012 and early 2013 are also noteworthy: Kelly and Gibson (2012) patented a cloudy-conditions tracker for General Motors Global Technology Operations. It automatically changes to a horizontal slope when the sun is occluded. This maximises diffuse radiation capture. In China, He *et al.* (2012) used a parallel links mechanism to track on two axes. They report motor power consumption reduction of up to 70%. Ghazali and Rahman (2012) investigated performance of amorphous, poly and mono crystalline solar panels under tracking conditions in Malaysia. They found that polycrystalline panels did best. In Bangladesh, Rahman *et al.* (2013) used LDRs and two amplifiers to demonstrate a gain of 52.78% energy yield between fixed slope and two axes tracking.

These technologies are yet to be fully adopted in Tropical Africa's homes. Apart from the fact that domestic solar energy systems are still few, there are issues with the technologies that may need to be addressed before widespread adoption.

4.1 Problems with the technologies

From tropical Africa's perspective, Table 1 summarises possible pertinent technology issues under the headings of energy sourcing; sensing and actuation.

5. Conclusion

In this paper, the more recent tracking technologies were reviewed. It was found that current technologies have many issues to resolve before adoption at a domestic level in rural Africa. Functionality, legality, security, operability and maintainability were some of the issues encountered.

In absence of empirical long term tracker performance data in the region, it is difficult to give definitive recommendations on type(s) of trackers which will be most successful. A particular tracker's acceptance elsewhere is not a guarantor of its success in the region. This is because the art of tracking can theoretically be implemented by many competing low level technologies as described in parts of the survey above. Never the less, single axis trackers showed that clock controlled passive trackers with weights of either solids or non-polluting liquids could possibly stand better chances of acceptability in the region.

Acknowledgement

This research is being funded by the Cape Peninsula University of Technology – to whom we are grateful.

References

Abdulrahim A.T., Diso I.S. and El-Jummah A.M. (2010). Solar concentrators' developments in Nigeria: a review, *Cont. J. Eng. Sci*. 5 (2010) 38-45.

ADB *see* Africa Development Bank.

Africa Development Bank, The Middle of the Pyramid: Dynamics of the Middle Class in Africa. http://www.afdb.org/fileadmin/uploads/afdb/Documents/Publications/The%20Middle%20of%20the%20Pyramid_The%20Middle%20of%20the%20Pyramid.pdf [14th July 2011].

Ahmed M.B. (2001). Design, Fabrication and Performance evaluation of an improved solar concentrating collector using slat-mirrors, Unpublished MSc. Eng. Thesis,.Mech. Eng. Dept. Ahmed Bello University, Zaria Nigeria, 2001.

Ajiya M. (1995). Design and Construction of a parabolic solar cooker, Unpublished B Eng project. Mech. Eng. Dept. University of Maiduguri, Nigeria, 1995.

Anonymous. (2011). Canadian Teen Makes Cheaper,

Table 1: Summary of key issues in surveyed solar tracking mechanisms

Area	Alternatives	Issues
Energy source	Manual	Not viable because it is labour intensive
	Weights	Counter weights for balancing and control
		Frequent reloading
	Solar thermal	Speed of response
		Availability in case of cloud cover
		Evening and morning collection effectiveness
	Hydraulic	Pressure head source
		Needs reliable working fluid supply
	Springs	Frequent re energising
	Electricity	Needs electric source
		Complex control system
Sensory system	Clock	Insensitive to diffuse radiation effects
	Shading	Affected by sky objects and delayed action
	Photo sensor	Needs electronic circuitry and unequal ageing of sensors
System Actuation	Manual	Tedious because it is labour intensive
	Clock	Separate programming
	Bimetallic strips	Low thermal efficiency
		Low tracking angle range
		'Wake up' and evening return problems
	Shape memory alloys	Low tracking angle
	Vapour pressure	Use of refrigerants which must be eco-friendly
		'Wake up' and evening return problems
	Electric motors	Possibly too costly – require sub system
		Maintenance of attendant control & drive elements
	Linkages	Power losses – require sub system
		Bulk and maintenance issues
	Hydraulic	Pressurised liquid reservoir
		Size and maintenance issues

More Efficient Solar Tech., *Altern. Energy Afr*. 6th June 2011.

Arafat K.Md.T. Shahrear T.S.M., Rifat R., and Shafiul A.S.M. (2010). Design and Construction of an Automatic Solar Tracking System. *ICECE*, 2010. 326 – 329. eeexplore.org/stamp/Stamp.jsp?tp=&arnumber=5700694 [23 Feb 2013].

Bakos C.G. (2006). Design and Construction of a two – axis sun tracking system for parabolic trough collector (PTC) efficiency improvement, *Renew. Energy*. 31 (2006) 2411-2421.

Barsoum N., and Vasant P. (2010). Simplified solar tracking prototype, *Glob. J. on Technol. & Optim*. 1 (2010) 38-45.

Bekker B. (2007). Irradiation and PV array energy output, cost, and optimal positioning estimation for South Africa, *J. Energy in S. Afr*. 18 (2) (2007) 16-25.

Bennett, L. (2008). Assets under Attack: Metal Theft, the Built Environment and the Dark Side of the Global Recycling Market. *Environmental law and Management*. 20(2008) 176-183.

Beringer S., Schilke H., Lohse I., and Seckmeyer G. (2011). Case study showing the tilt angle of PV plants is nearly irrelevant. *Sol. Energy*. 85 (2011) 470-476.

Brent, A. C. and Rogers, D. E. (2010). Renewable Rural Electrification: Sustainability Assessment of Mini-Hybrid off-grid Technological Systems in the African context. *Renewable Energy.* 35(2010) 257–265

Brew-Hammond, A & Kemausuor, F. (2009). Energy for all in Africa—to be or not to be?! *Environmental Sustainability*, 1 (2009) 83–88.

Bugaje, I.M. (2006). Renewable Energy for Sustainable Development in Africa: A Review. *Renewable and Sustainable Reviews.* 10 (2006) 603–612. Available from Science Direct [2014, July 3].

Chia – Yen Lee, Po – Cheng Chon, Che – Ming Chiang, and Chiu – Feng Liu. (2009). Sun Tracking systems: A review, Sensors 2009, 9 3875 – 3890; doi: 10.3390/S90503875. www.mdpi.com/journal/sensors [23 Feb 2013].

Chong K.K. and Wong S.W. (2009). General formula for on axis sun-tracking system and its application in improving tracking accuracy of solar collector, *Sol. Energy.* 83 (2009) 298 – 305.

Ciobanu D., Visa I., Jaliu C., and Burduhos B.G. (2010). Tracking system type linkage mechanisms. Annals of DAAAM for 2010 and proceedings of the 21st International DAAM symposium, 21 (1) ISSN 1726-9679, ISBN 978-3-901509-73-5. Ed. Kantalimo, DAAAM International, Vienna, Austria, EU 2010.

Clifford M.J. and Eastwood D. (2004). Design of a novel passive solar tracker, *Sol. Energy.* 77 (2004) 269–280.

Djeu D. (2004). Passive Solar Tracker for a Solar Concentrator, US Patent application. 20040112373, 2004. patents.com/us-20040112373.html – Cached [3rd April 2011].

Ellega˚rd a, Arvidson, A., Nordstro¨ma, b, Mattias, Kalumiana, O, S., and Mwanza, C. (2004). Rural People Pay for Solar: Experiences from the Zambia PV-ESCO Project. *Renewable Energy.* 29 (8) (2004) 1251–1263.

Elmer Z.K.G. (2006). Optimising solar tracking systems for solar cells, 4th Serbian – Hungarian Joint symposium on Intelligent systems. SISY (2006) 167-180.

Eveleens I. E. Africa's first solar-panel plant supports Kenya's clean energy push, AlertNet, 23rd Nov 2011.

Fluri T P. (2009). The Potential of Concentrating Solar Power in South Africa. *Energy Policy,* 37(2009) 5075–5080.

Fthenakis, V. M. (2000). End-of-life management and recycling of PV modules. *Energy Policy,* 28 (14) (2000) 1051-1058.

Full E. (2010). Appropriate Technologies in Mpala Village, Kenya: Solar, Water and Bamboo, [PPT] presentation www.princeton.edu/grandchallenges/health/...2010/Full_Eden_SOL.pptx [4th July 2011].

Ghazali A. M. and Rahman A. M. A. (2012). The performance of three different solar panels for solar electricity applying solar tracking device under the Malaysian climate condition, *Energy and Environment Research,* 2 (1) (2012) 235 -243.

He X., Wang B., Huang F., Zhu W. and Gao C. (2012). Solar Automatic tracker based on parallel mechanism, *J. Mech. & Elec. Eng*, (01) (2012).

Helwa N.H., Bahgat A.B.G., El Shafee A.M.R. and El Shenawy E.T. (2000). Maximum collectable energy by different solar tracking systems, *Energy Sources*, 22 (2000) 23-34.

Hernandez C. (2011). The 19-year-old innovator revolutionizing solar energy systems. http://www.smartplanet.com/blog/pure-genius/the-19-year-old-innovator-revolutionizing-solar-energy-systems/6436 [4th July 2011].

Hitchcock. R.D. (1976). Passive solar tracking system for steerable Fresnal elements, US Patent. 3986021, 1976. www.patentstorm.us/patents/3986021/description.html – Cached [3rd April 2011].

IEA *see* International Energy Agency.

International Energy Agency, Renewables and Waste in Africa in 2008. http://www.iea.org/stats/renewdata.asp?COUNTRY_CODE=11 [30th June 2011].

International Energy Agency IEA (2011). Energy for all: Financing access for the poor. *World Energy Outlook*, (2011) 11.

Kalogirou S. (2007). Recent patents in solar energy collectors and applications, *Recent Pat. on Eng*. 1(1) (2007) 23-33.

Kalogirou S. (2009). Thermal Performance, economic and environment life cycle analysis of thermo syphon solar water heaters. *Solar Energy*. 83 (1) (2009) 39-48.

Kanyarusoke, K.E., Gryzagoridis, J. and Oliver, G. (2012a). Issues in solar tracking for sub-Sahara Africa, 1st Southern African Solar Energy Conference (SASEC), Stellenbosch, South Africa 21st-23rd May 2012.

Kanyarusoke, K.E., Gryzagoridis, J. and Oliver, G. (2012b) Annual Energy Yields Prediction From Manufacturers' Photovoltaic Panel Specifications for Sub Sahara Africa, Proceedings of International

Conference on Engineering and Applied Science 2012 (ICEAS 2012), 24th-27th July 2012. Beijing China. pp. 223-235.

Karekezi S. (2002). Renewables in Africa – Meeting the Energy Needs of the Poor. *Energy Policy*. 30 (2002) 1059 -1069.

Kelly N.A. and Gibson T.L. (2010). Optimizing the Photovoltaic Solar Energy Capture on Sunny and Cloudy Days Using a Solar Tracking System. http://www.cormusa.org/uploads/CORM_2010_presentation_Nelson_Kelly_Optimizing_the_Photovoltaic_Solar_Energy.pdf [30th June 2011].

Kelly N.A. and Gibson T.L. (2012). Solar Photovoltaic output for cloudy conditions with a solar tracking system, US patent No. US 8,101,848B2 of Jan 24 2012.

Kraak, A. (2005). Human Resources Development and the Skills Crisis in South Africa: The Need for a Multi -Pronged Strategy. *Journal of Education and Work*. 18(1) (2005) 57-83.

Louchene A., Benmakhlouf A. and Chagai. (2007). Solar tracking system with Fuzzy reasoning applied to crisp sets, *Revue des Energies Renouvelables*. 10 (2) (2007) 231-240.

Markvart T. (ed.). (2000). *Solar Electricity* 2nd ed. John Wiley & Sons, Chichester 2000.

Martinez C.M.C. (2010). Bidirectional solar tracker, US Patent. 2010/0095955, 22nd April 2010.

Meyer S.M. (2010). Two Axes solar tracking system, http://www.freepatentsonline.com/y2010/0288062.html [15th June 2012].

Mills D. (2004). Advances in Solar thermal electricity Technology, *Sol Energy*. 76 (2004) 19 – 31.

Mousazadeh H., Keyhani A., Javadi A., Mobli H., Abrinia K., and Sharifi A. (2009). A review of principle and sun-tracking methods for maximizing solar systems output, *J. Renew. & Sustain. Energy* Rev. 13 (2009) 1800 –1818.

Mshelbwala S.A. (1996). Experimental investigation of a parabolic solar cooking device, Unpublished BEng Project. Mech. Eng. Dept. University of Maiduguri, Nigeria, 1996.

Mulugetta, Y., Nheteb T. and Jacksona T. (2000). Photovoltaics in Zimbabwe: Lessons from the GEF Solar Project. *Energy Policy*. 28 (140) (2000) 1069–1080

Murphy J.T. (2001). Making the energy transition in East Africa: Is Leapfrogging an alternative? *Technol. Forecast. & Soc. change*. 68 (2001) 173-193.

Musa U., Sambo A.S. and Bala E.J. (1992). Design, Construction and Performance test of a parabolic concentrator cooker, Paper presented at the 1992 National Energy Forum, Sokoto.

Mwithiga G. and Kigo S.N. (2006). Performance of a solar dryer with limited sun tracking capability, *J. Food Eng.* 74 (2006) 247–252.

Oyetunji S.O., Sawhney R.I. and Aro I.O. (1989). Design, Construction and Estimation of performance of composite conical concentration, *Directory of Renewable Energy Research and Development activities in Nigeria,* SERC Sokoto. 1:12.

Pauw, K., Oosthuizen, M., & Westhuizen, c. Van der. (2008). Graduate Unemployment in the Face of Skills Shortages: A Labour Market Paradox. *South African Journal of Economics.* 76 (2008) 1.

Pegels, A. (2010). Renewable Energy in South Africa: Potentials, Barriers and Options for Support. Energy Policy. 38 (2010) 4945–4954.

Pelemo D.A., Fasasi M.K., Owolabi S.A. and Shaniyi J.A. (2002a). Design, Construction and Performance of focusing type solar cooker, *Niger. J. Phys*., 4 (2) (2002) 109-112.

Pelemo D.A., Fasasi M.K., Owolabi S.A. and Shaniyi J.A. (2002b). Effective utilisation of solar energy for cooking, *Nig. J. Eng. Manag*. (NJEM), 3 (1) (2002) 13-18.

Pelemo D.A., Fasasi M.K., Owolabi S.A. and Shaniyi J.A. (2003). Application of solar concentrator for water boiling and distillation, *Niger. J. Sol. Energy*, 14 (2003) 51-54.

Peter, P. and Donnelly Jr., J. H. (2009). *Marketing Management* 9th ed. McGraw Hill, New York (2009).

Poulek V. (1994). New low cost tracker, *Sol. Energy Mater. & Sol. Cells*, 33 (1994) 287-291.

Rabinowitz M. (2011). Tracking and focusing adjustable fresnel lens array solar collector, US Patent. 7960641 B2. www.uspto.gov/web/patents/patog/.../US07960641-20110614.html – Cached [2nd August 2011].

Rahman S., Ferdaus R. A., Mannan M. A. and Mohammed M. A. (2013). Design and Implementation of a dual axis solar tracking system. Am. Acad. & Scholarly Res. J. 5 (1) (2013) 47 – 54.

Rizk J. and Chaiko Y. Solar Tracking system. (2008). More efficient use of solar panels, *World Acad. of Sci. and Techno*, 28 (28) (2008) 313-315.

Seme S., Stumberger G. and Vorsic J. (2011). Maximum efficiency trajectories of a two – axis sun tracking system determined considering tracking system consumption, *IEE Transactions on Power Electronics,* 26(4) (2011) 1280 – 1290.

Slama R.B. and Combarnous M. (2011). Study of Orange peels drying kinetics and development of a solar dryer by forced convection, *Sol. Energy*. 85 (2011) 570-578.

Sobamowo M.G., Kamiyo O.M, Ojolo S. J. and Ogundeko I.A. (2012). Design and Development of a Photovoltaic-Powered DC Refrigerator System with an Incorporated Solar Tracker, 1st Southern African Solar Energy Conference (SASEC), Stellenbosch, South Africa 21st-23rd May 2012.

Sobolewski. (2011). Roof mounted double axis tracker, US Patent. 20110120447, 26th May 2011.

Solar Buzz (2012). Solar Energy Market Growth.
http://www.solarbuzz.com/facts-and-figures/markets-growth/market-growth [7th April 2012].

Sovacool B. K., D'Agostino A. D. and Bambawale, M. J. (2011). The Socio-technical Barriers to Solar Home Systems (SHS) in Papua New Guinea: "Choosing pigs, prostitutes, and poker chips over panels. *Energy Policy*. 39 (3) (2011) 1532–1542

Suleiman A.K., Bajpai A.C. and Sulaiman A.T. (1989). Design, Fabrication and Testing of a low-cost cylindrical collector for steam generation, *Directory of Renewable Energy Research and Development Activities in Nigeria,* SERC, Sokoto, 1989, pp. 1-13.

Tina G.M. and Gagliano S. (2011). Probabilistic modelling of hybrid solar/wind power with solar tracking system, *Renew. Energy*, 36 (2011) 1719 –1727.

Tomson T. (2008). Discrete two positional tracking of solar collectors, *Renewable Energy*. 33 (2008) 400 – 405.

United Nations Energy Agency. (2007). Energy for Sustainable Development: Policy Options for Africa. Vol. 2008.

United Nations (2014). Division for Sustainable Development. Department of Economic and Social Affairs. A Survey of International Activities in Rural Energy Access and Electrification.

United Nations Economic Commission for Africa. (2006). African Regional Implementation review for the 14th Session of the Commission on Sustainable Development (CSD-14) (2006). Report on "Energy for Sustainable Development". United Nations Economic Commission on behalf of the Joint Secretariat UNECA, UNEP, UNIDO, UNDP, ADB and NEPAD Secretariat.

Vanek F. M., Albright L. D. and Angenent L.T. (2012). *Energy Systems Engineering: Evaluation and Implementation* 2nd ed. New York, McGraw Hill, (2012) 49-71.

Winston R. (2001). Solar concentrators, In Gordon, J. (ed.) Solar Energy: The state of the art – ISES position papers. James and James Science Publishers, London, 2001, pp. 357-436.

Wu Chun-Sheng, Wang Yi-Bo, Liu Si-yang, Peng Yan – Chang, and Xu Hong – Hua. (2008). Study on Automatic Sun-Tracking technology in PV Generation. *DRPT 2008*, 6-9 April 2008, Nanjing, China. *IEEEXplore* 2586 – 2591.

Yi J-H. and Hwang W-C. (2009). Solar tracking device with springs, US Patent. 7607427 B2, 2009. www.wikipatents.com/...Patent-7607427/solar-tracking-device-with-... – Cached) [3rd April 2011].

Zerlaut G.A. and Heiskell R.F. (1977). Solar Tracking device, US Patent. 4031385, 21st June 1977.

Zomeworks. (n.d.). PV trackers. http://zomeworks.com/products/pv-trackers/how-trackers-work [3rd April 2011].

Received 28 July 2014; revised 26 December 2014

Performance optimization of an air source heat pump water heater using mathematical modelling

Stephen Tangwe[a]

Michael Simon[a]

Edson L Meyer[a]

Sampson Mwampheli[a]

Golden Makaka[b]

a. Fort Hare Institute of Technology, University of Fort Hare, Alice, Eastern Cape South Africa
b. Department of Physics, University of Fort Hare, Alice, Eastern Cape, South Africa

Abstract
In South Africa, there is an ongoing constraint on the electricity supply at the national grid to meet the demand. Eskom is implementing various measures such as the Integrated Demand Management and the promotion and encouragement of the use of energy efficient devices like an Air Source Heat pump (ASHP) water heater to replace the high electrical energy consuming conventional geysers for sanitary hot water production. The ASHP water heater market is fast gaining maturity. A critical mathematical model can lead to performance optimization of the systems that will further result in the conservation of energy and significant reduction in global warming potential. The ASHP water heater comprises of an ASHP unit and a hot water storage tank. In this study, a data acquisition system (DAS) was designed and built which monitored the energy used by the geyser and the whole building, the temperature at the evaporator, condenser, tank outlet hot water, tank inlet cold water, the ambient temperature and relative humidity in the vicinity of the ASHP evaporator. It is also worthy to mention that the DAS also included to a flow meter and two additional temperature sensors that measured the volume of water heated and inlet and outlet water temperature of the ASHP. This work focused on using the mathematical equation for the Coefficient of Performance (COP) of an ideal Carnot's heat pump (CHP) water heater to develop basic computation in M-file of MATLAB software in order to model the system based on two reservoir temperatures: evaporator temperatures (T_{evp}) of 0°C to 40°C (approximated to ambient temperature, T_a) and condenser temperatures (T_{Con}) set at 50°C, 55°C and 60°C (approximated to the hot water set temperature of 50°C, 55°C and 60°C) respectively. Finally, an analytical comparison of a CHP water heater to the practical ASHP water heater was conducted on a hot water set point temperature of 55°C. From the modelling results, it can be deduced that at 0°C T_{evp}, the COP was 5.96 and 2.63 for CHP and ASHP water heater respectively, at a hot water set temperature of 55°C. Above 20°C T_{evp}, the rate of change of COP increased exponentially for the ideal CHP system, but was constant at 0.01/°C for the practically modelled ASHP water heater.

Keywords: Air source heat pump; coefficient of performance; data acquisition system; mathematical model; Carnot's heat pump

1. Introduction

Hot water heating constitutes a significant percentage of energy consumption in the industrial, commercial and residential sectors worldwide. In South Africa, water heating is the largest residential use of energy, with up to 50% of monthly electricity consumption being used for this purpose (Meyer and Tshimankinda, 1998). The Eskom strategic plan outlook for 2010 to 2030 envisages over 20% reduction of electricity production from coal (Digest of SA Energy statistics, 2009) as shown in Figure 1. One way to achieve this energy conservation could

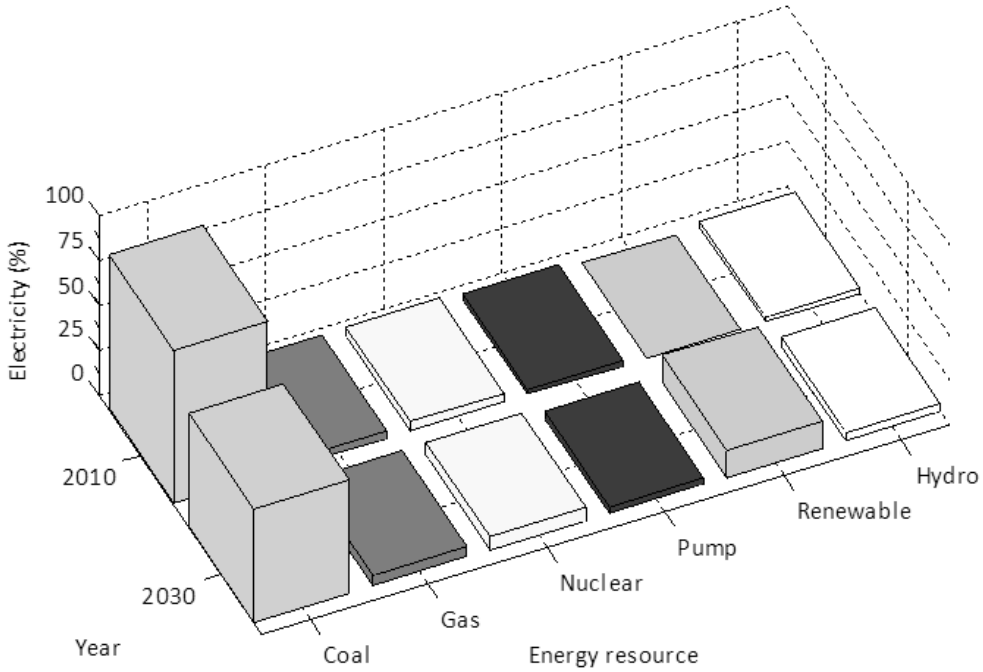

Figure 1: Illustration of energy outlook for sources of electricity production, according to Eskom *(Digest, 2009)*

be by the use of an energy efficient technology such as the implementation of a heat pump for sanitary hot water production. Figure 1 illustrates the statistical outlook for sources of electrical energy generation in South Africa.

In order to execute the afore-mentioned energy efficient technology, Eskom embarked in rolling out a rebate programme of approximately 65 580 units of residential ASHP to retrofit existing geysers until March 2013 (Eskom Report, 2010). Consequently, this strategy will go a long way to promote the use of this technology within the residential sector. Considering the fact that the ASHP technology has been recommended and accepted for demand and energy reduction, it is therefore imperative at this juncture to present a clear description of the ASHP. The ASHP water heater is an electro-mechanical close circuit system comprising of a heat pump and a water storage tank. The key components of the heat pump unit are the evaporator coil, vapour compressor, heat rejection condenser and an expansion valve. The ASHP water heater operates on the principle of a vapour compression refrigerant cycle (VCRC). It can be categorized into integrated and retrofit types. In the integrated type both the ASHP unit and the storage tank exist as a single system; the ASHP lies on top of the tank while in the split type, the ASHP unit is situated below the storage tank and connected to it by pipes. Generally, both types can further be classified as one passed circulation system and recirculation system. Studies have documented that the ASHP water heater could provide hot water at 40 to 100 percent of the rate of electric resistance units and 30 to 50 percent of the rate of gas units, but required warm ambient temperatures and a large heat pump or storage tank so as to provide a constant flow of hot water (Bodzin, 1997; CBEEDAC, 2005). The characteristic of a heat pump that enables it to provide such a very high efficiency of 300% is called the coefficient of performance (De Swardt *et al*., 2000). The COP of an ASHP water heater is dependent on various parameters including component design, heating load cycle, thermo-physical properties of the working fluids, relative humidity and air speed through the duct space. The instantaneous, seasonal or annual COP can be calculated using simulation with the TRYSYN software package (Kline *et al.,* 2000), and an analytic mathematical model that correlates COP and temperature for solar assisted ASHP water heater (Itoe *et al*., 1999).

2. Fundamental principles of ASHP water heater

The entire operational principle of an ASHP water heater is clearly illustrated in Figure 2. During a heating load cycle, the ASHP undergoes a VCRC. The cycle can only be achieved in the case of CHP by supplying electrical energy to the compressor and in a practical ASHP, energy is also needed to run the water circulation pump and fan as shown in Figure 2. The low pressure and temperature refrigerant extract aero-thermal energy from ambient air and the low pressure vapour flows to the compressor where it is compressed and discharged as superheated gas. The thermal energy absorbed by the gas is rejected at the condenser unit where incoming water from the ASHP inlet pipe is heated to hot

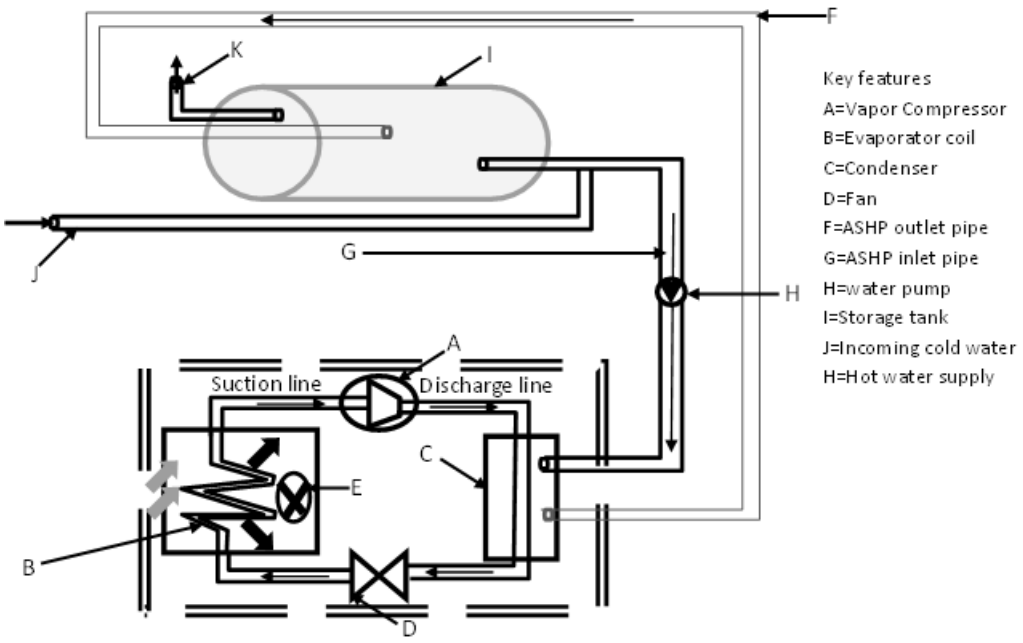

Figure 2: Illustration of an ASHP water heater schematic

water set point temperature. Finally, the refrigerant passes through an expansion valve where its pressure and temperature drops. The complete processes involved in the cycle are shown in the temperature versus entropy and pressure versus enthalpy graphs of Figures 3 and 4, respectively. From both figures, the saturated liquid and saturated vapour lines for the working fluid are distinguished by the critical temperature (T_c) and the critical pressure (P_c).

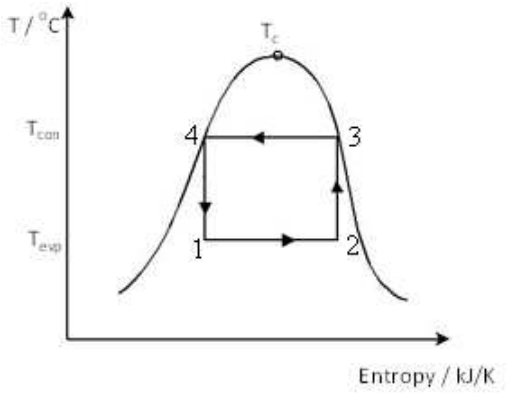

Figure 3: T-S graph of VCRC for the CHP water heater

The COP of the heat pump could be determined by either using the pressure versus enthalpy graph or the temperature versus entropy graph and the essential parameters were obtained for the final COP calculation. The analysis of the processes involved in each section of the two figures is explained below: where h and s are specific enthalpy and specific entropy of the system, respectively, E_{in} is input electrical energy and Q_{out} is the useful heat gain.

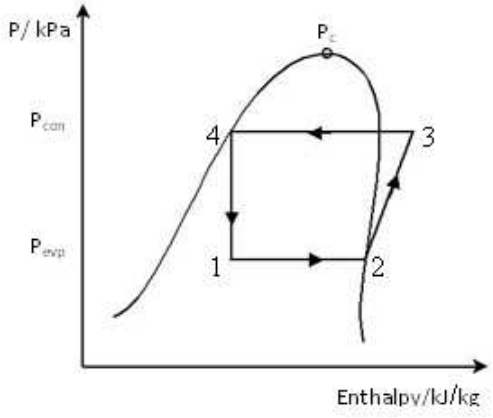

Figure 4: P-h graph of VCRC for the CHP water heater

In order to understand and mathematically represent the processes taking place in the evaporator, compressor, condenser and expansion valve sections of the heat pump, a set of equations (1-8) were deduced. Analysing Figure 4, the process 1 to 2 occurred in the evaporator and the heat gain was calculated using equation 1.

$$\Delta Q = mh_2 - mh_1 \quad (1)$$

Process 2 to 3 occurred at the compressor and heat gain was calculated as shown in equation 2

$$\Delta Q = mh_3 - mh_2 \quad (2)$$

Process 3 to 4 occurred in the condenser and the heat rejected was calculated using equation 3

$$\Delta Q = mh_3 - mh_4 \quad (3)$$

Process 4 to 1 occurred in the expansion valve and

enthalpy change was calculated as shown in equation 4

$$\Delta Q = mh_4 - mh_1 = 0 \quad (4)$$

Using the definition of COP in terms of energy factor, equation 5 was obtained

$$COP = \frac{Qout}{Ein} \quad (5)$$

From equation 5, both energies (Q_{out}, output thermal energy and E_{in}, input electrical energy) can be expressed in terms of h to give equation 6.

$$COP = \frac{m(h_3 - h_4)}{m(h_3 - h_2)} = \frac{h_3 - h_4}{h_3 - h_2} \quad (6)$$

The COP could also be derived from Figure 3 and by using the first law of thermodynamics. The COP can be defined by equation 7

$$COP = \frac{s_2 T_{con} - s_1 T_{con}}{(s_2 T_{con} - s_1 T_{con}) - (s_2 T_{evp} - s_1 T_{evp})} \quad (7)$$

Simplifying equation 7 gives equation 8

$$COP = \frac{T_{con}}{T_{con} - T_{evp}} \quad (8)$$

Both the evaporator and condenser temperatures were expressed in Kelvin (K). Equation 8 was the COP formulation applied to the CHP water heater. Based on this equation, a computational programme which modelled the COP variation with temperature lift was generated from the M-file script of the MATLAB software.

3. Methodology

3. 1 Variations of the modelled COP of the CHP water heater with evaporator temperature

The modelled COP of CHP derived from equation 8 was used for ambient temperature ranging from 0°C to 40°C with the hot water set point temperature (condenser temperature) of 50oC, 55°C and 60°C. Figure 5 illustrates Carnot's COP variation in relation to ambient temperature, which is equal to the evaporator temperature. From Figure 5, it can be depicted that Carnot's COP increased linearly with ambient temperature from 0°C to 20°C at a rate of 0.15 / °C and above this range, the COP increased exponentially.

It was also observed that at the condenser temperature of 55°C, the COP increased with increase in evaporator temperature. The COP of 5.96 could be obtained at ambient temperature of 0°C, since the air contained waste heat at such a temperature provided there is no frost formation. At an ambient temperature of 40°C, a COP of 21.8 could be achieved as deduced from Figure 5 provided no parasitic heat losses occurred at the condenser. This indicates that all the rejected heat in the condenser is absorbed by the inflow water into the CHP unit.

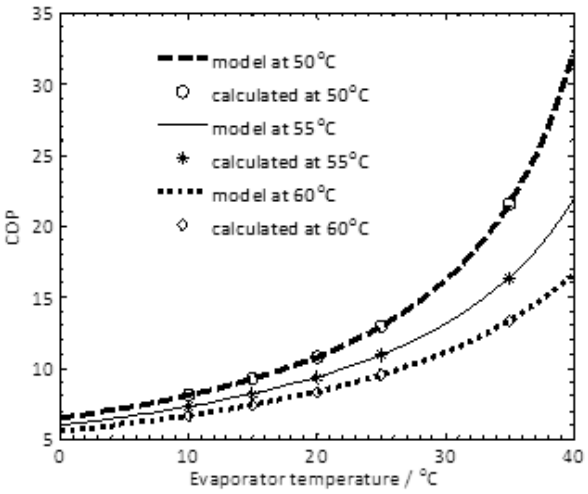

Figure 5: Variation of Carnot's COP in relation to evaporator temperature

3. 2 Mathematical modelling of practical ASHP water heater

The second aspect of this work, was to use the Marrison's COP correlation to mathematically model a practical ASHP water heater. Equation 9 illustrates the Marrison COP model while equation 10 shows the constraint COP equation used for the simulation.

$$COP = a_1 + a_2(T_t - T_a)\left[1 - a_3 \frac{T_t - T_w}{T_t - T_d}\right] \quad (9)$$

$$COP = a_1 + a_2(T_t - T_a) \quad (10)$$

Equation 10 is a constraint equation to optimize the COP; where the constants a_1 was the COP when $T_t = T_a$ and a_2 was the COP gradient determined for T_t = 50°C, 55°C and 60°C using the experimentally determined COP at an average ambient temperature of 10°C, 15°C, 20°C, 25°C and 35°C as shown in Table 1. The wet bulb temperature (T_w) was assumed to be equal to hot water set temperature (T_t) and (T_d) was the dew point temperature.

Table 2 shows the predictors and scaling constants for the three different hot water set point temperatures derived from the linear regression model of the COP obtained from the data shown in Table 1.

Figure 6 gives a presentation of measured and modelled COP at 50°C, 55°C and 60°C hot water set point temperatures. It can be delineated that if all other conditions affecting the COP remain con-

Table 1: Experimentally determined COP at specific ambient temperature

Average ambient temperature/°C	10.0	15.0	20.0	25.0	35.0
Calculated COP at HWSPT of 50°C	3.10	3.15	3.25	3.30	3.40
Calculated COP at HWSPT of 55°C	2.82	2.85	2.95	3.00	3.22
Calculated COP at HWSPT of 60°C	2.69	2.70	2.70	2.80	2.88

stant, then the lower the hot water set point temperature the better the COP of the modelled ASHP water heater.

Table 2: The predictors scaling constant at the different hot water set point temperature

Predictors	T_t-T_a	*constant*
Scaling variable	a_1	a_2
Scaling constant at HWSPT of 50°C	-0.010	3.510
Scaling constant at HWSPT of 55°C	-0.017	3.560
Scaling constant at HWSPT of 60°C	-0.008	3.080
Output	COP	

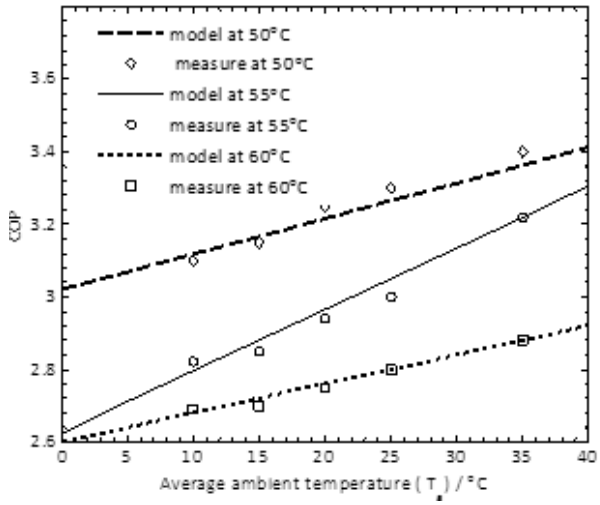

Figure 6: Variation of ASHP water heater COP versus T_a

The dash dot, solid and dot lines are the optimized linear equations obtained for hot water set at 50°C, 55°C and 60°C. The average cold water temperature of 25°C at the bottom of the tank and average relative humidity of 75% were used. The solid line is for hot water set point temperature of 55°C. The modelled COP equation from equation 10 was used in the simulation designed in Simulink, which required both ambient temperature and electrical energy as its input parameters.

3. 3 Methodology for determination of input parameters

The computation of the COP using mathematical modelling was performed for a typical week baseline profile of a 4kW, 200 litres convectional geyser installed in a domestic residence (occupied by four adults and two children) of a middle class family at Fort Beaufort, South Africa. The geyser was allowed to operate without interruption for 24 hours on a daily basis. Figures 7 and 8 illustrate the DAS used to determine the hot water profiles and the analogous parameters appropriate to determine the system performance.

The U30-NRC data logger shown in Figure 7 is a Hobo no remote communication data logger logging various temperatures, counts from hot water drawn off and relative humidity per minute. The Power track analysers logged power, current, voltage and power factor per minute for geyser and the whole building. The Smart connectors at the connecting end of the sensors were connected to the logger via jack ports. The digital pulse input adapters were incorporated to all the sensors and they convert analogue signals to digital in order to reduce errors. Finally, the solar radiation shield was used to protect the temperature and relative humidity sensor. Figure 8 shows the built programme flow chart.

In the schematic diagram (Figure 8), the different metering transducers and sensors to measure the respective parameters are shown. The main electric power consumption and total current drawn to the building was measured by power track analyser 1. The device was installed on the main distribution board with the positive voltage cable (red) and the negative voltage cable (black) connected to the live and neutral lines of the mains. The current transformer of the power track analyser was placed on the live line of the mains. Power track analyser 2 was placed in the line supplying current to the geyser and it measured the current and the total power utilized by the 200 litres, 4kW high pressure geyser. These power meters were configured to log at every 1 minute interval. All the temperature sensors were thermistor resistance sensors. The temperature sensor 1 was well insulated and placed in the cold water inlet pipe to the geyser. Similarly, the temperature sensors 2, 3 and 4 measured the hot water temperatures to the outlet from the geyser, hot water to the bathrooms and kitchen respectively. Furthermore, a flow meter (T-Minol-130) was placed in close proximity to temperature sensor 1 on the hot water pipe and it measured the flow rate of hot water drawn in number of counts per minute. The relative humidity and temperature sensor measured the relative humidity and ambient temperature respectively. The hobo no remote communication (U30 /NRC) was used to log counts equivalent to the volume of water drawn, various

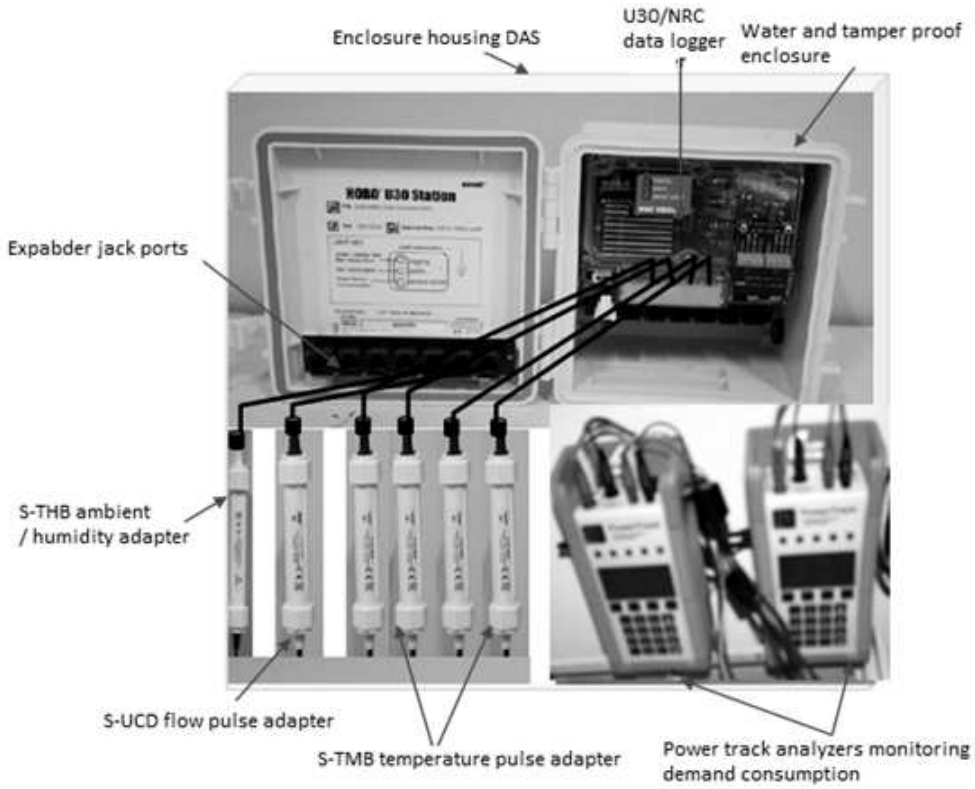

Figure 7: DAS designed and built for the research

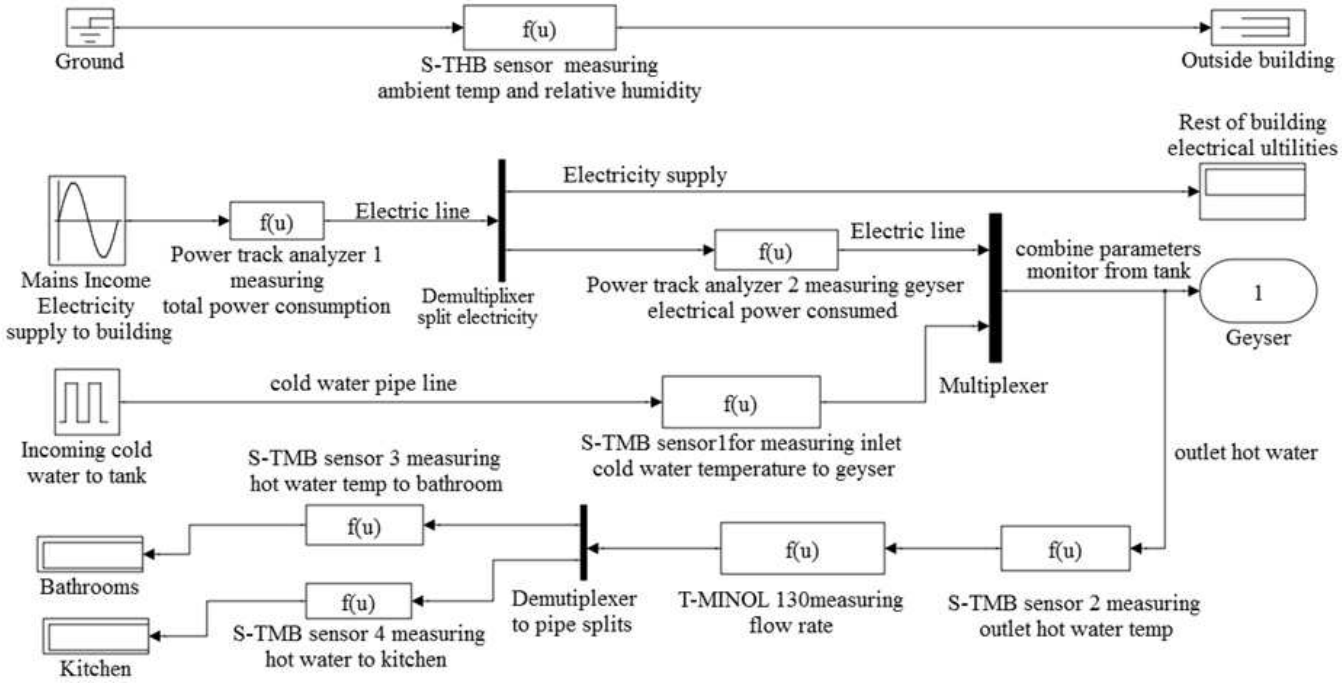

Figure 8: The schematic programme sequence

temperatures, relative humidity and ambient temperature measurements.

3. 4 Simulation application using Simulink

In order to simulate the processes illustrated in Figure 8, the Simulink platform was used as shown in Figure 9. Figure 9 shows the simulation, architectural and programming sequence for system COP and energy consumption. The input parameters (electrical energy used by geyser and ambient temperature) for the practical ASHP and CHP over 30 minute interval were loaded to the two input sources using the interpolation sequence source from Simulink library. The multiplication block acted as a heat pump extracting aero-thermal energy from the vicinity around the evaporator and

electrical energy via the compressor of CHP, while additional electrical energy was needed to drive the fan and water circulation pump of the practical ASHP. This combined energy was dumped into the storage tank as output thermal energy. Both the input and output energy profiles were displayed on the oscilloscope (energy profiles). The oscilloscope (COP profiles) displayed variation of the modelled COP of practical ASHP and of CHP water heaters versus time over 24 hours at 30 minutes interval. On the other hand, the oscilloscope (COP Vs T_a) also displayed variation of the modelled COP of practical ASHP water heater with the average ambient temperature within the duration of the simulation. After loading the respective input parameters into the discrete sources in the simulation model, the Simulink was set to start at time 0 and stop at time 23:30. Upon completion of the simulation, the three oscilloscopes would show the various desired output parameters. (thermal energy absorbed by hot water and COP). The performance of practical ASHP and CHP water heaters of the average weekday and average weekend from the 4-10th of June 2012 was used in the simulation application.

4. Results and discussion

4. 1 Analysis of the average weekday performance

The energy, the COP and temperature analysis of an average weekday (4-8 June 2012) over a 24 hour period are illustrated in Figures 10, 11, 12 and 13. Figure 10 shows the various energy profiles of an average weekday divided into three zones (zone A between 00:00 to 5:30, zone B between 5:30 to 12:00 and zone C between 12:00:23:30). Based on the energy consumed by a convectional geyser with an energy factor of 1, the electrical energy used is equal to thermal energy gained to heat water to set point temperature of 55°C. Hence, from Figure 10, the thermal output energy of practical ASHP water heater corresponded to the input electrical energy used by the geyser. Furthermore, the modelled output thermal energy of CHP water heater was also equal to the input electrical energy of the geyser. On the other hand, the CHP water heater input energy was displayed as Carnot heat pump water heater input energy (model CHPWH) using the ideal COP equation of heat pump. Similarly, the input electrical energy of practical ASHP water heater was achieved using the regression model for COP (model ASPHWH). This energy was much higher than the input energy of CHP water heater as justified by figure 11 (showing the variation of the modelled COP of practical ASHP water heater and COP of CHP water heater with the ambient temperature of an average weekday. From the temperature profiles (figure 12), the COP for both modelled practical ASHP and CHP water heaters depended on the ambient temperature.

At the 18:00 hour, the maximum average ambient temperature of 23.13°C was measured and corresponded to a COP of 3.00 and 9.98 for both of the systems. Despite the average ASHPWH modelled COP of 2.78 in zone A, there was very little or no hot water drawn which meant that the energy used up compensated for standby losses. Consequently, the energy saved was minimal (1.11 kWh) and the amount of input electrical energy was 0.63 kWh. In zone B, more than 60% of the total average input energy was used by the modelled practical ASHPWH between 6:00 to 12:00 (3.60 kWh) and the thermal energy output of 10.09 kWh

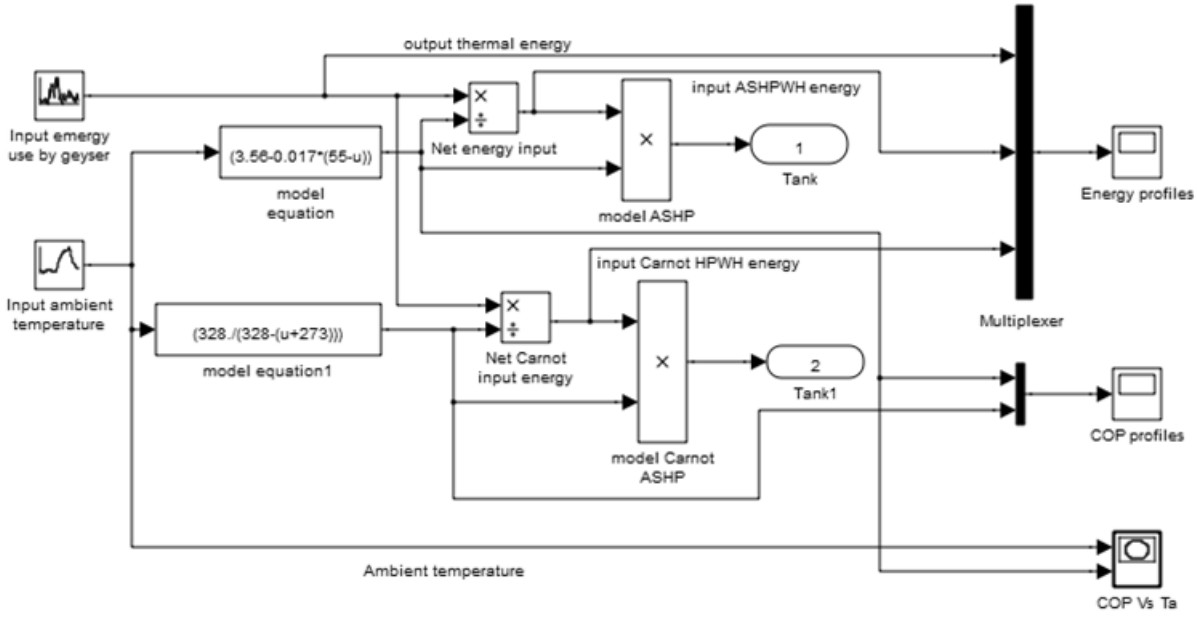

Figure 9: The simulation, architectural and programming sequence used in modelling the system COP and energy consumption

was produced, making a significant saving of 6.48 kWh but with an average COP of 2.80. Figure 12 shows the temperature profiles of the average weekday with the set point temperature for hot water at 55ºC. However, in practice, there are instances where hot water (below the set point temperature) could be supplied by the geyser due to huge water drawn off just like in the case of a heat pump water heater – thus, indicating that the COP would be higher. Figure 13 illustrates the COP variation in relation to ambient temperature of the average weekday over a 24 hour period. Although the maximum temperature was 22.13ºC at time 18:00, the energy saved was not maximum due to the low electrical input as depicted in Figure 10. Table 3 summarizes the comparative analysis of average values over 24 hours for the average weekday. It shows a modelled practical ASHP and CHP water heater's performance under the prevailing conditions using the mathematical modelling equations. The modelled ASHPWH is representing a practical heat pump water heater whose performance was determined from the mathematical model of COP while the CHP water heater represents a heat pump water heater whose performance was determined using the Carnot's equation of heat pump COP. It is also relevant to mention that the efficiency of the modelled ASHP water heater was the ratio of the modelled COP of ASHP water heater to the COP of CHP water heater. Table 3 summarizes the average weekday performance comparison analysis for the modelled ASHP and CHP water heater.

4. 2 Analysis of the average week-end performance

The energy, the COP and temperature analysis of the average weekend profiles over a 24 hour period are illustrated in Figures 14, 15, 16 and 17. From Figure 14, it can be depicted that the practical ASHP water heater used the least electrical input in zone A with a COP of 2.83 and an energy saving of 0.86 kWh. Comparing the COP of zone A to the COP of zone B (2.80), a larger energy saving of 7.93 kWh was achieved due to this significant level of input energy used during this period since the demand for hot water also increased. From Figure 15, the COP profile for both modelled ASHP and modelled CHP water heaters replicated a similar pattern to those profiles shown in Figure 11 (COP profiles of the average weekday).

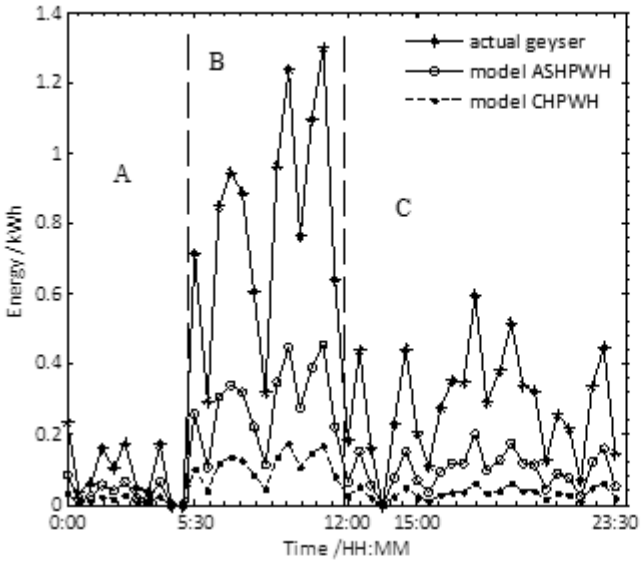

Figure 10: Average weekday energy profiles

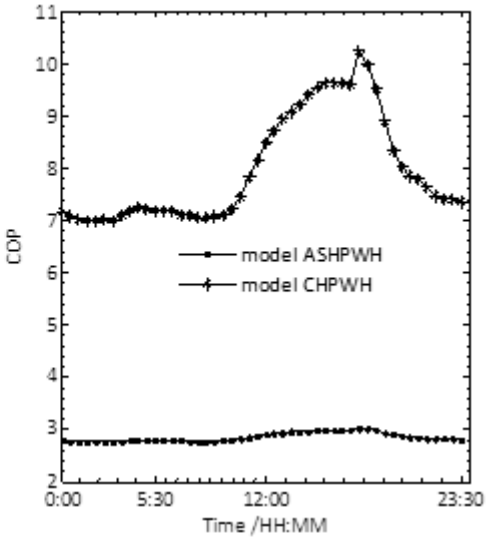

Figure 11: Average weekday COP profiles

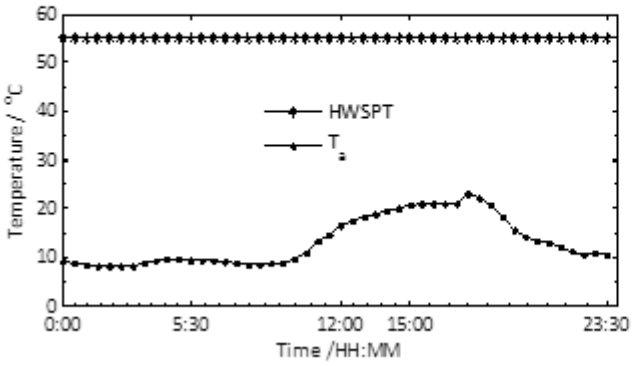

Figure 12: Average weekday temperature profiles

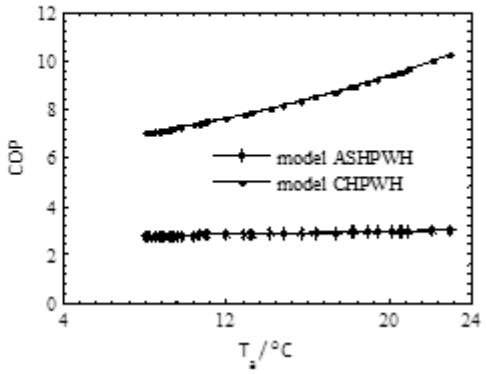

Figure 13: Average weekday COP vs T_a

Table 3: Performance comparison analysis

Average weekday	*Zone A (00:00 – 05:30)*		*Zone B (05:30 – 12:00)*		*Zone C (12:00 – 23:30)*	
Quantity	*Model ASHPWH*	*Carnot ASHPWH*	*Model ASHPWH*	*Carnot ASHPWH*	*Model ASHPWH*	*Carnot ASHPWH*
Average COP	2.775	7.105	2.803	8.709	2.916	8.753
Total input (kWh)	0.626	0.244	3.604	1.377	2.257	0.752
Total output (kWh)	1.738	1.738	10.086	10.086	6.595	6.595
Energy save (kWh)	1.112	1.494	6.482	8.709	4.338	5.843
Efficiency wrt Carnot	39.06	100.0	37.93	100.0	33.31	100.0

Table 4: Performance comparison analysis

Average week-end	*Zone A (00:00 – 05:30)*		*Zone B (05:30 – 12:00)*		*Zone C (12:00 – 23:30)*	
Quantity	*Model ASHPWH*	*Carnot ASHPWH*	*Model ASHPWH*	*Carnot ASHPWH*	*Model ASHPWH*	*Carnot ASHPW*
Average COP	2.830	7.621	2.800	7.342	2.884	8.287
Total input (kWh)	0.466	0.171	4.403	1.678	3.016	1.041
Total output (kWh)	1.322	1.322	12.334	12.334	8.729	8.729
Energy save (kWh)	0.856	1.151	7.931	10.656	5.713	7.688
Efficiency wrt Carnot	37.13	100.0	38.14	100.0	34.80	100.0

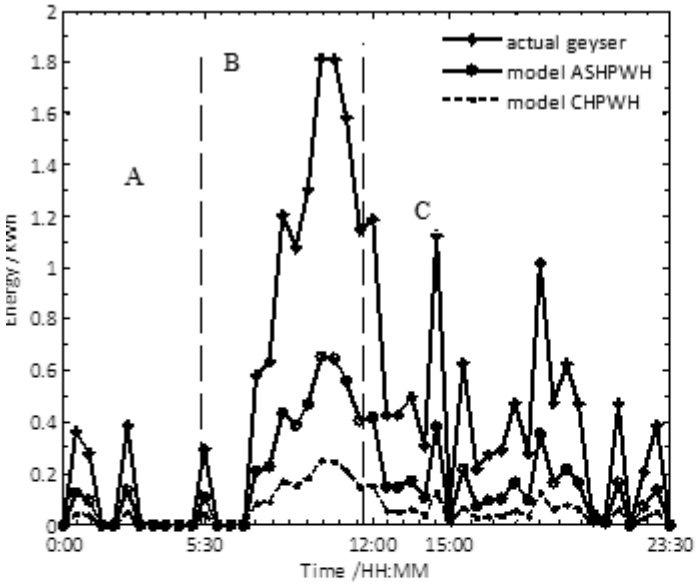

Figure 14: Average weekend energy profiles

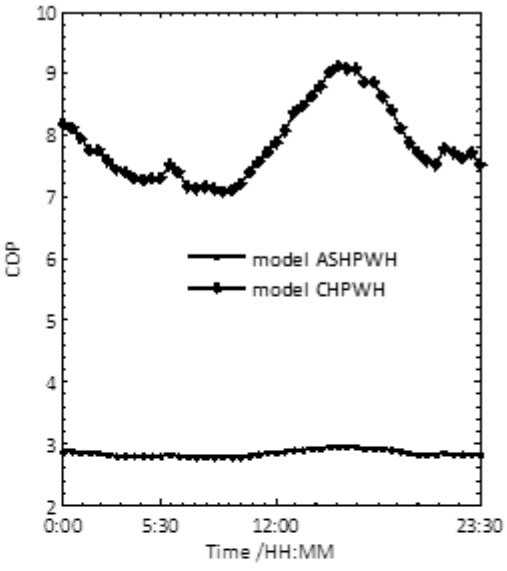

Figure 15: Average weekend COP profiles

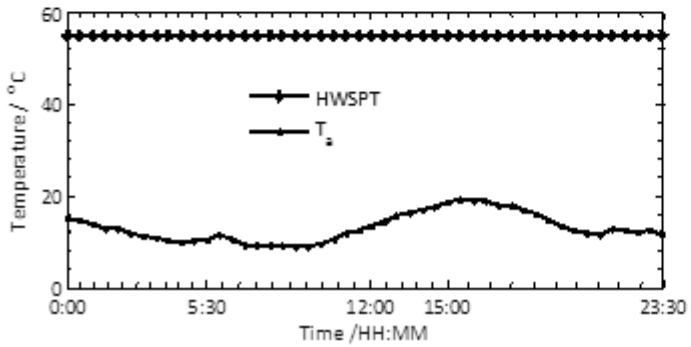

Figure 16: Average weekend temperature profiles

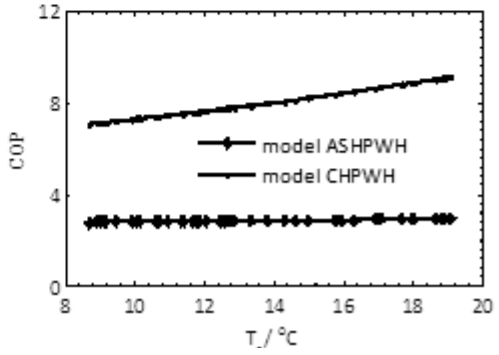

Figure 17: Average weekend COP vs T_a

In zone C, there was an increase in the average COP but with a slightly lower electrical input energy as represented by the values 3.02 kWh and 1.08 kWh respectively, compared to Zone B. The temperature ranges (8°C to 23°C) were equal for both the average weekend and average weekday. This argument holds for both the temperature profiles in Figure 16 and the COP variation with average ambient temperature as shown in Figure 17. The maximum average COP of model ASHP water heater was 2.95 and was achieved at time 15:30, when ambient temperature was maximum (19.10°C). The complete analysis is as shown in Table 4.

Table 4 summarizes the average weekend performance comparison analysis for the model ASHP and CHP water heater.

5. Conclusion

The modelled COP of practical ASHP water heater depicted the real life performance of the ASHP water heater with a minimal deviation error due to the exclusion of the other factors that affect COP. Seasonal and annual COP can be accurately determined for the ASHP water heater provided transient evaporator temperature (which in practice differ from the ambient temperature of more than or equal to 4°C) and hot water set temperatures are known. The ASHP water heater is an energy efficient technology for sanitary hot water production, but when compared to the Carnot's heat pump water heater, which does not have auxiliary energy consuming components, the ASHP water heater is 37% to 40% efficient owing to the extra input energy required to run the water circulation pump and axial propeller fan. Mathematical modelling and simulation of COP can be determined without actually measuring the primary factors (load cycle, cold water temperature, etc.) but using theoretical values from the literature. Based on the modelled COP, energy savings and performance can be determined with some degree of confidence for any intending retrofit The ASHP water heater going to be installed provided ambient temperature and hot water set point temperatures are known in conjunction with the baseline profile for the geyser intended to be retrofitted, using the simulation application developed and built in the Simulink environment.

Acknowledgement

We are grateful for Eskom and the Institute of Technology, University of Fort Hare. for their financial supports that facilitated the acquisition of equipment for the research.

References

Bodzin, S. (1997), Air-to-Water Heat Pumps for the Home, Home Energy Magazine Online, July/August 1997.

Digest of South Africa Energy Statistics (2009). Department of Energy.

Domestic water heating and water heater energy consumption in Canada (CBEEDAC, 2005).

Energy Management and conservation handbook (2008). Nitin Goel, Thermo physical properties of refrigerants, CRC Press.

Eskom (2010). Integrated Demand Management www.eskom.co.za/home/about.

Ito S, Miura N and Wang K. (1999). Performance of a heat pump using direct expansion solar collectors. *Solar Energy* V65, 189-196.

Kline, S. A., *et al.* (2000). TRNSYS 15 A Transient system simulation program. University of Wisconsin Solar Energy.

MATLAB and Simulink software package (Math work corporation 2011b, version 7.12)

Meyer, J.P., and M. Tshimankinda (1998). Domestic Hot Water Consumption in South African Townhouses, Energy Conversion and Management, 39:7, 679-684.

Morrison, G.L., Anderson, T. and Behnia M. (2004). Seasonal performance rating of heat pump water heaters. *Energy Conservation & Management. 76:147-152.*

Received 5 March 2013; revised 25 February 2015

Performance of an autonomous solar powered absorption air conditioning system

Tatenda J Bvumbe

Freddie L Inambao

Department of Mechanical Engineering, University of KwaZulu-Natal, South Africa

Abstract

The demand for air conditioning is increasing due to changing architectural trends and increased standards of living and indoor comfort conditions. Coupled to this, refrigerants used in conventional refrigeration systems have detrimental effects on the environment. As a result, there is an urgent need to implement environmentally cleaner ways of satisfying this air-conditioning demand. Absorption cooling systems have shown great potential to do so. In this study, system performance data for an autonomous solar heating and cooling system installed at the Vodafone Site System Innovation Centre, at the Vodacom Campus in Midrand was collected and analysed. The system comprises a 116 m^2 vacuum tube collector array, a 6.5 m^3 hot water storage tank, a 35 kW LiBr-Water absorption chiller, 1 m^3 of cold water storage, a dry cooler for the chiller, and two underground thermal stores to pre-cool the supply air to the building and the dry cooler respectively. System performance data was collected from the beginning of December 2011 to the end of January 2012 and used to estimate the system long term performance. The chiller has an average coefficient of performance (COP) of 0.51 whilst the solar COP has an average value of 0.24. The total installation cost is R2 822 436.89, with an annuity of R225 949.75 and a cost per kWh of R28.88.

Keywords: solar powered absorption cooling, LiBr-water, system performance, economic performance

Nomenclature

CV	Capital value
d	Basic interest rate
f	Inflation
G_t	Incident solar energy
N	Life time of the plan
PVF(N,f,d)	The present value factor
P(t)	Investment at time
t	Time
T_a	Ambient temperature
T_{am}	Collector average temperature

1. Introduction

Heating Ventilation and Air Conditioning (HVAC) contributes approximately 5 400 MW to electricity demand, which is roughly 15% of the peak load demand. In total, every year HVAC systems utilize 4 000 GW of electricity in South Africa (Eskom, n.d.). Due to the prevailing electricity shortages and ever increasing energy prices, there is now an increased need for cooling systems that use working cycles that can be driven by renewable energy such as solar, wind, geothermal and biogas, whilst at the same time, having minimum impact on the environment. The solar radiation levels in South Africa are among the highest in the world. As a result, solar energy has the potential to supply a sizeable percentage of the cooling energy demand. The annual 24-hour solar radiation average for South Africa is 220 W/m^2. Most of the interior geography of the country receives an average insolation in excess of 5 kWh/m^2/day with some parts of the Northern Cape averaging 6 kWh/m^2/day (Haw and Hughes, 2007). In general, solar cooling is an attractive idea because the cooling loads and availability of solar energy are approximately in phase.

The most common type of thermally driven technology used globally to produce chilled water is absorption cooling. The absorption cooling system is characterized by high reliability, silent operation, long service life, simple capacity control and low maintenance costs. This makes it a genuine candidate for efficient and economic use of solar energy

for cooling applications. Absorption systems use low temperature thermal energy collected from the sun without converting it into mechanical energy as is the case in vapour compression systems. The basic physical process in an absorption system consists of at least two chemical components, one of them serving as the refrigerant and the other as the absorbent. For air-conditioning applications, absorption systems commonly use lithium bromide-water or ammonia-water working pairs. LiBr-water absorption units are the most appropriate for solar applications since low cost solar collectors may be used to power the generator of the machine. The NH_3-water machine requires high generator temperatures in the range of 125-170°C (Duffie and Beckman, 2006). This temperature requires the use of medium concentration ratio parabolic collectors, which have increased maintenance requirements. The LiBr-water machine requires a temperature in the range 75-120°C, which is easily achieved using flat plate or evacuated tube collectors. The LiBr-water machine has a higher coefficient of performance (COP) than that of the NH_3-water machine and costs less (Duffie and Beckman, 2006; Mittal, Kasana and Thakur, 2006; Henning, 2005; Hang, Qu and Zhao, 2011; Agyenim, Knight and Rhodes, 2010; Casals, 2006). One of the reasons the NH_3-water machine is more expensive is because it requires a rectifier to prevent any water vapour entering the evaporator.

In this study, we monitor a solar powered HVAC system and report on its performance and cost.

2. System description

The Vodacom Campus is located in Midrand (within greater Johannesburg) at a latitude of 25°58'14"S and a longitude of 28°7'37". This area receives on average of 3 128.3 hours sunshine a year. The key weather parameters for Johannesburg are presented in Table 1.

The Vodafone Site Solution Innovation Centre (Vodafone SSIC) is the first 6 Green Star SA accredited building in South Africa. In this building, two types of solar technologies are used: a photovoltaic (PV) system to generate electricity and a solar thermal system that provides heating and cooling through a solar absorption system. This study focuses on the solar powered absorption system. This is a solar autonomous thermal heating and cooling system to maintain room temperature at comfortable levels throughout the year. Two rock storage facilities are located under the building: one pre-cools the supply air to the building so that the cooling load is reduced and the other pre-cools the supply air to the dry cooler at ambient air temperatures to facilitate heat rejection.

The system also includes a 116 m^2 evacuated tube collector array, a 6.5m^3 hot water storage tank, Yazaki WFC10 absorption chiller with a dry cooler for heat rejection, a 1m^3 cold storage tank, a thermally activated slab and a dehumidification system.

3. Building loads

In Johannesburg, the average ambient temperatures are highest in the period from November to April and the cooling requirements follow the same pattern. During this period, the temperatures fall to about 15°C after midnight and these mild temperatures are responsible for the observed low heating requirements. The outside ambient temperatures start falling below 10°C in April and hence the heating loads for the building start steadily increasing reaching their peak in July. The load profile for the office building in this study is shown in the Figure 1. The maximum cooling load is around 20 kW and is experienced during the period November to February whereas the maximum heating load is 22.5 kW and is recorded in July. The annual cooling demand is 18.4 MW and the annual heating demand is 3.2 MW.

The peak sizing for the cooling system was based on January 15, 2002. The cooling for the building increases steadily from morning as the ambient temperature and incident solar irradiation increases. The peak cooling load occurs later in the day instead of around midday when the solar energy is at its maximum. This delay is due to conduction of the incident solar energy by the walls, roof and windows of the building. This heat energy is transferred to the cooling space by convection. The peak load is 24.87 kW and occurs at 16:30 and the average load is 8.86 kW. This particular day experienced an average dry bulb temperature of 24.4°C, with a maximum of 30°C being recorded at 15:00. The distribution of the cooling for this day is shown in Figure 2.

In winter, the system provides heating for the building. A three-way valve is used to bypass the chiller in winter so that hot water can be delivered from the hot water storage tank directly to the air

Table 1: Weather parameters for Johannesburg
(New, Lister, Hulme and Makin, 2002)

Month	*Jan*	*Feb*	*Mar*	*Apr*	*May*	*Jun*	*Jul*	*Aug*	*Sep*	*Oct*	*Nov*	*Dec*
Insolation, kWh/m²/day	6.70	6.10	5.46	4.77	4.21	3.80	4.08	4.78	5.69	5.98	6.29	6.62
Maximum Temperature	25.6	25.1	24.0	21.1	18.9	16.0	16.7	19.4	22.8	23.8	24.2	25.2
Wind speed, m/s	3.62	3.50	3.37	3.54	3.74	4.04	4.18	4.74	4.95	4.73	4.31	3.77
Monthly sun hours	251.1	224	239	237	276	267	285.2	285.2	282	269.7	249	264

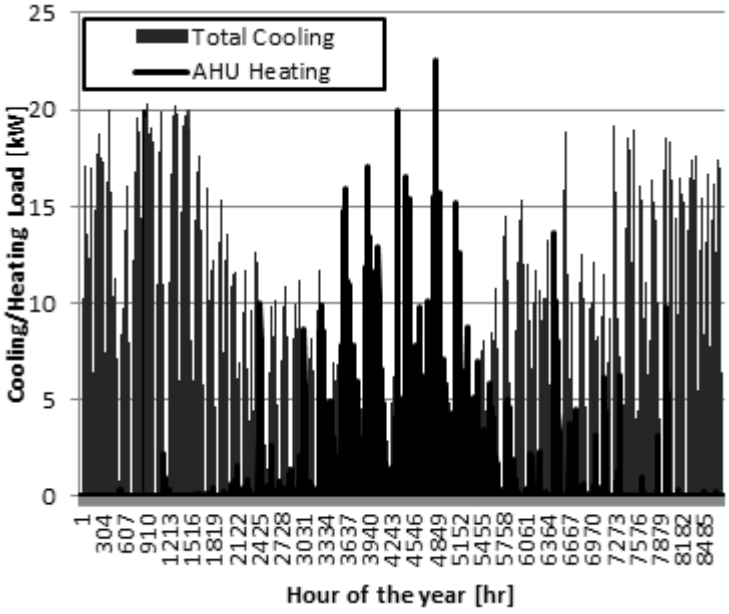

Figure 1: Load profile for the building

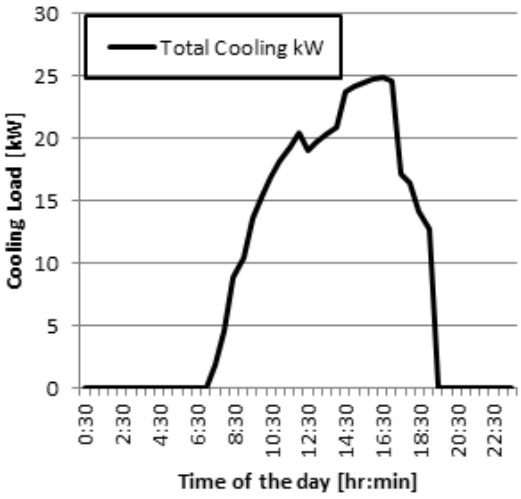

Figure 2: Distribution of the cooling load for January 15, 2002

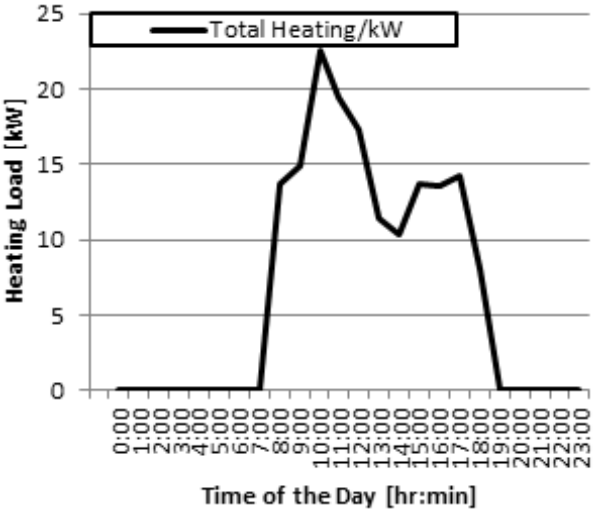

Figure 3: Distribution of heating load distribution on July 21, 2002

handling unit and the thermally active slab. The heating energy demand rises quickly in the morning and reaches its peak before midday. The high demand in the morning can be attributed to lower temperatures and incident solar irradiation in the morning. As the day progresses and this ambient temperature and incident solar radiation increases the building energy demand steadily decreases. In the summer of 2002 the highest heat demand experienced was July 21, with a maximum heating load of 22.5 kW and an average of 6.64 kW.

The distribution of the heating load on that day is shown in Figure 3.

4. Solar array performance

The collector had an average useful energy output of 31.43 kW with a maximum value of 143.7 kW on January 31, 2012, as shown in Figure 4.

There is a rapid rise in both the collector outlet and inlet temperatures at 7:45 because that is the time when the primary solar pump is switched on and starts to circulate water in the collectors that have already been warmed up by the early morning sun. The collector inlet is slightly greater than the outlet at the beginning which is why no useful energy is supplied by the collector. Once the outlet temperature becomes greater than the inlet then useful energy starts being supplied. The useful energy produced increases rapidly in the first hour and then stays approximately constant throughout the day. The graph shows that there is a fairly constant change in these parameters throughout the day.

The evacuated tube collectors that are used in this system are defined by the following equation:

$$\eta = 0.745 - 2.007\left(\frac{T_m - T_a}{G_t}\right) - 0.005\left[\frac{(T_m - T_a)^2}{G_t}\right] \quad (1)$$

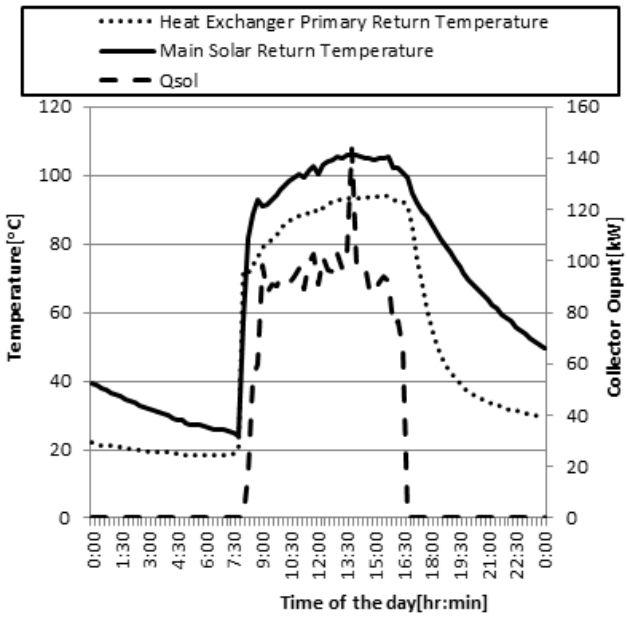

Figure 4: Distributions of collector energy output, inlet and outlet temperature on January 31, 2012

Where
T_a Ambient temperature
T_m Collector average temperature
G_t Incident solar energy

The third term on the right hand side of equation (1) can be neglected without any significant effect on the collector efficiency. In the morning, the collector average temperature is approximately equal to the ambient temperature so that the collector efficiency is equal to the nominal efficiency of 0.745. There is a rapid increase in the difference between the average collector temperature and the ambient temperature and hence the sharp decrease in the collector efficiency. As the incident solar energy increases, the efficiency starts increasing with a distribution similar in shape to the solar energy distribution and reaches its peak around midday. The incident solar then steadily decreases after midday and consequently the collector efficiency does the same. The distribution of the collector efficiency given by the above equation is shown in Figure 5.

5. Absorption chiller performance

The distribution of the temperature streams going in and out of the chiller is presented in Figure 6. The chiller can be operated using water with a temperature of between 70°C and 95°C, but the system control strategy states that the chiller will only start producing cooling energy if the hot water temperature that is being delivered into the generator exceeds 80°C. The system performance values were recorded at 15 minute intervals and there are 96 data points for January 31, 2012. As shown in Figure 6, 35 of the recorded values, representing

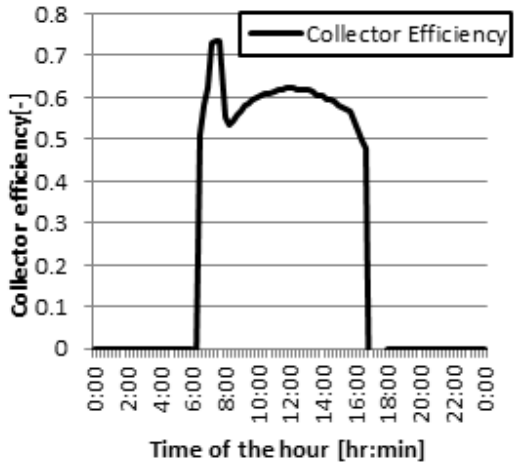

Figure 5: Distribution of collector efficiency on January 31, 2012

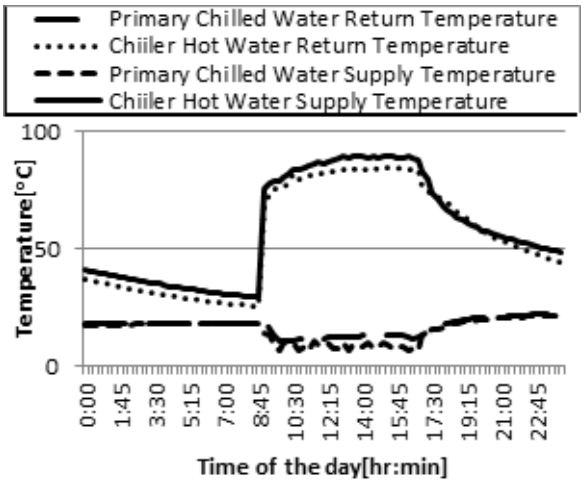

Figure 6: Temperature distributions of the chiller water streams on January 31, 2012

36.5%, were above 70°C. This means that the chiller could have run for 36.5% of the time period if required. The generator inlet temperature exceeds the threshold value of 80°C for 28 of the recorded values representing 29.2% of the time period.

It can be seen that the hot water stream temperatures rise sharply when the chiller is switched on at 9:00 after which they become fairly constant before gradually falling after the chiller is switched off at 17:00. The chilled water return temperature starts gradually decreasing at chiller switch on, and then evens out as the day progresses. This is different from the chilled water supply temperature, which shows an up and down trend. This is because the system control strategy requires that the chiller switches off if the chilled water supply temperature falls below 7°C. The same distribution is also seen in the variation of the chiller COP and solar COP as seen in Figure 7.

6. Thermally activated slab

Concrete Core Tempering also known as Thermally Activated Building Systems (TABS) is a method of

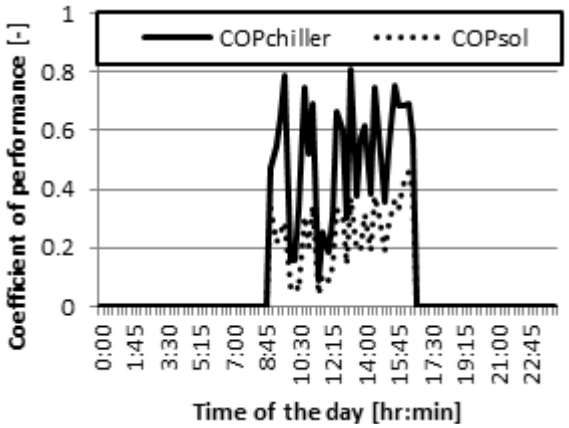

Figure 7: Distributions of COP and SCOP on January 31, 2012

introducing heating or cooling into a concrete structure by means of embedding a series of pipes in the concrete floor or cooling slab (REHAU Polymer Limited, n.d.).. The cooling energy produced is used to substitute the heating or cooling energy generated by a central air-conditioning system. The TABS acts by reducing the building cooling load through radiant and convective cooling as the cold water travels in the embedded pipes underneath the floor. On January 30, 2012 the thermal store provided an average energy output of 15.74 kW with a maximum of 45.52 kW. As a result of this large amount of cooling energy generated, the AHU had a cooling rate of 3.96 kW which is approximately 15.3% of the total cooling capacity. The thermal store satisfies the bulk of the cooling demand. The energy is generated from the moment that the slab pumps are switched on and the energy generation proceeds at a rate that is approximately constant. The input and outlet temperatures of the TABS are also fairly even throughout the day. The variations of these temperatures and the cooling energy produced are shown in Figure 8.

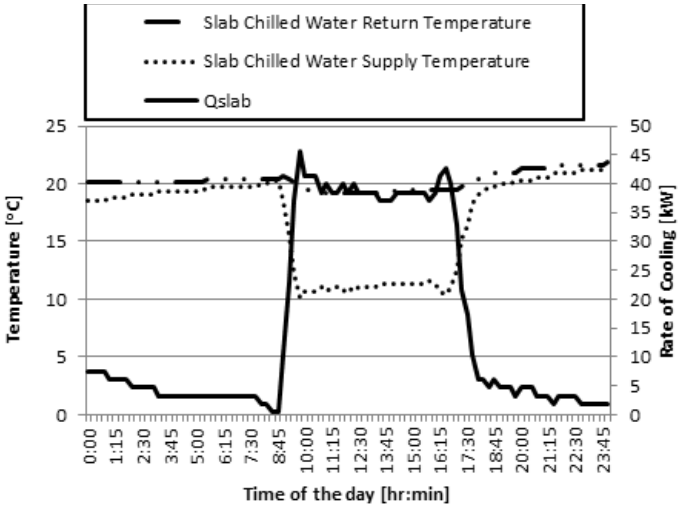

Figure 8: Distributions of the TAS water stream temperatures and the cooling energy on January 31, 2012

7. Dehumidification fins

The TABS lowers the air temperature when the air comes in contact with the cooled slab hence condensation of water vapour takes place on the floor. To solve this problem, a dehumidification system is integrated with TABS. The functions of the dehumidification fins are to maintain the building humidity in the range 30-65%. There is a control system that automatically switches the dehumidification fins on at 8:00 and switches them off at 17:00. The dehumidification is achieved by passing the air over a refrigerated coil. This cools the air below dew point and the moisture is condensed and drained out. The cold air produced is introduced into the building airspace and this produces a cooling effect. The fins provided an average cooling capacity of 2.6 kW with a maximum of 11.1 kW. The variations are shown in Figure 9.

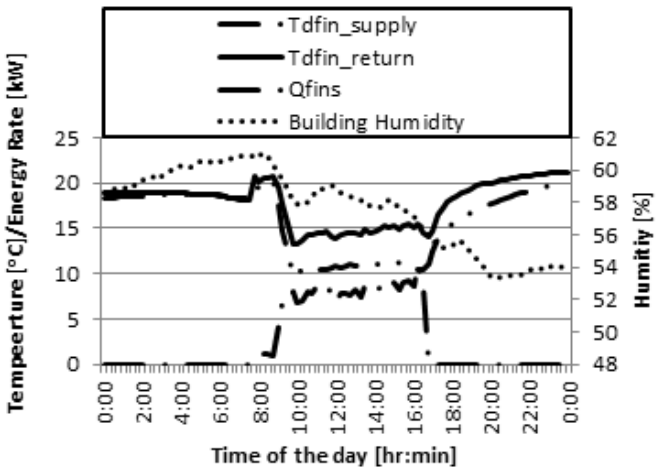

Figure 9: Distributions of the inlet and outlet water temperatures and the dehumidification fins cooling energy on January 31, 2012

8. Building environment

The system was designed to keep the building airspace temperature between 20°C and 25°C. The ambient conditions determine the amount of work that the system has to perform for these desired conditions to be maintained. On 31 January, 2012 there was an average ambient temperature of 23.82°C with a maximum temperature of 32.5°C. The ambient humidity had an average of 58.82% and a maximum of 76.6% as shown in Figure 10. The solar cooling system was able to maintain the temperature within the desired limits throughout the day; the average building temperature had a mean value of 22.47°C, a maximum of 24.9°C and a minimum of 20.4°C. The humidity had an average value of 57.6% with maximum and minimum values of 61.15 and 53.3% respectively.

9. Economic analysis

The costs of a solar powered cooling system can be broken down into capital costs, operating costs and

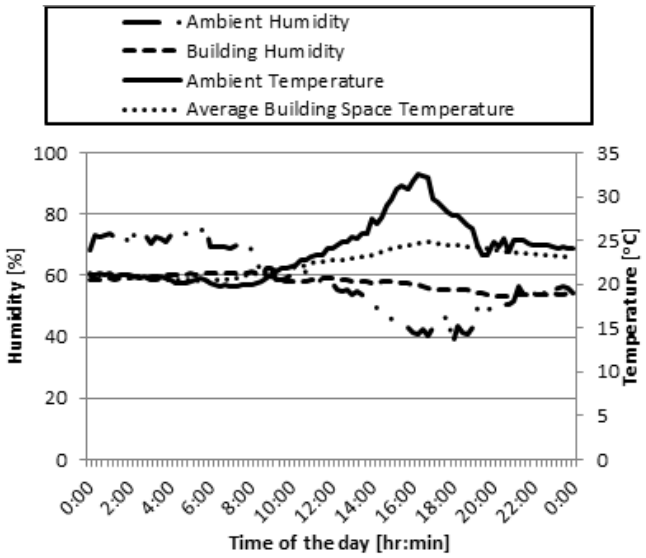

Figure 10: Distributions of the ambient and building humidity and temperatures on January 31, 2012

costs for energy. The capital costs for the Vodafone SSIC system are shown in Table 2.

Table 2: Vodafone SSIC system capital costs

Item	*Costs [Rands]*
Air conditioning equipment	1,918,544.00
Solar equipment	559,422.89
Thermal store	388,350.00
Total installation value	2,866,436.80

To measure economic performance we use the total cost of the cooling system. We make use of the annuity method, where all cash flows are connected into a series of annual payments of equal amounts. The annuity is found by first calculating the net present value (NPV) of all costs occurring at different times during the project, i.e. by discounting all costs to the time when the investment takes place. The NPV is the total present worth of the gains from the solar system compared to the electricity only system. The capital value of the investment is made up of the initial investment costs and any further investments for component exchange in subsequent years. This is calculated using the rate of inflation and the basic interest rate (Pietruschka, 2010). The capital value is given as:

$$CV = \sum P(t)\frac{(1+f)^t}{(1+d)^t} \qquad (2)$$

Where:
CV Capital value
p(t) Investment at time t
t Time
d Basic interest rate
f Inflation rate

The prime interest rate set by the South African Reserve Bank as of May 2012 was 5.75% and the inflation rate was 9% (South African Reserve Bank, 2012). With these values the CV is found as R1 934 844.90.

The annual expenses for maintenance and plant operation, which occur regularly during the life time of the plant, are discounted to the present value by multiplication of the expenses with the present value factor (PVF). The PVF is given by the following equation:

$$PVF(N,f,d) = \frac{1+f}{d-f}\left[1-\left(\frac{(1+f)}{(1+d)}\right)^N\right] \qquad (3)$$

Where:
PVF (N,f,d) The present value factor
N Life time of the plan
f 5.75
d 9
N 20
The PVF is calculated to be 2.08.

In the case of solar cooling plants, no annual income is generated (Pietruschka, 2010; Edwards, 2011; Sakellari, 2005; Li and Sumathy, 2002). As a result, the NPV is simply obtained from the sum of discounted investment costs and the discounted annual expenses. It is defined here with a positive sign to obtain annuity values:

$$NPV = CV + EX.PVF(N,f,d) \qquad (4)$$

Where: *EX* Annual expenses

The annual expenses include maintenance costs, energy and water costs. The maintenance costs over the lifetime of the system are taken as 2% of the initial capital investment and the average life

of the system is taken as 20 years (Pietruschka, 2010). The annual expenses (*EX*) are found to be R57 328.74. This consequently results in the NPV for the system being equal to R2 054 088.64

To obtain the annuity, the NPV is multiplied by a recovery factor,r_f which is calculated from the discount rate and the life time of the plant.

$$a = NPV.r_f(N,d) \quad (5)$$

Where:

r_f Recovery factor and is given as:

$$r_f = \frac{d(1+d)^N}{(1+d)^N - 1} \quad (6)$$

The recovery factor r_f is calculated and found to be 0.11. The annuity for the system is R225 949.75.

The cost per kWh of cooling energy produced is the ratio of the annuity divided by the annual cooling energy produced (Sakellari, 2005). The cost per kWh is R28.88.

10. Conclusions and recommendations

The use of solar energy to provide building cooling energy using the absorption cycle has been demonstrated. The costs of the installation and hence the cost per kWh of energy produced is very high. This is because the system is oversized to cater for periods when the incident solar energy is low. It is recommended that solar powered absorption systems should be installed in combination with conventional vapour powered system so as to reduce the initial costs of the solar system. Further research should be geared towards cost reduction and the government can also introduce a rebate in order to encourage uptake of solar powered absorption systems.

Acknowledgements

The authors would like to acknowledge the assistance provided by Voltas Technologies, particularly Messrs Frank Major and Hartmut Martin, and financial support from the Centre for Engineering Postgraduate Studies (CEPS) and the DVC-Research, Prof Nelson M. Ijumba.

References

Agyenim, F., Knight, I. and Rhodes, M. (2010). Design and experimental testing of the performance of an outdoor LiBr-water solar thermal absorption cooling system with a cold store, *Solar Energy*, 84(5): 735-744. doi:10.1016/j.solener.2010.01.013

Casals, X. G. (2006). Solar absorption cooling in Spain: perspectives and outcomes from the simulation of recent installations. *Renewable Energy*, 31(9): 1371–1389.

Duffie, J. A. and Beckman, W. A. (2006). *Solar engineering of thermal processes*. 3rd edition. New York: John Wiley.

Edwards, C. (2011). Performance assessment of solar absorption cooling for Ontario housing, MASc Thesis, Carleton University, Ottawa, Ontario, Canada.

Eskom. (n.d.) Demand side management: air conditioning facts [Online]. Available: www.eskom.co.za. (Accessed July 20 2012).

Hang, Y., Qu, M. and Zhao, F. (2011). Economical and environmental assessment of an optimized solar cooling system for a medium-sized benchmark office building in Los Angeles, California: *Renewable Energy*, 36(2), 648-658.

Haw, M. and Hughes, A. (2007). Clean energy and development for South Africa: Background Data. Report 1 of 3. Energy Research Centre, University of Cape Town.

Henning, M. (2005). Solar assisted air-conditioning of buildings – an overview. Proceedings of the Heat-SET 2005 Conference 5-7 April, Grenoble, France. Grenoble: Editions-GRET.

Li, Z. F. and Sumathy, K. (2002). Performance study of a partitioned thermally stratified storage tank in a solar powered absorption air conditioning system. *Applied Thermal Engineering*, 22(11):1207-1216.

Mittal, V, Kasana, K.S. and Thakur, N.S. (2006). Modelling and simulation of a solar absorption cooling system for India. *Journal of Energy in Southern Africa*, 17(3) 65-70.

New, M., Lister, D., Hulme, M. and Makin, I. (2002). A high-resolution data set of climate over global land areas. *Climate Research*, 21:1-21.

Pietruschka, D. (2010). Model based control optimisation of renewable energy based HVAC systems: solar driven absorption and open dessicant evaporative cooling. Ph.D Thesis: De Montfort University and University of Applied Sciences Stuttgart..

REHAU Polymer Limited. (n.d.). [Online] Available: http://www.rehau.co.za/094B4D9CA7EFB95BC12579590058BFFE_33BE485874AD15A0C12570EB002C8401.shtml. (Accessed 30 May 2012).

Sakellari, D. (2005). Modelling the dynamics of domestic low temperature heat pump heating systems for improved performance and thermal comfort – a systems approach. PhD Thesis: Royal Institute of Technology, Sweden.

South African Reserve Bank. (2012). [Online] Available: www.resbank.co.za. (Accessed 1 June 2012).

Received 10 January 2012; revised 21 January 2015

Theoretical investigation of a combined Kalina and vapour-absorption cycle

Mohammad Tariq
Department of Mechanical Engineering, Shepherd School of Engineering & Technology, SHIATS-DU, Allahabad, U.P. India

Vinod Kumar Nema
Department of Mechanical Engineering, Motilal Nehru National Institute of Technology, Allahabad, UP, India

Abstract
A program has been developed to calculate enthalpies at the salient points (later referred to as stations) of a combined power and cooling cycle provided pressure, temperature, mixture concentration and condition are known at these points. The ammonia-water mixture, which is taken as the working fluid, may be at one of the following seven conditions namely, superheated vapour mixture, mixture of superheated component of ammonia and pseudo vapour component of water, saturated vapour mixture, wet vapour mixture, saturated liquid mixture, mixture of subcooled water and pseudo liquid ammonia and subcooled mixture of subcooled components of ammonia and water. The mixture boiling-point temperature and dew-point temperature, needed to establish the condition of the working fluid, are functions of absolute pressure, critical pressure and critical temperature of the mixture; later two depend on the mixture concentration and the corresponding critical values of water at the given station. Using typical values of the variables as listed above, enthalpies at all stations are predicted. The predicted enthalpies are close (within 3%) to those available in the literature except at two stations where the mixture was weak in ammonia and its temperature was either in the near vicinity of the mixture boiling-point temperature or below the saturation temperature of pure ammonia at the concerned pressure. Using the predicted values of enthalpies, thermal efficiency of the combined power and cooling cycle has been calculated.

Keywords: *absorption, ammonia-water mixture, cogeneration cycle, combined power and cooling cycle, energy, refrigeration, Kalina cycle.*

1. Introduction

Many combined cycles have been proposed as an alternative to the conventional power cycles for improving the overall energy conversion efficiency. A typical combined cycle consists of a gas turbine operating on a Brayton cycle as a topping cycle. The hot exhaust gases from this cycle provide the energy for the bottoming steam Rankine cycle. The efficiency of the combined cycle is better than the efficiency of each cycle operating alone (Feng and Goswami, 1999). Another method of improving the performance of a thermal power plant is to use a cogeneration cycle which provides heating and power of both or a hybrid thermal power and cooling cycle which combines the Rankine cycle and absorption refrigeration cycle with power generation as primary goal in either case.

The research team of Kalina is recognized for introducing an ammonia-water mixture as the working fluid in power cycles [Kalina, 1984; Kalina and Tribus, 1990; Kalina *et al.,* 1986]. An absorption type power cycle using a mixture of ammonia and water as the working fluid was studied in the early fifties (Maloney and Robertson, 1953). Washam *et al.* (1994) suggested solar energy as input in the combined cycle to make it economically viable.

Park and Sonntag (1996) and Ibrahim and Klein (1993) analysed the Kalina cycle. Their studies show that the Kalina cycle was advantageous over the conventional Rankine cycle under certain conditions. Although the use of mixed working fluid, such as ammonia-water, provides a big advantage in utilizing a sensible heat source in the boiler, it presents a disadvantage in the condenser. The disadvantage can be overcome if a normal condensation process is replaced by an absorption condensation process (Park and Sonntag, 1996; Zeigler and Trepp, 1984).

The combined cooling and power cycle with power as the primary goal takes advantage of low

boiling temperature of ammonia so that its vapour can be expanded to a very low temperature while it is in a vapour state or a high quality two- phase state. This cycle is ideally suited for solar thermal power using low cost concentrating solar collectors with the potential of reducing the capital cost of a solar thermal power plant. This cycle can also be used as a bottoming cycle for any thermal power plant. A thermodynamic cycle proposed by Goswami and Feng (1999) combined the advantages of mixed working fluid and absorption condensation to improve the efficiency of the thermal cycle. Since the proposed cycle uses almost pure ammonia as the working fluid in the turbine, it is expanded to a temperature much below the ambient temperature. The net effects are the production of both the refrigeration effect and power output and the reduction of the effective sink temperature for the cycle.

1.1 Thermodynamic analysis of the combined cycle

The following assumptions have been made while determining enthalpies at various temperature conditions:

- The water and ammonia components form a single system and no chemical reaction takes place.
- In case of vapour mixture, each gas behaves as an ideal gas.
- In the liquid phase, when the mixture temperature is either equal to or less than the boiling point temperature, the enthalpy is calculated using the mixture properties suitable to the ideal solution and then the isothermal departure of the liquid mixture from the ideal solution properties added to it.

There are certain combinations of pressure and temperature at which the mixture is not in equilibrium condition. This occurs when at the given pressure, the mixture temperature lies between the dew point temperature and the saturated temperature of pure water (T_{sat2}). In this case, ammonia is in the superheated vapour form and water exists in the metastable vapour form. Another situation occurs when at the given pressure, the temperature lies between the boiling point and the saturation temperature of pure ammonia (T_{sat1}). Here ammonia is assumed to be in the metastable liquid state.

During the whole process of the combined cycle, the mixture may adopt any one of the following states, as shown in Figure 1, which will depend on its temperature relative to two temperatures namely, boiling point and dew point. Boiling point temperature, T_b, is the temperature at which the liquid of known composition and pressure begins to boil and dew point temperature, T_d, is the temperature at which a vapour of known composition and pressure begins to condense. The method used to determine them (Feng and Goswami, 1999) is given in the Appendix A.

Consider gradual cooling of a mixture, of a given pressure and concentration, from temperature greater than pure water saturation temperature (T_{sat2}) as shown in Figure 1. It passes through various states (numbered 1 to 7) which are detailed below. Expressions for the related mixture enthalpy in kJ/kg, with suffix 1 for ammonia and 2 for water, have also been provided.

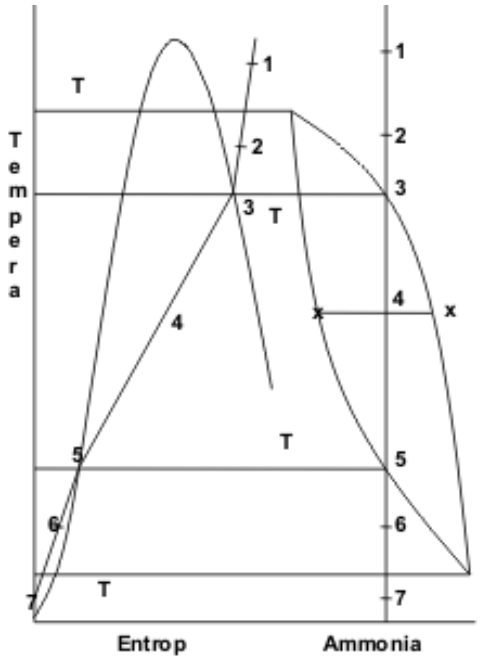

Figure 1: Various conditions on T-s and T-x plots during cooling of a mixture

1.1.1 State 1: ($T \geq T_{sat2}$)

In this condition the temperature is above the saturation temperature of water. The mixture then is the superheated mixture of a superheated component of ammonia and a superheated component of water. Its enthalpy is calculated using equations (Siddiqui, 1999) given below.

$$h_{vm} = xh_{v1} + (1 - x)h_{v2} \quad (1)$$

Where x is the mass fraction of ammonia in the mixture and and , the enthalpies of ammonia vapour and water vapour, respectively, are given by

$$hv_1 = a_1t_g - a_2t_{c1} + a_3 \quad (2)$$

$$hv_2 = b_1t_g - b_2t_{c2} + b_3 \quad (3)$$

where t_g is the temperature of the mixture in ^{0}C and t_c the critical temperature of respective component in ^{0}C. Constants in eqns. (2) and (3) are given below.

a_1=2.3678756;
a_2=0.72779902;

a_3=137908894;
b_1=1.925;
b_2=0.126;
b_3=2500.0;

1.1.2 State 2: ($T_{sat2} > T > T_d$)
The mixture is considered as the superheated mixture of superheated component ammonia and pseudo vapour component water. Enthalpy is found (Siddiqui, 1999) by linear interpolation with respect to temperature of superheated enthalpy at T_{sat2} and saturated vapour enthalpy at T_d,

1.1.3 State 3: ($T = T_d$)
In this condition, the temperature is equal to the dew point temperature of the mixture. For this condition, the enthalpy is calculated using equation (Siddiqui, 1999) given below.

$$hv_m = xh_{v1} + (1 - x)h_{V2} \quad (4)$$

where vapour enthalpies h_{v1} and h_{v2} are given by following equations.

$$h_{v1} = a_1 + a_2T_d + a_3T_d^2 + a_4T_d^3 + \left(\frac{a_5}{T_d^{11}} + \frac{a_6}{T_d^3} + a_7\right)P + a_8\frac{P^3}{T_d^{11}} \quad (5)$$

$$h_{v2} = w_1 + w_2T_d + w_3T_d^2 + w_4T_d^3 + \left(\frac{w_5}{T_d^{11}} + \frac{w_6}{T_d^3} + w_7\right)P + w_8\frac{P^3}{T_d^{11}} \quad (6)$$

and the constants are
a_1 = 780.3751592,
a_2 = 1.793463444,
a_3 = 2.438453,
a_4 = 5.887041*e*-1,
a_5 = -3.894205*e*+4,
a_6 = -1.618514*e*+2,
a_7 = -5.123027*e*-2,
a_8 = -5.946927*e*+2,
w_1 = 1995.675063,
w_2 = 1.854864237,
w_3 = -10194269*e*-4,
w_4 = 3.002761*e*-7,
w_5 = -2.566671*e*+28,
w_6 = -5.850564*e*+8,
w_7 = 90858336*e*-2,
w_8 = 0.0,
where T_d is in K and P is in bar.

1.1.4 State 4: ($T_d > T > T_b$)
In this condition, the temperature lies between the dew point temperature and boiling point temperature and enthalpy of two-phase mixture is calculated (Park and Sonntag, 1996) by:

$$h_m = (1 - D)h_{lm} + Dh_{vm} \quad (7)$$

where h_{lm} and h_{vm} denote the enthalpies of the saturated liquid mixture and saturated vapour mixture, respectively and D, the dryness fraction of the mixture, is given by:

$$D = \frac{x - x_l}{x_v - x_l}$$

where x_l and x_v are the mass fractions of ammonia in the liquid- and vapour-solution, respectively.

1.1.5 State 5: ($T = T_b$)
In this condition, the mixture is at the boiling point temperature as a saturated liquid. At this condition the enthalpy is calculated [Siddiqui, 1999] by:

$$D = \frac{x - x_l}{x_v - x_l} \quad (8)$$

where the constants are listed below:
C_0 = -2.25462*e*+3,
C_1 = 884209*e*+5,
C_2 = -1.239222*e*+8,
C_3 = 1.197489*e*+3,
C_4 = 4.686089*e*-2,
C_5 = -9.412826*e*+5,
C_6 = 1.797014*e*+8,
C_7 = -3.701820*e*+2,
C_8 = 2.935257*e*-3,
C_9 = 0.357491*e*+5,
C_{10} = 0.122989*e*+8,
and h_{l1} and h_{l2} are the enthalpies of saturated liquid ammonia and saturated liquid water component respectively, and are given by the following equations.

$$h_{l1} = w_0 + a_1T + a_2T^2 + a_3T^3 + (a_4 + a_5T^2)P + a_6P^2 \quad (9)$$

$$h_{l2} = w_0 + w_1T + w_2T^2 + w_3T^3 + (w_4 + w_5T^2)P + w_6P^2 \quad (10)$$

where the constants are given by:
a_0 = -1477.925379,
a_1 = 7.979672715,
a_2 = -1.584957*e*-2,
a_3 = 2.357889*e*-5,
a_4 = 1.938836*e*-1,
a_5 = -1.832123*e*-6,
a_6 = -4.370722*e*-6,
w_0 = -1296.803487,
w_1 = 5.6052326,
w_2 = -4.3682107*e*-3,
w_3 = 4.4796158*e*-6,
w_4 = 0.12685805,
w_5 = -3.8716726*e*-7,
w_6 = -2.3459764*e*-6.

It may be noted that T is in K and P is in bar in the equations (8) through (10). Further x_l and x_v should be used in place of x in equations (4) and (8), respectively

1.1.6 State 6: ($T_b > T > T_{sat1}$)

The mixture is considered as the mixture of subcooled water and pseudo- liquid ammonia. At this condition, the mixture enthalpy is calculated (Kalina et al., 1986) by interpolation of enthalpies at temperature T_b and T_{sat1} given by the equations, (8) and the forthcoming equation (11), respectively.

1.1.7 State 7: ($T \leq T_{sat1}$)

In this condition, the temperature falls below T_{sat1}. The enthalpy for this condition is calculated (Ibrahim and Klein, 1993) by using the equation:

$$h_{lm} = x_{hl1} + (1 - x)h_{l2} + H^E \quad (11)$$

where h_{l1} and h_{l2} are the enthalpies of the subcooled pure ammonia and the subcooled pure water, respectively to be calculated from eqn. (9) and (10), respectively. H^E accounts for the isothermal enthalpy departure from the real solution and is given by

$$H^E = -T^2 \frac{\partial}{\partial T}\frac{G^E}{T} \quad (14)$$

where G^E, the Gibb's excess energy for liquid mixtures, accounts for deviation from ideal solution behavior and its value can be obtained from two references (Kalina *et al.,* 1986 and Feng and Goswami, 1999). In reference (Kalina *et al.,* 1986), it is expressed by a Margule-type equation:

$$G^E = R_m T y(1 - y)[A + B(2y - 1) + C(2y - 1)^2 + ...] \quad (15)$$

where y is the mole fraction of ammonia and R_m stands for characteristic gas constant of mixture, given by:

$$R_m = xR_1 + (1\text{-}x)\, R_2,$$

Unfortunately, values of the constants appearing here are not available on the paper. G^E in the reference (Feng and Goswami, 1999) and is expressed in terms of reduced pressure and temperature, by the following equation:

$$G^E = R_m T_B\,(1\text{-}x)\{F_1 + F_2\,(2x\text{-}1) + F_3\,(2x\text{-}1)^2\} \quad (16)$$

where the constants are given below:

$$F_1 = E_1 + E_2P_r + (E_3 + E_4P_r)T_r + \frac{E_5}{T_r} + \frac{E_6}{T_r^2}$$

$$F_2 = E_7 + E_8P_r + (E_9 + E_{10}P_r)T_r + \frac{E_{11}}{T_r} + \frac{E_{12}}{T_r^2}$$

$$F_3 = E_{13} + E_{14}P_r + \frac{E_{15}}{T_r} + \frac{E_{16}}{T_r^2}$$

The coefficients F_1, F_2 and F_3 use reduced pressure ($P_r = \frac{P}{P_B}$) and reduced temperature ($T_r = \frac{T}{T_B}$) which are found with base pressure P_B = 10 bar and base temperature T_B = 100 K and their constants are given below:

E_1 = -41.733398,
E_2 = 0.02414,
E_3 = 6.702285,
E_4 = -0.011475,
E_5 = 63.608967,
E_6 = -62.490768,
E_7 = 1.761064,
E_8 = 0.008626,
E_9 = 0.387983,
E_{10} = 0.004772,
E_{11} = -4.648107,
E_{12} = 0.836376,
E_{13} = -3.553627,
E_{14} = 0.000904,
E_{15} = 24.361723,
E_{16} = -20.736547.

Gibb's excess free energy (G^E) can also be evaluated using reference (El-Sayed and Tribus, 1986):

$$G^E = R_m\, T\, y\, (1\text{-}y)\, [A+B\,(2y\text{-}1)] \quad (17)$$

where

$$A = (a_1 + a_2P) + \frac{(a_3+a_4P)}{T} + \frac{(a_5+a_6P^2)}{T^2} \quad (18)$$

$$B = (a_7 + a_8P) + \frac{(a_9+a_{10}P)}{T} \quad (19)$$

Values of the constants in equations (18) and (19) are given below:

a_1 = 18.1901,
a_2 = -0.121603,
a_3 = -99.5037,
a_4 = 0.67809,
a_5 = 84.4263,
a_6 = -1.02601,
a_7 = 2.43329,
a_8 = 0.026458,
a_9 = -1.28324,
a_{10} = -0.106125,

where P is expressed in MPa and T is the reduced temperature, T(K)/100 using 100 K as the reference temperature.

Thus, there are three equations namely, equations (15), (16) and (17) which may be used for calculating G^E. Equation (15) is not usable because of inadequate information. Equation (16) was tried but it could give values closer to Goswami and Feng (1999) only when the concentration (x) was changed from mass to molar, i.e. to y. Equation (17) also did not give the satisfactory results unless T, was changed from reduced value to base value, T_B. Incorporating the proposed corrections in equations (16) and (17), and comparing the predicted values of enthalpies, modified equation (17) gives the results closer to those in reference (Goswami and Feng, 1999). So it was used in the present work. For

completeness, it is rewritten as:

$$G^E = R_m T_B y (1-y) [A+B (2y-1)] \quad (20)$$

where A and B are the same as given in equations (18) and (19).

2. Calculation of mass flow rates

The conservation equations for mixture mass and ammonia concentration in the mixture for absorber may be written as:

$$m_9 = m_1 - m_{12},$$

and

$$m_1x_1=m_{12}x_{12}+m_9x_9$$

which lead to

$$m_{12} = m_1 \frac{x_1-x_9}{x_{12}-x_9} \quad (21)$$

Similarly, for condenser/rectifier

$$m_5 = m_6 \frac{x_6-x_4}{x_4-x_5} \quad (22)$$

$$m_4 = m_6 + m_5 \quad (23)$$

while the constant mass flow rates are obtained at stations (1, 2 and 3) and (6, 7, 8 and 9) i.e.

$$m_1 = m_2 = m_3$$

and

$$m_9 = m_3 = m_7 = m_6$$

where m is the mass flow rate of the mixture with a suffix denoting the station number.

Overall thermal efficiency is calculated as follows:

$$\eta = \frac{w_n+q_c}{q_s+q_b} \quad (24)$$

where
The net work output,

$$w_n = m_7 (h_7 - h_8) - m_1(h_2-h_1) \quad (25)$$

The refrigeration output

$$q_c = m_8 (h_9 - h_8) \quad (26)$$

The superheat input

$$q_s = m_6 (h_7 - h_6) \quad (27)$$

The boiler heat transfer

$$q_b = m_4h_4 + m_{10}h_{10} - m_3h_3 - m_5h_5 \quad (28)$$

where the suffixes of enthalpy and mass flow rate denote the station numbers as given in Figure 2.

3. Results and discussions

Dew point temperature and boiling point temperature

The variations of the dew- point temperature (T_d) and boiling-point temperature (T_b), with mixture concentration (x) were calculated at pressure 34.47

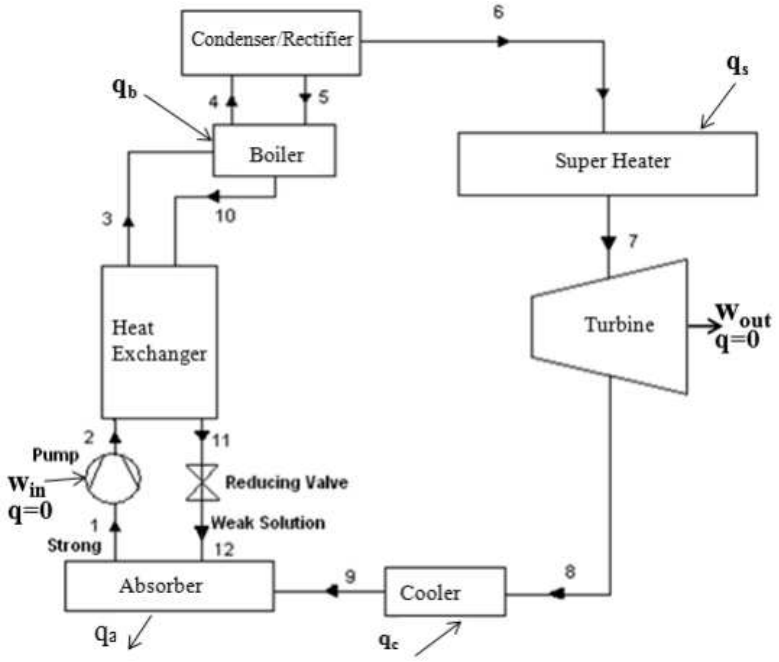

Figure 2: Schematic of the combined Kalina and aapour-absorption cycle

bar from equations A-1 and A-2, respectively and have been shown plotted in Figure 3a.

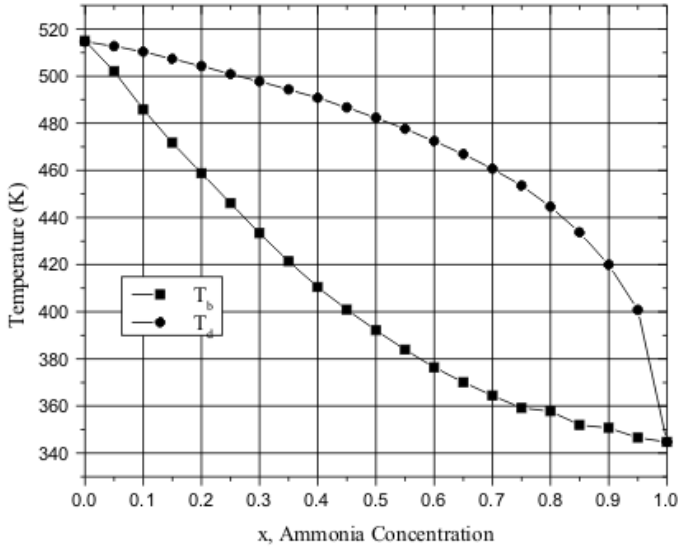

Figure 3a: T_d – T_b curve at p=34.47 bar using equations A-1 and A-2

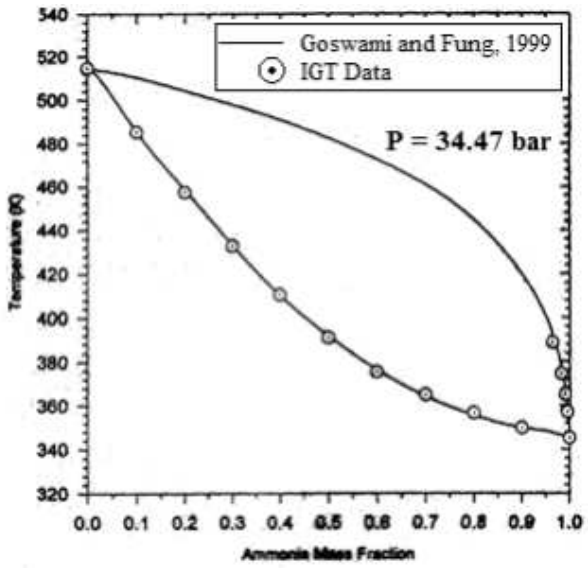

Figure 3b: Boiling- and dew- point temperatures at pressure 34.47 bar as given in two published references

In Figure 3b, T_d and T_b variations using the IGT (Institute of Gas Turbine) data is given by circled points and the continuous curves pertain to reference (Goswami and Feng, 1999), as explained in the insert. From Figures 3a and 3b, it is observed that the nature of curves from this work is similar to both of the IGT data and from above mentioned reference.

In an effort to have a further verification, the boiling point and dew point temperature, calculated from the methodology at low pressure of 2.067533 bar (30 psi) and other at high pressure of 20.67533 bar (300 psi) are shown in Figures 4, 5, 6 and 7 and compared with the reference (Bogart, 1981). It is observed from these figures that the predicted boiling point temperature and dew point temperature values, at both the typical high and low pressures deviate within ±1%. So the methodology adopted to predict dew point temperature and boiling point temperature gives fairly accurate results.

Besides this, the boiling point temperature and dew point temperature for various concentrations have been obtained for the entire concentration range from 0 to 1 for typical high and low pressure values that is 30 bar and 2 bar. This has been plotted in Figures 8 and 9. From these figures, it is found that the calculated boiling point temperature variation for concentration of ammonia beyond 0.8 at a very low pressure (<10 bar) do not join smoothly with the curves which join points for x<0.8. Such condition i.e. x<0.8 does not occur in the cycle, as discussed below,

With reference to Figure 2, low pressure exists in the cycle in cooler and absorber i.e. stations 8, 9, 1 and 12. At entrance to the cooler, though the ammonia concentration is quite high (>99%), it is a mixture of saturated liquid and saturated vapour in equilibrium, the saturated liquid concentration becomes much lower than 0.8. At exit from the cooler, mixture temperature increases and exceeds the dew-point temperature so liquid phase is no longer there.

It is absorbed by the weak solution coming from boiler (station 12) via the heat exchanger and reducing valve. So the mixture leaving absorber, this ammonia vapour of high concentration (station 1) reaches in the vicinity of boiling point temperature, yet the concentration is much less than 0.8 due to absorption of ammonia by weak aqua ammonia solution.

Having verified the application of the equations A-1 and A-2 for T_b and T_d, respectively, next to be considered is the enthalpy needed for the analysis of the cycle. At dew- and boiling-point temperatures, the predicted values of enthalpies calculated in this paper are tabulated in Tables 1 and 2 at two typical pressure values 30 psi (2.06753 bar) and 300 psi (20.6753 bar), respectively, because enthalpy values are available at these pressures in reference([Bogart, 1981) for the purpose of comparison.

In these tables, enthalpies within small parentheses are the values predicted using relevant equations, having prefix * represent the values from reference (Bogart, 1981), while those with prefix ** denote % enthalpy deviation from reference (Bogart, 1981).

These tables reveal that:

a. At high pressures, saturated liquid enthalpy values at boiling point temperature, h deviate by maximum 2.28% and saturated vapour enthalpy at dew point temperature, H deviate by a maximum of 1.54%.

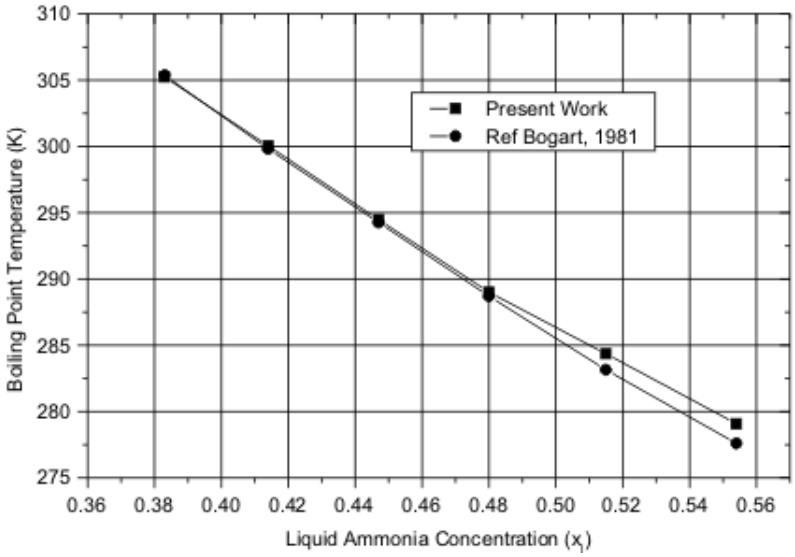

Figure 4: Variation of boiling point temperature with liquid ammonia concentration at a typical low pressure (p = 2.067533 bar, i.e. 30 psi)

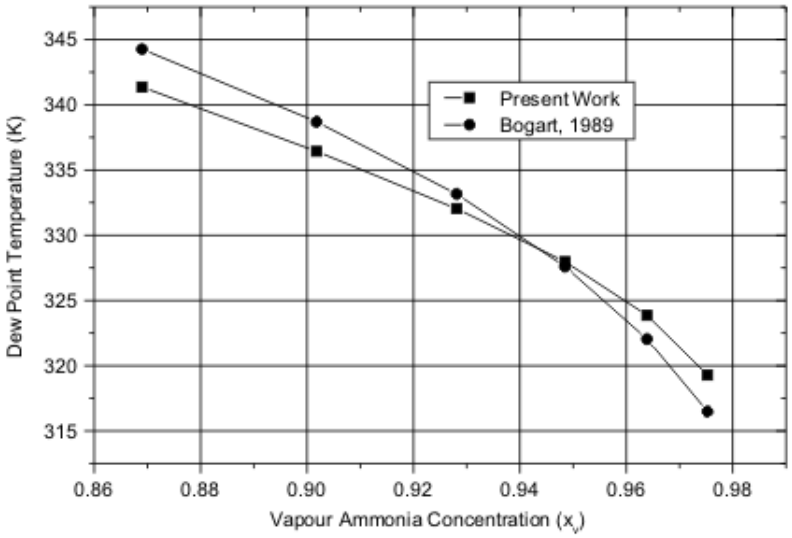

Figure 5: Variation of Dew point temperatures with vapour ammonia concentration at a typical low pressure (p = 2.067533 bar)

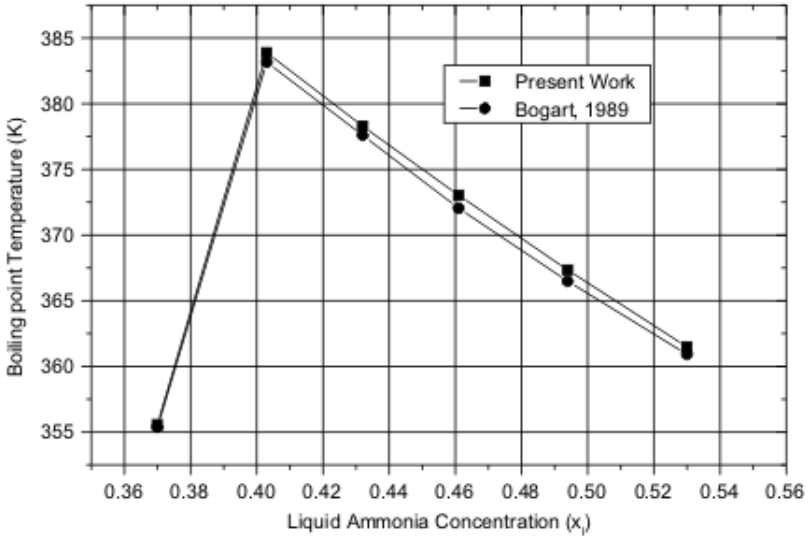

Figure 6: Variation of boiling point temperatures with liquid ammonia concentration at a typical high pressure (p = 20.67533bar)

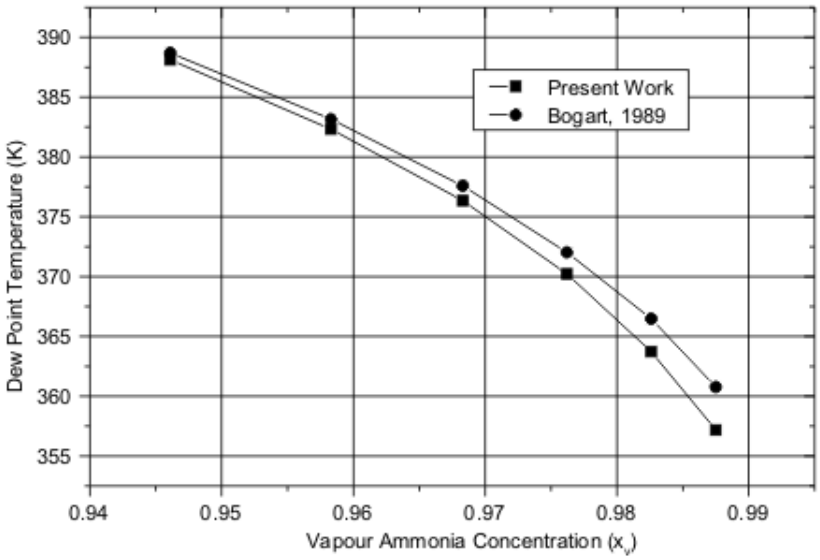

Figure 7: Variation of Dew-point temperature with liquid ammonia concentration at a typical high pressure (p = 20.67533bar)

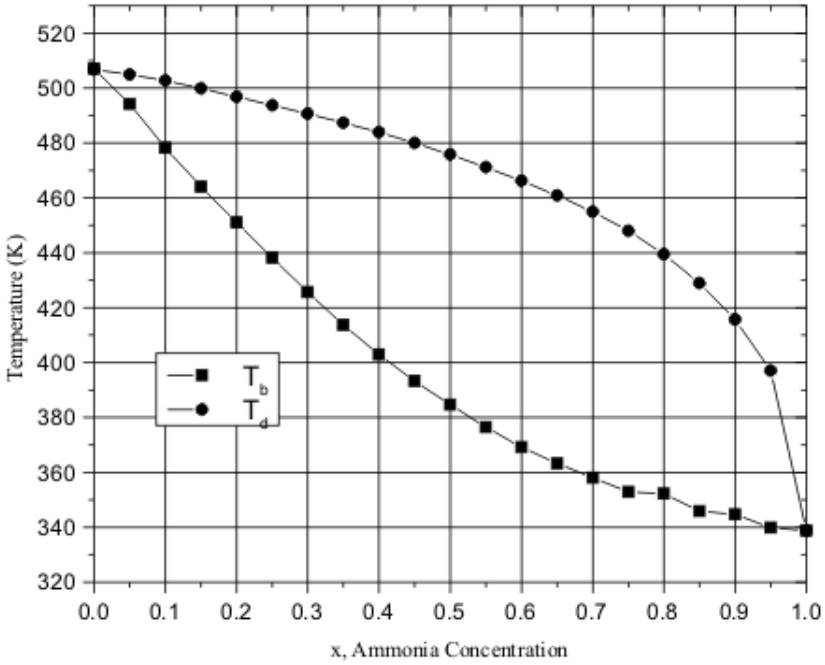

Figure 8: $T_d - T_b$ curves for p = 30 bar

b. The saturated vapour enthalpy for low pressure at dew point temperature, H deviate from reference (Bogart, 1981), by a maximum of 0.41% but at boiling point temperature saturated liquid enthalpy, h deviate more, by a maximum of 6.6%. The high value deviations are seen at temperature greater than 300 K.

With reference to the values of enthalpies at stations 2 and 11, where the ammonia exists as a subcooled liquid, have been compared with (Goswami and Feng, 1999). Percentage deviations calculated as mixture predicted by equation (20) is reasonably close (< 8%) to the one obtained in reference (Goswami and Feng, 1999). Having arrived at final equations, software was developed for calculating enthalpies at various mixture conditions.

Enthalpies are now compared with those given in (Goswami and Feng, 1999) for the values of pressure, temperature and concentration taken therein. The comparison is given in Table 3. The computed values of the enthalpies are compared with those tabulated in reference (Goswami and Feng, 1999) for the same typical operating conditions. The percentage deviations defined by

$$\left[\frac{h_{predicted} - h_{[Goswami\ and\ Feng,1999]}}{h_{[Goswami\ and\ Feng,1999]}}\right] \times 100$$

are within 4% at all stations except 11 and 12. The value of enthalpy deviates by 7.9% at station 11

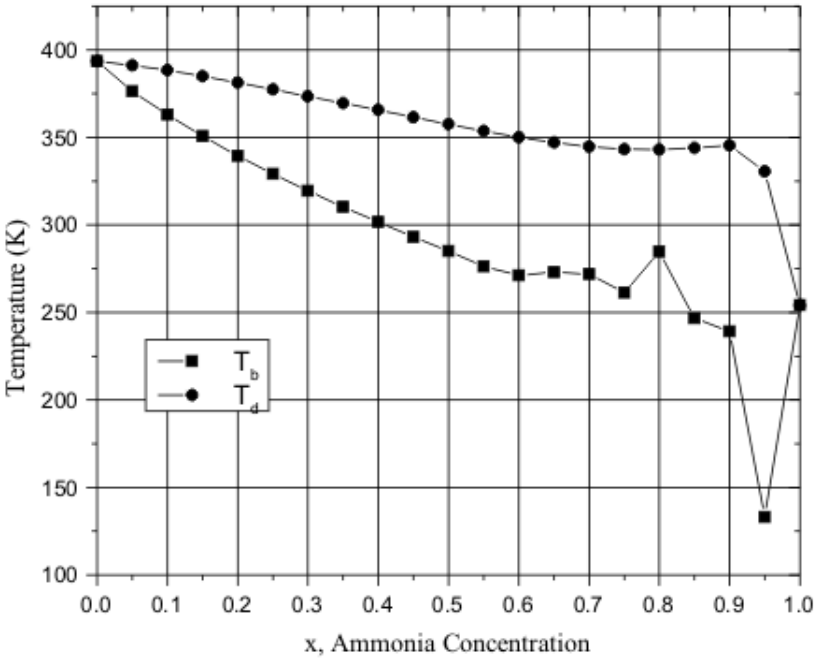

Figure 9: T_d – T_b curves for p = 2 bar

Table 1: Saturated liquid and saturated vapour enthalpies of the mixture at selected temperatures at typical low pressure (p = 2.06753 bar)

Temp. (K)	277.59	283.15	288.7	294.26	299.81	305.37
x_l	0.554	0.515	0.48	0.447	0.414	0.383
x_v	0.999378	0.99878	0.99777	0.9961	0.99345	0.9894
Saturated liquid enthalpy at T_b, h(kJ/kg)	(-230.0) *-224.23 **2.57%	(-209.65) 206.54 -1.5%	(-185.4) -185.15 -0.13%	(-158.11) -161.42 2.05%	(-128.09) -133.745 4.22%	(-95.81) -102.57 6.59%
Saturated vapour enthalpy at T_d, H(kJ/kg)	(1293.34) *-224.23 **0.36%	(1306.69) 206.54 0.41%	(1320.37) -185.15 0.41%	(1334.78) -161.42 0.36%	(1350.25) -133.745 0.36%	(1367.34) -102.57 0.26%

Table 2: Saturated liquid and saturated vapour enthalpies of the mixture at selected temperatures at typical high pressure (p = 20.67533 bar)

Temp. (K)	360.92	366.48	372	377.59	383.15
x_l	0.53	0.494	0.461	0.432	0.403
x_v	0.9875	0.9826	0.9762	0.9683	0.9583
Saturated liquid enthalpy at T_b, h(kJ/kg)	(161.93) *162.58 **-1.01%	(188.715) 186.31 1.28%	(214.6) 209.80 2.28%	(237.73) 237.25 0.2%	(267.7) 265.16 0.95%
Saturated vapour enthalpy at T_d, H(kJ/kg)	(1419.66) *1408.62 **0.78%	(1442.9) 1426.30 1.16%	(1465) 1446.30 1.29%	(1489.06) 1467.24 1.48%	(1515.23) 1492.13 1.54%

and by 15.5% at station 12. It means that the constants in the equations for determining enthalpy of the mixture still need revision where the mixture was weak in ammonia and it is at a temperature in the near vicinity of or much below the saturation temperature of ammonia at the concerned pressure.

4. Conclusions

Equations have been reviewed for calculating boiling point and dew point temperatures for the given mixture pressure and concentration and in turn the mixture enthalpy at various mixture states. After establishing the condition of the mixture from mixture temperature and boiling- and dew-point temperature, the procedure calculates the mixture enthalpy at the salient stations of a combined power and cooling cycle. The enthalpy values, so predicted are found close to those reported in the reference

Table 3: Result of the present work

Station no. (z)	*Mixture state no. (s)*	*T (K)*	*P (bar)*	*Ammonia mass fraction (x)*	*m*	*h (kJ/kg) enthalpy from Goswami & Feng (1999)*	*h (kJ/kg) enthalpy from present work*	*% deviation of enthalpies*	T_d *(K)*	T_{sat2} *(K)*	T_b *(K)*	T_{sat1} *(K)*
1	5	280	2	0.5300	1.00	-214.1	-210.36	3.74	371	393	280	254
2	7	280	30	0.5300	1.00	-211.4	-205.49	2.79	473	507	380	339
3	5	378	30	0.5300	1.00	246.3	258.04	2.65	473	507	380	339
4	3	400	30	0.9432	0.2363	1547.52	1547.15	0.003	400	507	346	339
5	5	360	30	0.6763	0.0366	205.8	206.15	0.17	458	507	360	339
6	2	360	30	0.9921	0.1997	1373.2	1368.51	-0.34	348	507	340	339
7	2	410	30	0.9921	0.1997	1529.7	1530.93	0.0008	348	507	340	339
8	4	257	2	0.9921	0.1997	1148.9	1194.87	4.00	266	393	255	254
9	2	280	2	0.9921	0.1997	1278.7	1308.24	2.31	266	393	255	254
10	5	400	30	0.4147	0.8003	348.2	348.33	0.037	483	507	400	339
11	7	300	30	0.4147	0.8003	-119.0	-109.55	7.94	483	507	400	339
12	5	300	2	0.4147	0.8003	-104.5	-120.70	-15.5	378	393	299	254

(Goswami and Feng, 1999), except at station numbers 11 and 12, where the mixture was weak in ammonia and it is at a temperature in the near vicinity of or much below the saturation temperature of pure ammonia at the concerned pressure. The deviations are 7.9% and 15.5%, respectively. This would require revision of the constants used for evaluating enthalpies under the said conditions. Thermal efficiency of the combined cycle is found reasonably accurate (20.68% against the published values of 23.54%). The efficiency is calculated from turbine work, pump work, superheater heat input and refrigeration/cooling effect. The latter are the functions of mass flow rates and enthalpies at the characteristic stations of the cycle. The mass flow rates, if not known, can be obtained from the mass and concentration conservation equations. Thus, the software is capable of predicting the performance of a combined power and cooling cycle, satisfactorily.

Acknowledgement

We are very thankful to Dr D. Yogi Goswami, Department of Mechanical Engineering, University of Florida, Gainesville, FL 32611, USA, for supporting us. He has sent us a number of research papers regarding the topic, without whose cooperation this paper could have not been produced.

Appendix A

$$T_b = T_c - \sum_{i=0}^{6}\left(c_i + \sum_{j=0}^{9} C_{ij}\, x^j\right)\left[\ln\left(\frac{P_c}{P}\right)\right]^i \quad \text{(A-1)}$$

$$T_d = T_c - \sum_{i=0}^{5} f_i + \sum_{j=0}^{3} n_{ij}[\ln(1.0001 - x)]^j\left[\ln\left(\frac{P_c}{P}\right)\right]^i \quad \text{(A-2)}$$

Where

$$T_c = T_{cw} - \sum_{i=0}^{3} a_i x^i \quad \text{(A-3)}$$

$$P_c = P_{cw}\exp\left(\sum_{i=0}^{7} b_i x^i\right) \quad \text{(A-4)}$$

It may be noted that P is in psia and T in ^{0}F for equations A-1 through A-4. The values of constants are listed below.

c[0] = 153.634521459,
c[1] = -13.0305543892,
c[2] = -1.14845282991,
c[3] = 0.550358094447,
c[4] = -.0753450148427,
c[5] = 0.0048111666267,
c[6] = -0.000120433757177,
a[0] = 205.8889,
a[1] = 280.930556,
a[2] = -317.0138889,
a[3] = 263.194444,
b[0] = 0.368105523897,
b[1] = -3.6679548875,
b[2] = 46.6000470809,
b[3] = -262.921061996,
b[4] = 732.99536936,
b[5] = -1076.0613489,
b[6] = 797.948078048,

b[7] = -235.903904222,
C[0][0] = -462.460321366,
C[0][1] = 2373909986309,
C[0][2] = -194504.35292,
C[0][3] = 639383.528867,
C[0][4] = -523748.057636,
C[0][5] = -2328271.47551,
C[0][6] = 7562418.53499,
C[0][7] = -9668295.89504,
C[0][8] = 5922081.87086,
C[0][9] = -1432405.52125,
C[1][0] = 421.443122208,
C[1][1] = -14560.354925,
C[1][2] = 53051.4495633,
C[1][3] = 382763.793582,
C[1][4] = -583589.86875,
C[1][5] = 12243265.3815,
C[1][6] = -22307970.0156,
C[1][7] = 22896656.8499,
C[1][8] = -12483324.8091,
C[1][9] = 2813311.71633,
C[2][0] = -248.783804168,
C[2][1] = 4807.07241098,
C[2][2] = 13565.1003309.
C[2][3] = -466407.780832,
C[2][4] = 2827083.44764,
C[2][5] = -8469715.15799,
C[2][6] = 14459588.8962,
C[2][7] = -14281087.5331,
C[2][8] = 7596403.59678,
C[2][9] = -1684002.64482,
C[3][0] = 126.965580728,
C[3][1] = -2090.45270574,
C[3][2] = 1993.17101166,
C[3][3] = 100706.510396,
C[3][4] = -687388.808612,
C[3][5] = 2132412.46959,
C[3][6] = -3699199.65914,
C[3][7] = 3688365.22546,
C[3][8] = -1975122.39296,
C[3][9] = 440201.446068,
C[4][0] = -33.5343446156,
C[4][1] = 601.878586689,
C[4][2] = -3064.82070658,
C[4][3] = 71.7954752052,
C[4][4] = 51780.666659,
C[4][5] = -209714.899856,
C[4][6] = 405011.985355,
C[4][7] = -428310.461566,
C[4][8] = 238153.698326,
C[4][9] = -54497.0973336,
C[5][0] = 3.97454953787,
C[5][1] = -77.026846469,
C[5][2] = 541.19105807,
C[5][3] = -1696.60270972,
C[5][4] = 1713.45942707,
C[5][5] = 4019.01019872,
C[5][6] = -14844.7928004,
C[5][7] = 19481.0094551,
C[5][8] = -12107.0794501,
C[5][9] = 2966.92804386,
C[6][0] = -0.170806170177,
C[6][1] = 3.48182859299,
C[6][2] = -27.7957587743,
C[6][3] = 113.762064546,
C[6][4] = -258.750496922,
C[6][5] = 311.002585218,
C[6][6] = -123.917993454,
C[6][7] = -123.480627492,
C[6][8] = 154.375042114,
C[6][9] = -48.5083828701,
f[0] = 153.17055346,
f[1] = -11.7705687461,
f[2] = -1.78126355957,
f[3] = 0.647385455059,
f[4] = -0.0719950751898,
f[5] = 0.00285423950786,
n[0][0] = 194.793913463,
n[0][1] = 74.236124188,
n[0][2] = 9.84103819552,
n[0][3] = 0.436843852745,
n[1][0] = -74.3508283362,
n[1][1] = -3.2941879809,
n[1][2] = -4.78866918581,
n[1][3] = -0.225416733476,
n[2][0] = 13.0175447367,
n[2][1] = 6.1586564117,
n[2][2] = 0.789740337141,
n[2][3] = 0.0321510834958,
n[3][0] = -0.90857587517,
n[3][1] = -0.356752691147,
n[3][2] = 0.0238067275502,
n[3][3] = 0.00495593933952,
n[4][0] = -0.00071863574153,
n[4][1] = -0.0251026383533,
n[4][2] = -0.0191664613304,
n[4][3] = -0.0017014253867,
n[5][0] = 0.00195441702983,
n[5][1] = 0.00280533348937,
n[5][2] = 0.0013899436563,
n[5][3] = 0.000116422611616.

Saturation temperature (T_{sat}) of pure components is given by:

$$T_{sat} = \frac{b}{a - \ln P} + c$$

where P and T_{sat} are in bar and K, respectively. Values of the constants, with subscript 1 for pure ammonia and 2 for pure water, are listed below:

a_1 = 10.77584068,
a_2 = 11.73544221,
b_2 = 3861.6302,
b_1 = 2324.262496,
c_1 = 23.624144,
c_2 = 43.66924.

References

Ballaney P. L., (2002). Refrigeration and Air Conditioning, Delhi: Khanna Publishers.

Bogart M., (1981). Ammonia Absorption refrigeration in Industrial Process, Houston: Gulf Publishing Company.

El-Sayed Y. M. and Tribus, M. (1986). Thermodynamic Properties of Water Ammonia Mixture: Theoretical Implementation for Use in Power Cycle Analysis, ASME Special Publication; AES (1): p. 89-95.

Feng Xu. and Goswami D. Y. (1999). Thermodynamic Properties of Ammonia-Water Mixtures for Power Cycle Applications, *Energy* (24) 525-536.

Goswami D. Yogi and Feng Xu (1999). Analysis of a New Thermodynamic Cycle for Combined Power and Cooling Using Low and Mid Temperature Solar Collectors, ASME *Journal of Solar Energy Engineering* May 1999; (121): 91-97.

Ibrahim O. M. and Klein, S. A. (1993). "Thermodynamics Properties of Ammonia Water Mixture", ASHRAE Trans Symposia, pp 1495-1502.

Kalina A. I. (1984). Combined Cycle System with Novel Bottoming Cycle, ASME *Journal of Engineering for gas turbines and power* 1984; (106): 737-742.

Kalina A. I. and Tribus, A. M. (1990a). Advances in Kalina cycle technology Part 1 Development of a practical cycle Energy for the Transaction age, Proceedings of the Florence World Energy Research Symposium, Firenze, Italy, Vol. 97,1990a. pp 111-124.

Kalina A. I. *et al.,* (1986). A Theoretical Approach to the Thermophysical Properties of Two Miscible Component Mixture for the Purpose of power Cycle Analysis, Dec. 7-12, 1986 ASME winter annual meeting, Anaheim, California. (86). Exergy Incorporation Houston, Texas: WA/HT-54. p. 1-8.

Koremenos D. A. *et al.,*. Cogeneration with Combined Aqua Ammonia Absorption Cycle, Thermodynamic and the Design, Analysis and Improvement of Energy Systems, R. J. Drane Ed., AES Vol. 33, pp 231-238.

Maloney J. D. and Robertson R. C., (1953). Thermodynamic Study of Ammonia-Water Heat Power Cycles, ORNL Report CF-53-8-43, Oak Ridge, TN.

Maskara P. N. and Satish Chand, (1987). Tables and Charts on Refrigerants & Psychometric Properties, Allahabad: Technical Publishers of India.

Moran J. M. and Howard N. S. (2000). Fundamentals of Engineering Thermodynamics", Singapore: 4th Edition John Wiley & Sons (ASIA) Pvt. Ltd..

Park Y. M. and Sonntag, R. E. (1990). "Thermodynamic Properties of Ammonia Water Mixture: A Generalized Equation of State Approach", Vol. 97, *ASHRAE Transactions*, .p. 150-159.

Rogdakis E. D. and Antonopoulos K. A. (1991). A High Efficiency NH_3-H_2O Absorption Power Cycle, Heat Recovery System 1991; (II): 263-275.

Siddiqui Altamash M. Analysis of Some Simple and Advanced Absorption Cycle, M. Tech. thesis submitted to Department of Mechanical Engineering, India: I.I.T. Kanpur Mechanical Engineering Department.

Tariq M. (2003). Computer Simulation of the Combined Cycle for Power and Cooling, M. Tech. Thesis submitted to India: M.N.N.I.T. Allahabad, Mechanical Engineering Department.

Washam B. *et al., (*1994). Integrated Solar Combined Cycle Systems (ISCS) Utilising Solar Parabolic through Technology-Golden Opportunities for the 90's. Presented at the 1994 Annual Meeting of the American Solar Energy Society, Paper available from Spencer Management Associates, Diablo, California: 1994.

Yadav R. (2001). Thermodynamics and Heat Engines", Allahabad: Central Publishing House.

Zeigler B. and Trepp C. (1984). Equation of State for Ammonia-water Mixtures, *Refrigeration* 7(2):101-106.

Received 29 April 2013; revised 9 January 2015

A comparative study of the stochastic models and harmonically coupled stochastic models in the analysis and forecasting of solar radiation data

Edmore Ranganai
Department of Statistics, University of South Africa, Florida Campus, South Africa

Mphiliseni B Nzuza
School of Mathematics, University of Zululand, KwaDlangezwa, South Africa

Abstract
Extra-terrestrially, there is no stochasticity in the solar irradiance, hence deterministic models are often used to model this data. At ground level, the Box-Jenkins Seasonal/Non-seasonal Autoregressive Integrated Moving Average (S/ARIMA) short memory stochastic models have been used to model such data with some degree of success. This success is attributable to its ability to capture the stochastic component of the irradiance series due to the effects of the ever-changing atmospheric conditions. However, irradiance data recorded at the earth's surface is rarely entirely stochastic but a mixture of both deterministic and stochastic components. One plausible modelling procedure is to couple sinusoidal predictors at determined harmonic (Fourier) frequencies to capture the inherent periodicities (seasonalities) due to the diurnal cycle, with SARIMA models capturing the stochastic components. We construct such models which we term, harmonically coupled SARIMA (HCSARIMA) models and use them to empirically model the global horizontal irradiance (GHI) recorded at the earth's surface. Comparison of the two classes of models shows that HCSARIMA models generally out-compete SARIMA models in the forecasting arena.

Keywords: irradiance, Box-Jenkins methodology, harmonic, periodogram, forecasting

1. Introduction

Sunshine levels, incident on a photovoltaic (PV) panel have the overriding influence on electrical output. This output is affected by the unpredictability of the prevailing whether conditions, which in turn, leads to the fluctuating nature of the solar resource. Hence, its efficient use requires reliable forecast information of its availability in various time and spatial scales depending on the application. Forecasts are critically important for use in monitoring solar systems, energy system sizing and optimization and utility applications. Utilities and independent system operators use forecasting information to manage generation and distribution. Therefore, appropriate solar data modelling and reliable forecasting of solar radiation is essential for the design, performance prediction and monitoring of solar energy conversion systems. One class of models used successfully in the literature to achieve this are the short memory Box-Jenkins Seasonal/Non-Seasonal Autoregressive Integrated Moving Average (S/ARIMA) stochastic models (Craggs *et al.,* 1999; Zaharim *et al.,* 2009; Voyant *et al.,* 2013a).

In the forecasting domain, literature shows that S/ARIMA models out-competed many competing models. Pedro and Coimbra (2012) found that the improvement in 2-hours ahead forecasting using the ARIMA model with respect to the persistent model as measured by the decrease in Root Mean Squared Error (RMSE) was comparable to that of Artificial Neural Networks (ANN), i.e., 10.3% and 11.3% respectively. Reikard (2009) compared the S/ARIMA model to five other forecasting techniques in predicting high resolution data and found the SARIMA models to give the best results in four out of six test stations in the study. Actually, in the literature S/ARIMA and ANN models are considered to be the most preferred prediction methods (Alados *et*

al., 2007; Altandombayci and Golcu, 2009; Balestrassi *et al*., 2009).

Extra-terrestrially, there is no stochasticity in the solar irradiance, hence, deterministic models are often used to model this data. At ground level, the success of SARIMA models is attributed to their ability to capture the stochastic component of the irradiance series due to the effects of the ever-changing atmospheric conditions. However, such irradiance data recorded at the earth's surface is rarely entirely stochastic as weather phenomena cause varying degrees of stochasticity and deterministic components in solar irradiance. One plausible modelling procedure is to couple sinusoidal predictors at determined harmonic (Fourier) frequencies to capture the inherent periodicities (seasonalities) due to the diurnal cycle with SARIMA models capturing the stochastic components. To model this unpredictable mixture, Badescu *et al.* (2008) used a sinusoidal predictor to model seasonality and then represented the resulting standardized residuals by an ARMA model. However, this approach is limiting. We therefore generalize this approach by combining a sinusoidal predictor(s) to model major seasonalities and then fitting SARIMA models to the resulting residuals. We term this class of models Harmonically Coupled SARIMA (HCSARIMA) models. Another motivation for the proposal of HCSARIMA models is that ARMA models give unacceptable errors for distant horizon forecasting such as for more than 2 hours in the hourly case and 2 days in the daily case (Voyant *et al.,* 2013b). In order to minimize the forecast errors for a longer horizon, i.e., 2 cycles-ahead (28 and 24 hours in the case hourly data; 168 and 132 10-minutely intervals for 10-minutely data (see Table 1)), in the SARIMA models we include seasonal parameters to model seasonality while in HCSARIMA models the major seasonalities are modelled by sinusoidal components. By modelling the seasonality in this way, distant horizon forecasts of up to 24 hours or more essential for power dispatching plans, optimization of grid-connected PV plants and coordination control of energy storage devices (Wang *et al.,* 2012) will be valid as seasonal models are able to capture the entire seasonal swing.

We undertake a comparative study of these two classes of models viz., SARIMA versus HCSARIMA in modelling and forecasting the horizontal solar irradiance (GHI) (comprising of both direct normal irradiance (DNI) and diffuse horizontal irradiance (DHI)) data series recorded at the University of KwaZulu-Natal (UKZN) Howard College (HC) campus (Durban, South Africa) Faculty of Engineering's recently established (February, 2010) radiometric broadband ground station. This station is located at 29.9° South, 30.98° East with elevation, 151.3m. Measurements recorded were obtained from the Greater Durban Radiometric Network (GRADRAD) database (www.gradrad.ukzn.ac.za). A shadow band type Precision Spectral Pyranometer (Model PSP) is used to obtain the three irradiances. The DHI obtained by blocking the direct solar beam must be corrected for additional sky band blockage; hence the DNI obtained by subtraction from GHI is less accurate than that obtained from Pyrheliometers. Therefore, we study the more accurate GHI.

Although most of the studies in the literature used a calendar year's historical data series (Zalwilska and Brooks, 2011) to learn repeatable patterns that may be inherent in the series, in some instances it is also useful to use a shorter historical data series to learn strongly fluctuating patterns that may be inherent in a shorter period such as a season, month or less (Craggs *et al.,* 1999; Yona *et al.,* 2013). We follow the later approach and make use of the February (summer) and July (winter) 2011 data series. The data series are in two time scales, viz., hourly and 10-minutely which we adjudged to provide a fair compromise between the now-casting solar irradiance problem on very short time intervals (15 seconds to 30 minutes) and one day ahead forecasts crucial for controlling a PV plant operation (Paulescu *et al.,* 2013).

In the next section, we give a brief overview of SARIMA models. In Section 3 we elaborate on the periodogram as well as its use in searching for periodicities in data series leading to the building of the HCSARIMA model. Model selection based on in-sample diagnostics and forecasting accuracy are given in Section 4, data series modelling is carried out in Section 5, model comparisons are carried in Section 6 and conclusions are given in the last section.

2. SARIMA Models

The generalized form of a multiplicative SARIMA model can be specified as

$$\Phi_P(L^S)\phi_p(L)(1-L^S)^D(1-L)^d X_t = \delta + \Theta_Q(L^S)\theta_q(L)Z_t \qquad (2.1)$$

(Cryer and Chan, 2008), where

$$\Phi_P(L^S) = 1 - \Phi_S L^S - \Phi_{2S}L^{2S} - \cdots - \Phi_{PS}L^{PS},$$

$$\phi_p(L) = 1 - \phi_1 L - \phi_2 L^2 L - \cdots - \phi_p L^p,$$

$$\Theta_Q(L^S) = 1 - \Theta_S L^S - \Theta_{2S}L^{2S} - \cdots - \Theta_{QS}L^{QS},$$

$$\theta_q(L) = 1 - \theta_1 L - \theta_2 L^2 L - \cdots - \theta_q L^q,$$

are the seasonal AR, non-seasonal AR, seasonal MA and non-seasonal MA factors, respectively, the constant δ coincides with the mean of the series and S is the seasonality. The operator, L is the backward shift operator such that $L^k X_t = X_{t-k}$, d

and D are the non-seasonal and seasonal order differences, respectively, taking positive integer values. For instance, $(1-L)^d X_t = \Delta^d X_t = X_t - X_{t-1}$ and $(1-L^S)^D X_t = \Delta_S^D X_t = X_t - X_{t-S}$ for $d = D = 1$. The powers PS, p, QS and q denote the seasonal AR, non-seasonal AR, seasonal MA and non-seasonal MA orders, respectively. It is assumed that Z_t is white noise, i.e., $Z_t \sim N(0, \sigma_Z^2)$. This model in (2.1) is usually abbreviated as $SARIMA(p,d,q) \times (P,D,Q)_S$. Note that the seasonal and non-seasonal AR and MA factors in (2.1) may be additive.

To build SARIMA models via the Box-Jenkins methodology (Box and Jenkins, 1976), time domain techniques are made use of. On the other hand, to build HCSARIMA models spectral methods (periodogram analysis) are used to determine the inherent periodicities in the data series.

3. The periodogram

Frequency Domain techniques are used to search for periodicities in data. The standard tool to carry out such an analysis is called the spectrum, which is a Fourier transform of the autocorrelation function (ACF). In practice, the sample estimator of the spectrum, the periodogram first introduced by Schuster (1898), is used to determine periodicities in data. An efficient way to compute the periodogram is to make use of the Fast Fourier transform (FFT) (Chatfield, 2003). For a realization of a time series, $\{X_t\}_1^n$, the periodogram is defined as:

$$I(\omega_p) = \frac{1}{\pi n}\left|\sum_{t=1}^{n} X_t e^{it\omega_p}\right|^2 = \frac{1}{n\pi}\left|\tilde{X}(\omega_k)\right|^2, \quad (3.1)$$

where $\omega_p = \frac{2\pi p}{n}$, $p = 1,\ldots,[n/2]$ are harmonic frequencies, $\tilde{X}(\omega_p) \equiv \sum_{t=1}^{n} X_t e^{-it\omega_p}$ is the FFT and $[.]$ denotes the integer part. Using the well-known result from the analysis of variance (ANOVA), the total sum of squares (SST) of the series can be partitioned into sum of the error terms (SSE) plus sum of squares due to a periodic component ($I(\omega_p)$), viz.,

$$\sum_{t=1}^{n}(X_t - \bar{X})^2 = SSE + Sum\ of\ squares\ due\ to\ periodic\ component\ at\ \omega_p \quad (3.2)$$

Dividing (3.2) by n throughout clearly, a large contribution of the sum of squares due to the periodic component to SST implies a large contribution to the variance of the series by $I(\omega_p)$ (Chatfield, 2003: 127). If this is the case, then much of the variability in the data series is attributable to the periodic component.

3.1 Searching for periodicities and construction of the HCSARIMA model

Suppose that a time series is dominated by a periodic sinusoidal component with a known wavelength. Then the natural model is:

$$X_t = \mu_t + R\cos(\omega_p t + \phi) + Z_t, \quad (3.3)$$

where ω_p is the frequency of the sinusoidal variation, R is the amplitude of the variation, ϕ is the phase and $\{Z_t\}$ as in (2.1). Equivalently, (3.3) can be expressed as:

$$X_t = \alpha\cos\omega_p t + \beta\sin\omega_p t + Z_t, \quad (3.4)$$

where $\alpha = R\sin\phi$ and $\beta = R\cos\phi$ with $\mu_t = 0$. In practice, a series may contain multiplicities of periodicities and the generalized form of (3.4) becomes

$$X_t = \sum_{k=1}^{m}(\alpha_k\cos\omega_k t + \beta_k\sin\omega_k t) + Z_t. \quad (3.5)$$

Note that ω_k has to be a harmonic frequency since ordinary least squares and ML (under normality) estimators at different general frequencies ω_k and ω_j are not independent because the sine-cosine and complex exponential systems are complete and orthogonal only over Fourier frequencies.

For the model (3.5), if in a periodogram analysis, a particular intensity $I(\omega_g)$ is the largest one, we can test the hypothesis whether the parameters α and β are indeed zero, at this frequency *i.e.*

$$H_0: \alpha_g = \beta_g = 0 \quad vs \quad H_1: \beta_g \neq 0\ or\ \alpha_g \neq 0$$

by making use of The Fisher's Kappa statistic Fuller (1976).

To detect general departures from white noise, Bartlett's Kolmogorov-Smirnov statistic can be used. Also, the usual F-test can be used to test the significance of any periodogram ordinate of interest e.g. the 2nd largest say $I(\omega_h)$ (Wei, 2006:292). Now, the seasonality at significant periodogram ordinates $I(\omega_g)$ is modelled by equations (3.4) or (3.5). In practice $\{Z_t\}$ is rarely white noise such that it is described by a SARIMA model. The non-stationary residuals are denoted by $\{W_t\}$. Thus, combining (3.4) or (3.5) with a trend component, and (2.1) gives a HCSARIMA model, viz.,

$$X_t = \mu_t + \alpha\cos\omega_p t + \beta\sin\omega_p t + \Phi_P(L^S)\phi_p(L)(1-L^S)^D(1-L)^d W_t = \delta + \Theta_Q(L^S)\theta_q(L)Z_t. \quad (3.6)$$

If there are multiplicities of seasonalities in the data series (3.6) becomes

$$X_t = \mu_t + \sum_{k=1}^{m} (\alpha_k \cos \omega_k t + \beta_k \sin \omega_k t) + \Phi_P(L^S)\phi_p(L)(1-L^S)^D(1-L)^d W_t = \delta + \Theta_Q(L^S)\theta_q(L)Z_t. \quad (3.7)$$

where μ_t is the trend function which is dropped if nonsignificant.

4. Model selection criteria

Model selection criteria are two-fold, i.e., we make use of in-sample diagnostics as well model prediction accuracy measures.

4.1 In-sample diagnostics

The selection of the best SARIMA model was carried out using the principle of parsimony (select the model with the least number of parameters), high R-square value and two Information Criteria, viz., Akaike's information criterion (*AIC*) and the Schwarz's Bayesian criterion (*SBC*) (Akaike, 1983; Schwarz, 1978) also known as the Bayesian information criterion (*BIC*). The lower the values of these statistics the better the model is. The *SBC* is preferred over *AIC* since the *AIC* criterion overestimates the order of auto-regression (Wei, 2006).

4.2 Prediction accuracy

We make use of four common measures, viz., Mean Bias Error (MBE) in W/m^2, Mean Percentage Error (MPE), Mean Absolute Percentage Error (MAPE) and Root Mean Squared Error (RMSE) in W/m^2, in assessing the model out-of-sample two 2 days (cycles)-ahead forecast errors. The smaller the values of these measures the better the forecasts. The formulations of these forecasting measures are:

$$MBE = \frac{1}{n}\sum_{l=1}^{n} (\hat{Y}_t(l) - Y_{t+l}) \quad W/m^2, \quad (4.1)$$

$$MPE = \frac{100\%}{n}\sum_{l=1}^{n} \frac{\hat{Y}_t(l) - Y_{t+l}}{Y_{t+l}}, \quad (4.2)$$

$$MAPE = \frac{100\%}{n}\sum_{l=1}^{n} \left|\frac{\hat{Y}_t(l) - Y_{t+l}}{Y_{t+l}}\right|, \quad (4.3)$$

$$RMSE = \left\{\frac{1}{n}\sum_{l=1}^{n} (\hat{Y}_t(l) - Y_{t+l})^2\right\}^{1/2} \quad W/m^2, \quad (4.4)$$

where Y_{t+l} and $\hat{Y}_t(l)$ are the actual and forecasted l -steps ahead forecasted values, respectively.

5. Data modelling

All the data analysis is done using a statistical analysis system (SAS). The readings are taken instantaneously at 6 seconds intervals and then averaged minutely. We further average the minutely data in 60-minutely and 10-minutely. The details of the data series are presented in Table 1, along with their daily cycle lengths.

The February 60-minutely daily data spans from 0500 hours to 1800 hours and that for July spans from 0600 hours to 1700 hours, while the February 10-minutely daily data spans from 0500 hours to 1850 hours and that for July spans from 0630 hours to 1720 hours. Most of the missing values generally occur before around 0635 hours and after around 1725 hours for the July month. This explains the difference in the percentage of missing values between the hourly and 10-minutely July data series.

The February series from the 1st to the 13th and the July data series from the 3rd to the 9th were used for model building. The next 2 days data series was used for validation in each case. We adjudge these days to have the best data quality by making use of the following minutely data series profiles for each day of the February and July months given in Figure 1. These profiles can be obtained from http://gradrad.ukzn.ac.za .

We confirm the periodicities evident by means of time domain techniques such as time ACFs (Figure 2) as well as search for hidden ones using periodogram analysis in the next subsection.

5.1 Periodogram analysis

For brevity we only give results for the February 60-minutely series. In Figure 3, the periodogram is plotted against the harmonics, ω_p. Table 2 shows the Fisher's Kappa test and BKS test results. Lastly, the F-test results for the same data series are given in Table 3.

The largest intensity is at period 14, the second largest is at period 7 and the third largest is at period 4.667 corresponding to harmonics $\omega_{14} = 2\pi/14$, $\omega_7 = 2\pi/7$ $\omega_{4.6667} = 2\pi/4.667$, respectively. Fisher's Kappa results in Table 2 show the presence of a strong periodic component since the test statistic, 66.875, is greater than the critical value, 8.882 at the 1% level of significance while the BKS statistic has a p-value< 0.05 indicating that generally the series is not white noise, i.e., the presence of at least one periodic component. The strongest periodic component is further confirmed by the F-test (p-val-

Table 1: Data details

		60 min			*10 min*		
		Series length	*Cycle length*	*% missing*	*Series length*	*Cycle length*	*% missing*
Summer	February 2011	210	14	5.79	1260	84	5.79
Winter	July 2011	108	12	9.66	594	66	1.45

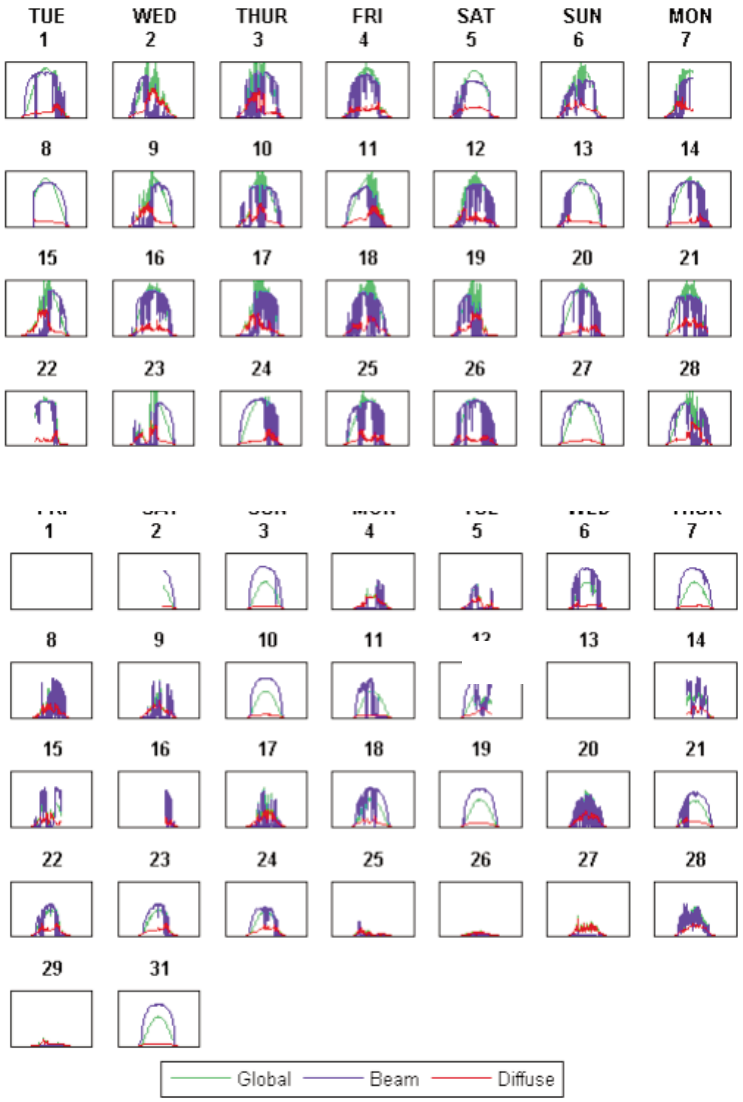

Figure 1: Minutely data series daily profiles in W/m^2. Upper panel February 2011 series; Lower panel July 2011 series

ues< 0.05) in Table 5.3, which also shows both the second largest and the third largest ordinates to be significant.

Table 2: White noise test output for 60-minutely series, February 2011

Test for white noise for variable global log	
M-1	90
Max(P(*))	263.305
Sum(P(*))	354.354
Fisher's Kappa: (M-1)*Max(P(*))/Sum(P(*))	
Kappa	66.875
Bartlett's Kolmogorov-Smirnov Statistic: Maximum absolute difference of the standardized partial sums of the periodogram and the CDF of a uniform(0,1) random variable.	
Test statistic	0.638
Test for whiote noise for variable global log	
Approximate P-Value	<.0001

Table 3: Periodogram analysis for all four data sets

	Obs	ω_k	*Period,*	$I(\omega_k)$	*p-value*
60-min	14	0.449	14.00	263.305	0.000
Feb	27	0.898	7.000	53.495	0.000
2011	40	1.346	4.667	15.194	0.0196

The harmonics used in HCSARIMA models G to H in subsection 5.2 were obtained in a similar fashion.

5.2 SARIMA and HCSARIMA Modelling

Both SARIMA and HCSARIMA models with significant (p-values< 0.05) parameters were fitted on all four data series (see Appendices A and B, respectively) via maximum likelihood (ML) estimation. To check the adequacy of these models, tables of residual analysis based the Box-Ljung statistics (p-values< 0.05), histograms (bell-shaped) of residuals, Q-Q plots (approximately straight line), and the

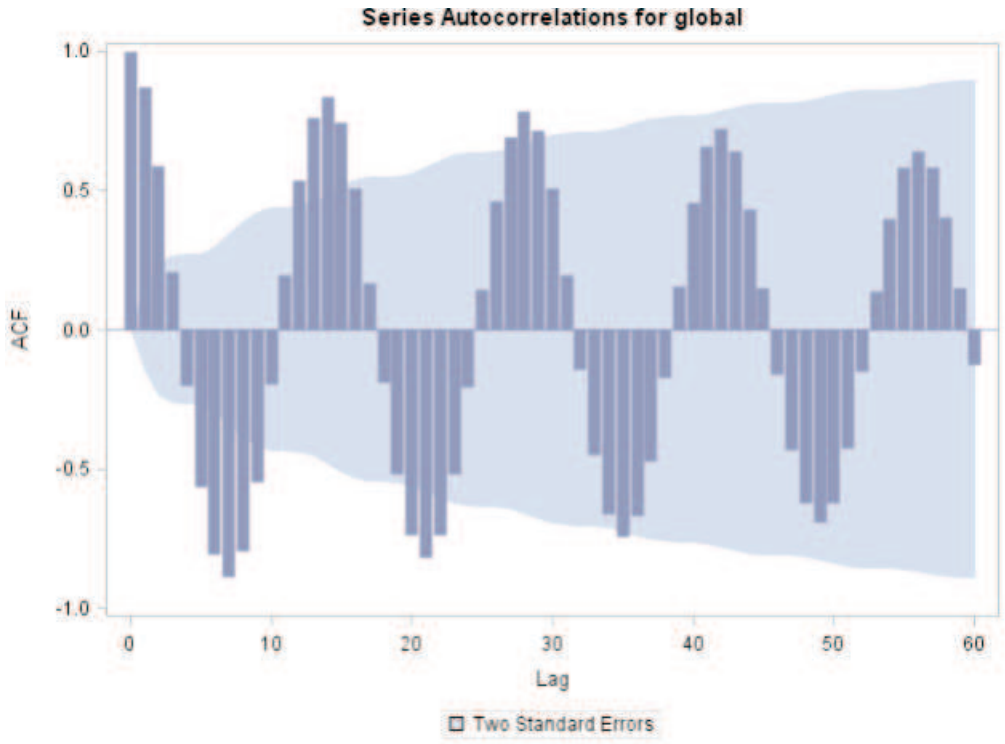

Figure 2: ACF plot of the 60-minutely averaged irradiance series (in W/m^2) for the period of the 1st to the 13th Feb 2011

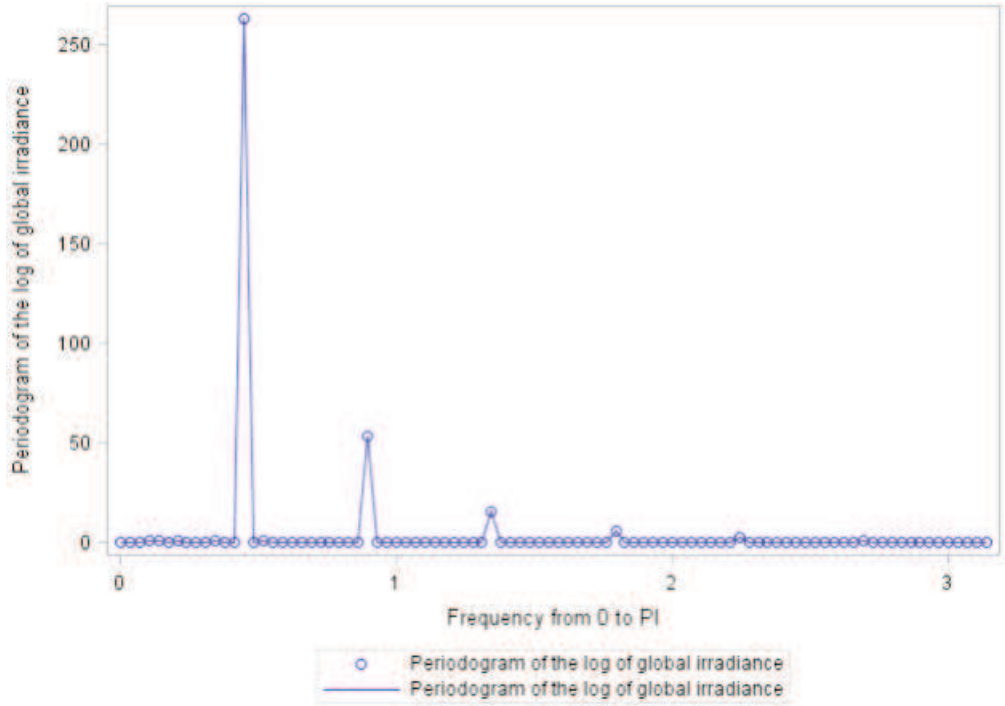

Figure 3: Periodogram plot for the log of the 60-minutely averaged irradiance series (in W/m^2) for the period of the 1st to the 13th Feb 2011

Anderson-Darling normality test (p-values < 0.05). Satisfying all criteria in parenthesis constitute adequacy. For brevity, only results for Model A are given in Appendix C.

SARIMA modelling

Parameter estimates for SARIMA models are given in Tables 4 to 7 in Appendix A. These are:

- *Model A, 60-minutely averaged February 2011 series:*

$$(1 + \phi_3 L^3 + \phi_{12} L^{12} + \Phi_{14} L^{14})(1 - L^{14}) X_t = (1 + \theta_1 L + \theta_2 L^2 + \Theta_{28} L^{28}) Z_t \,,$$

- *Model B, 60-minutely averaged July 2011 series:*

$$(1 + \phi_1 L + \phi_{12} L^{12} + \phi_{15} L^{15} + \Phi_{24} L^{24} + \Phi_{36} L^{36})(1 - L^{36}) X_t = (1 + \theta_1 L + \theta_2 L^2) Z_t,$$

- *Model C, 10-minutely averaged February 2011 series:*

$$(1 + \phi_1 L + \phi_2 L^2 + \phi_3 L^3 + \phi_6 L^6 + \phi_{10} L^{10} + \phi_{11} L^{11})(1 + \Phi_{84} L^{84} + \Phi_{168} L^{168})(1 - L^{84}) X_t = (1 + \theta_2 L^2 + \theta_4 L^4) Z_t,$$

- *Model D, on 10-minutely averaged July 2011 series:*

$$(1 + \phi_1 L + \phi_7 L^7 + \phi_{11} L^{11} + \phi_{12} L^{12} + \phi_{14} L^{14})(1 + \Phi_{66} L^{66} + \Phi_{132} L^{132})(1 - L^{66}) X_t = Z_t.$$

HCSARIMA modelling

Parameter estimates for HCSARIMA models are given in Tables 8 to 11 in Appendix B. These are:

- *Model E, 60-minutely averaged February 2011 series:*

$$X_t = \beta_0 + \alpha_1 \cos(2\pi/14) t + \beta_1 \sin(2\pi/14) t + \alpha_3 \cos(2\pi/7)\, t + (1 + \phi_1 L + \Phi_{56} L^{56}) W_t + Z_t,$$

- *Model F, 60-minutely averaged July 2011 series:*

$$X_t = \beta_0 + \alpha_1 \cos(2\pi/12)\, \mathrm{t} + \beta_1 \sin(2\pi/12)\, \mathrm{t} + (1 + \phi_1 L)(1 + \phi_{15} L^{15}) W_t + Z_t,$$

- *Model G, the 10-minutely averaged February 2011 series;*

Table 9 shows parameter estimates for the HCSARIMA model, G.

$$X_t = \beta_0 + \alpha_1 \cos(2\pi/84)\, t + \beta_1 \sin(2\pi/84)\, t + (1 + \phi_1 L + \phi_2 L^2 + \phi_3 L^3 + \phi_6 L^6 + \phi_7 L^7) W_t + Z_t,$$

- *Model H, the 10-minutely averaged July 2011 series;*

$$X_t = \beta_0 + \alpha_1 \cos(2\pi/66)\, t + (1 + \phi_1 L + \phi_7 L^7 + \phi_9 L^9 + \phi_{12} L^{12})(1 + \theta_{10} L^{10} + \theta_{54} L^{54}) W_t + Z_t.$$

6. Models comparison

In-sample model selection diagnostics

In-sample diagnostics used here are given in Table 4 viz., AIC, SBC (BIC), R-square and parsimony. The principle of parsimony selects the model with the least number of parameters.

SARIMA Model A is superior to HCSARIMA Model E in terms of criteria AIC and BIC but inferior with respect to R-square. Furthermore, the two models are equally parsimonious.

SARIMA Model B is superior to HCSARIMA Model F in terms of the two criteria, AIC and BIC but inferior with respect to the two measures, R-square and parsimony. SARIMA Model C and HCSARIMA Model G follow a similar pattern exhibited by SARIMA Model B and HCSARIMA Model F with respect to all measures, respectively. SARIMA Model D fares better than HCSARIMA Model H with respect to all diagnostics except R-square.

Prediction

Prediction accuracy diagnostics made use of here to compare the SARIMA models and HCSARIMA models are given in Table 5 viz., MBE, MPE, MAPE and RMSE. Also, the SARIMA and HCSARIMA models are compared graphically both with respect to point estimation and the 95% confidence intervals (CIs).

SARIMA Model A is out-performed by HCSARIMA E with respect to all the prediction accuracy measures except MPE, while SARIMA Model B performs better than HCSARIMA Model F in all the given prediction accuracy measures.

For both HCSARIMA Models G and H perform better than SARIMA Models C and D with respect to the MBE and RMSE and otherwise with respect to MPE and MAPE, respectively.

Graphically, the pair-wise forecasting accuracy comparisons of SARIMA models and HCSARIMA models are shown in Figures 4 to 7.

Note that the night times have been removed in order to get rid of the zero values.

The point forecasts of SARIMA Model A and HCSARIMA Model E in Figure 4 seem indistinguishable. However, the 95% CIs of SARIMA Model A are consistently wider than those of

Table 4: In-sample diagnostics for the fitted models

			In-sample model section diagnostics			
Scale	*2011 Month*	*MODEL*	*AIC*	*SBC*	*R-square*	*Parameters*
60-minutely	Feb	SARIMA A	1973.942	1992.686	0.946	6
		HCSARIMA E	2072.112	2091.336	0.961	6
	July	SARIMA B	841.435	857.372	0.840	7
		HCSARIMA F	946.258	958.413	0.883	5
10-minutely	Feb	SARIMA C	11613.350	11662.500	0.958	10
		HCSARIMA G	12195.330	12235.290	0.968	8
	July	SARIMA D	4381.669	4409.486	0.911	7
		HCSARIMA H	4955.966	4989.050	0.928	8

Table 5: Prediction errors for the fitted models

			Model forecast accuracy measure			
Scale	*2011 Month*	*MODEL*	*MBE(W/m^2)*	*MPE (%)*	*MAPE (%)*	*RMSE(W/m^2)*
60-minutely	Feb	SARIMA A	39.757	10.866	50.641	143.673
		HCSARIMA E	30.060	15.069	33.640	121.568
	July	SARIMA B	-31.802	-26.321	63.111	45.935
		HCSARIMA F	-89.076	-66.620	66.620	104.235
10-minutely	Feb	SARIMA C	38.075	25.119	44.692	155.747
		HCSARIMA G	17.134	47.301	64.775	146.817
	July	SARIMA D	-94.178	-28.119	38.167	122.249
		HCSARIMA H	-92.547	5.526	59.335	109.234

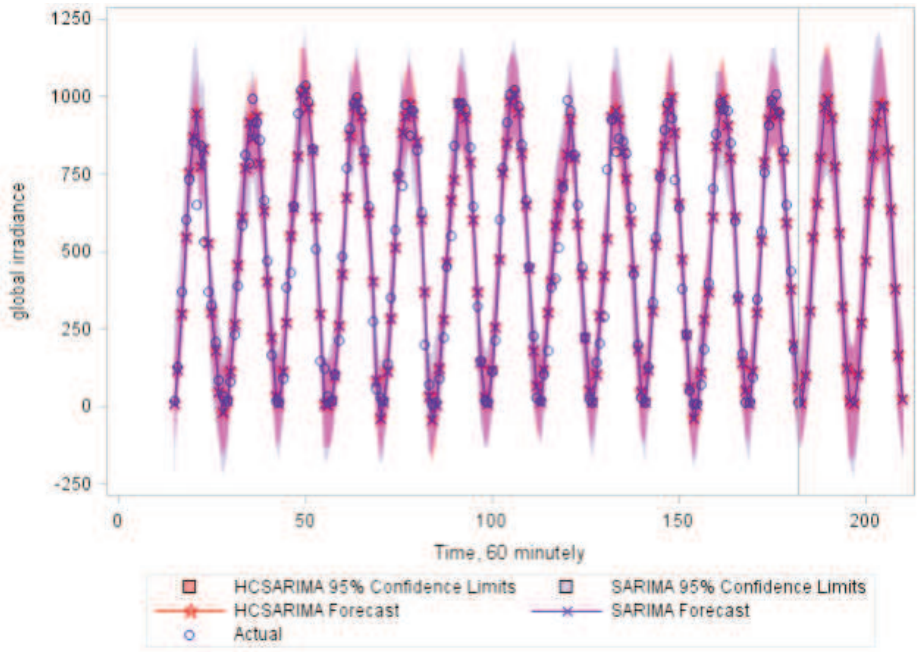

Figure 4: Forecasting accuracy comparison of SARIMA Model A and HCSARIMA Model E; 60-minutely averaged irradiance series (in W/m^2) for the period of the 1st to the 13th Feb 2011 and forecasts for the period 14th to the 15th Feb 2011

HCSARIMA Model E, hence the later model has a competitive. The picture is somewhat different for the 60-minutely series for July 2011, with respect to interval estimation as shown in Figure 5.

In these series, the 95% CIs for SARIMA Model B are wider those of HCSARIMA Model F in approximately a third of the estimation data series. Thereafter, both upper and lower confidents limits (CLs) tend to be alternating in size. However, in the hold out sample the upper CLs of SARIMA Model B, are wider than those for HCSARIMA Model F and vice-versa in the case of lower CLs.

The forecasting comparisons between SARIMA and HCSARIMA models for the 10-minutely series are given in Figures 6 and 7. The two figures exhibit a pattern similar to that in Figure 5, i.e., the point forecasts of SARIMA m\Models (C and D) and HCSARIMA Models (G and H) seem indistinguishable, while the 95% CLs for SARIMA models are generally wider than those of HCSARIMA models. Therefore, the HCSARIMA models have a competitive edge to SARIMA models.

Discussion

There is no clear 'winner' between the two classes of models, viz., SARIMA and HCSARIMA models, with respect to in-sample diagnostics. Empirically, it was observed that addition of a deterministic (sinusoidal) predictor would inflate the AIC and SBC diagnostics. As a consequence, these two measures were larger for HCSARIMA models compared to SARIMA models, giving SARIMA models a competitive edge in this regard. However, the opposite was true for the in-sample measures R-square and parsimony, where the HCSARIMA models performed better. To keep the values of AIC and SBC marginally larger we had to reduce the number of deterministic predictors, i.e., allowing some periodicities to be described by SARIMA model parameters in the HCSARIMA models. Thus, it was only at the

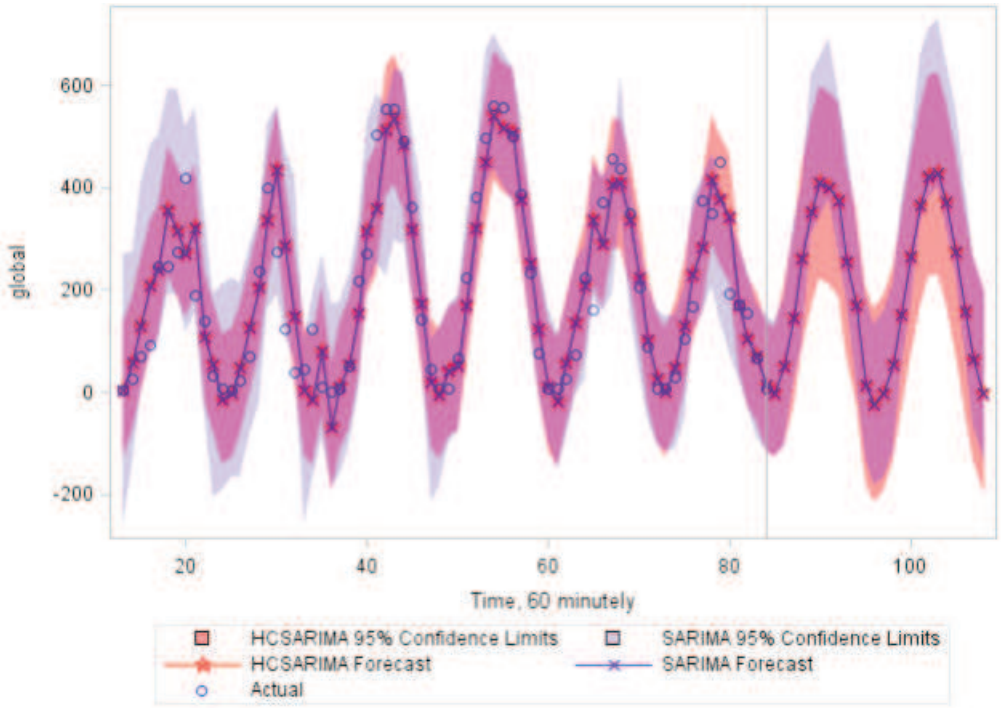

Figure 5: Forecasting accuracy comparison of SARIMA Model B and HCSARIMA Model F; 60-minutely averaged irradiance series (in W/m^2) for the period of the 3rd to the 9th for July 2011 and forecasts for the period 10th to the 11th July 2011

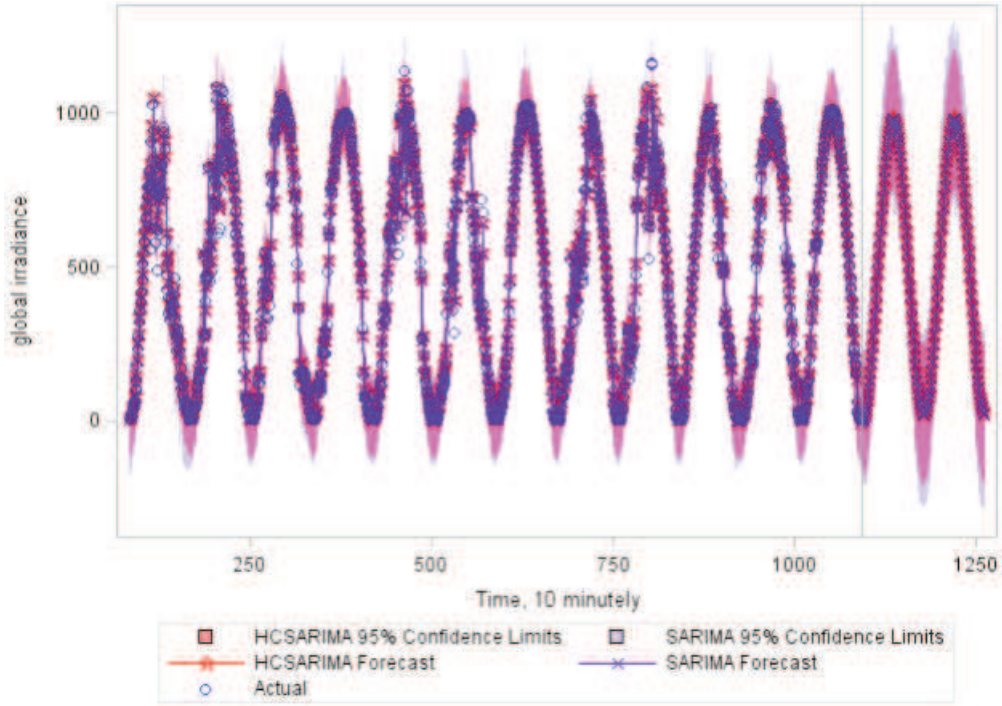

Figure 6: Forecasting accuracy comparison of SARIMA Model C and HCSARIMA Model G; 10-minutely averaged irradiance series (in W/m^2) for the period of the 1st to the 13th Feb 2011 and forecasts for the period 14th to the 15th Feb 2011

largest intensity (periodogram ordinate) that a sinusoidal predictor was used except for HCSARIMA Model E where a second sinusoidal predictor was added to model the seasonality at the second largest intensity. The addition of a sinusoidal predictor gives HCSARIMA models superiority with respect to R-square values and more or less better with respect to parsimony as HCSARIMA models have a single case of being marginally less parsimonious (HCSARIMA H).

In the prediction scenario, HCSARIMA models are found to be generally superior than SARIMA models. It is only in one data series (60-minutely July 2011) where SARIMA Model B out-performs

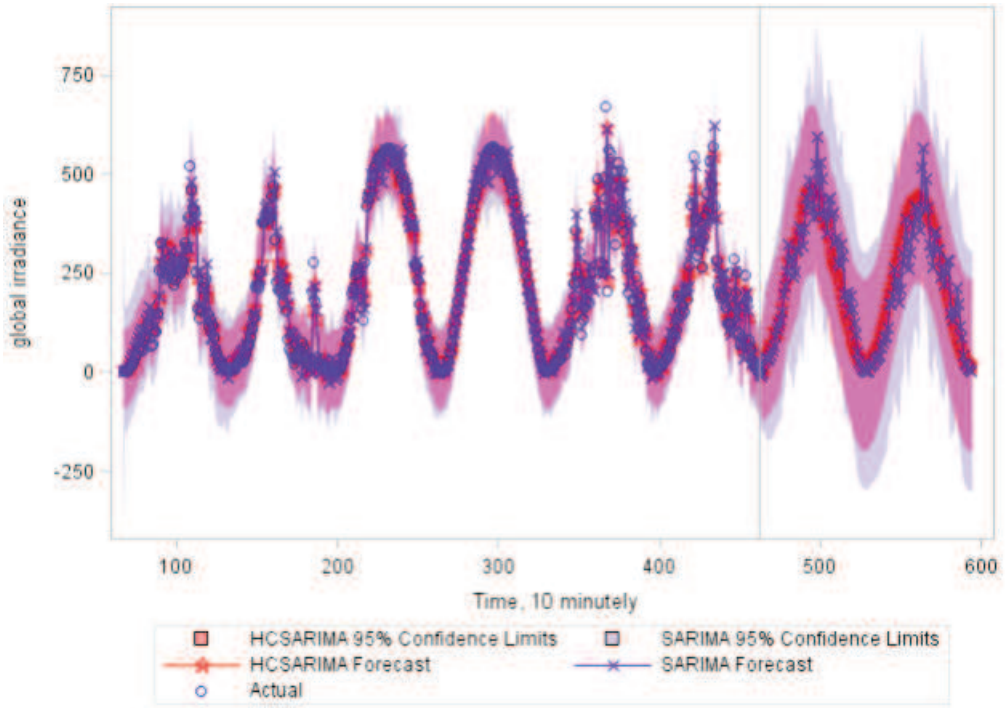

Figure 7: Forecasting accuracy comparison of SARIMA Model D and HCSARIMA Model H; 10-minutely averaged irradiance series (in W/m^2) for the period of the 3rd to the 9th for July 2011 and forecasts for the period 10th to the 11th July 2011

HCSARIMA Model F in all prediction measures. Furthermore, it was in this data series where in terms of the 95% CI estimation there was no clear better class of models. Otherwise in the other three data series the HCSARIMA models were found to be better than SARIMA models in the 95% CI estimation. However, we have reservations on this outcome of SARIMA model B versus HCSARIMA Model F due to the fact that the least amount of data series was available as well as the largest proportion of missing values inherent in this case.

7. Conclusions

While short memory SARIMA models are useful on their own, combining them with sinusoidal deterministic predictors to form HCSARIMA models generally has some competitive advantages in the prediction arena. However, the inclusion of sinusoidal predictors results in relatively larger AIC and SBC values. Using a smaller number of sinusoidal predictors gives a reasonable balance in the trade-off between the inflation of AIC and BIC values, and the improvement in forecasting. Alternatively, another proposal around this is to use SARIMA models for data generation and then use HCSARIMA models for forecasting. However, if the purpose of the models is only forecasting then there might be no need to restrict the number of sinusoidal predictors. In this scenario, all the harmonics found to be corresponding to significant periodogram ordinates using frequency domain techniques can be used to model the multiplicities of periodicities present.

Acknowledgements

Special thanks go to Michael Brooks of the UKZN School of Engineering for providing data, information and suggestions.

Appendix A: ML estimation for SARIMA models

Table 5: Parameter estimation for SARIMA model, A fitted on 60-minutely Feb 2011 series

Parameter	*Estimate*	*Approx* Pr > |t|	*Lag*
θ_1	-0.590	<.0001	1
θ_2	-0.447	<.0001	2
Θ_{28}	0.491	<.0001	28
ϕ_3	0.182	0.0015	3
ϕ_{12}	0.121	0.0198	12
Φ_{14}	-0.716	<.0001	14

Table 6: Parameter estimation for SARIMA model, B fitted on 60-minutely July 2011 series

Parameter	*Estimate*	*Approx* Pr > |t|	*Lag*
θ_1	-0.256	0.0493	1
θ_2	-0.350	0.0016	2
ϕ_1	0.199	0.0109	1
ϕ_{12}	-0.628	<.0001	12

ϕ_{15}	0.132	0.0234	15
Φ_{24}	-0.609	<.0001	24
Φ_{36}	-0.593	<.0001	36

Table 7: Parameter estimation for SARIMA model, C fitted on 10-minutely Feb 2011 series

Parameter	*Estimate*	*Approx* Pr > |t|	*Lag*
θ_2	-0.422	0.0018	2
θ_4	0.132	0.0038	4
ϕ_1	0.876	<.0001	1
ϕ_2	-0.597	<.0001	2
ϕ_3	0.504	<.0001	3
ϕ_6	0.094	0.0009	6
ϕ_{10}	-0.138	<.0001	10
ϕ_{11}	0.097	0.0003	11
Φ_{84}	-0.677	<.0001	84
Φ_{168}	-0.309	<.0001	168

Table 8: Parameter estimation for SARIMA model, D fitted on 10-minutely July 2011 series

Parameter	*Estimate*	*Approx* Pr > |t|	*Lag*
ϕ_1	0.863	<.0001	1
ϕ_7	0.112	0.0009	7
ϕ_{11}	-0.121	0.0155	11
ϕ_{12}	0.198	0.0003	12
ϕ_{14}	-0.124	0.0009	14
Φ_{66}	-0.781	<.0001	66
Φ_{132}	-0.323	<.0001	132

Appendix B: ML Estimation for HCSARIMA Models

Table 9: Parameter estimation for HCSARIMA model, E fitted on 60-minutely Feb 2011 series, where SINTWO = sin[2π/14)t], COSTWO = cos[2π/14)t] and COSTHREE = cos[2π/7)t]

Parameter	*Estimate*	*Approx* $Pr > \|t\|$	*Lag*	*Variable*
β_0	505.464	<.0001	0	global
ϕ_1	0.668	<.0001	1	global
Φ_{56}	-0.296	0.0002	56	global
β_1	-151.068	<.0001	0	SINTWO
α_1	-456.142	<.0001	0	COSTWO
α_3	-31.363	<.0001	0	COSTHREE

Table 10: Parameter estimation for HCSARIMA model, F fitted on 60-minutely July 2011 series, where SINTWO = sin[2π/12)t] and COSTWO = cos[2π/12)t]

Parameter	*Estimate*	*Approx* $Pr > \|t\|$	*Lag*	*Variable*
β_0	214.435	<.0001	0	global
ϕ_1	0.745	<.0001	1	global
ϕ_{15}	0.277	0.0193	15	global
β_1	-62.940	0.0009	0	SINTWO
α_1	-210.121	<.0001	0	COSTWO

Table 11: Parameter estimation for HCSARIMA model, G fitted on 10-minutely Feb 2011 series, where SINTWO = sin[2π/84)t] and COSTWO = sin[2π/84)t]

Parameter	*Estimate*	*Approx* $Pr > \|t\|$	*Lag*	*Variable*
β_0	498.676	<.0001	0	global
ϕ_1	0.858	<.0001	1	global
ϕ_2	-0.145	0.0002	2	global
ϕ_3	0.076	0.0167	3	global
ϕ_6	0.145	<.0001	6	global
ϕ_7	-0.067	0.0260	7	global
β_1	-48.184	0.0034	0	SINTWO
α_1	-478.809	<.0001	0	COSTWO

Table 12: Parameter estimation for HCSARIMA model, H fitted on 10-minutely July 2011 series, where COSTWO = sin[2π/66)t]

Parameter	*Estimate*	*Approx* $Pr > \|t\|$	*Lag*	*Variable*
β_0	228.483	<.0001	0	global
θ_{10}	-0.135	0.0140	10	global
θ_{54}	0.150	0.0037	54	global
ϕ_1	0.832	<.0001	1	global
ϕ_7	0.130	0.0006	7	global
ϕ_9	-0.143	0.0016	9	global
ϕ_{12}	0.091	0.0114	12	global
α_1	-211.674	<.0001	0	COSTWO

Appendix C: Checking adequacy for Model A

Table 13: Residual analysis for SARIMA model, A fitted on 60-minutely Feb 2011 series

Autocorrelation check of residuals									
To Lag	*Chi-Square*	*DF*	*Pr > ChiSq*	*Autocorrelations*					
6	.	0	.	0.112	-0.026	0.032	0.043	-0.124	-0.097
12	8.280	6	0.218	0.003	-0.012	0.018	-0.014	0.075	-0.011
18	12.620	12	0.397	-0.074	-0.053	-0.016	0.072	0.086	0.045
24	18.990	18	0.393	-0.008	-0.084	-0.048	0.055	0.090	-0.109
30	29.440	24	0.204	-0.080	0.007	-0.080	-0.120	-0.155	0.012

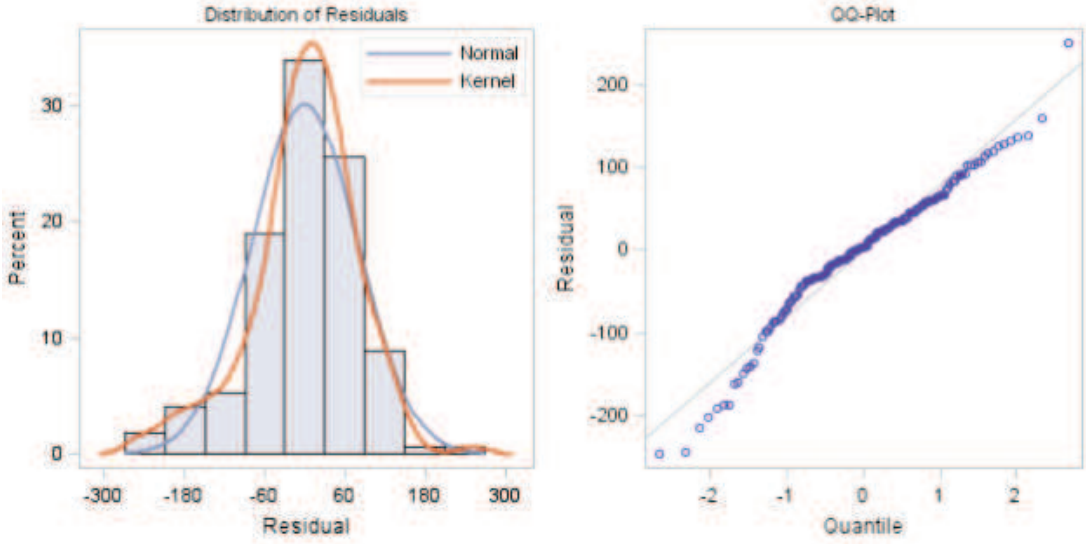

Figure 8: Normality check for the residuals of SARIMA Model A

Table 14: Fitted normal distribution for RESIDUALS

Goodness-of-fit tests for normal distribution		
Test	*Statistic*	*p Value*
Anderson-Darling	A-Sq 2.15090163	Pr > A-Sq <0.005

References

Akaike, H. (1983). Information Measures and Model Selection, *Bulletin of the International Statistical Institute,* 50, 277-290.

Alados I., Gomera M.A., Foyo-Moreno I., and Alados-Arboledas L. (2007). Neural network for the estimation of UV erythemal irradiance using solar broadband irradiance. *Int. J. Climatol.*, 27(13), 1791-9.

Altandombayci O, and Golcu M. (2009). Daily means ambient temperature prediction using artificial neural network method: a case study of Turkey. *Renew. Energy*, 34(4), 1158-61.

Balestrassi P., Popova E., Paiva A., and Marangonlima J. (2009). Design of experiments on neural network's training for nonlinear time series forecasting. *Neurocomputing*, 72(4-6), 1160-78.

Box, G. E., and Cox, D. R. (1964). An analysis of transformations. *J. Roy. Statist. Soc. Ser. B* 26:211–252.

Box, G. E. P. and Jenkins, G. M. 1976. *Time Series Analysis: Forecasting and Control*, Revised ed. USA, Holden-Day Inc.

Chatfield C. (2003). *The Analysis of Time Series: An Introduction*, 6th Edition, Chapman & Hall/CRC Press, London.

Craggs, C., Conway, E. and Pearsall N. M. (1999). Stochastic modelling of solar irradiance on horizontal and vertical planes at a northerly location. *Renewable Energy* 18, 445-463.

Cryer D.J. and Chan K, (2008). *Time Series Analysis with Applications in R*, 2nd Ed. Spring Street, New York Inc.

Davis H. T. (1941). *The Analysis of Economic Time Series*. Indiana: The Principia Press, Inc. Bloomington.

Fuller W. A. (1976). *Introduction to Statistical Time Series*. New York: John Wiley & Sons.

GRADRAD: The Greater Durban Radiometric Network. http://gradrad.ukzn.ac.za.

KZN Green Growth. http://www.kzngreengrowth.com.

Paulescu, M., Paulescu, E., Gravila P. and Badescu V. (2013). *Weather Modelling and Forecasting of PV Systems Operation*. Springer Verlag, London

Schwarz, G. (1978). Estimating the Dimension of a Model, *The Annals of Statistics*, 6, 461–464.

Pedro H. T. C. and Coimbra C. F.M. (2012). Assessment

of forecasting techniques for solar power production with no exogenous inputs. *Solar Energy*, 86, 2017-2028.

Reikard G. (2009). Predicting solar radiation at high resolutions: A comparison of time series forecasts, *Solar Energy*, 83, 342–349.

Schuster, A. (1898). On the investigation of hidden periodicities with application to a supposed 26 day period of meteorological phenomena, *Terrestrial Magnetism and Atmospheric Electricity*, 3 13-41.

Voyant C., Muselli M., Paoli C. and Nivet M. (2013a.) Hybrid methodology for hourly global radiation forecasting in Mediterranean area. *Renewable Energy*, 53, Complete, 1-11.

Voyant C., Randimbivololona P., Nivet M. L., Paolic C. and Musellic M. (2013b). Twenty four hours ahead global irradiation forecasting using multi-layer perceptron. *Meteorol. Appl.*, (2013), DOI: 10.1002/met.1387.

Wei W. W. S. (2006). *Time Series Analysis. Univariate and Multivariate Methods*. 2nd Ed. Addison Wesley.

Yona A., Senjyu T., Funabashi T., Mandal P. and Kim C-H. (2013). Decision Technique of Solar Radiation Prediction Applying Recurrent Neural Network for Short-Term Ahead Power Output of Photovoltaic System. *Smart Grid and Renewable Energy*, 2013, 4, 32-38.

Zaharim A., Razali A. M., Gim, T. P. and Sopian, K. (2009). Time Series Analysis of Solar Radiation Data in the Tropics. *European Journal of Scientific Research*. .25, 672-678.

Wang F., Mi Z., Su S. and Zhao H. (2012). Short-Term Solar Irradiance Forecasting Model Based on. Artificial Neural Network Using Statistical Feature Parameters. *Energies*, 5, 1355-1370.

Zawilska E. and Brooks M.J. An Assessment of the Solar Resource for Durban, South. Africa. *Renewable Energy*, 36:12, 3433-3438.

Received 31 October 2013; revised 11 December 2014

Details of authors

Khaled Bataineh *B Eng (Mech. Eng.) M Sc (Mech. Eng.) PhD (Mech. Eng.)*
Associate Professor of Mechanical Engineering
Jordan University of Science and Technology,
PO Box 3030, Irbid, 22110, Jordan
Tel: +962 2 720 1000
Fax: +962 2 720 1074
E-mail: k.bataineh@just.edu.jo
Rd. Khaled Bataineh is an Associate Professor of Mechanical Engineering. He received a B.S. from Jordan University of Science and Technology in 1999, and an M Sc from Carnegie Mellon University. He received his PhD in Mechanical Engineering from the University of Pittsburgh in 2005. Dr Bataineh's research interests are in micro scale fluidic system, machine design, and renewable energy technology. He is well –known in modelling of complex flows. His current group's research focuses on microfluidics, including micro pump and micro cone -plate viscometer. Currently, he is focusing on Concentrated Solar Power (CSP) which is a promising renewable energy technology for the Mediterranean and Gulf countries (World's Sun Belt region). He is the author of about 28 reviewed journal articles and other technical publications.

Michael Brooks *B Sc Eng (Mechanical), M Sc Eng (Mechanical), PrEng*
Senior Lecturer, Department of Mechanical Engineering, University of KwaZulu-Natal
Member: Group for Solar Energy Thermodynamics (GSET)
University of KwaZulu-Natal, Durban, 4041
Tel: +27 31 260 7667
Fax: +27 41 260 3217
E-mail: brooks@ukzn.ac.za
Mike Brooks is a senior lecturer in the Department of Mechanical Engineering at UKZN, where he is a member of the Group for Solar Energy Thermodynamics (GSET). His research interests include solar concentrator design and radiometry, and he leads the UKZN Aerospace Systems Research Group (ASReG). He is a registered professional engineer and the chairman of the steering committee for the Southern African Universities Radiometric Network (SAURAN). He is a member of SAIMechE and a senior member of the American Institute of Aeronautics and Astronautics (AIAA), where he has served on the Terrestrial Energy Systems Technical Committee since 2010.

Tatenda Joseph Bvumbe *BS Eng (Hons) (Mech Eng) MS Eng (Mech Eng)*
Doctoral Fellow
HySA System Systems
South African Institute for Advanced Materials Chemistry (SAIAMC)
University of the Western Cape,
Robert Sobukwe Road,
Bellville, Cape Town,
7535, South Africa
E-mail: engtatejose@yahoo.com
Tatenda J Bvumbe is a mechanical engineer with a BS Eng (Hons) in Mechanical Engineering from the University of Zimbabwe. He worked for the Civil Aviation Authority of Zimbabwe for three years as an Airport Mechanical Engineer. This role did not satisfy his wish to actively and effectively contribute to the development of sustainable energy systems so he left and enrolled at the University of KwaZulu-Natal and acquired his MS Eng in Mechanical Engineering in 2013. His research work focused on the utilisation of solar energy to power absorption cooling systems. He is currently a Doctoral Fellow with HySA Systems Competence Centre at the University of Western Cape and his work is focused on the internal humidification of low temperature Proton Exchange Membrane Fuel Cells.

Shuang Dai *Bachelor's degree (Textile Engineering)*
Graduate Year One, School of Management,
China University of Mining and Technology,
Xuzhou, 221116, P.R.China
Tel: +86 18761421689
E-mail:ds14511@126.com
Shuang Dai holds a bachelor's degree of Textile Engineering from Nantong University. Her research interests include energy economics and policy, and energy-related CO_2 emissions.

Reena das Nair *B Com (Hons), M Com (Economics); PhD Research Fellow (Economics)*
Senior Researcher: Centre for Competition, Regulation and Economic Development (CCRED), University of Johannesburg

Economist: Acacia Economics, Johannesburg
Cell: +27825469705
E-mails: reenadn@uj.ac.za and reena@acaciaeconmics.co.za
Reena das Nair is currently a Senior Researcher at the Centre for Competition, Regulation and Economic Development (CCRED) at the University of Johannesburg. Prior to joining CCRED, Reena was Programme Manager: Industrial Policy at Trade and Industrial Policy Strategies (TIPS), a not-for-profit research organisation undertaking economic research for policy makers. Before TIPS, Reena worked as a Principal Economist in the Policy and Research division at the Competition Commission of South Africa. She has extensive experience in leading investigations and economic analysis in mergers, abuse of dominance and cartel cases, including in case hearings before the Competition Tribunal and Appeal Court. She has further undertaken research in economic regulation, particularly in the energy sector. Reena is also an economist at Acacia Economics, a boutique consultancy that offers expertise in competition and regulatory economics in Africa.

Sven du Clou *B Sc Eng (Mech) M Sc Eng (Mech)*
Metrologist: Contact and Radiation Thermometry
National Metrology Institute of South Africa
Private Bag X 34, Lynnwood Ridge, 0040, South Africa
Tel: +27 12 841 2753
E-mail: sduclou@nmisa.org
Sven du Clou is a mechanical engineer with experience in thermal management, pyrometry and thermometry. He was previously employed by the University of KwaZulu-Natal as a Research Engineer, assisting in the development of the Southern African Universities Radiometric Network (SAURAN). Currently he is appointed as a metrologist at the National Metrology Institute of South Africa (NMISA). He is responsible for maintaining the ITS-90 temperature scale for contact and radiation thermometry and disseminating traceability to South Africa and abroad.

Paul Gauché *B Eng (Mech) M Eng (Mech)*
Senior Researcher: Solar Thermal Energy Research Group (STERG), Department of Mechanical and Mechatronic Engineering, Stellenbosch University
Private Bag X1, Matieland, 7602, South Africa
Tel: +27 21 808 4242
E-mail: paulgauche@sun.ac.za
Paul Gauché is a mechanical engineer with a master's degree in the thermal energy field. He has worked in a variety of R&D roles since 1995, initially in the cooling and ventilation fields and more recently as a systems engineering manager and strategic planning manager.
Currently he is appointed as a senior researcher in the Mechanical and Mechatronic Engineering Department, where he co-founded and directed the Solar Thermal Energy Research Group (STERG). He is currently the project leader for a TIA funded technology development project and is also completing his PhD.

Jasson Gryzagoridis *B Sc (Mech Eng) M Sc (Mech Eng PhD (Mech Eng) Pr.Eng*
Department of Mechanical Engineering, University of Cape Town, South Africa
Tel: 021 650 3229
Cell: 083 692 0931
E-mail: Jasson.Gryzagoridis@uct.ac.za
Jasson Gryzagoridis is an Emeritus Professor in Mechanical Engineering from the University of Cape Town. His academic career began as a Junior Lecturer in 1965 and culminated as a full Professor till retirement in 2004. Currently he is occupying the position of Senior Scholar at UCT engaged with NDT research for Armscor and is also a part time Adjunct Professor at Cape Peninsula University of Technology in the Mechanical Engineering Department as a Post Graduate student Mentor.
During his academic career he has supervised numerous students at MSc, M Tech, PhD and D Tech level sand is the author of over 80 Journal peer reviewed papers and in Proceedings of International Conferences. His research interests are in Heat Transfer, Thermo fluids, Refrigeration, Solar Energy and Non Destructive Testing. Past positions include:

- Head of Department, Department of Mechanical Engineering, UCT- (1996-2001) and (2003-2004);
- Chair of the Safety Committee, Faculty of Engineering, UCT;
- National Coordinator of NDT/E – IAEA/SA Atomic Energy;
- Referee and Inspector – Innovation Fund Projects, Department of Arts Science and Technology;
- Referee for a number of peer-reviewed journals; and
- Member of number of Scientific and Engineering Societies and Editorial Boards of Journals.

Freddie L Inambao *M SC, PhD (Volgograd)*
Senior Lecturer/Leader: Green Energy Solution Research Group, Department of Mechanical Engineering, Howard College, University of KwaZulu-Natal, King George V Avenue, Durban 4041, South Africa
Tel: +27 31 260 8530;
Fax: +27 31 260 8530
E-mail: inambaof@ukzn.ac.za

Freddie L. Inambao holds an MSc and PhD in Mechanical Engineering with specialisation in thermodynamics and internal combustion engines from Volgograd Polytechnic Institute, Russia. He has lectured in several universities in Southern Africa including the University of Zambia, University of Botswana, University of Durban-Westville (before the merger with the University of Natal) and currently a Senior Lecturer in the discipline of Mechanical Engineering of the University of KwaZulu-Natal, Howard College, Durban, South Africa. He is an expert in thermodynamics, internal combustion engines, renewable and alternative energy and energy management.

Adisa A Jimoh *Pr.Eng. (South Africa) B.Eng. (Elect. Eng.) M Eng. (Elect. Eng.)(ABU) PhD (Elect. Eng.)(McMaster) SMIEEE SMSAIEE MNSE*
Research Niche Area Leader: Energy and Industrial Power Systems
Head of Department: Electrical Engineering
Tshwane University of Technology, Building 6, Room 419, Pretoria Campus
Private Bag X680, Pretoria 0001, South Africa
Tel: +27 12 382 4964
Fax: +27 12 382 4964
Cell: +27 82 787 0251
E-mail: jimohaa@tut.ac.za
Adisa A. Jimoh (Senior Member, IEEE) is an electrical engineer with bachelor's, master's and PhD degrees. He has been a faculty member in several universities for 32 years.

Mohamed Tariq E Kahn
Faculty of Engineering
Head: Centre for Distributed Power and Electronic Systems
Cape Peninsula University of Technology
Cape Town
South Africa
E-mail: KhanT@cput.ac.za
Professor MTE Kahn is the Head of the Centre for Distributed Power Electronics Systems at Cape Peninsula University of Technology.

Kant E Kanyarusoke, *M-ASHRAE M-SASE M Sc. (Mech. Eng) B Sc. (Eng) 1st class Hons. HDHET cum laude PG cert. CIRDAFRICA int. rural devt*
Department of Mechanical Engineering, Cape Peninsula University of Technology, Cape Town, South Africa
E-mail: KanyarusokeK@cput.ac.za
Kant Kanyarusoke is an industrial-mechanical engineer with over 18 years of industrial experience in chemicals, foods and beverages industries across several sub-Sahara African countries. He also has over 11 years of full time university lecturing experience in Thermo-Fluids and Mechanical Eng. Design courses. He graduated from Makerere University, Uganda with a first class honours BSc. Eng. degree in 1982; obtained an M Sc in Mechanical Engineering (Design and Production Eng.) at the University of Lagos, Nigeria in 1985 and a cum laude Higher Diploma in Higher Education and Training at the Cape Peninsula University of Technology in 2009.
In his engineering, management and consultancy career, he first worked with multinational companies like British American Tobacco Company and Unilever PLC in Uganda with stints in Kenya, Malawi and Zimbabwe. Later, he helped set up 2 small scale detergents, cosmetics and drinks manufacturing companies in Uganda and Botswana. In South Africa, he has consulted on process steam plants maintenance. In Education, he has taught at Makerere University, University of Botswana, and now at the Cape Peninsula University of Technology. His current research work is on optimizing solar energy systems designs for rural Africa domestic applications.

Fatimah Kari *BA (Economics) MA (Economics) PhD (Economics)*
Department of Economics, Faculty of Economics and Administration, University of Malaya, 50603 Kuala Lumpur, Malaysia
Tel: +60 3 7967 3661
E-mail: fatimah_kari@um.edu.my
Associate Professor (Dr) Fatimah Kari earned a Bachelor's degree from the National University of Malaysia (UKM), a Master of Economics from the University of Leicester, UK and a PhD (Economics) from Mississippi State University, United States. She is formerly the Director of the Centre for Poverty and Development Studies (CPDS), University of Malaya and Associate Professor in the Department of Economics, Faculty of Economics and Administration, University of Malaya. She has published and presented many scholarly papers in the area of Environment and Poverty, Poverty Indexing and Environment and Growth. She has been a consultant for several consultancy project sponsored by the Ministry of Energy, Green Technology and Water (KeTTHA), Ministry of Natural Resources and Environment (MNRE) and Economic Planning Unit, Prime Ministers Department, Malaysia.

Durmus Kaya *B Eng (Mechanical Engineer) M Sc (Mechanical Engineer) PhD (Mechanical Engineer)*
Professor: (Mechanical Engineering-Energy)
Department of Energy Systems Engineering, Faculty of Technology, Kocaeli University, 41380 Umuttepe, Kocaeli, Turkey.
Tel: +90 532 402 60 74
Fax: +90 262 3032203

E-mails: durmuskaya@hotmail.com and durmus.kaya@kocaeli.edu.tr
Durmus Kaya graduated as a Mechanical Engineer from Yildiz University. He received his MS at Kocaeli University and a PhD in Mechanical Engineering at Sakarya University. His research areas are energy technologies, energy efficiency, renewable energies; biogas (mainly), new and clean energy technologies. He has contributed in many national and international projects as a project manager and a researcher. He has more than 50 academic papers published in different respectable journals. He is also the author of nine books, related to his main research areas. Currently, he is working as a professor at Kocaeli University, Department of Energy Systems Engineering, Faculty of Technology. He is managing two projects on biogas and energy efficiency, successfully.

Fatma Canka Kilic *B Eng (Mechanical Engineer) M Sc (Mechanical Engineer) PhD (Mechanical Engineer)*
Associate Professor (Dr) (Mechanical Engineering-Energy-)
Department of Electric and Energy Technologies, Air Conditioning and Refrigeration Technology, Kocaeli Vocational School, Kocaeli University, Kullar, Basiskele, Kocaeli, Turkey
Tel: +90 262 3493414
Fax: +90 262 3493997
E-mails:fatmacanka@hotmail.com and fckilic@kocaeli.edu.tr
Fatma Canka Kilic is Associate Professor (Dr) at the Kocaeli University, Kocaeli Vocational School in Air Conditioning and Refrigeration Program. She graduated Yildiz University, Department of Mechanical Engineering as a Mechanical Engineer in 1991. She worked as a mechanical engineer in the industrial area from 1991-1993. She received her Master's Degree from Kocaeli University, Institute of Science and Technology, at the Department of Mechanical Engineering, Heat and Energy Department, in 1996. The same year she started her PhD education at Sakarya University, Institute of Science and Technology. After completing her coursework, she went to the United States to prepare her PhD thesis at Clemson University, Department of Mechanical Engineering EIB, Graduate School of Applied Sciences, Energy Sciences, in English. She completed her PhD thesis in August 2000 and received her certificate. She began her academic career as a lecturer at Kocaeli University's Vocational School in Air Conditioning and Refrigeration Program, in October, 1994. She became Assistant Prof. (Dr) and the coordinator of that program in 2001 and served in this position until 2010. She was then appointed as the Chair of the Department of Electricity and Energy, a title that she still holds. She became Associate Professor (Dr) in June, 2012 and then she is also appointed as the International Student Coordinator at Kocaeli University. She has more than 20 academic papers published in different prestigious journals. She speaks English fluently and French at a secondary level.

Corli Leonard *B Eng (Industrial) M Sc Eng (Management)*
Research Engineer: Centre for Renewable and Sustainable Energy Studies, Stellenbosch University
Private Bag X1, Matieland, 7602, South Africa
Tel: +27 21 808 3605
Fax: +27 21 883 8513
E-mail: corli@sun.ac.za
Ms. Corli Leonard holds a B Eng degree in Industrial Engineering from the University of Pretoria. She completed her M Sc Engineering Management in 2010, specialising in aerospace quality assurance. Former work experience includes logistics in the automotive industry with the focus on the global supply chain management and also a research visit to Sweden as member of a team investigating the localisation of Volvo Aero Company's supply chain network. Currently her focus is project management of the Centre's research and commercial projects. Apart from management of various other projects for the industry, the daily processes of the Centre are also managed and streamlined. These tasks include the management of contracts, procurement processes, writing of funding proposals, organising and management of customised short courses for industry; and processing personnel's timesheets.

Chia-Wei Lin
Department of Food Science and Biotechnology, National Chung Hsing University, 250, Kuo-Kuang Rd., Taichung 402, Taiwan
Tel: 886 4 2284 0385 ext. 3070
Fax: 886 4 2287 6211
E-mail: d9643201@mail.nchu.edu.tw
Qualifications: 2007/09~up to now, National Chung Hsing University
Chia-Wei Lin is a PhD student in the Department of Food Science and Technology, National Chung Hsing, Taiwan, with achievements through scholarships and symposiums.

Golden Makaka *M Sc PhD (Applied Physics)*
Senior Lecturer (Renewable Energy), Physics Department, University of Fort Hare, Private Bag, X1314, Alice, 5700 South Africa
Tel: +27 (0)40 602 2207
Cell: +27 (0)71 8973 486
Prof Golden Makaka is a physicist with a Masters' degree in Applied Physics and a PhD in Physics. He is currently an Associate Professor and a post graduate coordinator in the Physics Department at Fort

Hare University. He specializes in renewable energy, energy efficiency and building physics. He is also a consultant in passive solar energy efficiency building design strategies in South Africa.

Sampson Mamphweli *PhD Physics, Menv Sc, Mini-MBA Associate*
Professor: (Renewable Energy), Institute of Technology, University of Fort Hare, Tel: +27 4060 22311
Fax: +27 4065 30665
Mobile: +27 82 2140 367
Prof Sampson Mamphweli is an Associate Professor at the Institute of Technology, University of Fort Hare, South Africa. He possesses a Doctor of Philosophy degree in Physics from the University of Fort Hare, and a Master of Environmental Sciences degree from the University of Venda, South Africa. He is also in possession of a Certificate in Financing Renewable Energy and Energy Efficiency from RENAC Renewables based in Germany.
Prof Mamphweli also possesses the Green Power Mini-MBA from the Green Power Academy based in Britain. He is a recipient of the prestigious University of Fort Hare Vice Chancellor's Emerging Researcher medal for the year 2012. He conducts research on renewable energy technologies and their applications, and he is a respected authority in the biomass to energy field. He has published 18 scientific papers in peer-reviewed journals and conference proceedings including two book chapters. Prof Mamphweli reviews papers for publication in several journals in the engineering and renewable energy fields of study. His current area of research interest includes biomass gasification for electricity generation, biogas digesters, co-gasification of coal and biomass for electricity generation as well as solar energy technologies.

AJ (Riaan) Meyer
Managing Director, GeoSUN Africa
Unit 1, CS Africa Building, 1 Meson Street, Techno Park
Stellenbosch, 7600, South Africa
Tel: +27 21 882 8354
Cell: +27 84 876 4816
E-mail: riaan.meyer@geosun.co.za
Website: www.geosun.co.za
Mr Riaan Meyer is an expert in solar resource assessment and has been working in this field since 2006. He holds a Bachelor's Degree in Electrical and Electronic Engineering and a Master's Degree in Mechanical Engineering. He is the Managing Director of GeoSUN Africa – a spin-off company from the Centre for Renewable and Sustainable Energy Studies (CRSES) at Stellenbosch University. GeoSUN Africa offers a wide variety of solar related services and products to utility scale solar plants as well as smaller on and off-grid installations. Riaan consults developers and operators of solar power plants, investors, financial and governmental institutions. GeoSUN operates in a number of Sub-Sahara Africa countries.Riaan remains a close link with the University of Stellenbosch and is involved in teaching of post graduate modules in renewable and specifically solar energy. He also serves as a reviewer of local and international solar energy conferences.

Edson Leroy Meyer *B Sc M Sc PhD (Physics) (NMMU) CEM CMVP*
University of Fort Hare, Institute of Technology, Private Bag X1314, Alice, 5700
Tel: 040 60220861
Fax: 040 6530665
Email:emeyer@ufh.ac.za
Prof Edson Meyer is the Director of the Fort Hare Institute of Technology, a research centre focusing on Renewable Energy areas such as Biomass, Solar Energy, ICT as well as Energy Efficiency.

Pamela Mondliwa *B Com (Hons)*
Researcher: Centre for Competition, Regulation and Economic Development (CCRED), University of Johannesburg
Economist: Acacia Economics, Johannesburg
Tel: +27115592717
E-mails: pamelam@uj.ac.za and pam@acaciaeconmics.co.za
Pamela is a Researcher at the Centre for Competition, Regulation and Economic Development (CCRED) at the University of Johannesburg. Prior to joining CCRED, Pamela worked as an Economist in the Policy and Research division at the Competition Commission of South Africa. Pamela has experience in conducting economic analysis on complex enforcement and cartel cases, and mergers and acquisitions in a wide range of sectors including petrochemicals. She has also conducted research for South African government on economic regulation, and industrial policy. Pamela is also an economist at Acacia Economics, a boutique consultancy that offers expertise in competition and regulatory economics in Africa.

Michael Mouzouris *B Sc Eng (Mechanical) M Sc Eng (Mechanical)*
Research Engineer at Helio100 project
10 Devon Valley Road, Stellenbosch, 7600, South Africa
Tel: +27 21 882 8681
E-mail: mjm@sun.ac.za
Michael Mouzouris is a mechanical engineer with a Master's degree focused in concentrating solar thermal energy systems. He was a lab research engineer at Stellenbosch University's Solar Thermal Energy Research Group (STERG) for 2 years conducting experiments and managing the lab's activities.

Currently he is appointed as a research engineer in the Helio100 project. The project is aimed at developing a 100% South African heliostat technology for the Concentrating Solar Power (CSP) industry.

Josiah L Munda *D Eng (Elect), PrEng*
Acting Executive Dean, Faculty of ICT
Tshwane University of Technology
Private Bag X680, Pretoria 0001, South Africa
Tel: +27 12 382 9689
Fax: + 27 12 382 9146
Cell: +27 84 415 6692
E-mail: mundajl@tut.ac.za
Josiah Munda holds a D Eng degree (2002) in electrical engineering. He has worked in a number of institutions in Africa and Japan on academic and engineering services for over twenty years.
Currently he is an Associate Professor of Power Systems, and the acting Executive Dean of the Faculty of Information and Communication Technology at Tshwane University of Technology, Pretoria, South Africa. His research areas are power system stability, renewable energy supplies, energy management, distributed power systems and intelligent control.

Sayed Mohammad Bager Najafi *BA (Economics) MA (Economics) PhD (Economics)*
Department of Economics, Faculty of Social Science, Razi University, Iran
Tel: +98 83 38388092
Sayed Mohammad Bager Najafi received his PhD in the field of Development Economics from Mofid University, Iran. His research interests include Economic growth and Development.

Vinod Kumar Nema *B.E. (Mech) M.E. (Mech), PhD (Rocket Propulsion)*
Tele: 919 6919 70473
E-mail: vinodnema1946@gmail.com
Vinod Kumar Nema retired from Motilal Nehru National Institute of Technology, Allahabad (India) in 2012. He had served as Director of MITRC, Alwar (Raj), India and Guru Ramdas Khalsa Institute of Science & Technology (GRKIST), Jabalpur (India) and is now serving as a Visiting Professor at GRKIST. He has guided many M.Tech. students and five PhD students. One PhD is in progress. All the theses are in the area of Heat and Mass Transfer. His field of Interest: is Thermal Engineering.

Mphiliseni B Nzuza *B Sc (Statistics & Applied Mathematics) BSc Hons (Statistics) MSc (Statistics)*
Lecturer: Statistics, School of Mathematical Sciences, University of Zululand
Private Bag X1001, KwaDlangezwa, 3886
Cell: +27 79 843 7670
Tel: +27 35 902 6497
E-mail: nzuzap@unizulu.ac.za
Mphiliseni Nzuza is a lecturer with a Masters' degree in Statistical Modelling of Solar Radiation. From 2009 to 2014, he served on a number of academic programmes and a variety of sections in the Faculty of Science and Agriculture at the University of KwaZulu-Natal. Currently he is appointed as a lecturer in the Statistics Department of Zululand University, where he is also set to take some part on the project about Renewable and Sustainable Energy to be established, furthering his studies towards obtaining his PhD.

Oludolapo A Olanrewaju *B Sc (Elect. Eng.) (University of Ibadan) M Sc (Industrial Eng.) (University of Ibadan)*
PhD Student, Industrial Engineering Department, Tshwane University of Technology, South Africa
Cell: +27 79 089 4923
E-mail: dlp4all@yahoo.co.uk
Oludolapo Olanrewaju is a PhD student in the Industrial Engineering Department, Tshwane University of Technology.

Atanda K Raji
Programme Coordinator: BTech: Electrical Engineering (Bellville Campus)
Stream Leader: Power Electronics
Senior Lecturer/Researcher
Centre for Distributed power and Electronics Systems
Electrical Electronic and Computer Engineering Department
Cape Peninsula University of Technology
Bellville Campus, Cape Town, South Africa
Tel.: 021 959 6563
Fax: 02 1 595 6117
Email: rajia@cput.ac.za
Mr Atanda K Raji is a doctoral student and lecturer in the Department of Electrical Engineering at Cape Peninsula University of Technology CPUT) and an active member of the Centre for Distributed Power Electronics Systems (CDPeS). He holds a Master degree in electrical engineering technology from CPUT and Masters of Science in electronics engineering from Ecole Supérieure d'Ingénieurs en Electrotechnique et Electronique (ESIEE-Paris) His area of specialization includes integration and interconnection of power electronics interface based grid-tied technology, modelling, control of power electronics and energy management systems, distributed generation and power system analysis.

Edmore Ranganai *B Sc Gen (Maths & Stats) B Sc Hons (Stats) M Sc (Stats) PhD (Stats)*
Senior Lecturer: Statistics
University of South Africa
College of Science Engineering and Technology

The Science Campus
Department of Statistics
C/nr Christiaan de Wet Road & Pioneer Avenue
Florida Park, Roodepoort, 1710
Private Bag X6, Florida, South Africa
Tel: +27 11 670 9257
E-mail: rangae@unisa.ac.za
Edmore Ranganai is a Statistician with a PhD in Statistics obtained from Stellenbosch University. Since 2000 he has been working in academia involved in research in general, consulting and lecturing both in main line statistics courses as well as servicing disciplines such as, Engineering and Natural Sciences. Recently, he has found new interests in renewable energy research. Currently, he is appointed as a senior lecturer in the Department of Statistics at the University of South Africa, Florida Science Campus.

Simon Roberts *BA Hons, MA, PhD*
Professor, Department of Economics and Econometrics, University of Johannesburg
Director, Centre for Competition, Regulation and Economic Development (CCRED), University of Johannesburg
Cell: +27 83 304 2567
E-mail: sroberts@uj.ac.za
Simon Roberts is Director of the Centre for Competition, Regulation and Economic Development and Professor of economics at the University of Johannesburg. Simon held the position of Chief Economist and Manager of the Policy & Research Division at the Competition Com-mission from November 2006 to December 2012. In addition, Simon has consulted extensively on competition and industrial development over the past 20 years and has been an expert economist witness in a number of major competition cases. He has advised competition authorities in a number of countries.

Nurulhuda Binti Mohd Satar *BA (Economics) MA (Economics) PhD (Economics)*
Department of Economics, Faculty of Economics and Administration, University of Malaya, 50603 Kuala Lumpur, Malaysia
Tel: +60 3 7967 3656
Fax: +60 3 7967 7252
E-mail: nurulhuda@um.edu.my
Nurulhuda Binti Mohd Satar is a lecturer in the Department of Economics, University of Malaya.

Michael Simon *B Sc (Hons) M Sc (Physics) PhD (Physics) (UFH)*
University of Fort Hare, Institute of Technology, Private Bag X1314, Alice, 5700
Tel: 040 6065302354
Fax: 040 6530665
E-mail: MSimon@ufh.ac.za
Michael Simon holds a PhD degree in Physics from the University of Fort Hare. He is presently the University of Fort Hare Energy Manager and Head of the Energy Efficiency Group in FHIT. He is also a certified Eskom M&V professional and Team leader of the Eskom M & V UFH Team. He is a Photovoltaic & an Energy Efficiency specialist. He is a SAEE member. He is a seasonal author and reviewer in many peer review journals and accredited national and international conference proceedings.

Saeed Solaymani *BA (Economics) MA (Economics) PhD (Economics)*
Department of Economics, Faculty of Social Science, Razi University, Iran
Tel: +98 918 387 1538
E-mail: saeedsolaymai@gmail.com
Saeed Solaymani received his Bachelors in Business Economics from Razi University, Iran. He also received his Master's degree in Economics from Shahid Bahonar University of Kerman, Iran. He received his PhD in the field of Energy and Environmental Economics from the University of Malaya, Malaysia. His research interests include Environmental and Energy Modelling, Microeconomics and Econometric Modelling.

Yan Song *PhD (Systems Engineering)*
Associate Professor, School of Management, China University of Mining and Technology, Xuzhou, 221116, P.R. China
Tel: +86 13952185360
E-mail: syan118@163.com
Yan Song holds a Doctorate in Systems Engineering from Nanjing University of Technology. His research interests include applied economy and theoretical economics.

Stephen L Tangwe *B Eng (ELEC) M Eng (ELEC)*
UFH Eskom M&V Engineer
MaATLAB Application Engineer
Energy Efficiency PhD Research Candidate at the Fort Hare Institute of Technology
Private Bag X1314, Alice, 5700, South Africa
Tel: +27 783076922
Fax: +27 40 653 0665
E-mail: acb@sun.ac.za
Stephen Tangwe holds a B.Eng.(Hons) and M Eng degree in Electrical Engineering from Atlantic International University. He is a member of the South African Institute of Electrical Engineers and IEEE. He's also a member of the South African Energy Efficiency Association and the World Sustainable Energy Technology Association. He is currently pursuing his PhD in Physics with the University of Fort Hare (UFH) and he is an adhoc Eskom Measurement and Verification Engineer with the UFH team. He is a seasonal author in several

accredited peer review conference proceedings and journals.

Mohammad Tariq *B. Tech. (Mech. Eng.) M. Tech. (Mech. Eng.) PhD (Gas turbine and Jet Propulsion)*
Assistant Professor (Senior) in the Department of Mechanical Engineering, Shepherd School of Engineering and Technology, SHIATS-DU, Allahabad
Tel: 919 7935 02977
E-mail: mohdtariq7@gmail.com
Mohammad Tariq has been working as an Assistant Professor (Senior) in the Department of Mechanical Engineering, Shepherd School of Engineering and Technology, SHIATS-DU, Allahabad, India, since 2005. He has guided more than 30 M. Tech. students and 5 PhD students are in progress. He had served as a lecturer in the United College of Engineering and Research, Allahabad, BBS College of Engineering & Technology, Allahabad, and ITM University, Gwalior, (India) for 4 years. His field of Interest is Thermal Engineering

Nic van der Westhuizen *B Eng (Mechatronic)*
Project Engineer: GeoSUN Africa (Pty) Ltd
Unit 1, CS Africa Building, 1 Meson Street, Techno Park,
Stellenbosch, 7600, South Africa
Tel: +27 21 250 0583
E-mail: nic.vanderwesthuizen@geosun.co.za
Nic van der Westhuizen holds a B Eng degree in Mechatronic Engineering. He has worked in a technical position for 5 years at a company that manufactures and exports road testing machinery before joining GeoSUN Africa as a project Engineer in mid-2013. He is responsible for projects pertaining to the installation of measurement stations across Africa. He is also involved with the technical setup of these stations which includes land owner liaison, exporting, training, data logger programming and data management.

Ernest E van Dyk *B Sc (Physics and Applied Mathematics) B Sc Hons (Physics) M Sc (Physics) PhD (Physics) Pr.Nat.Sci. Pr.Phys.*
Professor of Physics, Nelson Mandela Metropolitan University (NMMU)
Director: Centre for Energy Research, NMMU
Centre for Energy Research, PO Box 77000, Nelson Mandela Metropolitan University, Port Elizabeth, 6031
Tel: +27 41 504 2259
Fax: +27 41 504 1959
E-mail: ernest.vandyk@nmmu.ac.za
Web: http://energy.nmmu.ac.za
Prof Ernest van Dyk obtained his PhD in Physics at the University of Port Elizabeth in 1994. He teaches Physics at the NMMU and is also Director of the Centre for Energy Research (CER) at the NMMU since 2006. The CER is involved with several renewable energy research projects for industry and government agencies. Prof van Dyk's research interests are in the field of Solar Energy, specialising in Photovoltaics and Solar Thermal research. He has supervised 17 MSc and 7 PhD student projects to completion and is currently supervising 6 PhD students. He has published forty-nine scientific journal articles in the field of Photovoltaics and has authored or co-authored 39 international conference papers and 128 national conference presentations. Prof van Dyk has a passion for teaching Physics and researching Renewable Energy Technologies. He also regularly consults on Photovoltaics and Solar Energy to national and international companies.

Wikus van Niekerk *B Eng (Mechanical) M Eng (Mechanical) PhD (Mechanical)*
Director: Centre for Renewable and Sustainable Energy Studies,
Stellenbosch University
Private Bag X1, Matieland, 7602, South Africa
Tel: +27 21 808 4251
Fax: +27 21 883 8513
E-mail: wikus@sun.ac.za
Prof Wikus van Niekerk is a Professor in the Department of Mechanical and Mechatronic Engineering and Director of the Centre for Renewable and Sustainable Energy Studies at Stellenbosch University. He is registered as a Professional Engineer with the Engineering Council of South Africa, and was evaluated in the past by the NRF as a C2, internationally recognised, researcher. He is regularly consulted by industry on a variety of areas including renewable energy systems and technology; solar, wind and ocean energy; and energy policy and research strategy.

He completed his PhD on the active control of transient noise transmission at the University of California at Berkeley, working on a project for Mazda Corp. After holding the Sasol Chair in Vehicle Engineering at the University of Pretoria he moved to Stellenbosch University in 2000. At Stellenbosch he has been Head of the Mechanics Division, Chair of the Department of Mechanical Engineering and Director of the Institute for Thermodynamics and Mechanics. He is currently the Director of the Centre for Renewable and Sustainable Energy Studies and plays a leading role to establish research, education and training programmes in renewable energy and influence funding and policy priorities on the national level. He has a keen interest in solar and ocean energy and is investigating the exploitation of wave energy along the southwest coast and ocean current energy of the east coast of South Africa.Prof Van Niekerk serves

on the boards of various organisations and companies and founded GeoSUN Africa and SRL-SA as spin-out commercial ventures from his research and consulting activities. He has received numerous awards over the years, the most recent being the SANEA Energy Award for his contribution to renewable energy in South Africa (particularly in the field of solar energy).

Shuo-Wen Tsai *PhD*
Department of Food Science and Biotechnology, National Chung Hsing University, 250, Kuo-Kuang Rd., Taichung 402, Taiwan
Tel: 886 4 2284 0385 ext. 3070
Fax: 8864 2287 6211
E-mail: tsaishuowen@nchu.edu.tw
Shuo-Wen Tsai holds a PhD from the University of Tokyo and is an Assistant Professor in the Department of Food Science and Technology, National Chung Hsing, Taiwan.

Frederik J Vorster *B Sc (Physics, Mathematics) M Sc (Physics) PhD (Physics)*
Senior Lecturer: Physics
Senior Researcher: Centre for Renewable Energy, Nelson Mandela Metropolitan University
PO Box 770002, Nelson Mandela Metropolitan University, Port Elizabeth, 6031, South Africa
Tel: +27 41 504 3051
Fax: +27 41 504 2573
E-mail: Frederik.vorster@nmmu.ac.za
Frederik Vorster is a physicist with PhD specialising in photovoltaics. He teaches Physics and Engineering subjects at the NMMU and is closely involved with the management and development of various projects at of the Centre for Energy Research. He is currently a Senior Lecturer at the NMMU and actively involved with supervision of several Physics and Engineering masters and doctoral students. Dr Vorster's broad research interests include solar energy, heat engines and micro wind turbine development. His principal area of specialisation lies in concentrator and flat plate photovoltaics, specifically the development on new characterisation techniques for photovoltaic materials, modules and systems. He consulted to a variety of industry and public sectors in South Africa in the fields of photovoltaics and domestic solar water heating.

Ming Zhang *PhD (Energy and Environment Engineering)*
Associate Professor, School of Management, China University of Mining and Technology, Xuzhou, 221116, PR China
Tel: +86 1526 2028260
E-mail: zhangmingdlut@163.com
Ming Zhang holds a Doctor of Energy and Environment Engineering from the Dalian University of Technology. His research interests include energy economics and policy, energy efficiency, rural energy consumption, and energy-related CO_2 emissions.

INFORMATION FOR AUTHORS

The *Journal of Energy in Southern Africa* publishes papers covering the technical, economic, policy, environmental and social aspects of energy research and development carried out in, or relevant to, Southern Africa. Contributions from those working in these fields are welcome.

Submissions
All contributions should be submitted in English.

Only original work will be accepted, and by submitting an original work for publication the author grants the publisher a worldwide, non-exclusive, royalty-free and perpetual licence to reproduce, publish and distribute the author's work in any format or medium.

The suggested length for full-length articles is 3 000 to 5 000 words. All full-length articles are refereed, and amendments to scripts and formats may be required before final acceptance. The Editor reserves the right to make editorial changes to contributions.

The following shorter items are also welcome, but are not refereed:

- Research notes, Shorter communications and Case studies (500–2 500 words)
- Conference reports (100–1 500 words)
- Book reviews (800–1 000 words)

Format
Contributions should be in electronic format, and submitted either on disk or via e-mail. They should preferably be in a format compatible with MS Word. The Editor might also request the submission of a printed version.

Text should be single-spaced, with a wide left-hand margin. Standard international (SI) units must be used throughout.

An abstract of the article should be provided, not exceeding 500 words, resuming the contents and conclusions of the article. A maximum of six keywords should be included, reflecting the entries the author(s) would like to see in the annual Subject Index published in the last issue for the year. The keywords may consist of more than one word each, but the entire concept should not be more than 30 characters long.

References must be made according to the Harvard (author, date) system. See articles in the JESA for examples of this and of other aspects of its house style.

Notes, where unavoidable, should *not* be automatically embedded, but gathered at the end of the article and indicated in the text by means of sequential arabic numbers in superscript.

Numbers for headings, captions for tables and figures, etc should be manually inserted, rather than automatically generated.

Illustrations and tables
If the contribution is accepted, original electronic versions of graphs must be supplied; produced, where possible, with MS Office programmes (Excel, PowerPoint). The quality of the illustrations must be acceptable to the Editor. For photographs and non-electronically produced drawings, the originals will have to be provided, or scans of an acceptable quality (minimum 300DPI). Straight screen-grabs are never acceptable. All illustrations must be provided in monochrome, and readable as such (colour photographs can be converted by us).

Illustrations and tables should appear in their proper places in the submitted document (not gathered at the end). All should be referred to in the text, numbered sequentially (manually rather than automatically), and with accompanying captions. Tables must be submitted as text, rather than as images.

General
No material will be returned to the author(s) following publication unless this is requested by at the time of original submission.

At the time of submission, the author(s) must state that the contribution has not been published and is not being considered for publication elsewhere, and will not be submitted for publication elsewhere unless rejected by the *Journal of Energy in Southern Africa* or withdrawn by the author(s).

Authors must supply a brief CV (maximum of 500 words), which includes the following personal information (for the Details of authors section): surname, initials, address, contact telephone/fax numbers, email address, qualifications, occupation and/or employment.

Authors of accepted contributions will receive a free copy of the issue in which their contribution appears as well as a PDF version.

Neither the Editorial Committee nor the Publisher accepts responsibility for the opinions or viewpoints expressed, or for the correctness of facts and figures.

All contributions and enquiries should be addressed to: The Editor, Journal of Energy in Southern Africa, Energy Research Centre, University of Cape Town, Private Bag, Rondebosch 7701, South Africa. E-mail: richard.drummond@uct.ac.za